Sustainable Processes for Critical Metal Recovery using Oxalate Chemistry

By
© 2021
Ankit Verma
B.Tech., Indian Institute of Technology Madras, India, 2016

Submitted to the graduate degree program in the Department of Chemical and Petroleum Engineering and the Graduate Faculty of the University of Kansas in partial fulfillment of the requirements for the degree of Doctor of Philosophy.

Chair: Dr. Mark B. Shiflett

Dr. Alan M. Allgeier

Dr. Aaron M. Scurto

Dr. David R. Corbin

Dr. David A. Fowle

Date Defended: December 3rd, 2021

The dissertation committee for Ankit Verma certifies that this is the approved version of the following dissertation:

Sustainable Processes for Critical Metal Recovery using Oxalate Chemistry

Chair: Mark B. Shiflett

Date Approved: December 3rd, 2021

Dedicated to the loving memory of my grandfather, Ganpat Ram Verma.

Abstract

In the U.S., critical metals like aluminum (Al from bauxite), lithium (Li), cobalt (Co), and rare earth elements (REEs) are vital in various emerging technologies such as lithium-ion batteries (LIBs), solar cells, and high-tech electronics. Continuous growth in population with an increasing level of technological innovation has resulted in a rapid increase in resource consumption. Hence, sustainable, environmentally-friendly, and efficient use of available resources is required to preserve the natural resources for future generations. This dissertation introduces the utilization of oxalate chemistry to develop sustainable, environmentally-friendly, and closed-loop processes for recovery of critical metals like Li and Co from waste LIBs, Al and Fe from bauxite ore, and Fe and Ti from ilmenite ore. The oxalate anion ($C_2O_4^{2-}$) can be derived from organic sources, has minimal environmental impact, and forms moderately acidic reagents like oxalic acid ($H_2C_2O_4$), potassium hydrogen oxalate (KHC_2O_4), and ammonium hydrogen oxalate ($NH_4HC_2O_4$). The oxalate reagents are known for the chelation and precipitation properties, but the leaching and reduction properties had not been previously studied. This dissertation establishes oxalate reagents as an efficient route to recover and separate metals from various mixed metal oxide sources.

The demand for LIBs has significantly increased over the last 5 years, leading to a shortage in the supply of Li and Co. The LIBs economy can be stabilized by recycling the critical metals from spent cathodes. Currently, approximately 59% of the LIBs contain lithium cobalt oxide ($LiCoO_2$) as the cathode material. In this work, oxalate chemistry has been used to recover and separate Li and Co from $LiCoO_2$. Traditionally, inorganic acids like sulfuric and nitric acid with a reducing agent like hydrogen peroxide (H_2O_2) are used to recycle LIBs, but the emission of harmful pollutants like SO_X and NO_X pose a significant risk to the environment. The clean and green oxalate reagents like $H_2C_2O_4$ and $NH_4HC_2O_4$ can extract Li into the aqueous phase as lithium

oxalate ($Li_2C_2O_4$) and precipitate cobalt oxalate ($CoC_2O_4 \cdot 2H_2O$) from $LiCoO_2$ in a single step. The optimum acidity for Li and Co extraction and separation using oxalate reagents was pH < 2.0 at Co:$C_2O_4^{2-}$ (Co:Ox) molar ratio = 1:3, T = 100 °C and solid-to-liquid (S/L) ratio = 15 g/L. During the metal extraction, a green-colored Co^{3+}-oxalate complex was identified as an intermediate. This extracted Co^{3+} was reduced and precipitated in the form of $CoC_2O_4 \cdot 2H_2O$. The combined shrinking core model (cSCM) identified the rate-limiting mechanism to be the diffusion of aqueous $H_2C_2O_4$ through the solid product layer of $CoC_2O_4 \cdot 2H_2O$ forming on the surface of $LiCoO_2$. To improve the kinetics and avoid the loss of $C_2O_4^{2-}$ during oxidation, H_2O_2 was added as an additional reducing agent.

In the presence of H_2O_2, Li and Co were efficiently recovered and separated at Co:Ox:H_2O_2 molar ratio = 1:1.5:3, T = 55-75 °C, and S/L ratio = 15 g/L. The reduced concentration of $C_2O_4^{2-}$ ion led to the precipitation of $CoC_2O_4 \cdot 2H_2O$ in a micro-rod morphology. This micro-rod precipitate had 23% lower bulk density and higher porosity than the granular precipitate from extractions using only $H_2C_2O_4$. The lower density micro-rod precipitate formed a porous shell over the $LiCoO_2$ core and improved the diffusion of aqueous $H_2C_2O_4$. In this case, the chemical reaction at the $LiCoO_2$ surface was identified as the rate-limiting step at T = 55-75 °C. In both $H_2C_2O_4$ and $H_2C_2O_4$ + H_2O_2 processes, Li can be precipitated as Li_2CO_3 using K_2CO_3 and KOH at a pH > 13. The Co was separated from $CoC_2O_4 \cdot 2H_2O$ by dissolving and precipitating the metal oxalate (as $Co(OH)_2$) in the basic solution recovered after Li precipitation. Alternatively, micro-rod structure Co_3O_4 was synthesized by calcining $CoC_2O_4 \cdot 2H_2O$ at T > 400 °C in the presence of air.

In this work, oxalate chemistry was also used for efficient Fe and Al recovery from bauxite ore. Bauxite ore is the world's primary source for Al metal, and the Bayer process (based on NaOH) holds an exclusive status for its refining. The Bayer process is efficient for Al extraction,

but a massive quantity of "red mud" waste is generated. The red mud is an iron-containing caustic waste and is typically disposed in landfills or open ponds and reservoirs. The high alkalinity of the waste pollutes the land and ecosystem around it. With the growing demand for Al, the disposal methods of red mud needs global attention. Using oxalate chemistry, reagents like $H_2C_2O_4$, KHC_2O_4, and $H_2C_2O_4{\cdot}KHC_2O_4$ can efficiently recover Fe and Al from bauxite ore. From NIST SRM 600 bauxite ore, more than 90% of Fe and Al was extracted into the aqueous phase in less than 2 h with 0.50 M $C_2O_4^{2-}$ at 100 °C for all three reagents. Among the three oxalate reagents, $H_2C_2O_4$ is the most acidic, followed by $H_2C_2O_4{\cdot}KHC_2O_4$ and KHC_2O_4. The Fe can be selectively precipitated by hydrolyzing the aqueous phase to a pH = 13.80. After separating the Fe precipitate, the resulting filtrate can be acidified to a pH = 10.50 for efficient Al precipitation.

The recycling of acid after the efficient metal extractions is critical to minimize waste generation and improve economics. In this work, two unique acid recycling processes were developed to efficiently recover and reuse oxalate reagents. The first process utilizes strong acid cation-exchange resins to regenerate the oxalate reagent in acidic form. The amount of resins determines the final pH and the type of oxalate reagent regenerated. To recycle the aqueous phase as $H_2C_2O_4$, a pH < 1.0 was optimal, whereas, for KHC_2O_4 and $NH_4HC_2O_4$, a pH around 2.5 was required. Additionally, the low aqueous solubility of KHC_2O_4 and $H_2C_2O_4{\cdot}KHC_2O_4$ was utilized to precipitate 60-80% of acid by acidifying the aqueous phase after metal recovery to a pH = 1.5-2.5. Due to acid recycling, the $H_2C_2O_4 + H_2O_2$ process for LIBs recycling produced 50% less waste than the traditional H_2SO_4 process at a similar cost. The oxalate processes demonstrated in this work were closed-loop, environmentally-friendly, and economical and can offer similar advantages for recycling valuable metals from various waste streams.

Acknowledgments

First and foremost, I offer my sincerest thanks to my advisor and mentor, Dr. Mark Shiflett, for his guidance and support throughout my PhD work. This degree would not have been possible without the motivation and inspiration Dr. Shiflett has provided. I really appreciate the professionalism and safety culture that he has cultivated in this lab and in every group member graduating from here. Dr. Shiflett has immense knowledge in chemical engineering at both fundamental and industrial level. All the discussions I have had with him have expanded my knowledge tremendously in this area.

Second, I would like to express my deep gratitude to Dr. David Corbin for the valuable guidance in my PhD work. Dr. Corbin's knowledge in material science has expanded my knowledge and interest in this area immensely. I am glad that I got an opportunity to work at the forefront of chemical engineering and materials science under the guidance of two accomplished experts: Dr. Shiflett and Dr. Corbin. I will miss the weekly project meetings and the discussions we have had to solve numerous challenging problems.

I would like to thank Dr. Alan Allgeier, Dr. Aaron Scurto, and Dr. David Fowle for serving on my dissertation and comprehensive exam committee. The valuable comments, feedback, and insights that I have received from the committee throughout my PhD work have guided the work significantly. I also had the opportunity to interact with Dr. Laurence Weatherley on the ion-exchange processes. The scientific discussions with Dr. Weatherley were extremely helpful in developing the ion exchange process in this work. I am also thankful to Dr. Susan Williams for allowing me to use the ICP-OES and TGA instruments in her laboratory. She provided me with the flexibility to use both instruments at my convenience. This has helped a lot in completing the specific goals of my research on time.

I am also thankful to Dr. Victor Day and Dr. Prem Thapa for training me on the XRD and microscopy imaging, respectively. The composition of the solids produced in this work was characterized using PXRD and Dr. Day's training on analysis of the powder patterns played a crucial role in it. Dr. Prem Thapa has trained me on SEM, TEM, and XPS and has guided and motivated me during the PhD journey.

A special thanks go to the undergraduate team: Grant Johnson, Chris Lawrence, Ty Stranghoner, and Alex Henne. I had the opportunity to work with each of them during the various timespan of my PhD research. They have made an enormous contribution by assisting me in the experiment plans. I would like to give a special mention to the contribution of Grant Johnson and Alex Henne, who ideated the ion exchange resin process and performed most of the exchange experiments in the last two years. Ion exchange study was the most tedious process in this work and required patience to perform correctly.

I was also fortunate to have a fantastic set of colleagues in both Shiflett and Allgeier lab through my time here. Every member of both groups has supported me from my transition phase to the end of my PhD. I would specially like to acknowledge the impact of Tugba Turnaoglu on my PhD journey. Both of us had a similar beginning of our PhD studies, and the way she overcame all the challenges to be a successful researcher has motivated me tremendously. A special thanks also go to Simon Velasquez and Murilo Suekuni for being the support pillar during my time here. I have some amazing memories with everyone in the lab and will cherish those forever.

I am incredibly grateful for the amazing set of friends that I had outside the lab as well. In Amit and Riddhi, I had the best set of friends and housemates that always made me feel close to home. In Priya, Aparna, and Sayantani, I found the strongest pillars of my life in Lawrence. The amount of support that I got from them on every difficult day in my journey has been tremendous.

The little friends like family I had here will be extremely missed, particularly during every festival that we celebrated with outstanding enthusiasm and zeal. I would also like to acknowledge the support of my best friend Aditi during the last 8 years. Her motivation and encouragement have been vital for me in my professional and personal life.

At last, I would like to express my sincere gratitude to my amazing family. My mom, dad, and sister have been a continuous source of encouragement, positivity, and strength throughout my life. My parent's trust and belief have always allowed me to pursue my dreams with all my strength. All of this would not have been possible without the blessings of God, who has always been kind to me.

Additional Acknowledgments

Portions of this dissertation have been published as articles in journals by the American Chemical Society (ACS), Elsevier, and Wiley Online Library. One of the referenced articles (S.No. 1) was submitted to an ACS journal. The publishers allow the author to reuse published works in the author's thesis, which the author writes and is required to submit to satisfy the criteria of degree-granting institutions.

1. **Verma, A.**, Henne, A.J., Corbin, D.R., & Shiflett, M.B., Lithium and Cobalt Recovery from $LiCoO_2$ using Oxalate Chemistry: Scale-up and Techno-economic Analysis. *Industrial & Engineering Chemistry Research* (*submitted*)
2. **Verma, A.**, Corbin, D.R., & Shiflett, M.B., Extraction of Aluminum and Iron from Bauxite: A Unique Closed-Loop Ore Refining Process Utilizing Oxalate Chemistry, *AIChE Journal* **2021** (*in press*)
3. **Verma, A.**, Corbin, D.R., & Shiflett, M.B., Lithium and Cobalt Recovery for Lithium-Ion Battery Recycle using an Improved Oxalate Process with Hydrogen Peroxide. *Hydrometallurgy* **2021**, 105694
4. **Verma, A.**, Johnson, G.H., Corbin, D.R., & Shiflett, M.B., Separation of Lithium and Cobalt from $LiCoO_2$: A Unique Critical Metal Recovery Process Utilizing Oxalate Chemistry. *ACS Sustainable Chemistry & Engineering* **2020**, 8(15), 6100-6108
5. **Verma, A.**, Kore, R., Corbin, D.R., & Shiflett, M.B., Metal Recovery Using Oxalate Chemistry: A Technical Review. *Industrial & Engineering Chemistry Research* **2019**, 58(34), 15381-15393

Table of Contents

List of Figures

List of Tables

Chapter 1. Introduction

Portions of this chapter are adapted from the following published articles:

1. **Verma, A.**, Kore, R., Corbin, D.R., & Shiflett, M.B., Metal Recovery Using Oxalate Chemistry: A Technical Review. *Industrial & Engineering Chemistry Research* **2019**, 58(34), 15381-15393
2. **Verma, A.**, Corbin, D.R., & Shiflett, M.B., Extraction of Aluminum and Iron from Bauxite: A Unique Closed-Loop Ore Refining Process utilizing Oxalate Chemistry. *AIChE Journal* **2021**, (*in press)*

Chapter 1

"We do not inherit the earth from our ancestors;
we borrow it from our children"
- Wendell Berry in "Life is a Miracle"

Energy-efficient metal recovery and separation processes from a mixture of valuable metal are vital to the metallurgy and recycling industries. The oxalate process has great potential to replace many of the existing metal recovery processes that use inorganic acids such as sulfuric, hydrochloric, and nitric acid. In this chapter, the importance of oxalate chemistry and its use in four major metal recovery applications is discussed, namely, spent lithium-ion batteries (LIBs), spent catalysts, valuable ores, and contaminated and unwanted waste streams. The learnings from this chapter are critical in developing sustainable, green and closed-loop processes for recovery of critical metals like lithium and cobalt, from the cathode of LiBs and aluminum and iron, from bauxite by hydrometallurgical routes utilizing oxalate chemistry.

1.1. Oxalate Anion and Oxalic Acid: A Greener Source for Metal Extraction

The oxalate anion ($C_2O_4^{2-}$) is the conjugate base of oxalic acid ($H_2C_2O_4$), the simplest dicarboxylic acid. Oxalic acid is commercially available in dihydrate form. Scheele first synthesized oxalic acid in 1776 by oxidation of sugar with nitric acid. In 1824 oxalic acid was synthesized by Wöhler by the hydrolysis of cyanogen.[1,2] In nature, it is formed by an enzymatic pathway of hydrolysis of oxaloacetates in *Aspergillus niger*, fungi (genus *Aspergillium*), bacteria (*Acetobacter*), and mammals by carbohydrate metabolism via the tricarboxylic acid cycle.[3-5] The urine of humans and most mammals contains a small amount of oxalate, usually bound to calcium. An increase in the concentration of calcium oxalate content can lead to the formation of kidney stones. Industrially, it is typically used as a rust remover in metal treatment, a precipitant in rare

earth extraction processes, a mordant for printing, dyeing of cotton and wool, tanning and bleaching of leather, bleaching of pulpwood, and in the synthesis of esters and salts.[6-8]

1.1.1. Oxalate Chemistry

Depending on the pH, oxalic acid can exist in solution as several different species ($H_2C_2O_4$, $HC_2O_4^-$, $C_2O_4^{2-}$). The structure of the oxalate anion is shown in Figure 1. $H_2C_2O_4$ is the predominant species below pH 1.23, and $C_2O_4^{2-}$ is the dominant species at pH 4.19 or greater. The oxalic acid speciation curve is shown in Figure 2, which was created by performing the mole balance around the pKa values of oxalic acid. The oxalate ion (IUPAC: ethanedioate ion) is a bidentate anionic ligand that can donate two pairs of electrons to a metal ion. Also, this ligand is commonly known as a chelate because of its ability to attach to a metal cation in two places. There has been tremendous interest in the study of oxalates as a precipitant, chelate, and reducing agent.[2] Most of the simple oxalate compounds (like $FeC_2O_4 \cdot 2H_2O$) are insoluble in water, but with excess oxalate, the possibility of forming various oxalate complexes (i.e., $Fe(C_2O_4)_2^{2-}$) widens the application of oxalates as leaching agents. In metal complex ion, a metal center is present with a number of ligands attached via a coordinate bond providing a net cationic or anionic charge, whereas a compound is formed by two or more elements connected via a covalent or ionic bond. As a precipitating agent, oxalate has historically been used in rare earth extraction processes.[8,9] Oxalate/oxalic acid can also be used as a mild reducing agent with the following oxidation reaction[10]:

$$C_2O_4^{2-} \leftrightarrows 2CO_2 + 2e^- \quad E^\circ = 0.49\ V \tag{1.1}$$

This positive potential indicates the thermodynamic feasibility of this oxidation reaction and provides a possibility where it can potentially reduce a metal ion. Oxalate has been reported to

reduce Co^{3+} to Co^{2+} and Fe^{3+} to Fe^{2+}.[11-15] This reduction property can affect the leaching efficiency, particularly when solubility changes with the reduction of the metal. This kind of variation in solubility is seen commonly with the iron oxalate complexes where iron(III) oxalate is soluble, but iron(II) oxalate is insoluble.[13-15]

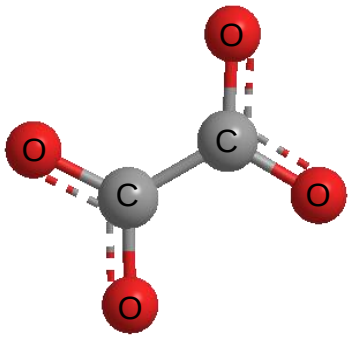

Figure 1. Structure of oxalate anion.

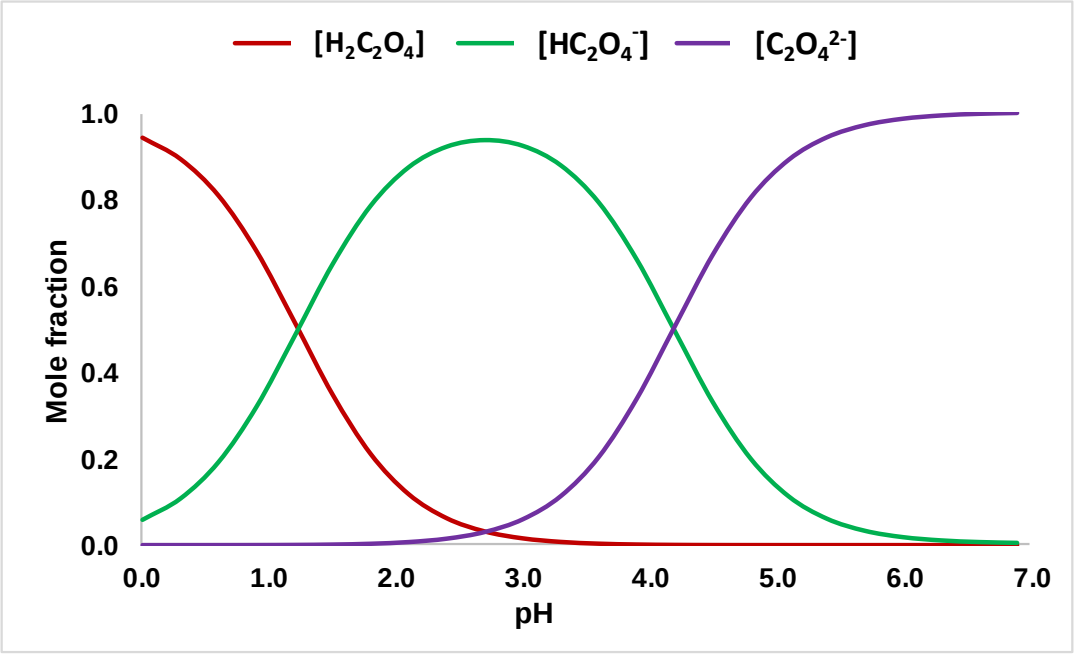

Figure 2. Oxalic acid speciation as a function of pH (pKa_1 = 1.23 and pKa_2 = 4.19) at room temperature.

1.1.2. Derivatives of Oxalic Acid

As discussed in the previous section, oxalic acid can exist in the solution as several different species ($H_2C_2O_4$, $HC_2O_4^-$, $C_2O_4^{2-}$) at different pH. Hence, in the presence of compounds like diammonium oxalate ($(NH_4)_2C_2O_4$), potassium oxalate ($K_2C_2O_4$), or sodium oxalate ($Na_2C_2O_4$) under specific conditions, binoxalate species ($HC_2O_4^-$ containing) like $NH_4HC_2O_4$, KHC_2O_4, and $NaHC_2O_4$ can be synthesized. The stoichiometric reaction for the synthesis of MHC_2O_4 where M^+ is either NH_4^+, Na^+, or K^+ is shown in Eq 1.2. For metal extraction and recovery applications using binoxalate species, the presence of the H^+ provides the required acidity for the initiation of leaching process. Corbin et al. used the synthesis process shown in Eq 1.2 and used $NH_4HC_2O_4$ as a digestion reagent for Fe and Ti recovery from ilmenite.[16] The use of $NH_4HC_2O_4$ as the digestion acid is a closed-loop process in which the acid can be efficiently recovered and recycled for additional digestions as shown in Figure 3.[16] This was the only recovery and recycling process known for oxalic acid before the work involving $H_2C_2O_4$ and KHC_2O_4 presented in later chapters. In terms of its aqueous solubility, $NH_4HC_2O_4$ is the most soluble acid after $H_2C_2O_4$, as shown in Table 1.[17] High aqueous solubility of acid is required to achieve a concentrated solution and process the maximum amount of source material in every cycle.

$$H_2C_2O_4(aq) + M_2C_2O_4(aq) \rightleftharpoons 2MHC_2O_4(aq) \quad (1.2)$$

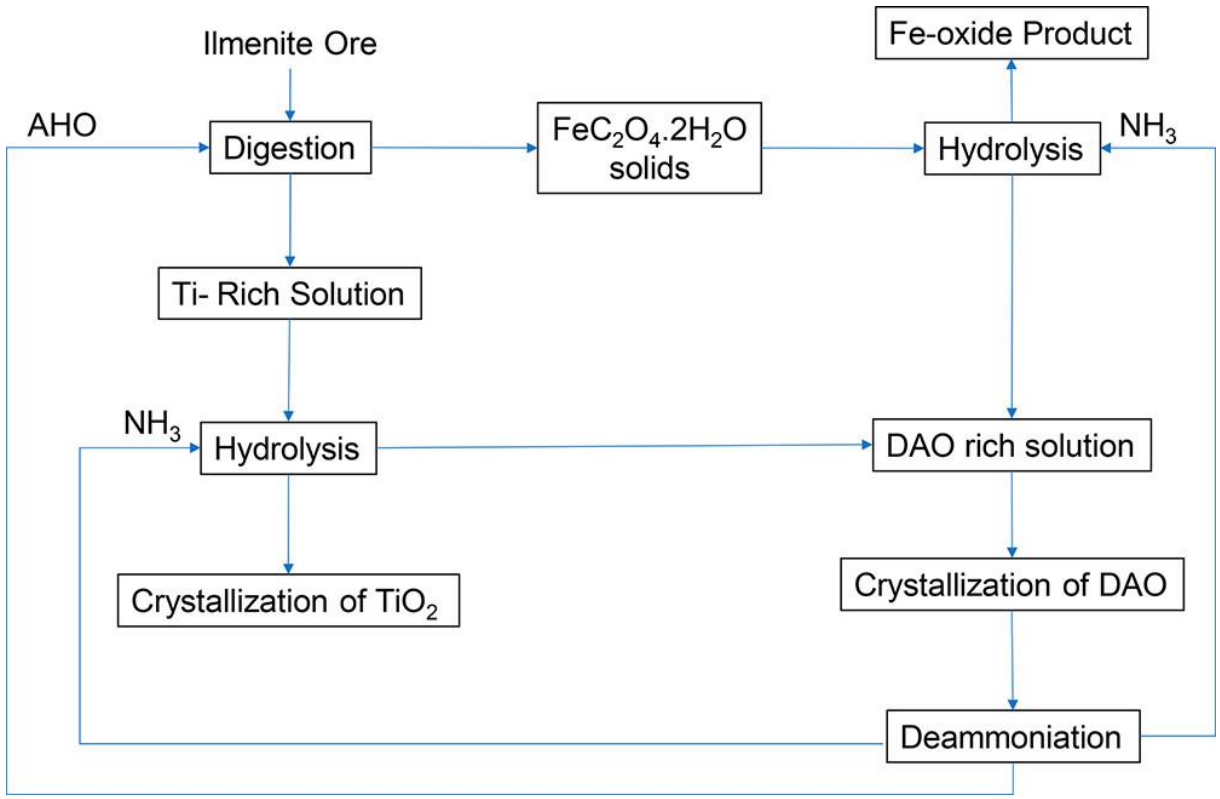

Figure 3. Simplified process flow diagram for ilmenite treatment with ammonium binoxalate.[16]

Table 1. Solubilities of common oxalate compounds relevant to this work.

Compound Formula	Aqueous solubility at 20 °C (g/100 ml)	Reference
$NH_4HC_2O_4 \cdot 0.5H_2O$	12.03 ± 0.42	Experimental
KHC_2O_4	5.73 ± 0.33	Experimental
$KHC_2O_4 \cdot H_2C_2O_4 \cdot 2H_2O$	2.97 ± 0.20	Experimental
$NaHC_2O_4 \cdot H_2O$	2.8 ± 0.22	Experimental
$K_2C_2O_4 \cdot H_2O$	36.4	CRC Handbook
$H_2C_2O_4 \cdot 2H_2O$	13.3	CRC Handbook
$(NH_4)_2C_2O_4 \cdot H_2O$	5.20	CRC Handbook
$Na_2C_2O_4$	3.61	CRC Handbook

1.1.3. Metal-Oxalate Chemistry: Solubility of Metal-Oxalates

Most metals form either simple oxalate compounds and/or oxalate complexes. Simple oxalate compounds can be either water soluble (like $Li_2C_2O_4$) or insoluble (like $FeC_2O_4 \cdot 2H_2O$) depending on the metal-ligand interactions, whereas all oxalate complexes are water soluble. The increase in the solubility of simple oxalate compounds in the presence of excess oxalate provides the basis for forming the oxalate complexes.[2,18] Most of the oxalate complexes formed by various metals are summarized in Table 2. Figure 4 summarizes the literature on the tendency of metals to form simple oxalate compounds and/or oxalate complexes. As might be expected all of the alkali metals (Group 1) are reported to form only soluble oxalate compounds. Many of the simple oxalate compounds are reported to be insoluble, with their solubilities ranging from 10^{-1} to 10^{-30} g/100 mL water.[2,19,20] Table 2 summarizes the possible metal oxalate complexes, and Table 3 classifies the insoluble and soluble oxalate compounds formed by most of the metals.

The variation in solubility of different metal oxalate species can be utilized effectively for the separation of metals.[21,22] Metal separation and recovery processes are commonly needed in any industry that has a mixture of metals as its primary material source. The metallurgy and recycling industries are two of the largest sectors that deal with mixed metal sources and are in need of sustainable, energy-efficient technologies for metal separation and recovery.[23-25] Oxalate, which can be derived from organic sources, has minimal to no environmental effects, is generally safer to work with than typical inorganic acids and may offer the opportunity for developing a more energy-efficient process. Oxalate has tremendous potential for creating an effective platform for future metals recovery and separation.

For the application of metal separation and recovery using oxalates, it is important to understand the qualitative metal oxalate solubility and possible complexes that can be formed.

Hence, for any metal, the use of Figure 4, Table 2, and Table 3 can help to determine the best choice of separation based on the solubility of the simple and complex oxalates. The uniqueness of using an oxalate for the separation of metals from a mixed metal source is due to the selectivity which it offers. In addition, understanding the behavior of metal mixtures in the presence of oxalate anions is necessary.

Table 2. Classification of metal-oxalate complexes.

No. of oxalate ligands attached	Formula of species	Metal Ion (M)
1	$M(C_2O_4)^+$	Al(III), Fe(III), Sb(III), Cr(III), Y(III), Yb(III), Ce(III), Mn(III), In(III), Nd(III), Tb(III)
1	$M(C_2O_4)^-$	Ag(I), TiO^+, Tl(I), MoO^{2+}
2	$M(C_2O_4)_2^-$	Al(III), Y(III), Yb(III), Cr(III), In(III), Rh(III), Mn(III), Sb(III), Ir(III), Fe(III), Ce(III), Po(III), Co(III), Nd(III), Pu(III), Ga(III), Gd(III)
2	$M(C_2O_4)_2^{2-}$	Be(II), Co(II), Pt(II), Mg(II), Ni(II), TiO^{2+}, Ca(II), Cu(II), VO^{2+}, Sr(II), Zn(II), OsO_2^{2+}, Ba(II), Cd(II), Mn(II), Pb(II), Fe(II)
3	$M(C_2O_4)_3^{2-}$	Ge(IV), Ir(IV), Pu(IV), Ru(IV), Th(IV)
3	$M(C_2O_4)_3^{3-}$	Al(III), Co(III), Ir(III), Sc(III), Ga(III), Ce(III), V(III), Y(III), Cr(III), Sb(III), Pu(III), Mn(III), Ru(III), Fe(III), Rh(III)
3	$M(C_2O_4)_3^{4-}$	Co(II), Zn(II), Ni(II)
4	$M(C_2O_4)_4^{4-}$	Sn(IV), Hf(IV), U(IV), Zr(IV), Th(IV), Pu(IV)
4	$M(C_2O_4)_4^{5-}$	Pu(III)

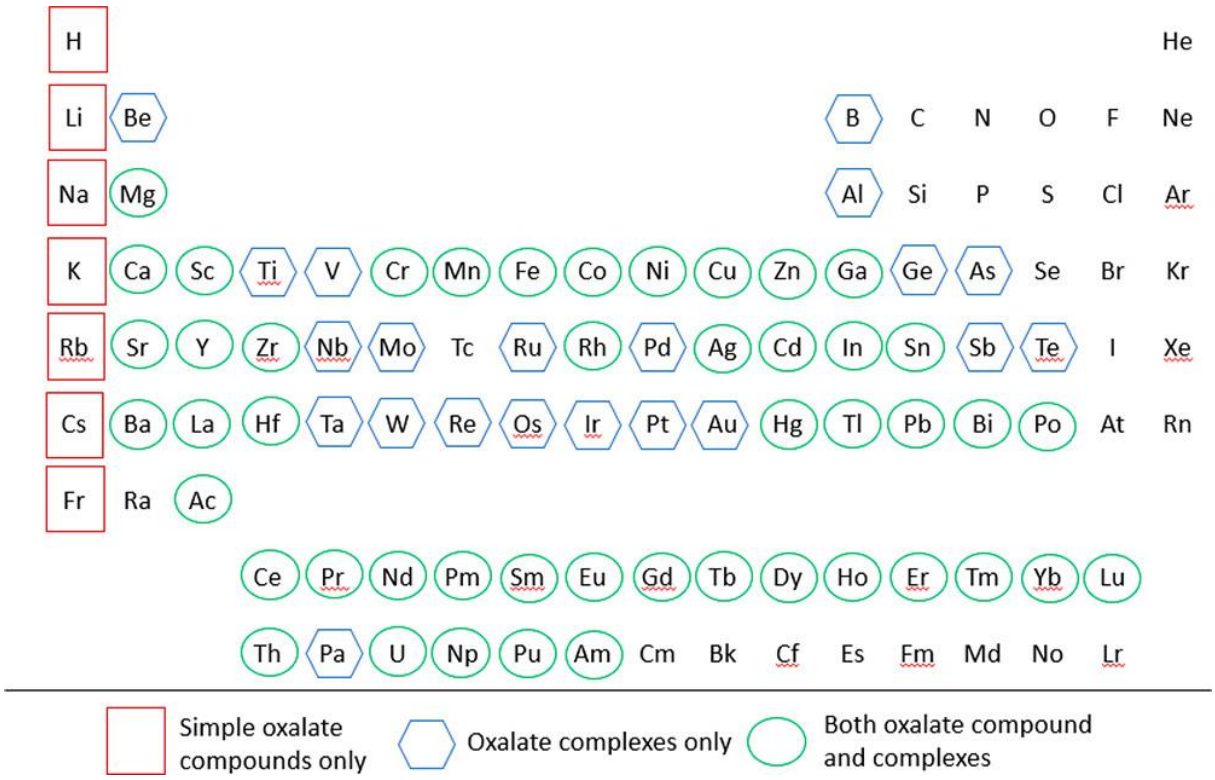

Figure 4. Tendency of metals to form simple oxalate compounds and/or complex oxalates.

Table 3. Qualitative solubility of common oxalate compounds in water at 20 °C

Formula	Qualitative solubility in water at 25 °C	Ref
$Ac_2(C_2O_4)_3 \cdot 10H_2O$	Insoluble	19
$Al_2(C_2O_4)_3 \cdot H_2O$		20
BaC_2O_4		26
$Bi_2(C_2O_4)_3$		20
CdC_2O_4		20
CaC_2O_4		20
$Ce(C_2O_4)_3 \cdot 9H_2O$		20
$CoC_2O_4 \cdot 2H_2O$		20
$CuC_2O_4 \cdot 0.5H_2O$		20
$FeC_2O_4 \cdot 2H_2O$		20
$La_2(C_2O_4)_3 \cdot xH_2O$		19
PbC_2O_4		20
MgC_2O_4		20
$MnC_2O_4 \cdot 2H_2O$		20
$Hg_2C_2O_4$		20
HgC_2O_4		20
$NiC_2O_4 \cdot 2H_2O$		20
$Ag_2C_2O_4$		20
$SrC_2O_4 \cdot 2H_2O$		20
SnC_2O_4		20
$Y_2(C_2O_4)_3 \cdot 9H_2O$		19
$ZnC_2O_4 \cdot 2H_2O$		20

Formula	Qualitative solubility in water at 20 °C	Ref
$BeC_2O_4 \cdot 3H_2O$	Soluble	20
$CrC_2O_4 \cdot H_2O$		20
$Fe_2(C_2O_4)_3$		20
$Li_2C_2O_4$		20
$K_2C_2O_4$		20
$Na_2C_2O_4$		20
$Ti_2(C_2O_4)_3 \cdot 10H_2O$		19
VOC_2O_4		27

1.2. Literature Review

The primary applications chosen to understand the application of oxalate chemistry include the recovery of metals from the cathode of spent lithium-ion batteries, spent catalysts, ores, and waste streams. The applications have been summarized in Figure 5.

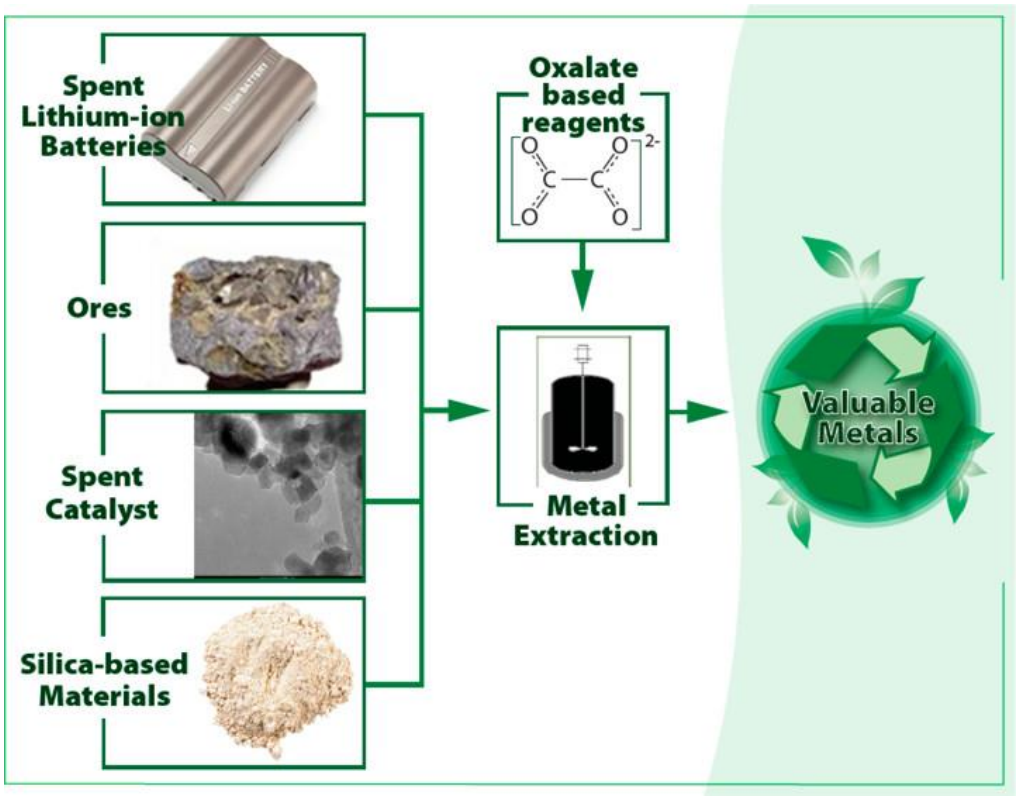

Figure 5. Applications of oxalate chemistry

1.2.1 Metal Recovery from the Spent LiBs

Lithium-ion batteries (LIBs) provide power for millions of people each day. Their usage has expanded from cellphones and laptops to powering hybrid and electric cars, homes, and electrical grids. The sustainability of the LIBs life cycle depends entirely on the recycling abilities for all the components of the battery. Metals like cobalt and nickel, which are found in the positive electrode (cathode during discharge) of LIBs, have significant economic value.[28] The positive electrode usually contains an oxide of Li along with another transition metal. Common electrode materials include lithium cobalt oxide ($LiCoO_2$ referred as LCO),[11,12,29-32] lithium nickel cobalt oxide ($LiNi_xCo_{1-x}O_2$),[33,34] lithium nickel manganese cobalt oxide ($LiNi_{0.33}Mn_{0.33}Co_{0.33}O_2$) (NMC),[34-36] and lithium iron phosphate ($LiFePO_4$).[34,37,38] To separate metals from the electrode, strong inorganic acids like H_2SO_4,[35,39] HCl,[36] and HNO_3[39,40] along with external reducing agents like H_2O_2 are used, but they have adverse environmental impacts because of emission of harmful pollutants like SO_x, Cl_2, and NO_x. Hence, replacing an inorganic acid with an organic acid minimizes this environmental impact, making the recycling process more sustainable. In this section, the separation of valuable metals from different electrode materials using oxalates will be discussed.

For the separation of Li and Co from LIB electrodes, $H_2C_2O_4$ functions as both a reducing and precipitating agent. Sohn et al.[30] compared the H_2SO_4/H_2O_2 leaching process with the $H_2C_2O_4$ leaching process. In the presence of 2 M H_2SO_4 with 10 vol % H_2O_2 at 75°C for 1.25 h, more than 99 wt% of Li and Co were leached into the aqueous phase. Using 3 M $H_2C_2O_4$ at 80 °C for 1.5 h as shown in, Table 4 more than 99 wt% of the Li leaches into the aqueous phase and 96 wt% of the Co precipitates out as $CoC_2O_4{\cdot}2H_2O$. In the H_2SO_4 process, Co needs to be recovered separately in the form of $Co(OH)_2$ by the addition of another precipitating agent. The requirement

of another precipitating agent for H_2SO_4 and other inorganic/organic acids provides a unique advantage for using oxalic acid/oxalates to recover metals efficiently from the electrode of LIBs. The concentration of $H_2C_2O_4$ can be used to adjust the solid-to-liquid ratio to further improve the separation and process economics. Theoretically, a stoichiometric molar ratio of 2 between $H_2C_2O_4$ and $LiCoO_2$ should be enough to ensure complete recovery and precipitation of Li and Co respectively according to the following reaction:[11,12,31]

$$4H_2C_2O_4(aq) + 2LiCoO_2(s) \leftrightarrows Li_2C_2O_4(aq) + 2CoC_2O_4 \cdot 2H_2O(s) + 2CO_2(aq) \qquad (1.3)$$

Zeng et al.[11] used a lower concentration of $H_2C_2O_4$ (1 M) with a longer reaction time (2.5 h), higher temperature (95 °C), higher mixing rate (400 rpm), and lower solid-to-liquid ratio (15 g/L). Under these conditions, 98 wt% of the Li leaches into the aqueous phase and 97 wt% of the Co precipitates out as $CoC_2O_4 \cdot 2H_2O$. The addition of H_2O_2 was found to be insignificant in the presence of excess $H_2C_2O_4$.[12] The effect of other leaching parameters such as solid-to-liquid ratio, temperature, and reaction time has also been studied.[12,30] Most experiments have been run over a temperature range of 80 to 100 °C, at atmospheric pressure. The optimum solid-to-liquid ratio for maximizing reaction rate depends on the acid concentration. For example, for an $H_2C_2O_4$ concentration of 1 M, the reaction rate begins to decrease above a solid-to-liquid ratio of 50 g/L.[12] Aaltonen et al.[32] compared $H_2C_2O_4$, H_2SO_4, HCl, and HNO_3 both in the presence and absence of H_2O_2 as a reducing agent (Table 5). The oxalic acid has both reducing and chelating properties, and the Co precipitates as $CoC_2O_4 \cdot 2H_2O$. The addition of H_2O_2 increases the leaching efficiency for most acids. In the case of $H_2C_2O_4$, the effect was less.

Zhang et al.[41] used $H_2C_2O_4$ to leach metals from $LiNi_xMn_yCo_zO_2$ (NMC) electrodes at the conditions shown in Table 4. Under these conditions, 84 wt% of the Li leached into the aqueous phase, and the transition metals (Ni, Mn, Co) formed oxalates that precipitated out of solution. The

unreacted material and oxalate precipitate was calcined with Li_2CO_3 at 900 °C for 14 h to regenerate the NMC electrode. In some studies, Ni from spent catalysts has been reported to form soluble oxalate complexes,[42,43] which complicates the separation of lithium from transition metals. Therefore, the pH of the $H_2C_2O_4$ leachate plays a significant role in the efficient separation and leaching of metals.

Another route is to perform the metal recovery using $H_2C_2O_4$ generated by the fungi, *A. niger*. The *A niger* has the potential to generate malic, gluconic, oxalic, and citric acid.[44] Hence, the culture conditions (direct or indirect) for the growth of fungi plays a major role in determining the acid, which would be generated in the maximum amount. Horeh et al.[44] found that $H_2C_2O_4$ was produced at higher concentration when the growth of fungi was done in the presence of cathodic material (direct process) whereas citric acid becomes the majorly produced acid in the absence of cathodic material (indirect process). The reason behind this observation could be the metals like Mn and Cu acting as an inhibitor for citric acid accumulation. Under the conditions of 30°C at 130 rpm for 30 days and on the addition of cathodic material from 3rd day, 100 wt% Li and 10 wt% Mn leached into the aqueous phase. 100 wt% Ni, Co and 90 wt% Mn precipitated in the form of their insoluble oxalate compounds.[44] Like chemical leaching, bioleaching also has an efficient separation but requires a longer reaction time, which is energy intensive.

Lithium iron phosphate batteries (LIPBs) contain a $LiFePO_4$ (LFP) electrode. LIPBs pose environmental challenges due to the hazardous electrolyte ($LiClO_4$ and ethylene carbonate-dimethyl carbonate) and phosphorous found in $LiFePO_4$, which causes eutrophication of natural water. For this reason, the Li and Fe should be recovered and the phosphorous treated in an environmentally-friendly process.[37] Treatment of the $LiFePO_4$ electrode with oxalate is beneficial because it can directly chelate and precipitate iron in the form of $FeC_2O_4{\cdot}2H_2O$. However, under

certain reaction conditions, the presence of an oxidizing agent can oxidize insoluble $FeC_2O_4 \cdot 2H_2O$ to soluble $Fe(C_2O_4)_3^{3-}$.[37,38,45,46] This reduces the advantage of the direct separation of Li from transition metals as previously reported for $LiCoO_2$. For $LiFePO_4$ electrodes, the Li goes into the aqueous phase along with the phosphorous in the form of phosphoric acid and other phosphate salts, which can be treated safely. The Li is separated using ionic sieves such as spinel type MnO_2 sieves, and $Ca(OH)_2$ is used to precipitate the PO_4^{3-} ion.[37] In some cases, $H_2C_2O_4$ was used to precipitate soluble Co from the aqueous phase when leaching with a combination of inorganic acids.[47-50] In most cases, the positive electrode material may contain additional metals in small concentrations as well as components from the current collector that require further separation.

Table 4. Summary of the digestion processes for metal recovery from LiBs positive electrode

Reaction Conditions				Metal recovery (wt%)	Ref
Electrode - Digestion agent	**Temperature (°C)**	**Solid-to-liquid ratio (g/L)**	**Reaction time**		
LCO – 4 M hydrochloric acid	80	20	2 h	Li, 97 % Co, 99 %	51
LCO – 4 M sulfuric acid, 10 vol% H_2O_2	85	100	2 h	Li, 96 % Co, 95 %	52
LCO - 3 M oxalic acid	80	50	1.5 h	Li, 99 % Co, 96 %	30
LCO - 1 M oxalic acid	95	15	2.5 h	Li, 98 % Co, 97 %	11
LCO - 1 M oxalic acid	80	50	2 h	Li, 96 %	12
LCO - 1 M oxalic acid	25	5	24 h	Li, 74 %	32
LCO - 1.25 M ascorbic acid	70	25	20 min	Li, 98.5 % Co, 94.8 %	53
LCO - 1.5 M succinic acid, 4 vol% H_2O_2	70	15	40 min	Li, 96 % Co, 99.5 %	54
LCO - 1.25 M citric acid, 1 vol% H_2O_2	90	15	0.5 h	Li, 100 % Co, 91 %	55
LCO - *Leptospirillum ferrooxidans*, and *S. thermosulfidooxidans*	42	15	7 h	Li, 91.4 % Co, 94.2 %	56
NMC - *A. niger*	30	10	30 days	Li, 95 % Co, 45 % Ni, 38 % Mn, 70 %	44
NMC – 0.6 M oxalic acid	75	20	2 h	Li, 84 % Ni, Mn, Co, 98 %	41
LFP – 0.3 M oxalic acid	80	60	1 h	Li, 98 % Fe, 92 %	37

Table 5. Summary of experiments performed by Aaltonen et al. on $LiCoO_2$.[32]

Acid Concentration	Metal Recovery (wt%)	
	No H2O2	1 vol% H2O2
2 M citric acid	Li – 62 %, Co – 41 %	Li – 65 %, Co – 46 %
1 M oxalic acid	Li – 74 %, Co in precipitate	Li – 79 %, Co in precipitate
2 M sulfuric acid	Li – 88 %, Co – 79 %	Li – 92 %, Co – 85 %
4 M hydrochloric acid	Li – 91 %, Co – 85 %	Li – 98 %, Co – 92 %
1 M nitric acid	Li – 85 %, Co – 75 %	Li – 90 %, Co – 83 %

Note: All experiments were carried out with a slurry density of 5 wt% at 25 °C for 24 h

1.2.2. Recovery of Metals from Spent Catalysts

Spent catalysts are another secondary source of valuable metals that can be recovered using appropriate technology. In the petroleum refining industry, hydrodesulfurization (HDS) catalysts are widely used to remove sulfur. HDS catalysts commonly consist of Mo, Ni, Co, and Al.[42,43,57,58] Pt- and V-based catalysts are also valuable, and the metals need to be recovered and recycled.[59-61] The metals in these catalysts can be recovered by treatment with inorganic acids such as H_2SO_4 and HNO_3.[62,63] For the treatment of spent catalysts, the focus has always been to leach these metals into the aqueous phase and then separate the metals from the deactivated catalyst. Oxalates, which have a high tendency to form insoluble metal oxalates in water, can precipitate transition metals on the catalyst support, which can negatively affect metal recovery. However, oxalates have shown some potential for effective leaching under appropriate conditions. This section summarizes the reaction conditions that can provide efficient leaching of the metals from spent catalysts using oxalates, as summarized in Table 6.

Recovery of Ni and Mo using $H_2C_2O_4$ from spent catalysts has been demonstrated by several researchers.[42,43,64,65] Ni tends to form both oxalate compounds and oxalate complexes,

whereas Mo forms only oxalate complexes (Figure 4). Ni leaching is dependent on the pH and oxalate concentration but is limited by the low solubility of the $NiC_2O_4{\cdot}2H_2O$ compound. The Mo leaching efficiency was more than 90 wt% in two different studies with oxalic acid concentrations of 1 M.[42,65] However, Ni has been reported to have varying leaching efficiencies of 86 wt% and 37 wt% with 1 M $H_2C_2O_4$.[42,65] The presence of other metals such as V and Al, which can form complexes with oxalate, can also affect the solubility by consuming the available oxalate ions. The oxalate availability in an aqueous environment and in the presence of insoluble $NiC_2O_4{\cdot}2H_2O$ is demonstrated by the following reaction:

$$Ni^{2+} + 3C_2O_4^{2-} \leftrightarrows NiC_2O_4{\cdot}2H_2O(s) + 2C_2O_4^{2-} \leftrightarrows Ni(C_2O_4)_2^{2-} + C_2O_4^{2-} \leftrightarrows Ni(C_2O_4)_3^{4-} \quad (1.4)$$

Depending on the conditions, the addition of H_2O_2, which has been reported to act as either an oxidizing or reducing agent,[66,67] did not seem to have a significant effect on either Mo or Ni leaching efficiency. Szymczycha-Madeja[43] considered the effect of adding H_2O_2 in the oxidation of low valence metal sulfides (e.g., hydrodesulphurization (HDS) catalysts) to high valence metal oxides that can complex with oxalate. It should be noted that some reports have achieved 90 wt% leaching efficiency of Mo even without the addition of H_2O_2.[42,65]

Vanadium is another major metal that can be found in many spent catalysts[43,45,60,61,65,68] and is reported to form only soluble oxalates, as shown in Figure 4, Table 2, and Table 3. Mazurek[60] and Erust et al.[61] attempted to recover V from a spent catalyst using $H_2C_2O_4$. The VOC_2O_4 is formed, which is soluble in the aqueous phase. Mazurek also demonstrated the step-wise separation of V from a mixture containing Fe. This separation was achieved using both Fe precipitation and ion-exchange techniques. Wu et al.[45] reported leaching of V and Fe from denitrification catalysts. The V and Fe exist as VO^{2+} and Fe^{2+} after leaching in the aqueous phase. The VOC_2O_4 is a soluble species and was expected to be present in the aqueous phase after

leaching. The Fe was proposed to exist in the form of $Fe(C_2O_4)_2^{2-}$, also a soluble species. This hypothesis was confirmed by quantitatively measuring the moles of CO_2 released during the redox reaction. Lee et al.[68] studied the regeneration of desulfurization catalysts using 0.9 M $H_2C_2O_4$ solution to leach the V. This vanadium-rich liquor was used to synthesize dehydrogenation catalysts on silica supports, which closes the recycling loop making this a sustainable process.

Ni, Mo and V recovery from spent catalysts through bioleaching route where $H_2C_2O_4$ is generated by *A. niger*, fungi have also been demonstrated.[69,70] Similar to the leaching of metals from cathodic material, direct leaching was found to be an optimum method that led to maximum production of $H_2C_2O_4$ and higher metal extraction than indirect leaching.[69,70] Aung and Ting[69] suggested that the fungus participates in the leaching process through bioaccumulation of generated $H_2C_2O_4$, which shifts the equilibrium towards consumption of additional acid. Other than the culture conditions, pulp density (solid-to-liquid ratio) also plays a major role in the growth of fungi. Higher pulp density (more than 1 g/L) affects the leaching efficiency because of the inability of the fungus to grow well under a high concentration of heavy metals.[69,70] Optimum conditions for metal extractions from spent catalysts via bioleaching from spent refinery catalysts are reported in Table 6. Reaction and fungal culture conditions play a major role in the amount of oxalic acid generated, and that has a direct impact on the leaching efficiency. Apart from longer reaction time, another difference between bioleaching and chemical leaching is the lower solid-to-liquid ratio (1 g/L to 10 g/L (average)). This means that to extract metals from 10 g of spent catalyst, ten times more reaction volume is required in bioleaching, which will directly impact the process economics.

Table 6. Examples of Metal Recovery from Spent Catalysts.

Source	Reaction conditions	Leaching efficiency (wt%)	Ref
Spent HDS catalyst (Ni-Mo/Al_2O_3)	1 M oxalic acid at 40 °C with 300 rpm stirring for 3 h	92 % Mo, 86 % Ni, 30 % Al and 73 % P	42
	0.5 M oxalic acid and 0.66 M H_2O_2 at 70 °C for 3 h	63 % Mo, 80 % V, 66 % Ni and 58 % Al	43
Spent refinery processing catalyst	Two-step bioleaching (*A. niger*) at 30 °C with 1 g/L S/L ratio for 60 d	82.3 % Mo, 58.2 % Ni and 54.5 % Al,	70
Spent fluid catalytic cracking catalyst	Two-step bioleaching (*A. niger*) at 30 °C with 1 g/L S/L ratio for 46 d	37% V, 9 % Ni and 30 % Al	69
Spent hydrotreating catalyst	0.45 M oxalic acid and 1.67 M H_2O_2 at 100 °C for 1 h	69.87 % Mo and 24.63 % Ni	64
	9 M H_2SO_4 at 90 °C for 2 h	99 % Mo and 98 % Ni	71
Spent residue hydroprocessing catalyst	1.12 M oxalic acid at 50 °C with a S/L ratio of 1:40 for 6 h	97 % Mo and V, 37 % Ni	65
Pt on alumina – Spent reforming catalyst	0.3 M oxalic acid at 80 °C with 10 g/L S/L ratio for 24 h	90 % Pt and almost 100 % Al	59
Spent desulfurization catalyst (V contaminant)	0.9 M oxalic acid at 100 °C for 1 h	More than 90 % V recovered	68
Spent vanadium catalyst	0.25 M oxalic acid at 50 °C with 40 g/L S/L ratio for 4 h	91 % V, 92 % K and 63 % Fe	60
	0.5 M oxalic acid and 2 M H_2O_2 at 50 °C with 20 g/L S/L ratio for 2 h	68 % V	61
Spent SCR denitrification catalyst	1 M oxalic acid at 90 °C for 3 h	84 % V and 96 % Fe	45

1.2.3. Extraction of Metals from Ores

Ores are a naturally occurring source of metals usually in the form of oxides or hydroxides. Ores typically contain multiple important metals that need to be both recovered and more importantly separated. Similar to the spent catalyst recovery processes, inorganic acids are used to leach the metals into the aqueous phase.[72-75] However, because of the environmental hazards associated with the emission of SO_x and NO_x gases from the use of inorganic acids, research using environmently-friendly reagents like organic acids has increased. In this section, metal recovery from ores using oxalates is discussed.

Ilmenite is an iron titanate ($FeTiO_3$) low-grade ore mainly used for the production of TiO_2. The TiO_2 is used as a white pigment in paints, plastics and paper applications. Separation of Fe from Ti is the key step and Ti forms a soluble oxalate complex, whereas Fe^{2+} forms an insoluble oxalate compound. Ilmenite can also contain Fe and Ti impurities such as magnetite, hematite, and rutile. Corbin et al.[16] digested ilmenite using $NH_4HC_2O_4$ (AHO) under different reaction atmospheres as shown in Figure 6. The titanium oxalate was soluble and the $FeC_2O_4{\cdot}2H_2O$ was insoluble and formed a precipitate providing an effective and simple separation. In the presence of an inert atmosphere such as N_2, He, or Ar, Fe^{2+} will not oxidize and precipitate in the form of $FeC_2O_4{\cdot}2H_2O$; however, in an oxidative atmosphere, Fe^{2+} will oxidize to Fe^{3+} that forms a soluble oxalate complex. This oxidative digestion is particularly useful for separation of impurities and unwanted materials present in the ore. Usually, oxidative digestion is followed by reduction step in an inert atmosphere, and a reducing agent like metallic Fe, Zn, or Al is added to reduce all the available Fe^{3+} into Fe^{2+} that can precipitate out of solution. The reaction atmosphere is not often considered for improving the leaching efficiency.

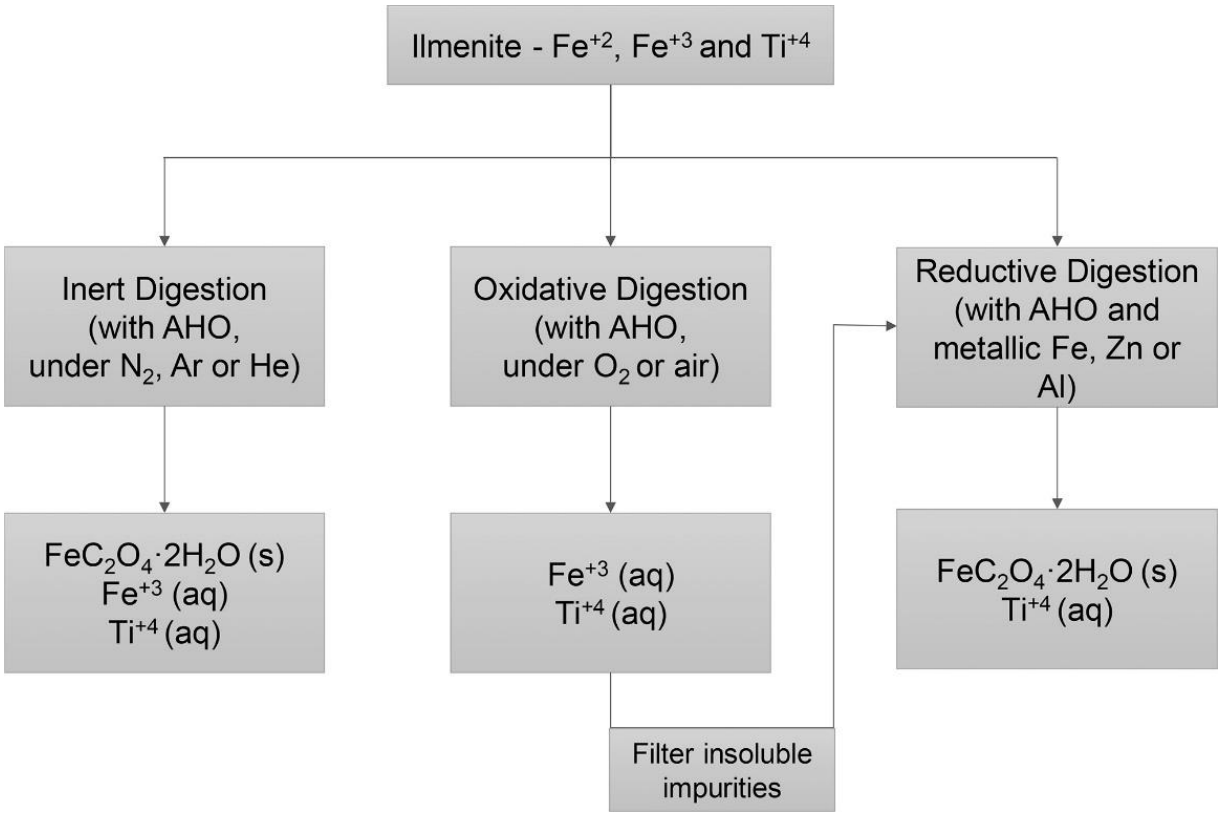

Figure 6. Summary of different digestion experiments for ilmenite.
Adapted from Corbin et al.[16]

Corbin et al.[16] developed a process to leach Ti from ilmenite and tried to completely recover the oxalate reagent as shown in the process flow diagram in Figure 6. In this case, AHO was used for leaching Ti and Fe from ilmenite. The titanium oxalate complex goes into solution and the $FeC_2O_4 \cdot 2H_2O$ species forms a precipitate, which enables the separation. The NH_3 or NH_4OH is used to precipitate the Ti as $Ti(OH)_4$ that can be converted into TiO_2. The $FeC_2O_4 \cdot 2H_2O$ precipitate is reacted with NH_3 or NH_4OH to form $(NH_4)_2C_2O_4$ (DAO) and $Fe(OH)_2$ that can be converted into an FeO co-product. DAO is also produced during the Ti precipitation step and combined with DAO from the Fe precipitation step. The DAO is crystallized and undergoes a deammoniation step to recover AHO and NH_3, which are both recycled as shown in Figure 3.[16] Another closed-loop process was reported by Corbin et al.[76] using trimethylammonium hydrogen oxalate ($(TMAH)HC_2O_4$). This closed-loop process is similar to the one with AHO, and its process flow

diagram is shown in Figure 7. Recovery of the oxalate provides a significant advantage for the overall process economics and reduces waste streams.

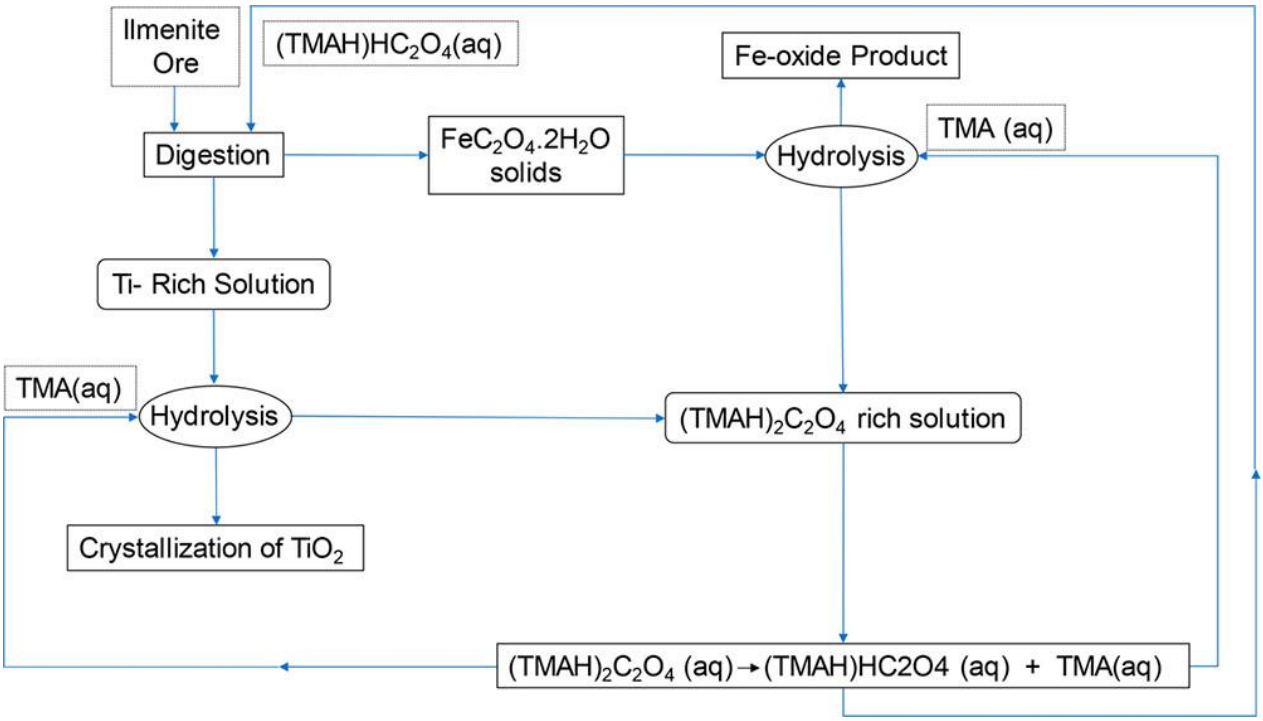

Figure 7. Simplified process flow diagram for ilmenite treatment with $(TMAH)HC_2O_4$. Adapted from Corbin et al.[76]

Another iron-based ore is laterite. Laterites are a source of Fe and Ni present in the form of their oxides. As discussed in Section 1.1.3, Ni forms both oxalate compounds and oxalate complexes, which can limit the ability to separate it using oxalates. Similarly, Fe can also form both soluble iron(III) oxalate complexes and insoluble iron(II) oxalate. Tzeferis and Agatzini-Leonardou,[77] Kursunoglu and Kaya,[78] and Sahu et al.[79] have used $H_2C_2O_4$ to leach metals from laterites collected from different parts of the world. Tzeferis and Agatzini-Leonardou tested the ability of $H_2C_2O_4$ to solubilize Ni and Fe from Greek laterite ores. Under their reaction conditions, Ni forms an insoluble $NiC_2O_4 \cdot 2H_2O$, and 40.3 wt% of the Fe leached into the aqueous phase. The

$H_2C_2O_4$ reduced Fe^{3+} to Fe^{2+}, and it was claimed that iron(II) oxalate was soluble in the aqueous phase. However, this contradicts the solubility reported in the previous studies.[20,80] Iron(III) oxalate is the soluble species and iron(II) oxalate is insoluble. A possible explanation is the formation of an oxalate complex of Fe^{2+} in an aqueous environment, as shown in Eq. 1.5:

$$Fe^{2+} + 3C_2O_4^{2-} \leftrightarrows FeC_2O_4 \cdot 2H_2O(s) + 2C_2O_4^{2-} \leftrightarrows Fe(C_2O_4)_2^{2-} + C_2O_4^{2-} \leftrightarrows Fe(C_2O_4)_3^{4-} \quad (1.5)$$

Kursunoglu and Kaya[78] reported 52 wt% leaching of Fe from Caldag laterite ore. In this example, the oxidation state of Fe in leachate was not determined. If reduction of Fe^{3+} was achieved, it would probably form additional complexes under the specified reaction conditions. Another possibility could be the incomplete reduction of Fe^{3+} using $H_2C_2O_4$ that could lead to a mixture of iron(III) oxalate and iron(II) oxalate. Iron(III) oxalate will remain in the aqueous phase and can be detected using atomic absorption spectroscopy (AAS) or inductively coupled plasma – atomic emission spectroscopy (ICP-AES). Another important difference between the two processes was the reaction temperature and time. Greek laterite required 20 days at 50 °C and Caldag laterite required 6 h at 90 °C to achieve equal weight percentages of iron dissolution. Although the reaction temperature is higher, the geographical location where ore is mined plays a significant role in the leaching efficiency. In general, the more an ore is weathered (i.e., oxidized), the longer the reaction time. Sahu et al.[79] worked with Sukinda laterite and found that 23 wt% Ni was leached into the aqueous phase under the conditions reported in Table 7. Bioleaching of Ni from Sukinda laterite using *Aspergillus humicola* SKP102 was demonstrated by Ghosh and Paul.[81] In their work, 54 % Ni was leached in direct one-step leaching (ore and fungus together from starting), whereas indirect leaching (fungi was initially incubated for 8 days, followed by addition of ore) led to 65 % Ni leaching into the aqueous phase. Higher leaching efficiency for indirect leaching was attributed to the reduced interaction between fungi and heavy metals.[81] This trend in the result is contradictory

to the observations by Aung and Ting for Ni leaching from spent catalysts. Possibly both factors: the amount of $H_2C_2O_4$ generated and interaction between heavy metals and fungi plays a determining role in extraction of metals.

Das et al.[82] and Sahoo et al.[83] attempted to recover Mn from low-grade manganese ores. Manganese also forms both oxalate compounds and complexes similar to Fe and Ni. Both ores were extracted from the Keonjhar region in Orissa, India. In these ores, Mn is present in the form of MnO_2. Das et al.[82] recovered 66 wt% of Mn in 6 days by using a 2 M $H_2C_2O_4$ concentration at a very dilute solid-to-liquid ratio (0.02 kg/m^3) and 25 °C. The Mn^{4+} was reduced to Mn^{2+} and formed an insoluble oxalate compound. Significant improvement in the leaching efficiency was demonstrated by Sahoo et al.[83] by using a mixture of H_2SO_4 and $H_2C_2O_4$ as the leaching agent. The mixed acid recovered almost 99 wt% of the Mn from these ores. The $NiC_2O_4{\cdot}2H_2O$ formed a precipitate layer on the ore and the reaction was proposed to follow the diffusion through product layer model. Azizi et al.[84] studied the kinetics and developed models for optimizing the leaching process for low-grade manganese ores. A series of experiments were carried out to determine the optimum operating conditions for Mn and Fe recovery as a function of the amount of H_2SO_4, the amount of $H_2C_2O_4$, temperature, and time. Under optimum conditions, 93.4 wt% Mn and 15.8 wt% Fe can be leached using 0.7 M H_2SO_4 and 0.5 M $H_2C_2O_4$ for 1 h at 63 °C. Hazek et al.[85] performed a similar study as Sahoo et al.[83] on a polymetallic Mn ore and leached 98 wt% Mn, 94 wt% Zn, and 92 wt% Cu using the optimum conditions for H_2SO_4 leaching with $H_2C_2O_4$ as a reductant. These studies prove that the addition of H_2SO_4 can improve the leaching efficiency for Mn.

Scheelite is a calcium tungsten ore with the chemical formula $CaWO_4$. In the work by Kalpakli et al.,[86] synthetically prepared $CaWO_4$ was dissolved in $H_2C_2O_4$. This dissolution took

place in two steps. In the first step, a calcium aqua oxalate tungstate intermediate ($Ca[WO_3(C_2O_4)H_2O]$) was formed. In the second step, a water-soluble hydrogen aqua oxalate tungstate ($H_2[WO_3(C_2O_4)H_2O]$) and insoluble $CaC_2O_4{\cdot}H_2O$ were formed. The proposed mechanism was based on a theoretical equilibrium calculation. In the method by Osthoff,[87] scheelite ore was first treated with an aqueous solution of $H_2C_2O_4$ that led to the formation of soluble tungstic acid (H_2WO_4) and insoluble $CaC_2O_4{\cdot}H_2O$. Ammonium hydroxide was added to precipitate tungsten in the form of ammonium paratungstate. Davey[88] found another process to extract tungsten from scheelite using HCl and $H_2C_2O_4$ where W goes into the solution and via hydrolysis is precipitated. According to Figure 4, W forms only oxalate complexes, which leads to efficient leaching.

Table 7. Examples of metal extraction from ores using oxalic acid.

Source	Reaction conditions	Recovery efficiency (wt%)	Ref
Ilmenite	6.6 M of trimethylammonium hydrogen oxalate at 60 °C for 120 h	Fe/Ti ratio of 0.048 compared to 0.404 of starting leachate	76
	7.16 M ammonium hydrogen oxalate at 100 °C for 72 h	100 % Ti in leachate	16
Greek laterite	0.5 M oxalic acid at 50 °C for 20 days	40.30 % Fe and 0.71 % Ni in leachate	77
Caldag laterite	0.5 M oxalic acid at 90 °C for 6 h	52 % Fe and 20 % Ni and Co in leachate	78
Sukinda laterite	1 M oxalic acid at 90 °C for 40 h	23 % Ni in leachate	79
	Direct bioleaching (*A. humicola*) at 30 °C for 30 days with 2 g/L solid-to-liquid ratio	54 % Ni in leachate	81
	Indirect bioleaching (*A. humicola*) at 30 °C for 30 days (8 days incubation) with 2 g/L solid-to-liquid ratio	65 % Ni in leachate	81
Low-grade Mn ore	2 M oxalic acid at 25 °C for 6 days with 2 g/L solid-to-liquid ratio	66 % Mn in leachate	82
	0.6 M sulfuric acid with 0.3 M oxalic acid at 95 °C for 3 h	99.4 % Mn, 24.3 % Fe and 44.6 % Al	83
Polymetallic Mn ore	0.5 M sulfuric acid with 0.24 M oxalic acid at 85 °C for 1.75 h	98 % Mn, 94 % Zn and 92 % Cu	85
Scheelite	1 M oxalic acid at 55 °C for 3 h	99 % W in leachate	86

1.2.4. Recovery of Metals from Waste Streams

In this section, the recovery of precious metals from different kinds of waste streams will be discussed. These waste streams contain important metals such as Co, Ni, and Fe.

Alumina extraction from bauxite produces a waste commonly referred to as "red mud" that contains primarily Fe_2O_3. Yang et al.[89] proposed using $H_2C_2O_4$ to leach Fe^{3+} in the form of $Fe(C_2O_4)_3^{3-}$ into the aqueous phase. To separate the Fe^{3+} ions from the leachate, metallic Fe was added to reduce and precipitate $FeC_2O_4{\cdot}2H_2O$. The observation of $H_2C_2O_4$ acting only as a chelating agent and not as a reducing agent contradicts other reports in the literature.[13,15,90] The occurrence of a combined reduction and complexation to form a soluble species such as $Fe(C_2O_4)_2^{2-}$ is another possibility that should be studied. Vakilchap et al.[91] studied the leaching of red mud using organic acids excreted by *A. niger* and found out that under direct one-step leaching process, 69.8 % Al, 60 % Ti and 25.4 % Fe were leached into the aqueous phase. In the case of bioleaching of red mud, the combined effect of all the acids excreted over the whole incubation period (citric, oxalic, gluconic) plays a major role in metal leaching, although the formation of insoluble $FeC_2O_4{\cdot}2H_2O$ could be the reason behind the low leaching efficiency observed for Fe.[91]

Electroless plating is a non-galvanic process where a metal is deposited on a surface without the use of external electrical power and generates an aqueous waste containing metals. Gyliene et al.[92,93] demonstrated the recovery of Ni, Cu, and Co from plating solutions using oxalic acid under specific pH conditions to recover more than 90 wt% of the metals in the form of insoluble metal oxalates (Table 8). It is important to understand the role that pH can play in the solubility of any metal oxalate species. Pickling liquor is another waste generated by the plating industry that contains mainly Zn. Oxalate can be effective for the recovery of Zn from pickling liquor waste because of the formation of insoluble ZnC_2O_4 that can be easily separated.[94]

Chromate copper arsenate (CCA) treatment is still used to preserve timber and extend the life of wood-based products. There is a threat to the environment due to toxic As and Cr leaching from the wood. In addition, burning the wood releases toxic smoke. Yu et al.[95] demonstrated the possibility of using $H_2C_2O_4$ for the extraction of As and Cr, but found it to be ineffective for Cu. The As and Cr have been reported to form soluble oxalate species confirming the effectiveness of $H_2C_2O_4$ in the extraction process.[20,96,97] To effectively extract all three metals from wood, a two-step acid treatment using $H_2C_2O_4$ and CH_3COOH was attempted by Shupe et al.[98] However, even in this process, Cu extraction was limited by the formation of insoluble CuC_2O_4, which led to only 34 wt% recovery (Table 8).

Table 8. Examples of extraction of metals from waste streams.

Source	Reaction conditions	Recovery efficiency (wt%)	Ref
Red mud	1:1 ratio of oxalic acid with red mud was used at 95 °C for 1.5 h	94.15 % Fe and 21.12 % Al	89
	A. niger at 30 °C for 30 days with 2 g/L solid-to-liquid ratio	69.8 % Al, 60 % Ti and 25.4 % Fe	91
	3 M H_2SO_4 at 60 °C with 5 g/L solid-to-liquid ratio for 4 h	37 % Al, 64.5 % Ti and 46 % Fe	99
Spent electroless plating solution	0.3 M oxalic acid at 25 °C at pH 9	99 % Ni and Co, 90 % Cu	92
Galvanic solution	Selective precipitation at different pH using oxalic acid	> 95 % recovery of Cu, Ni, Co, Sn	93
CCA – treated pinewood	20 mL mixture of acetic and oxalic acid with 1 g of wood at 160 °C for 0.5 h	98 % As, 99 % Cr and 34 % Cu in leachate	98
Zinc pickling solution	Tributyl phosphate for leaching and 1 M oxalic acid for precipitation at 25 °C	95 % Zn	94

1.2.5. Removal of Iron Oxides from Silica-based Materials

The dissolution of iron oxides using $H_2C_2O_4$ is an important process in several fields, such as the removal of oxides from metal surfaces and the beneficiation of minerals such as pottery stone and clays. Clays like kaolin are usually contaminated with Fe^{2+} and Fe^{3+} ions that directly affect the whiteness of the ceramics formed from them.[100,101] Inorganic acids are considered to be unsuitable for the removal of metals because of additional contamination and environmental pollution associated with sulfate and chloride ions.[102,103] Dissolution of iron oxides using $H_2C_2O_4$ has been extensively studied by many researchers. In this section, a few references are provided for understanding the dissolution mechanism, and applications will also be discussed. Baumgratner et al.,[104] Panias et al.,[13,14] and Taxiarchou et al.[15] have studied the dissolution of pure iron oxides and established a mechanism that has been verified by Veglio et al.,[102,103] Lee et al.[90,105,106], and Ubaldini et al.[107] Panias et al.[13] described a three-step dissolution mechanism: (1) adsorption of organic ligands on the iron oxide surface, (2) non-reductive dissolution, and (3) reductive dissolution. Non-reductive dissolution is a simple desorption process that can remove only the most reactive sites from the oxide surface. The reductive dissolution involves the reduction of Fe^{3+} to Fe^{2+} that involves a slow induction period followed by a fast dissolution via an autocatalytic mechanism. Factors such as pH of the initial solution, temperature, and the presence of UV light can affect the dissolution. Panias et al.[14] also studied the autocatalytic effect exclusively for hematite dissolution in oxalic acid by the addition of Fe^{2+} at the beginning of the reaction. This reduced the induction time for reductive dissolution and increased the rate of the autocatalytic reaction. Taxiarchou et al.[15] carried out the hematite dissolution in an inert atmosphere under visible light and found that the dissolution proceeded much faster. In the absence of visible light under an oxidizing atmosphere, the induction time was much longer, and the photocatalytic

reduction decreased. Another important point to note here is that although $FeC_2O_4 \cdot 2H_2O$ is an insoluble compound, its solubility increases at higher pH forming $Fe(C_2O_4)_2^{2-}$, and $Fe(C_2O_4)_3^{3-}$.

Vegliò et al.[102,103] studied the Fe removal process from quartz, an essential raw material for ceramics, paper making, and high-value products such as optical fibers. For optical fiber production, the Fe content in the quartz should be less than 10 g/tonne; however, the Fe content is normally around 77 g/tonne in regular quartz. Quartz from two different sources was leached with oxalic acid and a mixture of $H_2C_2O_4$ and H_2SO_4 as shown in Table 9.[102,103] Using only $H_2C_2O_4$, roughly 98-100 wt% of the Fe was extracted, whereas in the presence of the $H_2C_2O_4$ and H_2SO_4 mixture, only 35-45 wt% of the Fe could be extracted. This extreme difference in the Fe recovery was due to the presence of 52 wt% iron in the micaceous fraction for the quartz used in the combined acid process. The Fe content from the micaceous fraction is extremely difficult to remove. Additionally, in the $H_2C_2O_4$ experiment, the ore was ground to an average particle size of about 20 µm that provides additional surface area and improves the dissolution process. This comparison also emphasizes the importance of geographical location for minerals used in the metal leaching process, as discussed in Section 2.4.

Table 9. Summary of iron oxide dissolution from quartz using oxalates.

Source	Reaction Conditions	Fe extraction (wt%)	Ref
Quartz	3 g/L oxalic acid with 10 % solid-to-liquid ratio at 80 °C for 3 h	98-100 %	103
	2 kg/t sulfuric acid and 3 kg/t oxalic acid at 90 °C for 5 h	35-45 %	102

Lee et al. studied iron oxide removal from clay[90] and dissolution of iron oxide[106] using $H_2C_2O_4$. The non-hematite iron oxides dissolved faster than the hematite, confirming the mechanism reported earlier. In this study, grinding was performed to decrease the average particle diameter to 150 µm. Although the particle size was larger than the previous study with quartz,[103]

higher $H_2C_2O_4$ concentrations of 0.19 M at 100 °C for 2 h led to 90 wt% Fe removal from clay. In this case, the pH of the solution was reported to be 1.23. As discussed previously, the dissolution of iron oxide is controlled primarily by pH, temperature, and oxalate concentration. Lee et al.[90] used NH_4OH to control the pH in the range of 2.5-3.0 for optimizing the reaction rate for hematite and iron oxide rust. Iron extraction efficiency from both of these materials reached a maximum at a pH of about 2.5. This behavior is attributed to the predominant oxalate species being $HC_2O_4^-$ in the pH range of 2.5-3.0. This is responsible for the reduction of Fe^{3+} to Fe^{2+}.

1.2.6. Removal of Toxic Metals from Soil

Soil contamination with potentially toxic heavy metals like As, Pb, Cd, and Zn is common around the world. This is more predominant in developing countries where there has been a sudden increase in activities such as mining due to increasing industrialization. Soil can be decontaminated by ex-situ washing using acids, surfactants, and chelating agents. Chelating agents such as ethylenediaminetetraacetic acid (EDTA) and ethylenediamine-N, N'-disuccinic acid (EDDS) form stable complexes with heavy metals over a broad pH range but have adverse health effects on humans.[108] On the other hand, strong acids like HCl and H_2SO_4 degrade the soil structure. Therefore, organic acids such as $H_2C_2O_4$, which are milder and have metal complexing and dissolution properties, can be used to remove toxic metals from contaminated soil.

The composition of toxic metals in the soil varies depending on the source of the industrial pollutants that contaminate the soil. The variation in the extraction of toxic metals like Cd from different soils is shown in Table 10. An interesting observation is the inability of $H_2C_2O_4$ to leach Cu(II) and Pb(II). For example, $H_2C_2O_4$ was more effective than citric and acetic acid at leaching As from soil samples collected in the vicinity of a lead battery plant in the Czech Republic, but it was ineffective at extracting Pb.[97] The ineffectiveness of $H_2C_2O_4$ to remove Cu and Pb may have

more to do with the extremely low solubility of these metal oxalates compared to other heavy metals.[94] Their tendency to form oxalate complexes is mentioned in Figure 4, but the extremely low leaching into the aqueous phase suggests that the oxalate complexes of Pb and Cu are not easily formed.

In general, the extraction of heavy metals from contaminated soil using oxalates is affected by several factors. A major factor is the presence of Ca^{2+} and Na^{+} ions in the soil that form extremely stable complexes with $H_2C_2O_4$ reducing the oxalate available to complex with other metals of interest. Also, the variability of soils from one region to the next can make an effective decontamination process difficult to control. The form of the heavy metals is another factor that controls the efficiency of any extractant. Arsenic occurs in the form of a residual fraction (O-As: oxygen bound arsenic) that is the most stable fraction and in the form of Fe-As (Fe bound), Al-As (Al bound), and Ca-As (Ca bound), which are inter-transformed fractions. These inter-transformed fractions have limited mobility and are difficult for a mild acid like $H_2C_2O_4$ to extract As. Also, for Cd, the adsorbed fraction (exchangeable fraction) in the soil is the most active, followed by iron/manganese oxyhydroxides bound, organic matter bound, and sulfides bound. For these different forms, pH and atmospheric conditions can lead to difficulty and variability in extraction.[96,97]

Table 10. Summary of soil decontamination using different chemistries.

Source of soil	Leaching procedure	Metal extraction (wt%)	Ref
Zinc-lead smelting plant (Iran)	12 step washing with 0.01 M oxalic acid	34.3 % Zn, 2.4 % Cd, and 0 % Cu	109
Sandy loam soil	20 mmol/kg oxalic acid for 24 h	40 % Cd, 15 % Cu, 5 % Mn, 35 % Ni, 3 % Pb, and 10 % Zn	110
Surface soil near mining area (China)	0.05 M phosphoric acid, 0.075 M Na_2EDTA, 0.075 M oxalic acid in sequence for 0.5 h per step	41.9 % As, 89.6 % Cd	96
Brass smelter plant (Switzerland)	0.4 M Na_2EDTA at pH 7 for 24 h	17 % Zn, and 29 % Cu	111
	0.4 M EDDS at pH 7 for 24 h	19 % Zn, and 53 % Cu	111

1.3. Dissertation Objectives and Motivation

The goal of this dissertation is to investigate the oxalate chemistry for efficient extraction and separation of metals from mixed metal oxide sources. In addition, the recovery of acid is critical to minimize waste production and offset the high cost of oxalate reagents used. The sub-goals of this dissertation are as follows:

a) *Establishing oxalate chemistry as a viable candidate for $LiCoO_2$ recycling*: Recycling of LIBs is critical to develop a sustainable energy economy and reduce the energy dependence on fossil fuels. Currently, 59 % of LIB waste contains $LiCoO_2$ as the cathodic material from which Li and Co can be recycled. Both Li and Co metals have an unstable economy, and a secondary source is needed to make LIBs affordable. Commercially, H_2SO_4 is the most popular leaching agent (high acidity and low cost) for the recycling of LIBs waste. Oxalate processes suffer from the high cost and low leaching capabilities of various transition metals. Therefore, a major goal for this dissertation is to establish the oxalate reagents as an environmentally-friendly and economical acid

for LIBs recycling. In this work, first, the oxalate reagents: $H_2C_2O_4$, $NH_4HC_2O_4$, KHC_2O_4 with and without H_2O_2 were tested for the efficient extraction and separation of Li and Co from $LiCoO_2$. The use of $H_2C_2O_4$ has been demonstrated well in the literature (Table 4), but its individual leaching and reduction mechanism and its interaction with H_2O_2 need more understanding. Other oxalate reagents: $NH_4HC_2O_4$, KHC_2O_4 have been explored for the first time in this work for Li and Co extractions. The only prior study with $NH_4HC_2O_4$ for metal extractions was performed by Corbin et al. on Fe and Ti recovery from ilmenite ore, whereas KHC_2O_4 has never been reported as a reagent for metal extractions. These oxalate derivative reagents are expected to have convenient recycling routes and could improve the economics. Each of these oxalate reagents have a different operating pH and the importance of pH in efficient extraction and separation was identified. The other reaction parameters like temperature, acid concentration, agitation speed and solid-to-liquid ratio were also optimized for the best performing cases.

b) *Developing an efficient and environmentally-friendly closed-loop process*: A major challenge in the oxalate processes is to recover the oxalate reagents to minimize the acidic waste and offset the high costs. In any commercial inorganic acid process, the acidic waste is usually neutralized, and heavy metals are removed before disposing it in water bodies. Therefore, the downstream processes like Li precipitation and oxalate recovery from $CoC_2O_4{\cdot}2H_2O$ must be carefully designed to minimize the waste production. As discussed earlier, $NH_4HC_2O_4$ is the only oxalate reagent that can be recycled conveniently using a thermal treatment process. The recycling of the other two reagents ($H_2C_2O_4$ and KHC_2O_4) was demonstrated for the first time in this work. For the recycling of KHC_2O_4, a solubility-based acid regeneration was devised and demonstrated. The recycling of $H_2C_2O_4$ was performed using an ion-exchange resin process. Both recycling processes were optimized, and the optimized closed-loop processes were used in performing a techno-

economic analysis. The developed oxalate processes for LIBs recycling were compared with a commercial H_2SO_4 process to understand the benefits of an environmentally-benign process.

c) *Extending the developed oxalate process for refining of ores*: The oxalate processes were developed initially for extraction and separation of Li and Co for LIBs recycling. But the wide application of the developed process for different starting materials must be studied. Therefore, the oxalate chemistry was tested on a variety of mixed metal oxides sources such as bauxite ore, ilmenite ore and NMC cathode material. Bauxite refining is commercially done using the Bayer process and has never been explored using organic acids. The Bayer process is efficient for Al extraction, but a massive amount of caustic iron-rich "red mud" waste is produced. This red mud is typically disposed in open landfills or ponds and pose significant environmental hazards. Hence, it was important to extend the oxalate process for the refining of bauxite ore. The reaction conditions for the Fe and Al extraction and separation from bauxite ore were optimized, and a closed-loop process was designed.

1.4. Outline of Chapters

The introduction chapter had emphasized the importance of oxalate chemistry, summarized the available literature, and discussed the objectives and motivation of this work. Additionally, there are seven additional chapters that discuss different aspects of oxalate chemistry for developing metal extraction processes.

Chapter 2 describes the metal extraction experiments from $LiCoO_2$ using the oxalate reagents particularly: $H_2C_2O_4$, $NH_4HC_2O_4$, and $H_2C_2O_4$ with H_2O_2. The results for other possible reagents like KHC_2O_4 and $NaHC_2O_4$ are predicted based on the results observed with $NH_4HC_2O_4$. Based on the experimental observations, a mechanism of extraction is developed, and the importance of pH for efficient metal extraction is explained.

In Chapter 3, the kinetics of the optimized processes for Li extraction is studied in detail. A combined shrinking-core model is developed and used to identify the rate-limiting step. To improve the kinetics of the $H_2C_2O_4$ process, a novel solution is proposed to produce Co product in the micro-rods morphology. The kinetic study, reaction conditions for the micro-rods formation and their characterization, along with the experimental modeling study, are covered in this chapter.

Chapter 4 discusses the general strategy of metal precipitation in oxalate-rich solutions with an emphasis on Li precipitation from $Li_2C_2O_4$ solution. Additionally, the dissolution of $CoC_2O_4{\cdot}2H_2O$ in the aqueous phase and re-precipitation in the form of $Co(OH)_2$ is also discussed.

In Chapter 5 the regeneration of $H_2C_2O_4$ and KHC_2O_4 for recycling of the acid after metal extraction and separation is discussed. An ion exchange method using strong acid cation exchange resin for regeneration of most of the oxalate reagents discussed in this work is demonstrated. A solubility-based approach, specifically for the regeneration of KHC_2O_4 is also been discussed.

In Chapter 6, the closed-loop process for Li and Co extraction and separation from $LiCoO_2$ with acid recovery is demonstrated at a higher solid-to-liquid ratio. The subsequent metal extraction using the regenerated acid is also demonstrated and the results are used to perform a techno-economic analysis. A comparative economic analysis of the cost of reagents required between the closed-loop oxalate process with sulfuric acid over 100 cycles is discussed to understand the benefits.

Chapter 7 extends the application of oxalate chemistry to bauxite refining for extraction and separation of Fe and Al. The learnings from previous chapters around the metal hydroxide precipitation and acid recovery are used to develop a green, closed-loop process for bauxite refining with minimal waste production.

Finally, Chapter 8 completes the dissertation by providing conclusions and recommendations for future research in this area.

Chapter 2. Recycling of Lithium-ion Batteries Cathode Using Oxalate Chemistry

Portions of this chapter are adapted from the following published article:

Verma, A., Johnson, G.H., Corbin, D.R., & Shiflett, M.B., Separation of Lithium and Cobalt from $LiCoO_2$: A Unique Critical Metal Recovery Process Utilizing Oxalate Chemistry. *ACS Sustainable Chemistry & Engineering* **2020**, 8(15), 6100-6108

Chapter 2

"There is no such thing as AWAY.
When we throw anything AWAY it must go somewhere"
- Annie Leonard (Greenpeace USA)

2.1. Abstract

The demand for lithium-ion batteries (LiBs) is significantly increasing, leading to a shortage in supply for critical metals, such as lithium and cobalt. Recycling $LiCoO_2$ cathodes can provide a secondary source for these critical metals, which are necessary raw materials for synthesizing modern LiB cathodes, such as nickel manganese cobalt oxide (NMC). In this chapter, an environmentally-friendly, closed-loop process for the recovery and separation of lithium and cobalt from $LiCoO_2$ cathodes has been developed using oxalate chemistry. Oxalic acid and ammonium hydrogen oxalate are utilized as digestion reagents to extract lithium into the aqueous phase ($Li_2C_2O_4$) and precipitate cobalt oxalate ($CoC_2O_4 \cdot 2H_2O$) in the solid phase resulting in a low-temperature, cost-effective separation of these metals. A green-colored intermediate was identified as a Co(III)-oxalate complex; this complex further reduces and precipitates as a Co(II)-oxalate complex ($CoC_2O_4 \cdot 2H_2O$). The optimum acidity for digestion and metals separation using oxalate containing acids was a pH < 2.0. The minimum amount of oxalic acid required for digestion was determined in order to develop the most economical process with more than 97 wt% Li and Co recovery. The proposed process is an energy-efficient, cost-effective, environmentally-friendly process for recovering high-value, critical metals, such as lithium and cobalt from LiBs cathodes

2.2. Motivation

One of the major challenges in the 21st century is to tackle the environmental issues resulting from greenhouse gas emissions, the dumping of waste in landfills and water bodies, and many more. In the past two decades, a major effort has been made towards making the earth a

better place for future generations by following three R's: "Reduce, Reuse, Recycle." The first global challenge in these efforts is reducing the dependence on fossil fuels to meet energy requirements. The global annual energy demand is predicted to increase by almost 20 % by the end of 2030, out of which under the current scenario, 79 % of energy will still be met from fossil fuels. Hence, a significant push is needed for energy-efficient processes along with development in the renewable energy sector to reduce the energy dependence on fossil fuels.

In this process, technological advancement and commercialization of lithium-ion batteries (LiBs) have gained tremendous interest, particularly for their application as an energy storage device in electrical grids and electric vehicles. The global market for LiBs is expected to be tripled by 2025, growing at a CAGR of 17.1 %. But, as the production of LiBs consumes finite natural resources like lithium and cobalt, a sustainable LiB recycling process is needed for a broader impact. Hence, for the conservation of active metal resources and development of an alternative secondary raw material for LiBs production, "Recycling of LiBs" is necessary. This chapter covers the fundamentals of LIBs and the details of a sustainable closed-loop process for the recovery of critical metals like Li and Co from the cathode of LiBs utilizing a hydrometallurgical route of oxalate chemistry.

2.3. Lithium-ion Batteries

The term "battery" was first coined by Benjamin Franklin in 1749 to describe an array of charged glassed capacitors used for storing energy. Subsequently, this term was commonly used for a group of two or more similar electrochemical objects functioning together. Nowadays, even a single electrochemical cell that extracts electrical energy from chemical energy is commonly referred to as a "battery." The batteries can be widely classified into primary and secondary batteries. Primary batteries are non-rechargeable, where the reaction of active material limits the

energy capacity of the battery. Once the chemically active materials are completely consumed, no additional electrical energy can be extracted. Secondary batteries are rechargeable batteries, where active materials are regenerated for additional electrical energy production.[112] Lithium-ion batteries (LiBs) are secondary batteries that can store electrical energy in the form of chemical energy. Secondary batteries have a history of over 200 years, with lead-acid batteries being the first of this type. Like any typical battery, LiBs consist of lithium ions in the negative electrode, which move through an electrolyte to the positive electrode during discharge, and back when charging.

2.3.1. History of Lithium-ion Batteries

The first commercial LiB was developed by Sony in 1991 and was soon followed by the Asahi Kasei team in 1992, but the numerous studies before 1991 provide the origin of LiBs.[113] The idea of a battery where a Li^+ ion moved reversibly between two intercalation electrodes was developed by Armand in the 1970s and was termed as a rocking chair battery.[114] This idea was implemented in a lithium tungsten oxide electrode and titanium disulfide electrode by Lazzari and Scrosati, where Li^+ ions flow forward and backward between two electrodes.[115] In 1976, Whittingham, then a research scientist at Exxon, invented a low-temperature, high-energy battery consisting of lithium metal and titanium disulfide as electrodes.[116,117] Although the high volatility of lithium metal resulting in fires and explosions was still an issue that needed to be resolved. Soon after that, the ability of the family of lithiated transition metal oxides (Li_xMO_2) to reversibly intercalate and deintercalate the Li^+ ions was discovered by Goodenough.[118] These lithiated transition metal oxides had a structure similar to $NaFeO_2$, where Ni, Co as well as their mixtures with Mn, Fe, Al, etc. had the similar reversible intercalation ability and further in 1991, $LiCoO_2$ formed the electrode in the first commercial LiBs. Later, J.C. Hunter of Eveready laboratories

discovered $LiMn_2O_4$ in spinel structure that can also perform the reversible redox reactions at a high potential similar to $LiCoO_2$.[119]

For the negative electrode, initially, graphite and carbonaceous material demonstrated the possibility of lithium-ion intercalation. Still, the issue of solvent intercalation along with Li^+ ions was prevalent in these. The breakthrough in the negative electrodes was using the low-temperature carbon such as petroleum coke by Yoshino and coworkers at Asahi Kasei. In the first commercial battery, $LiCoO_2$ and petroleum coke were used as the electrodes, and a water-free electrolyte consisting of $LiPF_6$ with propylene carbonate was used. The charging voltage was as high as 4.1 V and had an energy density of ~80 Wh/kg which soon led to the mobile electronics revolution. Later, it was also discovered that the graphite could be used as a negative electrode with ethylene carbonate in the electrolyte.[116] This invention was readily adopted by the scientific community, and batteries with a graphite electrode with a charging voltage of 4.2 V were developed. In 2019, John B. Goodenough, M. Stanley Whittingham, and Akira Yoshino were awarded the Nobel Prize in Chemistry for developing lithium-ion batteries.[116,117] Modern LiBs are still close to the traditional composition of LiBs containing lithium metal oxide ($LiMO_2$) as the positive electrode, graphite as the negative electrode, and $LiPF_6$ along with ethylene carbonate as electrolyte. Research in the last decade has focused more on decreasing the cost by introducing cheaper positive electrode materials like $LiNi_xMn_yCo_zO_2$ (NMC) containing less cobalt.[120]

2.3.2. Major Components and Operating Principle

As discussed briefly in previous sections, LiBs mainly composed of a negative electrode (anode during discharge), a positive electrode (cathode during discharge), an electrolyte, and separators and current collectors. Commonly, an intercalated lithium-containing transition metal oxide (such as $LiMO_2$) is used as the positive electrode, graphite is used as the negative electrode,

and an organic solvent in which a Li compound is dissolved and used as the electrolyte. The discharging (forward) and charging (backward) reactions are shown in Eqs. 2.1 and 2.2.

$$\text{Positive Electrode: } Li_{1-x}MO_2 + xLi^+ + xe^- \rightleftarrows LiMO_2 \quad (2.1)$$

$$\text{Negative Electrode: } Li_xC_6 \rightleftarrows xLi^+ + xe^- + C_6 \quad (2.2)$$

Operating principle and electrode terminology: Li^+ ions intercalated between the graphite planes of the negative electrode, are extracted during the discharge process, and dissolve in the electrolyte. A Li^+ ion from the electrolyte solution moves into the metal oxide planes of positive electrodes to maintain charge neutrality. The Li^+ ions that entered into the positive electrode plane combine with the electrons traveling via an external circuit. The discharge process is a galvanic cell operation, and hence, the cathode ($LiMO_2$) is positive, whereas the anode (graphite) is negative. The opposite reactions occur during the charging process, where electrons are withdrawn from the negative electrode ($LiMO_2$) and combine with the traveling lithium ions at the positive electrode (graphite). The charging process is an electrolytic cell operation, and hence, cathode (graphite) is negative, whereas anode ($LiMO_2$) is positive.[112,121] The terminology of anode and cathode depends on whether a battery is charging or discharging. It will be easier to constantly refer, to $LiMO_2$ as the positive electrode and graphite as the negative electrode, which remains the same irrespective of the operation the battery is performing. A schematic of a lithium-ion battery is shown in Figure 8.[122]

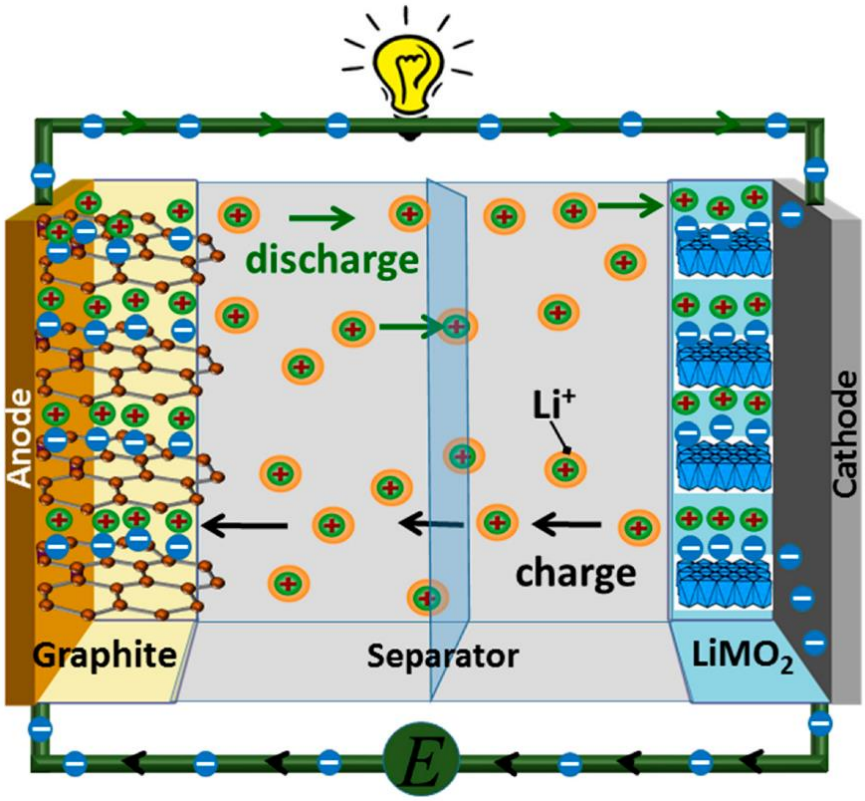

Figure 8. Schematic of the operation principles for rechargeable lithium-ion batteries. Reprinted with permission from Madian et al. Copyright (2018), MDPI.[122]

2.3.3. Types of Lithium-ion Batteries

This work is restricted to the recovery of active metals from LIBs, and a majority of active metals are found in the positive electrode. Hence, this section will classify various modern LIBs based on active metals used in the positive intercalation electrodes (cathode during discharge). An intercalation electrode is a solid host network where guest ions can be inserted and removed reversibly without disturbing the solid structure.

Lithium Cobalt Oxide. $LiCoO_2$ (LCO) is one of the first commercially developed layered intercalation electrodes used in most commercial LiB applications.[118] In LCO, Li and Co occupy the octahedral sites in alternating layers and form a hexagonal symmetry. Its structure is shown in Figure 9a.[34] LCO electrodes have high theoretical capacity and low self-discharge but suffer from

high cost and low thermal stability. The amount of Co required in this electrode is a major reason behind its higher cost.[34,112]

Lithium Nickel Oxide and Lithium Nickel-Cobalt-Aluminum Oxide. $LiNiO_2$(LNO) and $LiNi_xCo_yAl_zO_2$ (NCA) are structurally similar to the LCO. The presence of Ni increases the energy density of the electrode, decreases the cost but suffers from the lower thermal stability and diffusion of Ni ions along with Li during the delithiation.[123] Addition of Al along with Ni improves the thermal stability and electrochemical performance of the standard LNO electrode. However, increased resistance and cracks at the solid-electrolyte interface are observed because of local structural changes in electrodes.[124]

Lithium Manganese Oxide and Lithium Nickel-Manganese-Cobalt Oxide. $LiMnO_2$ (LMO) and $LiNi_xMn_yCo_zO_2$ (NMC) are also structurally similar to the LCO electrode. These electrodes are promising because of cheaper and less toxic Mn.[125] Although LMO suffers from structural changes during reversible intercalation and deintercalation, which was improved by combining LCO, LNO, and LMO to synthesize NMC electrode. $LiNi_{0.33}Mn_{0.33}Co_{0.33}O_2$ is the most common type of NMC material with wide commercial applications. NMC has a higher specific capacity than LCO while having lower costs because of less Co content. Numerous researchers are working towards improving the thermal stability, reversible cycling capacity, and power density of NMC electrode.[126,127]

Spinel Lithium Manganese Oxide. $Li_2Mn_2O_4$ (LMO) is a spinel-type material consisting of cheap and less toxic Mn as the active metal with Li. In this structure, Li occupies tetrahedral sites, whereas Mn is located in octahedral sites, as shown in Figure 9b.[34] The Li intercalation and deintercalation happen through the vacant tetrahedral and octahedral interstitial sites in the structure. However, it suffers a similar problem of Mn dissolution as the layered LMO electrode.

Currently, various research investigations are ongoing towards improving the spinel LMO properties, making it one of the promising electrodes for the future.[128,129]

Olivine Lithium Iron Phosphate. $LiFePO_4$ (LFP) is a thermally stable material where large polyanions (PO_4^{3-}) occupy lattice positions and increase the redox potential.[130] In the olivine structure, $Li^{+,}$ and Fe^{2+} ions occupy octahedral sites, and P is present at tetrahedral sites in a slightly distorted hexagonal closed-pack oxygen structure (HCP) as shown in Figure 9c.[34] A major issue with the LFP is the low electrical and ionic conductivity, and extensive research has continuously being done to improve it by carbon coating and size reduction.[130,131]

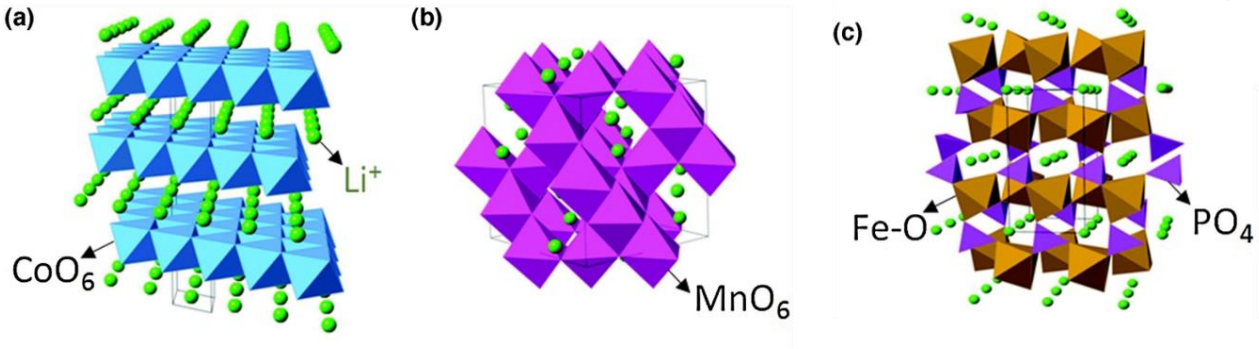

Figure 9. Crystal structures of intercalation electrodes: (a) layered $LiCoO_2$, (b) spinel $LiMn_2O_4$, and (c) olivine $LiFePO_4$. Reprinted with permission from Nitta et al. Copyright (2015) Elsevier.[34]

2.3.4. Degradation Mechanism of Lithium-ion Batteries

Understanding the LIBs degradation is critical before developing the recycling process for it. The technology of Li^+ ion reversible intercalation in electrodes has proven useful because of low volume expansion and contraction that provides required electrochemical and mechanical stability for the lifespan.[132] The multiple mechanisms responsible for the degradation of LIBs are shown in Figure 10. However, two known mechanisms are the major factors responsible for the degradation of LIBs and are discussed here briefly:

a) Solid electrolyte interphase (SEI) layer growth: SEI is a thin passive layer formed at the negative electrode and liquid electrolyte interface during the first charge-discharge cycle. This layer commonly consists of inorganic compounds such as Li_2CO_3 and Li_2O.[133-135] The SEI is an electrically insulating protective layer to avoid further decomposition of electrolyte but allows the conduction of Li^+ through it. However, the thickness of the SEI layer increases over time. This growth could be due to the deposit of side reaction products from metal ions leached in the electrolyte. Additionally, the plating of Li^+ on the negative electrode at low temperatures can initiate side reactions that can lead to SEI growth.[136] As a result of the increasing thickness of SEI, the free Li in the battery decreases, resulting in capacity loss.[137] Thick SEI also slows down the charge and discharge process because of increased diffusional resistance for the available ions.

b) Positive electrode degradation: The layered electrode structures (commonly high Ni electrodes), after delithiation, can decompose into disordered spinel and rock salt phases, as shown in Eq. 2.3. The decomposition results in the destruction of layered structures and releases oxygen inside the battery compartment.[138,139]

$$Li_xMO_2 \text{ (layered)} \rightarrow Li_xM_3O_4 \text{ (spinel)} \rightarrow Li_xMO \text{ (rock salt)} \quad (2.3)$$

[O] releases in each step

This decomposition becomes more thermodynamically favorable at high delithiated states.[139] The electrochemical oxidation of oxide anions within the structure can also take place, resulting in the collapse of layered structures into spinel or rock salt structures.[140] Higher Co content is critical in providing chemical stability to the layered material.[136]

As discussed earlier, the LiB electrolyte is a highly reactive non-aqueous organic compound, $LIPF_6$. The electrolyte can react with the available moisture to produce HF, leaching

the transition metal ions into the electrolyte.[141,142] This can be avoided by a better design for sealing the LIB packs.

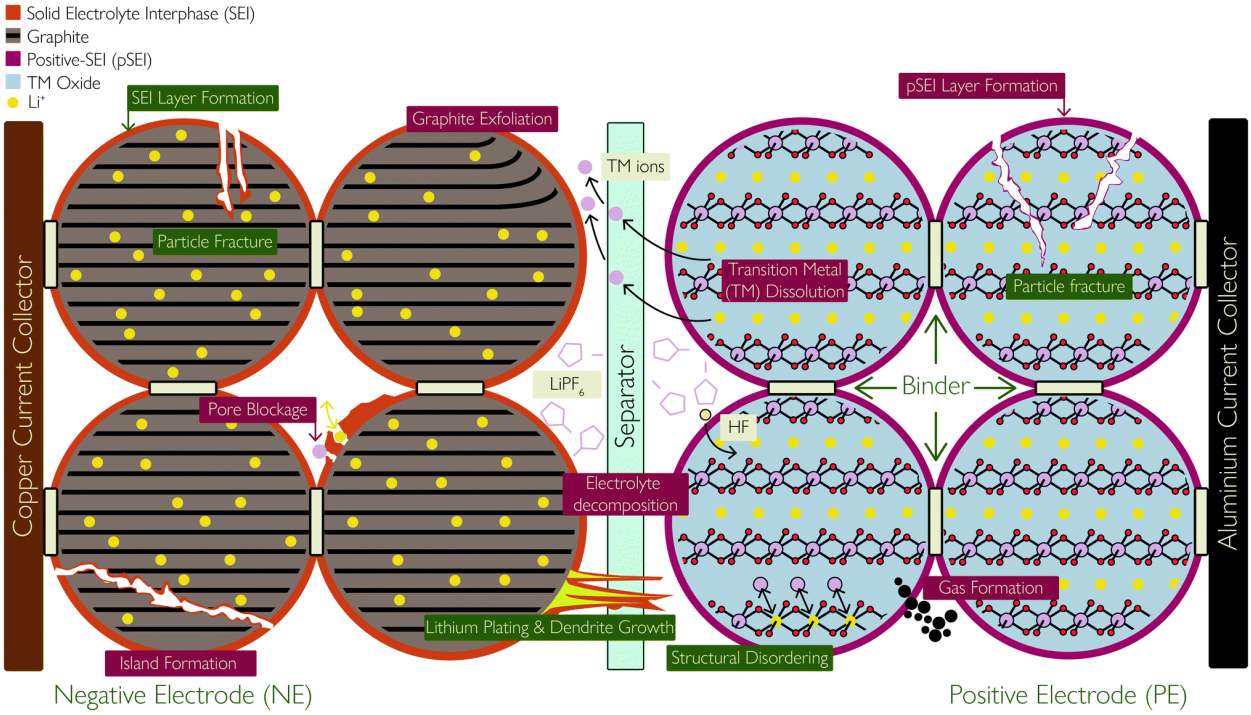

Figure 10. Schematic showing the major degradation mechanism in a lithium-ion battery cell. Reprinted with permission from Edge et al. Copyright (2021), Royal Society of Chemistry[136]

2.4. Recycling of Lithium-ion Batteries

Lithium-ion batteries are consumable products with an average life span of 1-3 years. In the rapid growth phase of electric vehicles, LiBs production will automatically increase.[143] In terms of the natural resource's utilization, one ton of Li production requires 750 tons of brine, whereas only 28 tons of waste LiBs can produce the same amount of Li.[144,145] A more significant concern is Co reserves, which are geographically concentrated mainly in the politically unstable Democratic Republic of Congo (DRC).[143] Co prices have experienced long-term fluctuations over the past decade and have raised numerous social, ethical, and environmental concerns around the prevalent mining practices.[143,146] Given the global impact of the LiB industry, international coordination is required to globally push the circular economy of metals and recycling of LiBs.

Apart from the social issues, numerous environmental problems caused by landfills dumping of LiBs are also an area of concern. In their metallic state, active metals like Co and Ni have serious health hazards ranging from gastrointestinal disorders, dermatitis, and even damage to the nervous systems. Metallic Ni is also a known carcinogen and, once dissolved in the blood, can induce lung cancer. Common electrolytes used in LiBs ($LiPF_6$ and $LiClO_4$) are highly corrosive and volatile. These compounds can react with oxygen and form hazardous byproducts like HF, P_2O_5, and Li_2O.[31,143] Overall, LiBs discarded with no-approved guidelines can cause significant damage to the environment through heavy metal pollution, air pollution, water pollution, and may even enter the human body through the contaminated soil, air, or water. This could lead to severe diseases and extreme health conditions, which can even result in death.[143]

The LIB recycling technologies can be divided into three main categories: pyrometallurgy, hydrometallurgy, and direct recycling.[31,143] Pyrometallurgy is the most flexible technology and can be adapted for all kinds of LIBs with minimum pre-processing. However, the high energy requirements and significant carbon footprint from fossil-based fuels are the major issues.[147] Direct recycling requires physical separation methods to separate the LIB components and efficiently reuse the cathode after re-lithiation. However, the continuously changing cathode chemistries and battery designs are the major obstacles for this technology in the circular battery economy.[148] For the recycling of predominant LCO batteries, re-lithiation via direct recycling may not be appropriate as the cathode composition cannot be pushed towards reducing the dependence on Co. Hydrometallurgy is based on wet chemistry with high efficiency in recovering pure metal compounds. These metal compounds can be used to synthesize new cathode materials. However, pre-processing and separation of individual components from spent LIBs is necessary for effective

metal extraction.[31,149] Hydrometallurgical processes are adaptable with the continuously evolving cathode metal oxides formulations and can recycle the LCO batteries into NMC batteries.

This dissertation explores hydrometallurgical processes developed using oxalate chemistry. Hence, the discussion in the further sections is limited to hydrometallurgical recycling processes. A hydrometallurgical recycling process typically comprises both physical and chemical processes. The physical separation processes discussed in the following section can be employed in direct recycling as well.

2.4.1 Physical Processes: Pretreatments and Separations of Electrode Material

Most of the spent LiBs usually contain a small charge, which is dangerous if disassembled directly in the air. Hence, the first and foremost step is to discharge the battery completely. After that, a series of pretreatment steps are commonly used to disassemble and separate the various components of the battery based on density, weight, shape, conductivity, or magnetic properties.[31] The pretreatment processes required will differ from manufacturer to manufacturer. Hence, a generalized sequence is difficult to predict, but common physical separation techniques like crushing, sieving, ultrasonic washing, and magnetic separations are typically used. With physical pretreatments, the aim is to separate materials and components with similar physical properties. Figure 11 contains the flowchart of typical processes used in the recycling of spent LiBs.[150] As discussed previously, positive electrode materials contain critical metals. Hence, it is important to recover the positive electrode with minimal impurities (like Al, Fe, and binders). If additional metallic impurities are present, it can create additional complications for separating and recovering critical metals from electrode material in downstream processes.

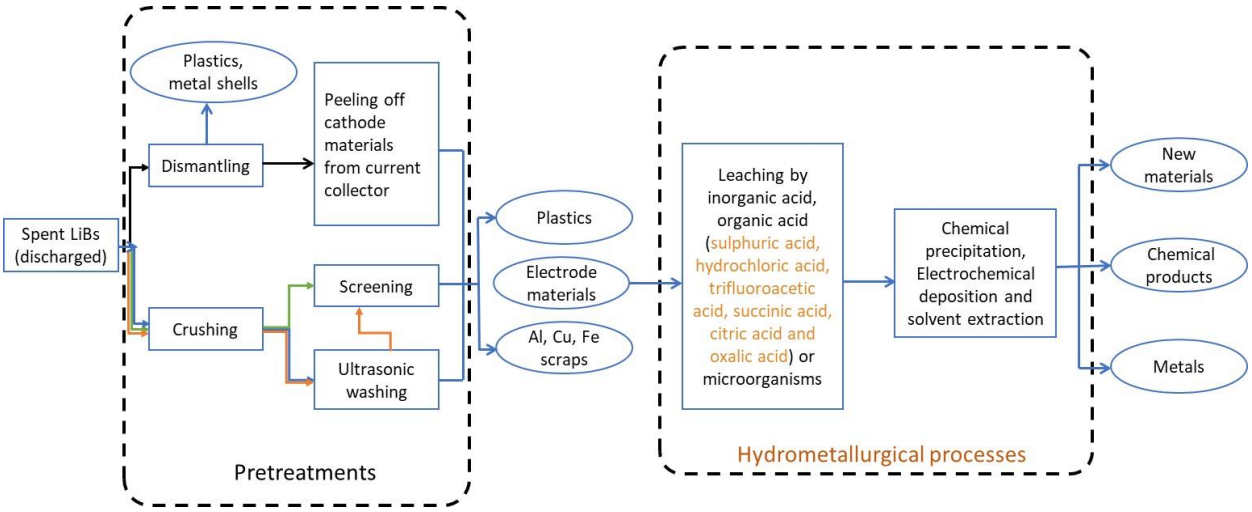

Figure 11. Flowchart of a typical process for recycling spent LiBs.

2.4.2. Chemical Processes: Critical Metal Recovery from Positive Electrode

Recovery of metals from the positive electrode materials is the critical process for LiBs recycling. Critical metals like Li, Co and Ni are valuable, and their efficient recovery in a green and sustainable manner will drive the economy of such a recycling process. Therefore, the chemical leaching reagents and separation processes used in this step are important for the overall success both in terms of its global implementation and adaptability. Hydrometallurgy commonly involves leaching the cathode in concentrated inorganic acids like HCl, H_2SO_4, and HNO_3 after a series of mechanical pretreatments to separate various components from spent LiBs.[12,31] The dissolved metals can be recovered by multiple precipitation steps; however, the separation process is complex. Inorganic acid leaching processes often require the addition of a reducing agent like H_2O_2 to increase the efficiency.[35,36,39,40] Under the optimum conditions reported, more than 98 wt% of Li and Co can be recovered using these inorganic acids; however, the emission of pollutants like Cl_2, SO_x, and NO_x and acidic wastewater after the leaching process pose a significant threat to the environment. Organic acids like acetic acid, citric acid, oxalic acid, succinic acid, ascorbic acid, and malic acid have also been proposed for the recovery of Li and Co

from $LiCoO_2$ cathodes removed from spent LiBs.[32,53,54,151-154] All of the organic acids except ascorbic acid and oxalic acid need an additional reducing agent like H_2O_2 for recovery of Co. Fungi and bacteria have also been used to leach Li and Co from spent LiBs cathode. These micro-organisms produce acid, which leaches the metals from cathodic material.[44,56] A summary of different organic acids and micro-organisms used for leaching of Li and Co from $LiCoO_2$ is presented in Table 4 in Section 1.2.1.

2.5. Extraction of Li and Co from $LiCoO_2$ using Oxalate Chemistry

The structure of $LiCoO_2$ consists of layers of Li^+ cations intercalated between anionic sheets of Co^{3+} and O^{2-} ions, which are arranged in an edge-sharing octahedron.[155] Cobalt exists in a trivalent oxidation state, and the reduction of Co^{3+} to Co^{2+} is carried out by the oxidation of C(III) present in $C_2O_4^{2-}$ to C(IV) in CO_2. The reduction and oxidation reactions during digestion are shown in Eqs. 2.4 and 2.5. The positive standard potential of both reactions indicates the thermodynamic feasibility of this redox couple.[20] The final products after digestion in the presence of oxalate are a solid precipitate of $CoC_2O_4 \cdot 2H_2O$ and $Li_2C_2O_4$, which remains in solution. The high solubility of $Li_2C_2O_4$ in the aqueous phase allows for a simple separation after the digestion in any oxalate containing acid.

$$\text{Cobalt Reduction: } Co^{3+} + e^- \rightleftharpoons Co^{2+} \qquad E^0 = 1.92 \text{ V} \qquad (2.4)$$

$$\text{Oxalate Oxidation: } C_2O_4^{2-} \rightleftharpoons 2CO_2 + 2e^- \qquad E^0 = 0.49 \text{ V} \qquad (2.5)$$

Oxalate can exist in solution in the following forms: $H_2C_2O_4$, $HC_2O_4^-$, and $C_2O_4^{2-}$ depending upon pH. The presence of other cations in the aqueous phase can also affect the speciation of oxalate. However, irrespective of the other cations, at a pH > 4, $C_2O_4^{2-}$ becomes the predominant oxalate species in the aqueous phase (see Figure 2, oxalate ion speciation curve at 25 °C[150]). The possibility of cobalt(II) oxalate complexes containing more than two oxalate ligands increases the solubility

of $CoC_2O_4 \cdot 2H_2O$ in the aqueous phase. Such complexes are usually formed in the presence of excess $C_2O_4^{2-}$ ion, and hence the separation efficiency between Li and Co will be sensitive to the pH.[156,157] The availability of oxalate in the presence of insoluble cobalt(II) oxalate in an aqueous environment is shown in Eq. 2.6.

$$Co^{2+} + 3C_2O_4^{2-} \leftrightarrows CoC_2O_4 \cdot 2H_2O(s) + 2C_2O_4^{2-} \leftrightarrows Co(C_2O_4)_2^{2-} + C_2O_4^{2-} \leftrightarrows Co(C_2O_4)_3^{4-} \quad (2.6)$$

2.5.1. Experimental Setup for Metal Extraction Experiments

One aim of this work was to carefully understand the mechanistic details while collecting the fundamental kinetic data during the metal extraction experiments. Therefore, the extraction reactor was specifically designed to maintain the temperature while avoiding any water loss. All hydrometallurgical experiments were carried out in a 1-L glass reactor enclosed in a heating jacket with a 5-neck DURAN® head from which two thermocouples (sensory and over-temperature), electric agitator, and a reflux condenser were connected. The reactor temperature was maintained at 100 °C throughout the metal extraction process. The stirring speed was maintained at 600 rpm to eliminate any external mass transfer limitations and was kept constant for all the experiments. A reflux condenser connected to a chiller operating at 5 °C was used to avoid the loss of water during the metal extraction process. From the fifth neck, a syringe was connected to withdraw solid and aqueous samples for characterization and measuring metal concentrations. A simple schematic of the reactor is shown in Section A.1 (Appendix).

All the hydrometallurgical experiments were carried out by heating the reagents to a set temperature, and then the required amount of $LiCoO_2$ was added in the extraction reactor. The molar ratio between $LiCoO_2$ and $C_2O_4^{2-}$ (reactants and referred to as Co to oxalate ratio from here on) was considered important since $C_2O_4^{2-}$ can act as both a chelating and reducing agent in the Li and Co extraction from $LiCoO_2$. This molar ratio was used as one of the experimental variables,

which was optimized for maximum metal extraction. After completion of the digestion reaction, Li remains in the aqueous phase, whereas Co precipitates in the form of $CoC_2O_4 \cdot 2H_2O$. Insoluble $CoC_2O_4 \cdot 2H_2O$ can be separated using vacuum filtration.

The mixed metal oxide digestion and subsequent metal extraction is a solid-liquid reaction, and the reaction rate is a function of the acid concentration, temperature, solid-to-liquid ratio, and stirring speed. The optimum Co to oxalate ratio should be close to the stoichiometric ratio based on a chemically balanced digestion reaction. Solid-to-liquid (S/L) ratio of $LiCoO_2$ to aqueous oxalate solution was kept constant in all the experiments at an optimum value of 15 g/L as reported by Zeng et al.[11]

2.5.2. Materials and Materials Characterization

In this study commercially available $LiCoO_2$ (99.8 %, Sigma-Aldrich), $H_2C_2O_4 \cdot 2H_2O$ (99.5 %, ACROS Organics), $(NH_4)_2C_2O_4 \cdot H_2O$ (99 %, ACROS Organics), H_2O_2 (30 %, Fisher Chemical) were used for the digestion reactions. The concentration of Li and Co in the aqueous phase was measured using inductively coupled plasma – optical emission spectrometry (ICP-OES, Varian/Agilent 725 ES). Solid precipitates were characterized using a powder X-ray diffraction technique (PXRD) on a Bruker D2 Phaser XRD instrument with a CoKα (1.78897 Å) radiation source. The collected patterns were matched with the patterns in ICDD database at $\lambda = 1.78897$ Å. Ultraviolet−visible (UV−vis) spectroscopy was used to confirm the oxidation state of cobalt metal present in the aqueous phase and was performed using a Vernier UV−vis spectrophotometer (220−850 nm). Additional details about the instruments can be found in Section A.1 (Appendix).

2.5.3. $LiCoO_2$ in Oxalic Acid

Oxalic acid ($H_2C_2O_4$, OA) is the simplest oxalate and is the most acidic among all oxalate containing acids ($pK_{a1} = 1.23$ and $pK_{a2} = 4.19$ at 25 °C). The complete digestion reaction of $LiCoO_2$

with $H_2C_2O_4$ is summarized in Eq. 2.7. The Co to oxalate molar ratio according to the stoichiometry in the balanced reaction is 1:2 Co:OA. The effect of oxalate concentration on the metal extraction efficiency was investigated at 1:1.5, 1:2, 1:3, and 1:4 Co to oxalate molar ratios (Co:OA). These ratios are equal to 0.23 M (1:1.5 Co:OA), 0.30 M (1:2 Co:OA), 0.46 M (1:3 Co:OA), and 0.61 M (1:4 Co:OA) of oxalic acid maintaining 15 g/L S/L ratio in the aqueous phase. The Co to oxalate molar ratio was varied to find an optimum ratio for efficient digestion and separation between Li and Co, keeping other reaction parameters constant. Figure 12a summarizes the metal extraction kinetics and efficiency from $LiCoO_2$ by varying the Co to oxalate molar ratios. The temperature in all the metal extraction experiments was kept constant at 100 °C; S/L ratio was maintained at 15 g/L, and the agitator speed was set at 600 rpm.

$$4H_2C_2O_4(aq) + 2LiCoO_2(s) \leftrightarrows Li_2C_2O_4(aq) + 2CoC_2O_4{\cdot}2H_2O(s) + 2CO_2(aq) \qquad (2.7)$$

As shown in Figure 12a, maintaining the Co to oxalate molar ratio at 1:3 (Co:OA 1:3) and 1:4 (Co:OA 1:4), produced similar kinetic performance and extraction efficiencies indicating the requirement of excess oxalate for a complete separation of Li and Co. In both cases, more than 90 wt% of Li was extracted into the aqueous phase in a 2 h digestion, whereas less than 2 wt% of Co was extracted. This led to the precipitation of the remaining Co in the form of $CoC_2O_4{\cdot}2H_2O$ confirmed by the XRD pattern shown in Figure 13. Sun and Qiu, and Zeng et al., have reported more than 97 wt% recovery of Li and Co under similar reaction conditions of 1 M $H_2C_2O_4$ and high temperature (>80 °C).[11,12] In our work, a similar Li and Co recovery was obtained at a lower concentration of $H_2C_2O_4$ (0.46 M), which explains the importance of using S/L ratio and Co to oxalate ratio to find the optimum concentration. For metal extractions using micro-organisms, more than 90 wt % recovery of Li was observed at even a lower temperature (<50 °C), but the reaction duration was longer.[44,56] For Co to oxalate (Co:OA) molar ratios of 1:2 and 1:1.5,

incomplete digestion was observed, where Li extraction was found to be only 81 wt% and 73 wt%, respectively. Solid precipitates from the Co:OA 1:2 and Co:OA 1:1.5 digestions were found to be a mixture of unreacted $LiCoO_2$ and $CoC_2O_4 \cdot 2H_2O$. The XRD results are summarized in Figure 14. For the Co:OA 1:1.5 and Co:OA 1:2 digestions, higher concentration of Co was measured in the aqueous phase that produced a light pink color. Increasing the Co to oxalate molar ratio requires a higher acid concentration, which leads to a faster and more efficient extraction of metals into the aqueous phase. In addition, at higher $H_2C_2O_4$ concentrations (Co:OA $\geq$ 1:3), no $CoC_2O_4 \cdot 2H_2O$ dissolved in the solution; however, at lower $H_2C_2O_4$ concentrations (Co:OA $\leq$ 1:2) when the solution is less acidic, $CoC_2O_4 \cdot 2H_2O$ dissolution was observed. Similar phenomena for $CoC_2O_4 \cdot 2H_2O$ dissolution at lower oxalic acid concentration was observed by Sun and Qiu as well.[12]

2.5.4. $LiCoO_2$ in Ammonium Hydrogen Oxalate

A major advantage for using ammonium hydrogen oxalate ($NH_4HC_2O_4$, AHO) as the oxalate reagent was to create a closed-loop process so that the AHO could be efficiently recovered and recycled for additional cycles. A closed-loop metal recovery process was demonstrated by Corbin et al. using AHO for Ti and Fe extraction and separation from ilmenite ($FeTiO_3$).[16] AHO is a monoprotic acid, whereas OA is a diprotic acid. Hence, a higher concentration of AHO will be required for efficient metal extraction. In this work, the extraction using Co to oxalate molar ratio of 1:4 was attempted with AHO, and the results were compared to the Co:OA 1:4 digestion. The other reaction parameters (T = 100 °C, S/L = 15 g/L, agitator speed = 600 rpm) were kept constant similar to the OA experiments. The Li and Co extraction reaction from $LiCoO_2$ using AHO is shown in Eq. 2.8.

$$8NH_4HC_2O_4(aq) + 2LiCoO_2(s) \leftrightarrows Li_2C_2O_4(aq) + 2CoC_2O_4 \cdot 2H_2O(s) + 4(NH_4)_2C_2O_4(aq) + 2CO_2(aq) \quad (2.8)$$

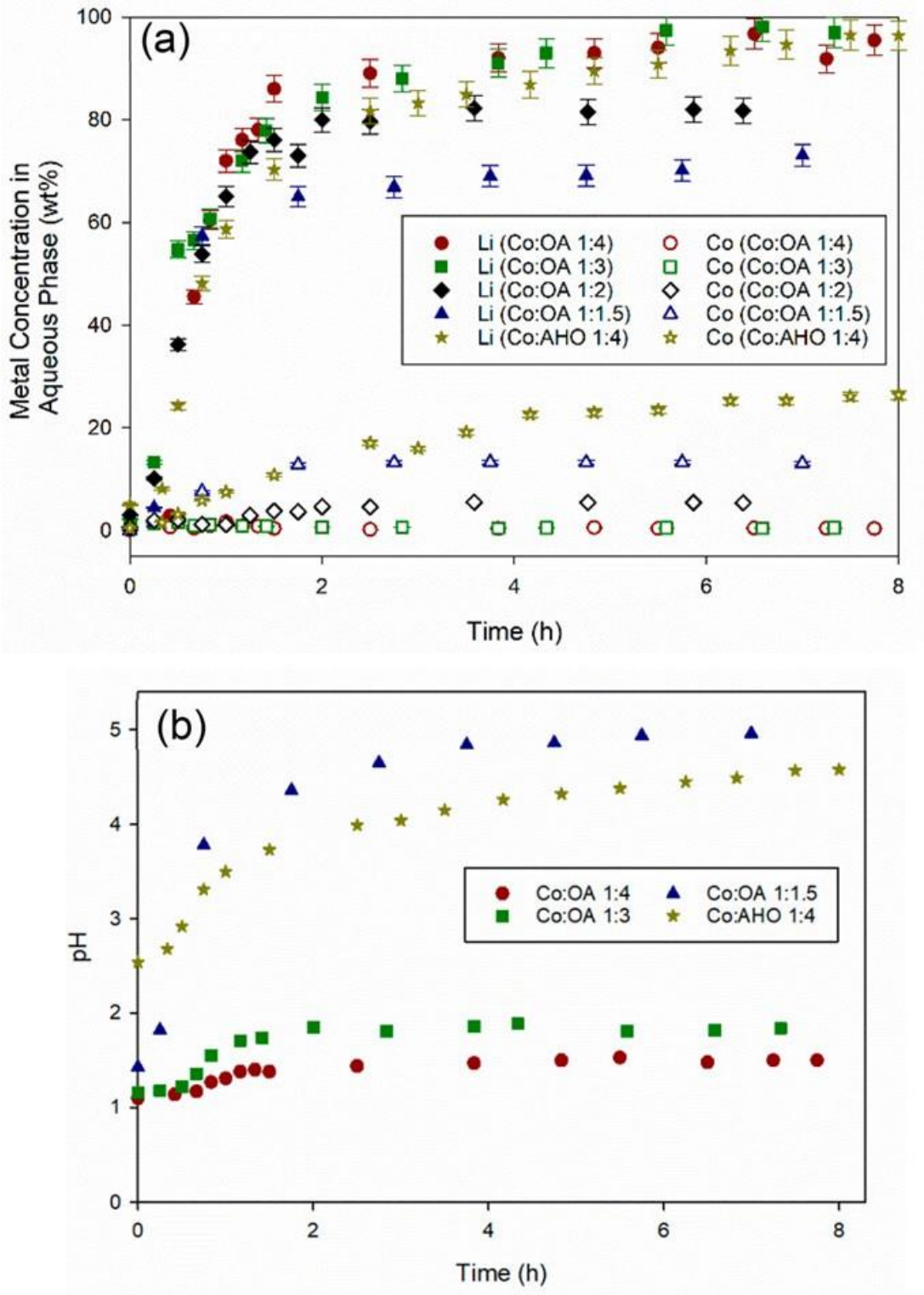

Figure 12. **(a)** Li and Co metal concentration as a function of time in the aqueous phase at Co:OA ratios of 1:4, 1:3, 1:2, 1:1.5 and Co:AHO 1:4 **(b)** pH as a function of time in the aqueous phase at Co:OA ratios of 1:4, 1:3, 1:1.5 and Co:AHO ratio of 1:4 at T = 100 °C.

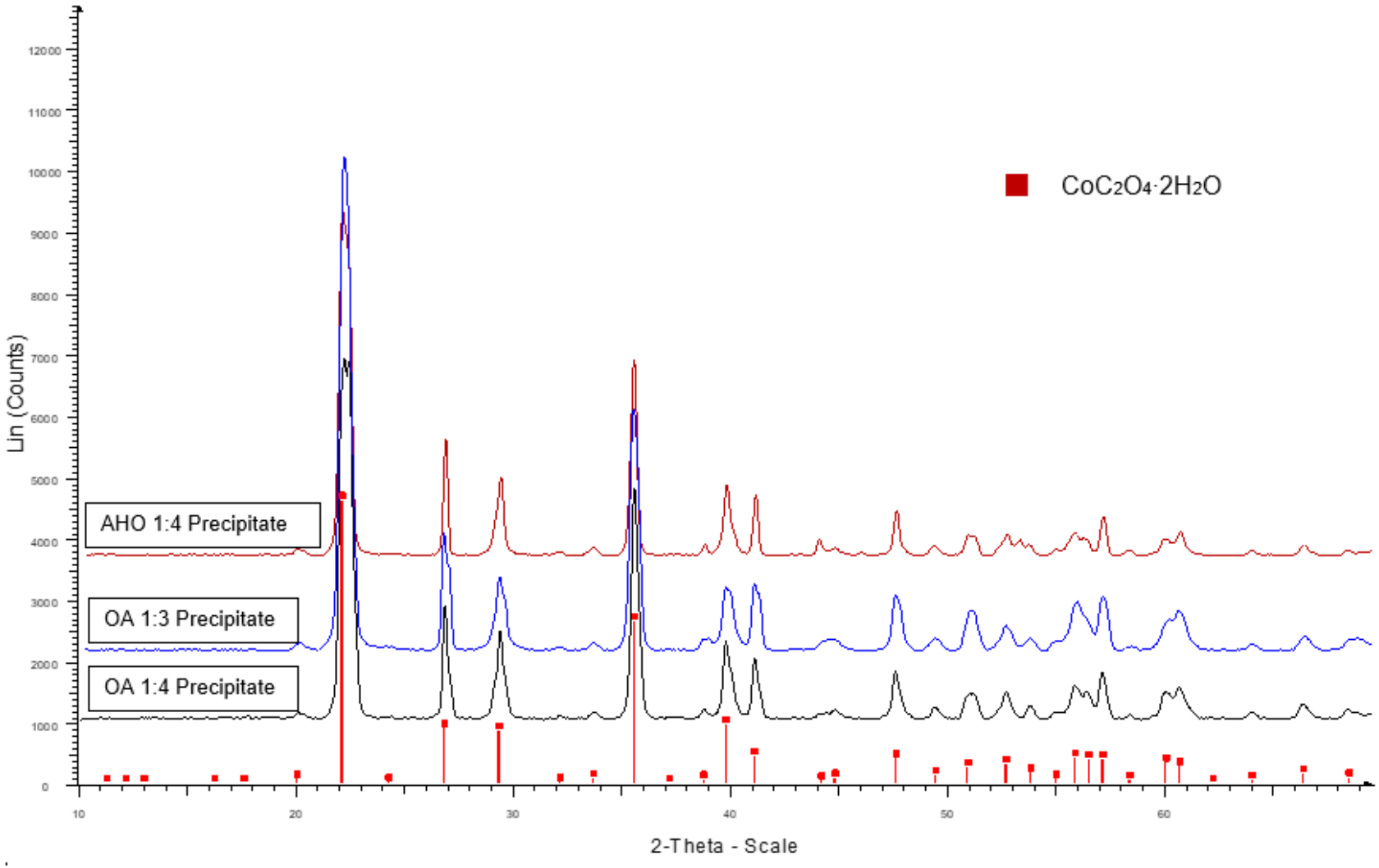

Figure 13. XRD pattern of solid precipitate recovered during extractions.
The XRD pattern of $CoC_2O_4 \cdot 2H_2O$ is monoclinic structure with P21/n space group and 110° being the major peak at d-spacing of 3.633 Å. $LiCoO_2$ pattern corresponds to the layered structure with R3m. All the patterns shown are corresponding to $\lambda = 1.78897$ Å.

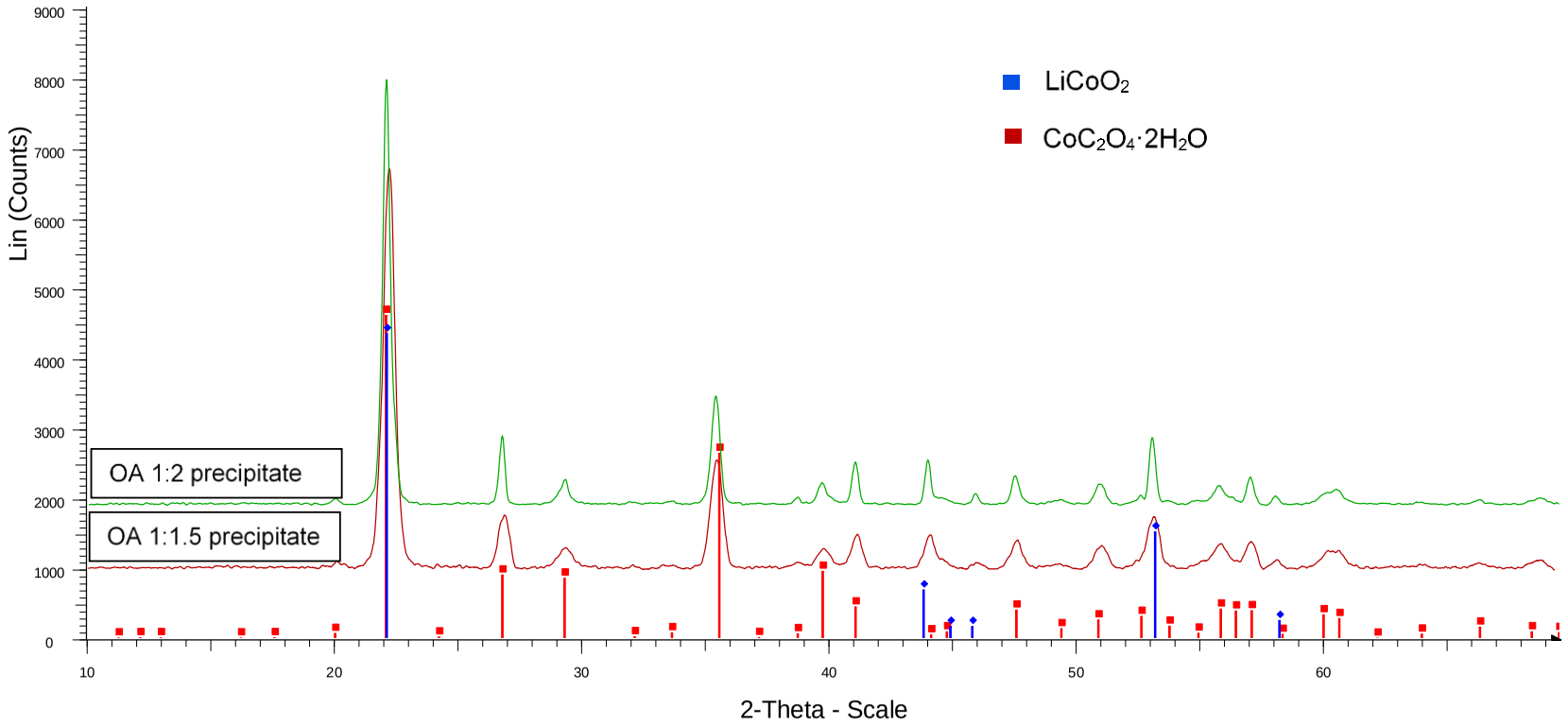

Figure 14. XRD pattern of recovered solid precipitate during extractions. The XRD pattern of $CoC_2O_4 \cdot 2H_2O$ is monoclinic structure with P21/n space group and 110° being the major peak at d-spacing of 3.633 Å. $LiCoO_2$ pattern corresponds to the layered structure with R3m space group. All the patterns shown are corresponding to $\lambda = 1.78897$ Å.

The metal extraction kinetics and yield are shown in Figure 12a. The Li metal extraction kinetics for AHO is slower than for the OA (Co:OA 1:4), and the metal extraction efficiency only reached about 90 wt% after 5 h. Another important difference between the AHO and OA extractions (Co:OA 1:4) was the physical appearance of the aqueous phase. The aqueous phase from the AHO extractions had a dark pink color (Figure 15) due to the 25 wt% of Co dissolved in the solution. The higher concentration of Co in the aqueous phase for the AHO extraction required an additional Co precipitation step for the complete separation. This precipitation process is discussed in Chapter 4.

The higher concentration of Co in the aqueous phase is a result of the complexation of $CoC_2O_4 \cdot 2H_2O$, as shown in Eq. 2.6. Also, in the Co:OA 1:1.5 and Co:OA 1:2 extractions, a significant amount of Co was measured in the aqueous phase, as shown in Figure 12a. Therefore, to develop a better understanding, the pH of both OA and AHO extractions were measured as a function of time and plotted as shown in Figure 12b. It is apparent that the amount of Co dissolved in the aqueous phase via $CoC_2O_4 \cdot 2H_2O$ complexation is a function of the pH. This experimental observation supports our claim that at higher acidity (pH > 4.2), $C_2O_4^{2-}$ is the predominant oxalate species in the aqueous phase, which forms soluble cobalt complexes ($CoC_2O_4 \cdot 2H_2O$) consisting of anions such as $Co(C_2O_4)_2^{2-}$ and $Co(C_2O_4)_3^{4-}$.[11,150]

2.5.5. Importance of pH in the Efficient Li and Co Separation

It is apparent from Figures 12a and 12b that the lower the pH or higher the acid concentration, the more efficient the separation between Li and Co. However, using a concentrated acid will increase the total operating cost for the process; therefore, the effect of pH on the dissolution of Co in the aqueous phase was studied by spiking the pH with acid and base during the extractions. During the Co:OA 1:4 extraction, 0.5 g of NaOH (in pellets form) was added to

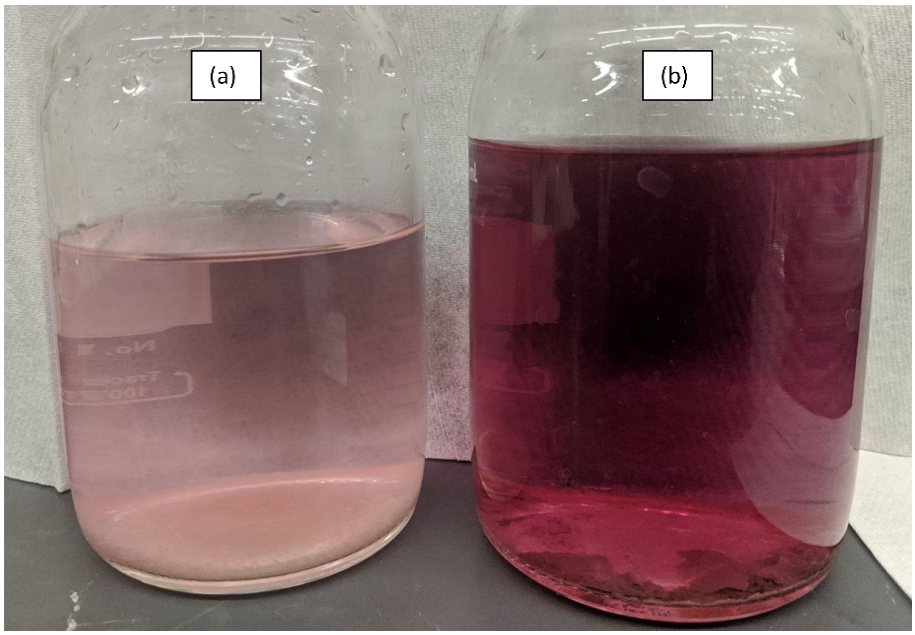

Figure 15. Physical appearance of the filtrate recovered in extractions from (a) oxalic acid (Co:OA 1:1.5) and (b) ammonium hydrogen oxalate (Co:AHO 1:4).

the reactant at 1.3 h as shown in Figure 16a. Due to the addition of a base, the pH increased from 1.5 to 3.5, and the Co concentration in the aqueous phase increased from around 2 wt% to 20 wt% within one hour, which provides evidence of the sensitivity of cobalt oxalate complexation to the pH of digestion. Oxalic acid was also added to the 1:4 Co:AHO digestion, and similarly, Co concentration in the aqueous phase decreased, as shown in Figure 2b. The AHO digestion shown in Figure 16b had an initial Co to oxalate molar ratio of 1:2.2 and a pH of 2.5, which increased to a pH of 4.75 in 3 h with a concentration of 80 wt% of Li and 20 wt% of Co in the aqueous phase. Upon addition of 0.5 g of OA, the pH decreased to 3.5 and immediately dissolved Co from the cobalt oxalate complexation began to precipitate, which reduced the concentration in the aqueous phase to 10 wt%. The extractions were continued for an additional 4 h and as additional protons were consumed, the pH of the aqueous phase increased again, leading to an increase in the Co concentration in the solution. Overall, from both Figures 16a and 16b, it is apparent that to minimize the cobalt oxalate complexation, a pH < 2.5 is required, which results in an efficient

separation of Li and Co after extraction from $LiCoO_2$. Similar pH-dependent metal oxalate chemistry is expected if other cathodic materials containing Ni and Mn as active metals are treated with oxalate reagents.[150,156] The $LiCoO_2$ in the presence of AHO and a Co to oxalate molar ratio of 1:4, 20 to 23 wt% of the Co was extracted into the aqueous phase. In order to separate additional Co, the pH was reduced using both OA and H_2SO_4. In both cases, pure $CoC_2O_4 \cdot 2H_2O$ precipitated from the filtrate providing an additional method for recovery of Co from the aqueous solution.

2.5.6. Mechanistic Insights and the Identification of an Intermediate

In all the extractions experiments of Li and Co from $LiCoO_2$ in both OA and AHO, the aqueous phase turned green within about 30 to 45 mins after starting the digestion and then slowly became light pink (OA) to dark pink (AHO) in color as the extraction proceeded towards completion. To identify the intermediate and final species present in the aqueous phase, absorbance was measured in the visible region, as shown in Figure 17. For the green-colored intermediate, peaks at 400 nm and 600 nm were observed whereas for the final pink-colored aqueous phase, peaks at 520 nm and 650 nm were observed. Adamson and Sporer report that the maximum absorbance peaks of a 0.1 M $K_3[Co(C_2O_4)_3]$ solution at 420 and 605 nm.[2,158] Although the peaks are slightly shifted, the similar green colored solution and the possibility of a Co^{3+} ion complexation suggests the formation of a $[Co(C_2O_4)_3]^{3-}$ intermediate at 30 to 45 mins. The peak shift for maximum absorbance was attributed to the difference in the cation, which can lead to a higher energy gap between the bonding and antibonding orbital of $Li_3[Co(C_2O_4)_3](aq)$ compared to the energy gap in $K_3[Co(C_2O_4)_3](aq)$. Concerning the final pink-solution, Co^{2+} ion is reported to have a maximum peak absorption at a wavelength of 520 nm.[159,160] In the work by Majumdar et al., electronic absorption spectra of Co^{2+} in $[(CH_3)_3NH]CoCl_3 \cdot 2H_2O$ were reported with two peaks

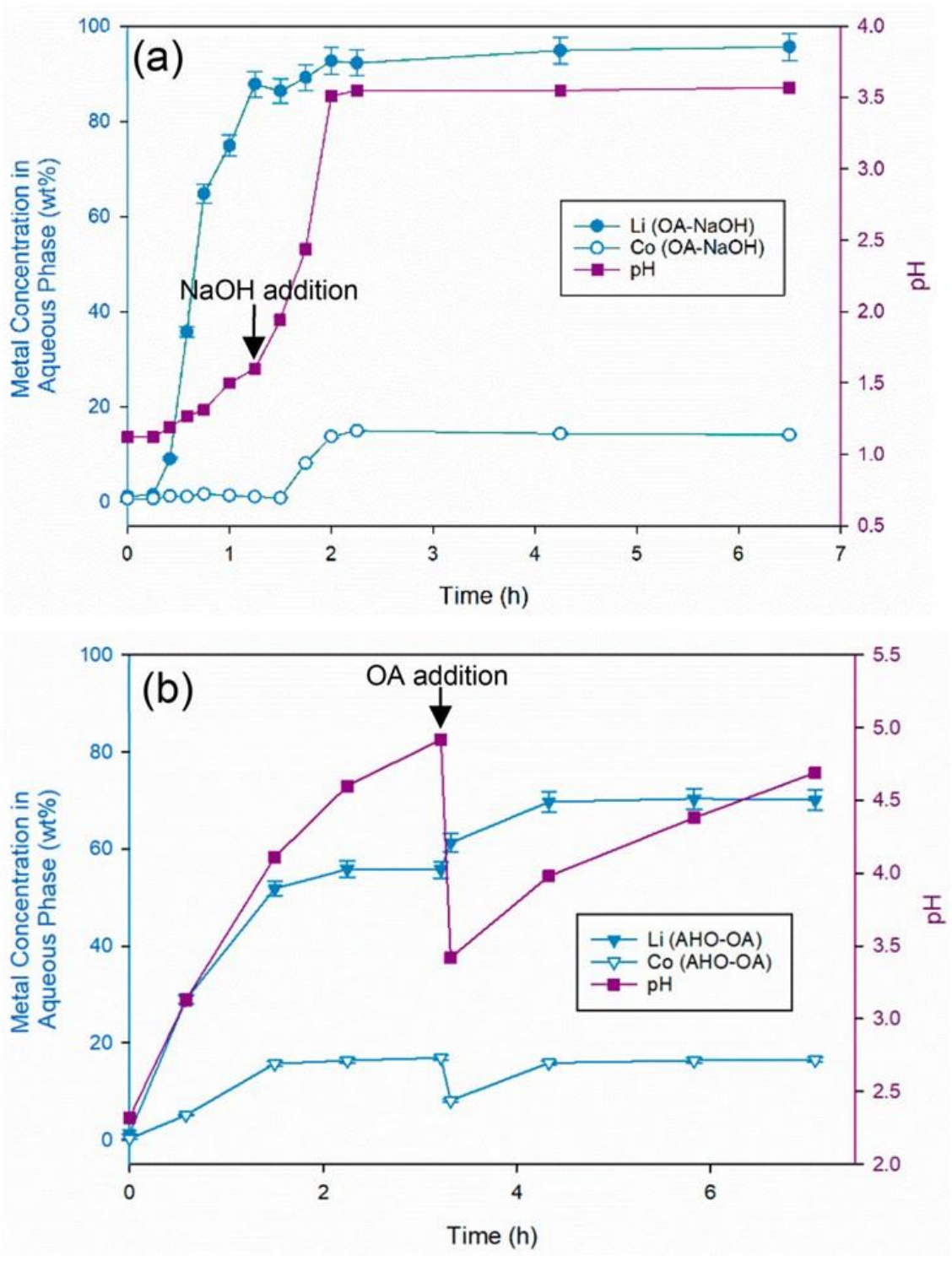

Figure 16. Impact of pH on Li and Co metal concentration as a function of time in the aqueous phase at T = 100 °C, S/L = 15 g/L, and agitator speed = 600 rpm for **(a)** the addition of NaOH at Co:OA ratio of 1:4 and **(b)** the addition of OA at Co:AHO ratio of 1:2.2.

at the wavelengths of 520 nm and 610 nm.[161] Hence, the information from the earlier work supports the formation of a Co^{2+} complex upon the dissolution of $CoC_2O_4 \cdot 2H_2O$ in excess $C_2O_4^{2-}$ anion. The final Co(II)-oxalate complexes imparting a pink color to the solution is due to the formation of $[Co(C_2O_4)_2]^{2-}$ and $[Co(C_2O_4)_3]^{4-}$species in the aqueous phase.

These observations and measurements support that the reaction between $LiCoO_2$ and oxalate reagents begins with the extraction of Co^{3+}, followed by the reduction to Co^{2+} with oxidation of the $C_2O_4^{2-}$ anion into CO_2 (Eqs. 2.6 and 2.7) followed by Co^{2+} precipitating in the form of $CoC_2O_4 \cdot 2H_2O$. In addition, the extraction, reduction, and precipitation processes are assumed to be simultaneous and fast because the Co concentration in the aqueous phase remains low. The XRD patterns of the solid phase, which was withdrawn from the reactor during the extraction, are shown in Figure 18 and indicate that $CoC_2O_4 \cdot 2H_2O$ precipitates from the reaction even at an early time (i.e., $t \leq 30$ min).

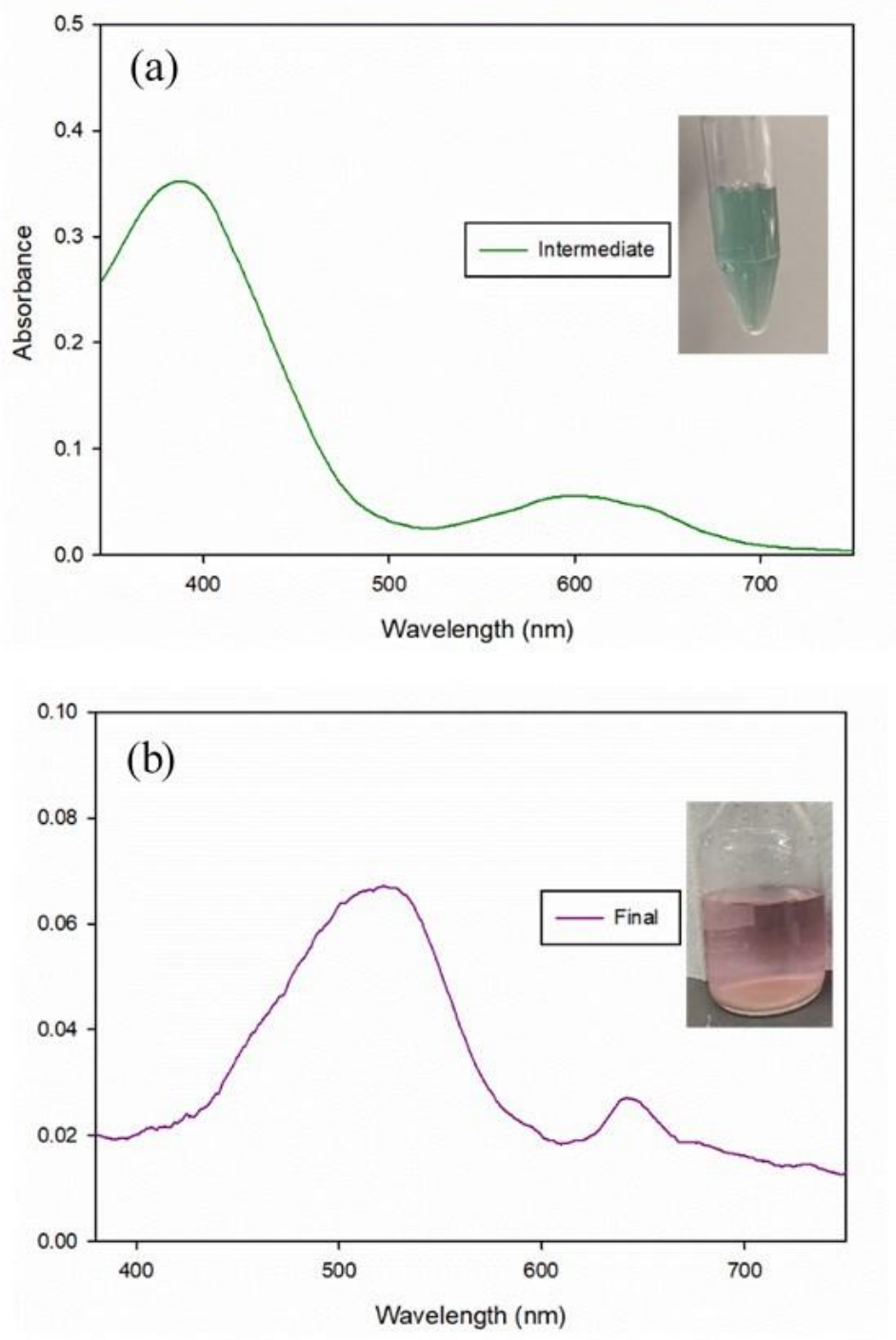

Figure 17. Absorbance measurement for the aqueous phase at 30 min **(a)** and at the end **(b)** for Co:OA 1:1.5 extraction experiment

.

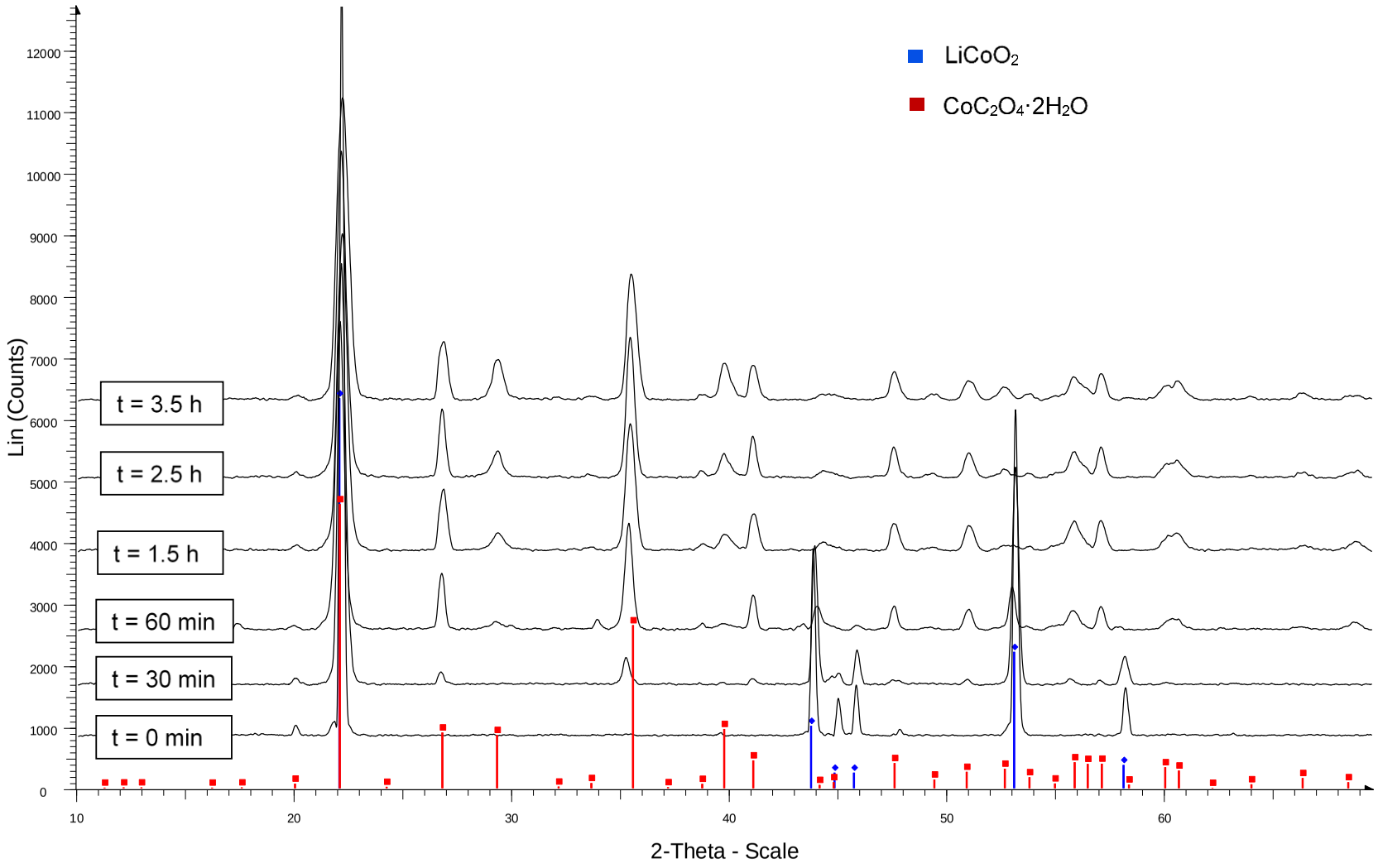

Figure 18. XRD pattern of solid phases withdrawn over time during the Co:OA 1:4 digestion.
The collected XRD pattern clearly showed the final product as $CoC_2O_4 \cdot 2H_2O$ monoclinic structure with P21/n space group and 110 being the major peak at d-spacing of 3.633 Å. All the patterns shown are corresponding to $\lambda = 1.78897$ Å.

2.5.7. $LiCoO_2$ in Oxalic Acid and Hydrogen Peroxide

Extraction of Li and Co from $LiCoO_2$ using oxalic acid at a Co to oxalate molar ratio of 1:3 provides efficient recovery and separation. A 1.5 molar equivalent of $C_2O_4^{2-}$ is required for Li^+ and Co^{2+} cations as shown in Eq. 2.7. An additional 0.5 molar equivalent of $C_2O_4^{2-}$ is used for the reduction of Co^{3+}; therefore, an external reducing agent like H_2O_2, reduces the consumption of $H_2C_2O_4$. The H_2O_2 can act both as an oxidizing agent and a reducing agent, as shown in Eqs. 2.9 and 2.10.[10,66,67]

$$H_2O_2 \text{ Reduction: } H_2O_2 + 2H^+ + 2e^- \rightleftharpoons 2H_2O \qquad E^0 = 1.763 \text{ V} \qquad (2.9)$$

$$H_2O_2 \text{ Oxidation: } H_2O_2 \rightleftharpoons O_2 + 2H^+ + 2e^- \qquad E^0 = -0.68 \text{ V} \qquad (2.10)$$

Based on the standard potentials shown in Eqs. 2.9 and 2.10, it is evident that the H_2O_2 reduction is thermodynamically more feasible than the oxidation. Based on these potentials, even if the H_2O_2 oxidation is coupled with a feasible Co^{3+} to Co^{2+} reduction, the H_2O_2 reduction will still occur; therefore, an excess of H_2O_2 was used in order to provide a sufficient amount of reducing agent for converting the available Co^{3+} into Co^{2+}.

To determine the optimum amount of H_2O_2 required, the Co to oxalate molar ratio was kept constant at 1:1.5, and the Co to H_2O_2 molar ratio was varied from Co:OA:H_2O_2 1:1.5:0 to 1:1.5:3. The Li extraction for the Co:OA:H_2O_2 1:1.5:3 case, reached 95 wt% after 3 h, whereas in the Co:OA:H_2O_2 1:1.5:0 and Co:OA:H_2O_2 1:1.5:2 cases, the Li extraction reached about 67 wt% and 78 wt%, respectively as shown in Figure 19. The Co:OA:H_2O_2 1:1.5:3 extraction had a 1:3 Co to H_2O_2 molar ratio, which was enough for efficiently extracting Li from the starting cathodic material. For the Co:OA:H_2O_2 1:1.5:3 case, the lowest amount of Co (< 4 wt%) was dissolved in the aqueous phase, resulting in an efficient one-step separation of Li and Co.

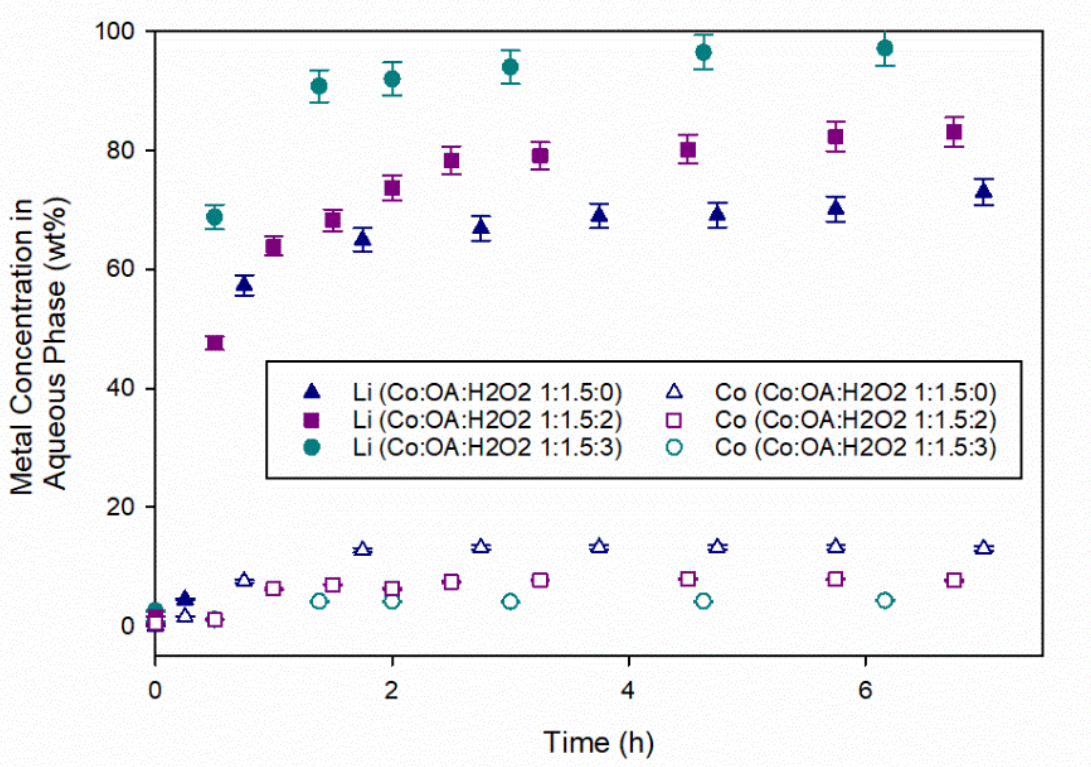

Figure 19. Li and Co metal concentration as a function of time in the aqueous phase using OA and H_2O_2 at Co:OA:H_2O_2 ratios from 1:1.5:0 to 1:1.5:3 at T = 100 °C, S/L = 15 g/L, and agitator speed = 600 rpm.

2.5.8. $LiCoO_2$ in Sodium Hydrogen Oxalate and Potassium Hydrogen Oxalate

The alkali metal hydrogen oxalates like $NaHC_2O_4$ (NaHO) and KHC_2O_4 (KHO) can be synthesized using the respective oxalate compounds ($M_2C_2O_4$) and $H_2C_2O_4$ as shown in Eq. 1.2. In comparison to the AHO, NaHO and KHO have a higher operating pH because of the increased cation size. As discussed in Section 2.5.5, a high operating pH during the Li and Co extraction from $LiCoO_2$ will lead to a higher amount of Co being dissolved in the aqueous phase. The extraction kinetics will also be slower as the H^+ concentration plays a significant role in initiating the extraction process by weakening the Co-O bond present in $LiCoO_2$. To confirm the importance of H^+, a metal extraction was attempted with only $Na_2C_2O_4$ as the reagent. In this experiment, no Li and Co were leached in the aqueous phase. Because of the higher operating pH that results in

low H^+ concentration, the metal extractions using KHC_2O_4 and $NaHC_2O_4$ were not preferred for $LiCoO_2$.

2.6. Conclusions

In summary, critically important metals, such as Li and Co, can be recovered efficiently from spent $LiCoO_2$ cathodes of LiBs using an environmentally-friendly process based on oxalate chemistry. In this work, a thorough investigation was conducted to understand the effect of important reaction parameters for Li and Co separation using oxalic acid and ammonium hydrogen oxalate. To achieve an efficient separation between Li and Co using oxalate chemistry, the acidity during the digestion should be below a pH of 2.5 to avoid the complexation and dissolution of $CoC_2O_4 \cdot 2H_2O$. To minimize the use of oxalic acid, an external reducing agent like hydrogen peroxide can be added, which slows the $CoC_2O_4 \cdot 2H_2O$ precipitation. However, the Li and Co extractions using hydrogen oxalate reagents like ammonium hydrogen oxalate may not be suitable because of poor separation efficiency between Li and Co. To gain mechanistic insight into the Co extraction and precipitation, green-colored intermediate from the aqueous phase was isolated and identified as $[Co(C_2O_4)_3]^{3-}$. From this investigation, the Co^{3+} extraction, reduction to Co^{2+}, and further precipitation were confirmed to occur simultaneously. A current challenge for commercializing this chemistry is the development of an efficient, cost-effective process for the recovery and recycling of oxalate and preferably oxalic acid. The discussions around the Li precipitation and oxalate recovery will be covered in future chapters. This simple and novel process using oxalic acid provides an efficient, sustainable, and environmentally-friendly route for recovering and separating critical and precious metals such as Li and Co. This sustainable oxalate-based process chemistry can also be applied to a number of other mixed metal oxide sources like

bauxite and ilmenite ores and other types of spent LiBs cathodes for metals recovery and separation, as shown in future chapters.

Chapter 3. An Improved Oxalate Process for Recycling of Lithium-ion Batteries Cathode

Portions of this chapter are adapted from the following published article:

Verma, A., Corbin, D.R., & Shiflett, M.B., Lithium and Cobalt Recovery for Lithium-Ion Battery Recycle using an Improved Oxalate Process with Hydrogen Peroxide. *Hydrometallurgy* **2021**, 105694

Chapter 3

"Discovery consists of seeing what everybody has seen and thinking what nobody has thought."
- *Albert Szent-Györgyi (Biochemist, Nobel Prize Winner)*

3.1. Abstract

Lithium cobalt oxide ($LiCoO_2$) is the first and most commercially successful form of layered transition metal oxide cathode used in lithium-ion batteries (LIBs). Recycling $LiCoO_2$ cathode is critical for stabilizing the Li and Co economy. In this work, a kinetic investigation of a closed-loop oxalate-based process for recovery and separation of Li and Co from $LiCoO_2$ has been developed. Metal extraction from $LiCoO_2$ is a non-catalytic solid-liquid reaction with both solid and aqueous products. To understand the kinetics and identify the rate-limiting mechanism, a combined shrinking core model (cSCM) was used for $LiCoO_2$ digestions. $LiCoO_2$ in the presence of aqueous oxalic acid ($H_2C_2O_4$) at the optimum concentration of 0.46 M and 100 °C, resulted in efficient extraction and separation of Li and Co. Diffusion of $H_2C_2O_4$ into $LiCoO_2$ occurs through a product layer of cobalt oxalate dihydrate ($CoC_2O_4 \cdot 2H_2O$) that forms on the surface, and this process was identified as rate-limiting. The $CoC_2O_4 \cdot 2H_2O$ was precipitated in a micro-rod morphology when 0.46 M hydrogen peroxide (H_2O_2) was added along with 0.23 M $H_2C_2O_4$ and the reaction was carried out at a temperature of 55-75 °C. In this case, the chemical reaction at the $LiCoO_2$ surface was identified as the rate-limiting step. Addition of H_2O_2 results in a 33% reduction in the overall activation energy, a 50% reduction in energy consumption, and a 13% reduction in the cost of reagents. This work signifies the importance of a cost-effective, environmentally-friendly, and energy-efficient process for recovering critical metals such as Li and Co from spent LIB cathodes.

3.2. Introduction

Oxalic acid has tremendous potential for developing environmentally-friendly critical metal recovery processes. The oxalate anion ($C_2O_4^{2-}$), which is a bidentate ligand, can donate two pairs of electrons to a metal ion.[150] The oxalate anion chelating properties can easily form complexes with many of the critical metal ions with varying degrees of solubility in water. This difference in water solubility plays a major role in the separation and recovery of Li and Co from used $LiCoO_2$ cathodes. The lithium oxalate ($Li_2C_2O_4$) is soluble in water while the cobalt oxalate dihydrate ($CoC_2O_4 \cdot 2H_2O$) is insoluble. This difference in oxalate solubilities allows for an efficient and easy solid-liquid separation of Li and Co using a hydrometallurgical extraction process.[150,162] To reuse Co in the manufacturing of LiBs, battery-grade Co with >99.9% purity needs to be the final product of a recycling process.[163] A one-step metal separation and precipitation process during the extraction increases the possibility of producing a battery-grade purity for the final products. The reaction conditions, mechanism, and the economics for an oxalate-based process for separation and recovery of Li and Co from $LiCoO_2$ were discussed in detail in Chapter 2.[162]

Leaching kinetics for the metals in hydrometallurgical processes can identify the mechanism of metal extraction and elucidate the interaction between aqueous reactants and the reacting solid. This is the first study of the Li extraction mechanism from $LiCoO_2$ in aqueous $H_2C_2O_4$ (OA). Metal extraction from $LiCoO_2$ falls under the classification of a non-catalytic solid-liquid (S-L) reaction with solid and aqueous products. This type of system involves five mechanistic steps: (1) diffusion of the oxalate reactant through the aqueous film and porous product layer surrounding the solid particle, (2) adsorption of the oxalate reactant at the solid reacting core surface, (3) chemical reaction with the solid reacting core, (4) desorption of the

product from the solid surface, and (5) diffusion of the product from the solid surface through the porous product layer (product and inert reactant) and aqueous film. Among these consecutive steps, if one of the steps is slower than the others, that step becomes rate-limiting. $LiCoO_2$ is a low-porosity material, which makes it impervious to the aqueous oxalate reactant, and as such the reaction begins at the solid surface and a product layer forms at the interface between the solid surface and the aqueous reactant layer. This confines the reaction zone to the interface between the unreacted solid surface and the porous product layer. For such cases, the shrinking core model developed by Yagi and Kunii can be applied.[164]

The shrinking core model (SCM) has been previously applied by other researchers to investigate the metal extraction kinetics for cathodic materials using various acids. For example, Gao et al. evaluated the metal extraction kinetic mechanism of a spent $LiNi_{0.33}Mn_{0.33}Co_{0.33}O_2$ (NMC) cathode with acetic acid. The group identified the rate-limiting step to be the ion diffusion in the residue layer.[165] SCMs have also been used by Yuliusman et al. and Takacova et al. to understand the kinetic mechanism of metal extraction for spent $LiCoO_2$ cathodes with nitric and sulfuric acid, respectively.[166,167] In addition, SCMs have been used to understand the leaching of lead from galena with ferric chloride in sodium chloride solutions and nickel from spent NiO/alumina catalyst in sulfuric acid.[168,169] In this work, to understand the Li extraction kinetics from $LiCoO_2$ using aqueous $H_2C_2O_4$ (both with and without H_2O_2), a SCM was used to guide the fundamental understanding of the mechanism and determine the rate-limiting step. To the best of our knowledge, no kinetic study of $LiCoO_2$ using aqueous $H_2C_2O_4$ (with or without H_2O_2) has been performed to understand the S-L interfacial phenomenon. This kinetic study is a continuation of the work in Chapter 2 and provides a detailed kinetic model for Li and Co extraction from $LiCoO_2$ using $H_2C_2O_4$ and $H_2C_2O_4 + H_2O_2$.

3.3. Metal Extraction Study and Kinetics Measurement

Hydrometallurgical experiments were carried out using aqueous $H_2C_2O_4$ or $H_2C_2O_4 + H_2O_2$ by adding $LiCoO_2$ after reaching the setpoint temperature. The molar ratio between $LiCoO_2$ and $C_2O_4^{2-}$ is important and was set at 1:3 (in the absence of H_2O_2) based on an optimization study from Chapter 2.[162] Solid-to-liquid (S/L) ratio is also an important parameter that indicates the amount of solid $LiCoO_2$ added to the aqueous reagent solution. For the experiments in this work, the S/L ratio was 15 g/L; therefore, to maintain a $LiCoO_2$ to $C_2O_4^{2-}$ molar ratio of 1:3, 0.46 M of $H_2C_2O_4$ was required. When using an additional reducing agent such as H_2O_2 in combination with $H_2C_2O_4$, a $LiCoO_2$ to $C_2O_4^{2-}$ molar ratio of 1:1.5 was required with a $LiCoO_2$ to H_2O_2 molar ratio of 1:3. This corresponds to a concentration of 0.23 M $H_2C_2O_4$ and 0.46 M H_2O_2 to maintain a S/L ratio of 15 g/L.

3.3.1. Materials

Commercial-grade lithium cobalt oxide ($LiCoO_2$, Sigma-Aldrich 99.8%), $H_2C_2O_4 \cdot 2H_2O$ (99.5%, Acros Organics), H_2O_2 (30 wt %, Fisher Chemical), and deionized water were used for the hydrometallurgical experiments.

3.3.2. Characterization

The aqueous phase metal concentrations were measured using a Varian/Agilent 725 ES inductively coupled plasma - optical emission spectrometer (ICP-OES). Solid samples were characterized on a Bruker D2 phaser powder X-ray diffraction (PXRD) with a Co Kα radiation source ($\lambda = 1.78897$ Å). The source voltage and current were set at 30 kV and 10 mA, respectively. For probing the solid phase morphology, a FEI 3D Dual Beam scanning electron microscope (SEM) was used. To identify the oxidation state of Co on the surface of solid particles, an X-ray photoelectron spectrometer (XPS) (PHI 5000 VersaProbe II) operating under ultrahigh vacuum (1

$\times 10^{-9}$ bar) with an AlKα X-ray source and a monochromator was used. The X-ray beam size was 100 μm, and survey spectra were recorded with a pass energy (PE) of 117 eV, step size of 1 eV, and a dwell time of 20 ms.

The tapped density for the solids was measured by filling a graduated cylinder with a known amount of material. The filled cylinder was gently tapped multiple times with an initial height of 5 cm to standardize the measurement. The final volume occupied by the solids was measured to calculate the tapped density. The tapped density measurement was repeated five times, and the average has been reported.

3.3.3. Shrinking-Core Model: Fundamentals

The digestion of $LiCoO_2$ with aqueous $H_2C_2O_4$ is shown by Eq. 3.1, where Li and Co are separated into aqueous ($Li_2C_2O_4$) and solid phases ($CoC_2O_4 \cdot 2H_2O$), respectively.[162] $LiCoO_2$ is a layered intercalated material where Li and Co occupy the octahedral sites in alternating layers and form a hexagonal symmetry.[170] The Co extraction process involves the chelation and subsequent reduction of the Co^{3+} ion resulting in the precipitation of a stable $CoC_2O_4 \cdot 2H_2O$. The redox equations involved in this process are summarized in Eqs. 3.2 and 3.3

$$4H_2C_2O_4(aq) + 2LiCoO_2(s) \leftrightarrows Li_2C_2O_4(aq) + 2CoC_2O_4 \cdot 2H_2O(s) + 2CO_2(aq) \quad (3.1)$$

$$\text{Cobalt Reduction: } Co^{3+} + e^- \rightleftharpoons Co^{2+} \qquad E^0 = 1.92 \text{ V} \qquad \Delta G° = -185.25 \text{ kJ} \quad (3.2)$$

$$\text{Oxalate Oxidation: } C_2O_4^{2-} \rightleftharpoons 2CO_2 + 2e^- \qquad E^0 = 0.49 \text{ V} \qquad \Delta G° = -94.55 \text{ kJ} \quad (3.3)$$

As discussed previously, the Li extraction from $LiCoO_2$ using aqueous $H_2C_2O_4$ can be classified as a non-catalytic S-L reaction with solid (e.g., $CoC_2O_4 \cdot 2H_2O$) and aqueous (e.g., $Li_2C_2O_4$) products. A combined shrinking core model (cSCM) was developed to understand the kinetics and identify the rate-limiting step for Li extraction while the solid product ($CoC_2O_4 \cdot 2H_2O$) is forming on the surface of the $LiCoO_2$. In cSCM, the $LiCoO_2$ particles are assumed spherical

with a diameter that decreases with time, and the $CoC_2O_4 \cdot 2H_2O$ layer is assumed to form uniformly around the core. The consumption of $LiCoO_2$ as the reaction progresses depicts the shrinking core. The formation of an inert $CoC_2O_4 \cdot 2H_2O$ layer around the spherical shrinking core resembles an ash-layer model. The shrinking core and formation of an inert product layer simultaneously during leaching can be modeled using the cSCM. The SCM originally derived by Yagi and Kunii, describes the rate of Li extraction as being limited by the slowest of the three simultaneous kinetic processes occurring during the extraction: (1) diffusion of the $H_2C_2O_4$ within the liquid film surrounding the particle, (2) diffusion of the $H_2C_2O_4$ through the $CoC_2O_4 \cdot 2H_2O$ product layer formed around the core, or (3) chemical reaction of the $H_2C_2O_4$ with $LiCoO_2$ at the surface of the core.[164] To identify the rate-limiting step, the kinetic model was fitted to the experimental data, and the controlling mechanism was defined by the model that best fits the data. Several researchers have used this method to investigate the kinetics of hydrometallurgical processes;[165-167] however, this method of fitting individual kinetic models has certain drawbacks. For example, the correlation coefficients of different kinetic models are often similar and as a result, the wrong rate-limiting step might be identified. Also, fitting individual kinetic models prevents the identification of a mixed control mechanism that is possible in numerous hydrometallurgical systems. To overcome these deficiencies, a cSCM was developed:[153,168]

$$t = \tau_R \left[1-(1-X)^{\frac{1}{3}}\right] + \tau_P \left[1-3(1-X)^{\frac{2}{3}} +2(1-X)^{\frac{1}{3}}\right] + \tau_F X \qquad (3.4)$$

where, τ_R is the time required for complete conversion under the chemical reaction control model, τ_P is the time required for complete conversion under the diffusion through product layer control model, and τ_F is the time required for complete conversion under the diffusion through film layer control model. The variables (τ_R, τ_P and τ_F) can be used as the constants for the individual kinetic

models and X is the fraction of Li extracted at time *t*. The individual kinetic models were developed by Yagi and Kunii.[164]

The X versus time data were collected experimentally and the model parameters were fit using the method of least squares. The method of least squares and the standard error calculations for the cSCM are described in the Section A.3. (Appendix). In some cases, only one rate-limiting mechanism was found (i.e., only one fitting parameter was nonzero) and in other cases, a mixed-control mechanism (i.e., more than one fitting parameter was nonzero) fit the experimental data best. The cSCM model eliminates the need to fit individual kinetic models and can help identify mixed-control mechanisms.

3.3.4. $LiCoO_2$ in aqueous $H_2C_2O_4$ as a function of temperature

To investigate the kinetics and identify the rate-limiting step for Li extraction, $LiCoO_2$ was digested in aqueous $H_2C_2O_4$ at temperatures of 65°C, 75 °C, 85 °C, and 100 °C as shown in Figure 20. The experimental Li extraction kinetics at different temperatures were fitted with the cSCM model shown in Eq. 3.4. The model parameters that provided the best fit are shown in Table 11, along with the standard regression error. The nonzero value for τ_P indicates that the digestion of $LiCoO_2$ at temperatures between 65 °C and 100 °C is limited by the diffusion of $H_2C_2O_4$ through the solid product layer of $CoC_2O_4 \cdot 2H_2O$. It should also be noted that the sum of the model parameters ($\tau_R + \tau_P + \tau_F$) indicate the time required for Li conversion (X) to reach complete extraction (X = 1). The decreasing τ_P value with increasing temperature, as shown in Table 11, agrees with the expected result of a faster rate at higher temperatures. The identification of the rate-limiting step as the diffusion of $H_2C_2O_4$ through the $CoC_2O_4 \cdot 2H_2O$ product layer suggests a shell-core model for modeling the digestion. In order to confirm this hypothesis, the agitation speed was varied to eliminate bulk diffusion limitations.

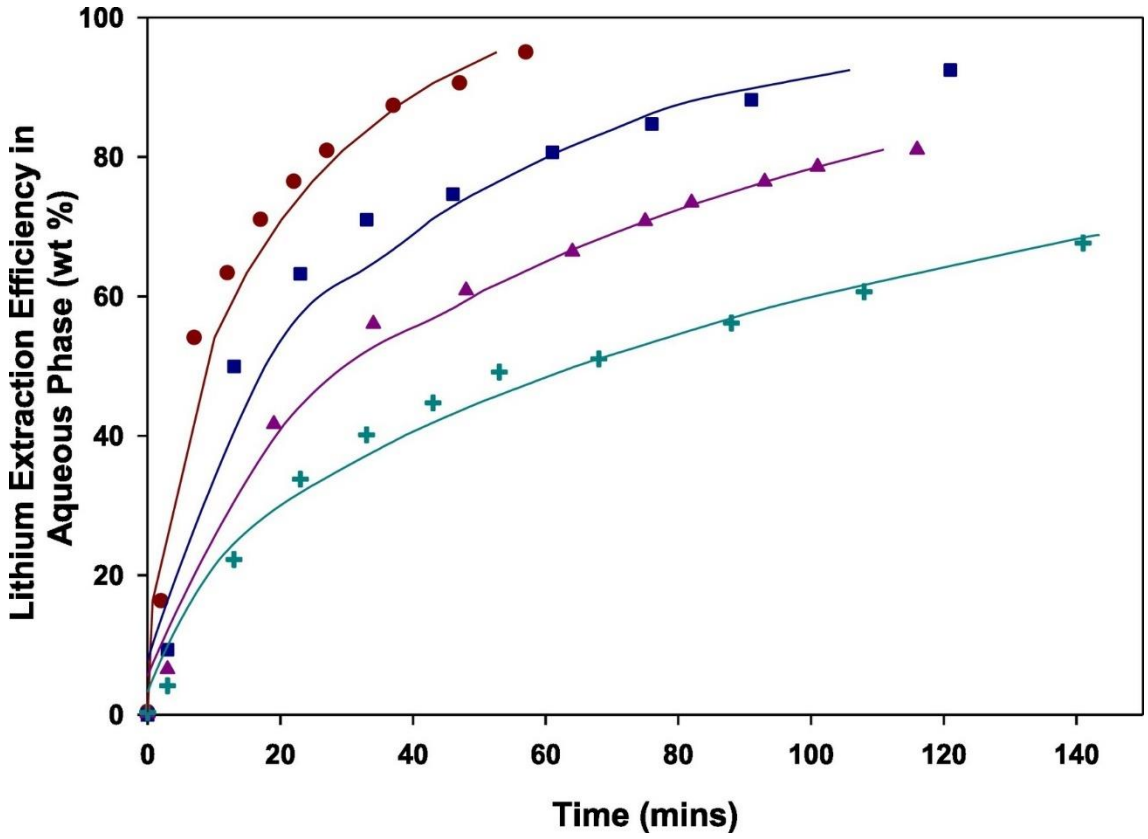

Figure 20. Li extraction efficiency as a function of time in the aqueous phase at Co:OA ratio = 1:3, S/L = 15 g/L, agitation speed = 600 rpm, and various temperatures (65 °C - +; 75 °C - ▲; 85 °C - ■ and 100 °C - ●). Each spline curve corresponds to the best fit.

Table 11. Model parameters for the cSCM shown in Figure 20.

Temperature (°C)	Model parameters for the best fit			Standard Error (min)	Apparent Rate Constant (min^{-1}) $\left(\frac{1}{\tau_R+\tau_P+\tau_F}\right)$
	τ_R (min)	τ_P (min)	τ_F (min)		
100	0	75.7	0	3.4	0.013
85	0	160.8	0	6.9	0.0062
75	0	284.8	0	3.7	0.0035
65	0	587.2	0	5.7	0.0017

3.3.5. $LiCoO_2$ in aqueous $H_2C_2O_4$ as a function of agitation speed

The Li extractions shown in Figure 20 were run at an agitation speed of 600 rpm. In order to evaluate whether any bulk diffusion limitations occur in the extraction reactor, agitation speed was varied from 125 to 875 rpm, as shown in Figure 21. An optimum agitation speed is required to ensure uniform concentration and temperature of the aqueous reactant. The bulk diffusion limitation can arise from the concentration gradient present in the aqueous reactant phase. The other operating parameters (Co:OA molar ration = 1:3, S/L ratio of 15 g/L, and T = 90 °C) were kept constant. The Li extraction kinetics at speeds above 200 rpm were the same confirming that there were no bulk diffusion effects. Greater than 90 wt% of the Co was present in the solid phase as $CoC_2O_4{\cdot}2H_2O$ with less than 5 wt% of Co present in the aqueous phase. The average τ_P was 101.76 ± 2.69 min for the cSCM model fit to the Li digestion kinetics over the range of agitation speeds from 200 to 875 rpm as shown in Figure 21 and Table 12. The other model parameters (τ_R and τ_F) were essentially zero indicating the rate-limiting step to be the diffusion of $H_2C_2O_4$ through the $CoC_2O_4{\cdot}2H_2O$ layer. The minor differences in τ_P values at agitation speeds higher than 200 rpm confirm the only rate limitation is due to the slow diffusion of $H_2C_2O_4$ through the $CoC_2O_4{\cdot}2H_2O$ product layer. Even at a low speed of 125 rpm, τ_P was the only non-zero parameter with a value of 189 min. The higher value of τ_P at the lowest speed (125 rpm) indicates the presence of an additional bulk diffusion limitation because of inefficient mixing. This hypothesis was also tested by starting with an agitation speed of 125 rpm and then increasing the speed to 600 rpm after about 0.75 h (★ data points in Figure 21). The Li extraction kinetics followed the 125 rpm kinetics initially and, after increasing the speed, followed the same kinetics as the 600 rpm experimental data. This confirms the presence of a bulk diffusion limitation along with the resistance from the solid $CoC_2O_4{\cdot}2H_2O$ product layer for the diffusion of $H_2C_2O_4$ at the low speed

of 125 rpm. The bulk diffusion limitation in the reactor can be eliminated by operating at an agitation speed above 200 rpm.

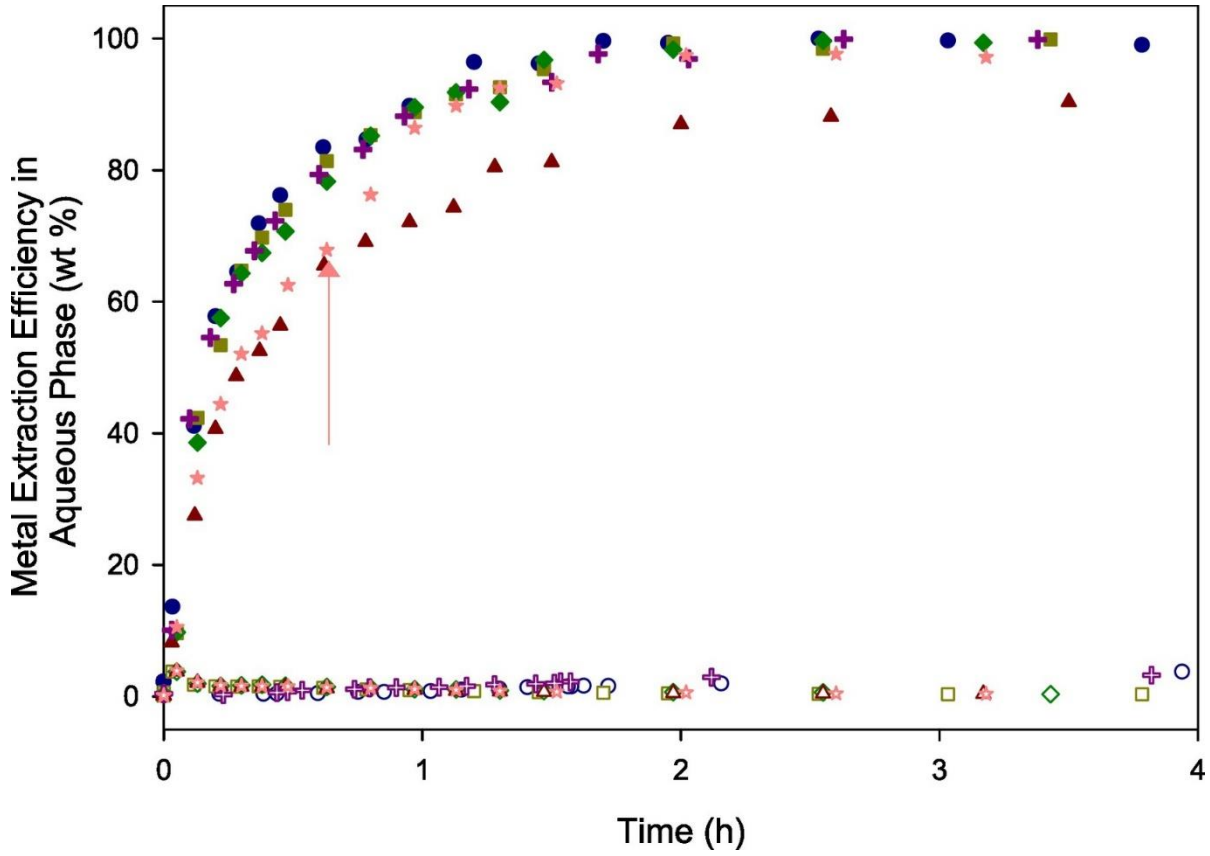

Figure 21. Metal extraction efficiency as a function of time in the aqueous phase at Co:OA ratio = 1:3, S/L = 15 g/L, various agitation speeds (125 rpm, Li - ▲, Co - △; 200 rpm, Li - ◆, Co - ◇; 350 rpm, Li - ■, Co - □; 600 rpm, Li - ●, Co - ○; 875 rpm, Li - ✚, Co - ✙; 125 to 600 rpm, Li - ★, Co - ☆) and *T* = 90 °C. Arrow indicates t = 0.75 h when agitation speed was increased from 125 rpm to 600 rpm.

Table 12. Model parameters for the cSCM shown in Figure 21.

Agitation Speed (rpm)	Model parameters for the best fit			Standard Error (min)	Apparent Rate Constant (min^{-1}) $\left(\frac{1}{\tau_R+\tau_P+\tau_F}\right)$
	τ_R (min)	τ_P (min)	τ_F (min)		
875	0	102.1	0	3.1	0.0098
600	0	98.1	0	3.7	0.010
350	0	101.2	0	4.2	0.0098
200	0	105.6	0	3.5	0.0095
125	0	189.1	0	4.9	0.0053
125/600	0/0	192.5/103.7	0/0	-	-

3.3.6. Core-Shell Model

Based on the absence of any bulk diffusion limitation in the reactor, a solid intermediate consisting of a $LiCoO_2$ core with a $CoC_2O_4{\cdot}2H_2O$ shell is possible. To confirm the presence of this $CoC_2O_4{\cdot}2H_2O$ shell, PXRD and XPS were performed on the starting $LiCoO_2$ reactant (Sample A), solid intermediate withdrawn from the digestion reactor at t = 15 min (Sample B), and the solid product recovered at the end of the reaction (Sample C). These samples were taken from the metal extraction experiment of $LiCoO_2$ with aqueous $H_2C_2O_4$ at a Co:OA ratio = 1:3, S/L = 15 g/L, agitation speed = 600 rpm, and T = 100 °C.

The PXRD patterns collected for the three samples are provided in Figure 22. Sample A and Sample C were confirmed as pure $LiCoO_2$ and $CoC_2O_4{\cdot}2H_2O$, respectively. Sample B was confirmed to be a mixture of both $LiCoO_2$ and $CoC_2O_4{\cdot}2H_2O$ supporting the hypothesis that a solid intermediate layer (i.e., $CoC_2O_4{\cdot}2H_2O$ shell) forms around the $LiCoO_2$ core.

XPS has a probing depth of less than 10 nm and can provide information on the surface composition. XPS spectra, along with the peak fitting in the Co 2p region (770-815 eV), are shown in Figures 23-25. As expected, Sample B (Figure 24) and Sample C (Figure 25) showed similar

spectra in the binding energy range of 770-815 eV with Co $2p_{1/2}$ and Co $2p_{3/2}$ peaks at 797 eV and 782 eV, respectively, with their shake-up satellite peaks at approximately 5 eV above the Co 2p peaks. In sample B (solid intermediate at t = 15 minutes), $CoC_2O_4 \cdot 2H_2O$ should be the only compound present at the surface and should show signals corresponding to Co^{2+}. Sample C was confirmed as pure $CoC_2O_4 \cdot 2H_2O$, and the similar XPS spectra of Sample B and Sample C strengthened the hypothesis of a shell-core model as an intermediate. For Sample A (starting material - $LiCoO_2$) less intense shake-up satellite peaks were observed compared to the XPS spectrum of Sample B and C. This observation fits the hypothesis well because Co^{3+} (surface species in Sample A: $LiCoO_2$) does not exhibit any intense shake-up satellite features in the Co 2p spectra.[171,172]

A major impact of forming a $CoC_2O_4 \cdot 2H_2O$ shell over the $LiCoO_2$ core (Figure 26) was found for the rate-limiting step of the Li extraction kinetics. Using the cSCM, it was found that the rate-limiting step for Li extraction from $LiCoO_2$ was the diffusion of $H_2C_2O_4$ through the $CoC_2O_4 \cdot 2H_2O$ product layer. This occurs because of the high density and low porosity of the product layer formed. The average bulk density of the $CoC_2O_4 \cdot 2H_2O$ product formed from the aqueous $H_2C_2O_4$ metal extraction (Co:OA = 1:3, S/L = 15 g/L, agitation speed = 600 rpm and T = 100 °C) using the tapping method was found to be 0.82 g/mL. The rate-limiting step was identified as the diffusion of $H_2C_2O_4$ through the $CoC_2O_4 \cdot 2H_2O$ shell surrounding the $LiCoO_2$; therefore, to improve the Li extraction kinetics, a novel idea was envisioned to precipitate the solid product in a morphology with lower bulk density and higher porosity. The hypothesis assumes this would lead to faster transport of $H_2C_2O_4$ through the $CoC_2O_4 \cdot 2H_2O$ shell and reduce or eliminate these diffusion limitations.

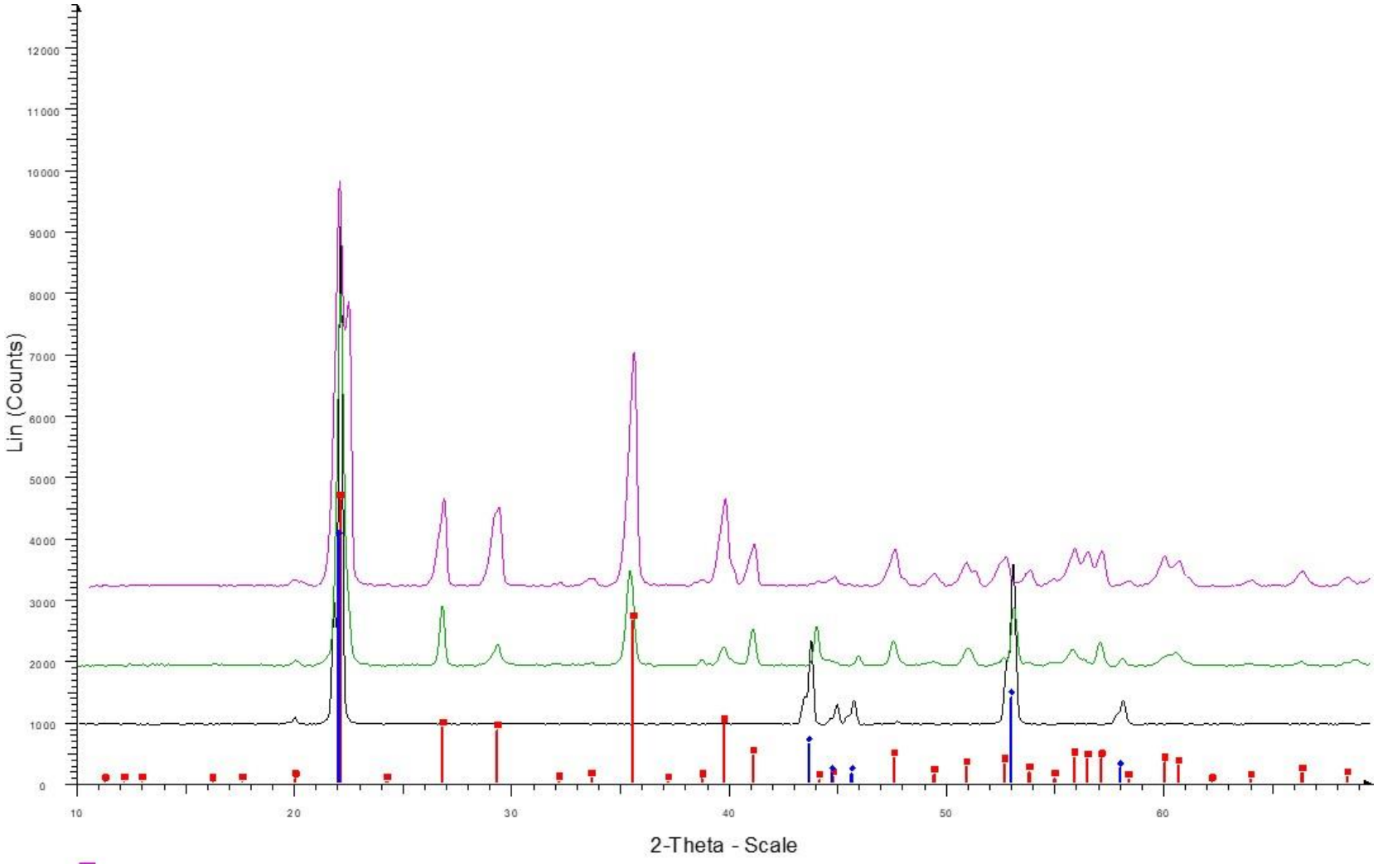

Figure 22. PXRD spectra of solids recovered from $LiCoO_2$ digestion at t = 0 min (Sample A, ─), t = 15 min (Sample B, ─), t = 60 min (Sample C,─) with pure $LiCoO_2$ (◆, PDF [01-075-0532]) and $CoC_2O_4 \cdot 2H_2O$ (■, PDF [00-001-0296]); (Co:OA ratio = 1:3, S/L ratio = 15 g/L, agitation speed = 600 rpm, and T = 100 °C). All the patterns shown are corresponding to λ = 1.78897 Å.

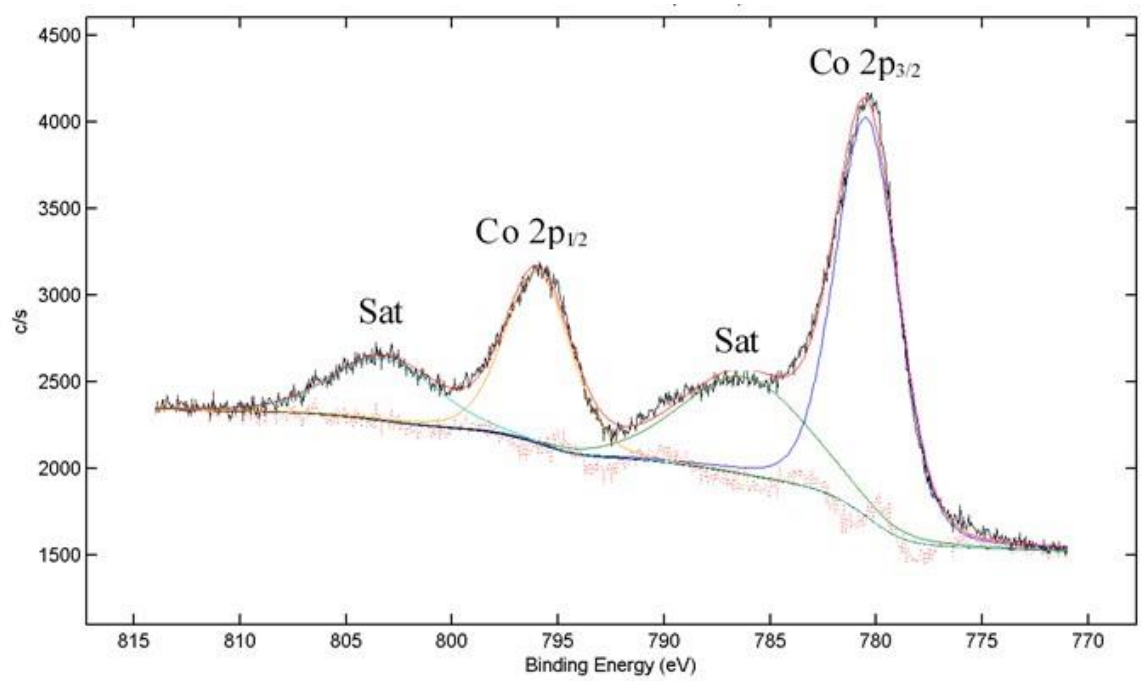

Figure 23. XPS spectrum in the Co 2p region for $LiCoO_2$ (Sample A)

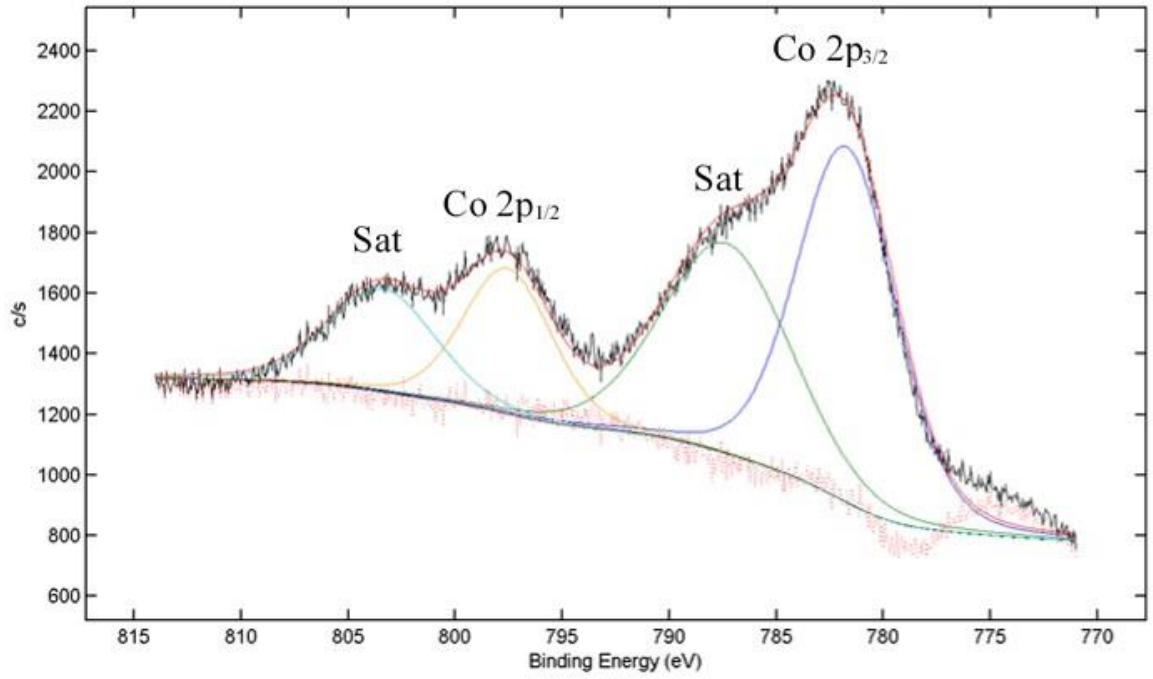

Figure 24. XPS spectrum in the Co 2p region for solids withdrawn at *t* = 15 min (Sample B)

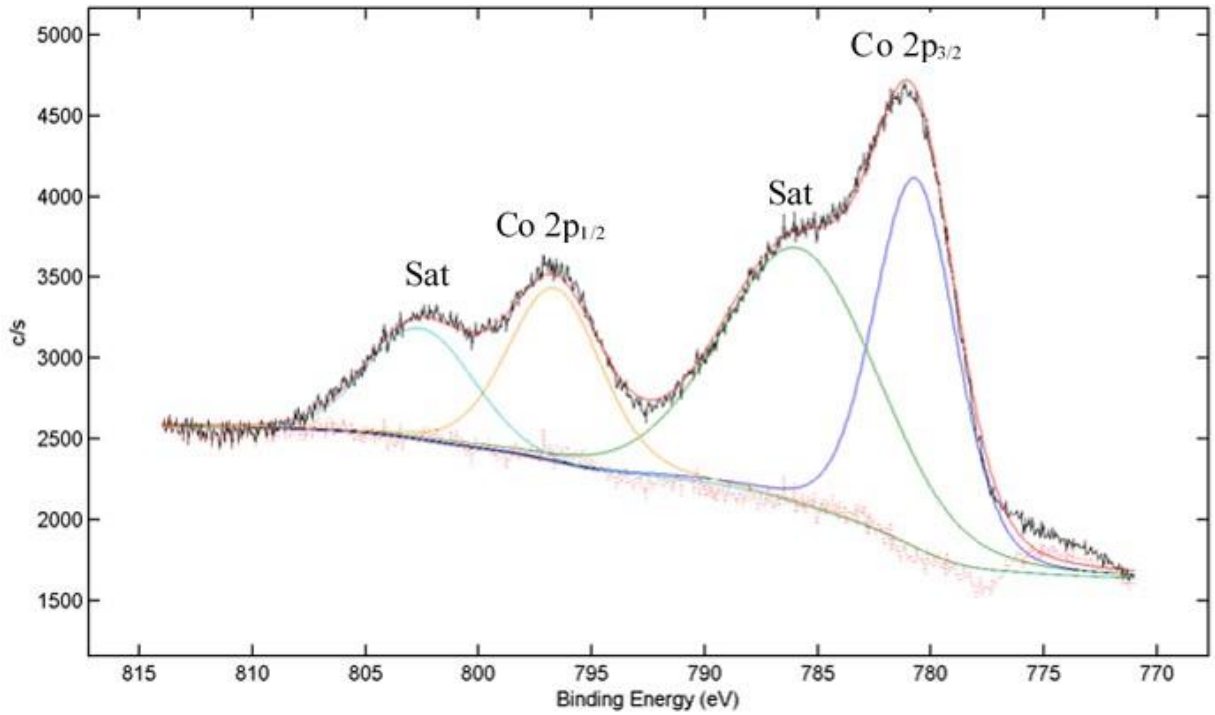

Figure 25. XPS spectrum in the Co 2p region for $CoC_2O_4 \cdot 2H_2O$ (Sample C)

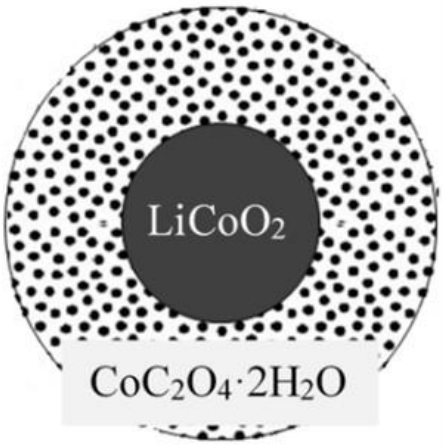

Figure 26. Simple schematic of proposed core-shell solid intermediate.

3.3.7. Impact of H_2O_2 in Metal Extraction: Micro-rods Formation

In Eq. 3.1, it can be seen that the reduction of Co^{3+} to Co^{2+} is coupled with $C_2O_4^{2-}$ oxidizing to CO_2. In this step, $C_2O_4^{2-}$ is transformed into a stable gas phase (CO_2) from which it cannot be easily recovered. An additional reducing agent such as H_2O_2 can be used to minimize the amount of $H_2C_2O_4$ that is lost in this redox process. This redox reaction has been discussed briefly in the previous chapter.[162] From the standard reduction potential shown in Eqs. 3.5 and 3.6 only the H_2O_2 reduction is thermodynamically feasible. The H_2O_2 oxidation reaction can occur by coupling it with a thermodynamically feasible reaction with a high positive standard potential like Co^{3+}/Co^{2+} (3.2). However, to compensate for the amount of H_2O_2 that reduces into H_2O, excess H_2O_2 will be required.

$$H_2O_2 \text{ Reduction: } H_2O_2 + 2H^+ + 2e^- \rightleftharpoons 2H_2O \qquad E^0 = 1.76 \text{ V} \qquad \Delta G° = -339.63 \text{ kJ} \qquad (3.5)$$

$$H_2O_2 \text{ Oxidation: } H_2O_2 \rightleftharpoons O_2 + 2H^+ + 2e^- \qquad E^0 = -0.68 \text{ V} \qquad \Delta G° = 131.22 \text{ kJ} \qquad (3.6)$$

$$3H_2C_2O_4(aq) + H_2O_2(aq) + 2LiCoO_2(s) \leftrightarrows Li_2C_2O_4(aq) + 2CoC_2O_4 \cdot 2H_2O(s) + 2O_2(aq) \qquad (3.7)$$

The reactant concentrations for efficient extraction were optimized at 15 g/L S/L ratio, 600 rpm agitation speed, and T = 100 °C.[162] A Co:OA molar ratio of 1:1.5 with a Co:H_2O_2 molar ratio of 1:3 were determined to be the optimum concentrations. The optimum concentration for the Co:H_2O_2 molar ratio of 1:3 is six times greater than the stoichiometric molar ratio of 1:0.5. The excess H_2O_2 is required to provide sufficient H_2O_2 for the unavoidable but feasible redox couple of H_2O_2 reduction (Eq. 3.5) and oxidation (Eq. 3.6). The addition of H_2O_2 changes the morphology of the $CoC_2O_4 \cdot 2H_2O$ precipitate from a granular shape to a micro-rod structure, as shown in Figure 27. The micro-rod morphology produced by the addition of H_2O_2 had a 23% lower average bulk density of 0.63 g/mL compared to the density of the granular precipitate (0.82 g/mL) produced with only $H_2C_2O_4$. The visual volume difference between 1 g of $CoC_2O_4 \cdot 2H_2O$ precipitate with either a granular or micro-rod morphology can be easily seen in Figure 28. The hypothesis for the

rod-shaped morphology with H_2O_2 is the more dilute concentration of $C_2O_4^{2-}$ leads to a slower precipitation and increased hydrogen bonding between the cobalt oxalate planes.[173] The micro-rods have an average aspect ratio (length-to-diameter) of 10 while the granular structure has an average aspect ratio of 1.5. The approximate order of magnitude higher aspect ratio for the micro-rod morphology results in a lower packing/bulk density.[174]

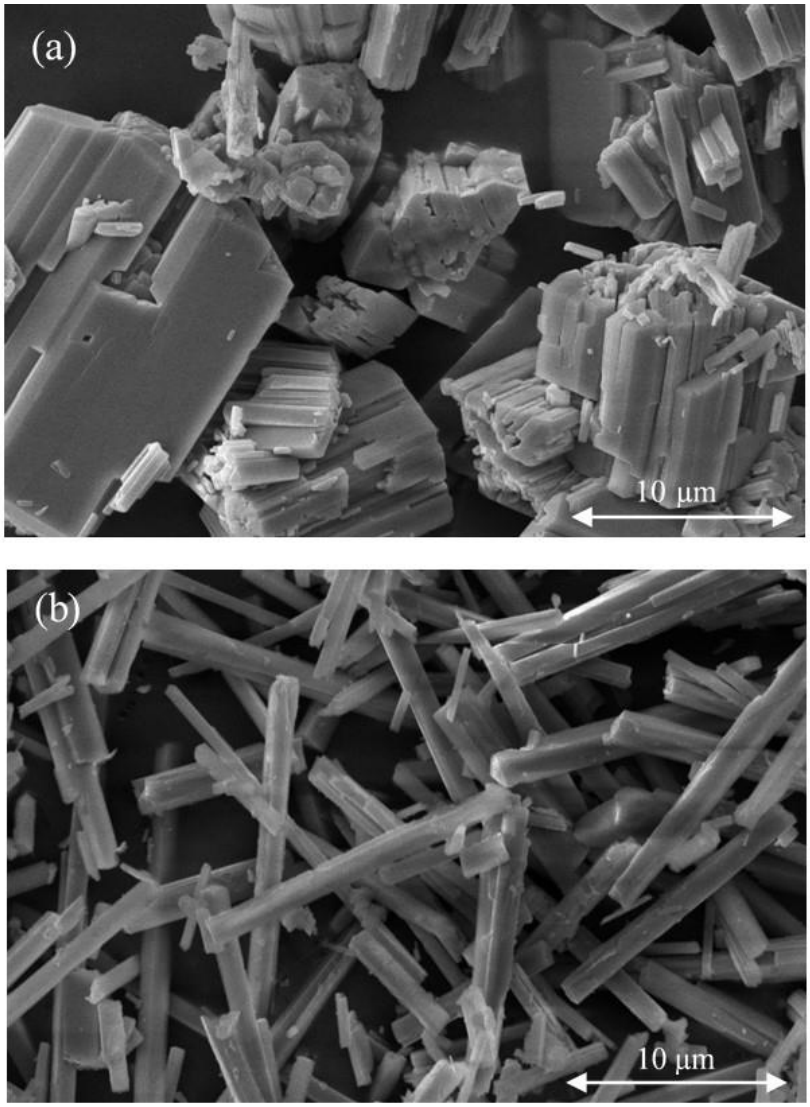

Figure 27. SEM images of (a) $CoC_2O_4 \cdot 2H_2O$ precipitate from $H_2C_2O_4$ digestion (Co:OA ratio = 1:3) and (b) $CoC_2O_4 \cdot 2H_2O$ precipitate from $H_2C_2O_4$ + H_2O_2 digestion (Co:OA ratio = 1:1.5 and Co:H_2O_2 ratio = 1:3).

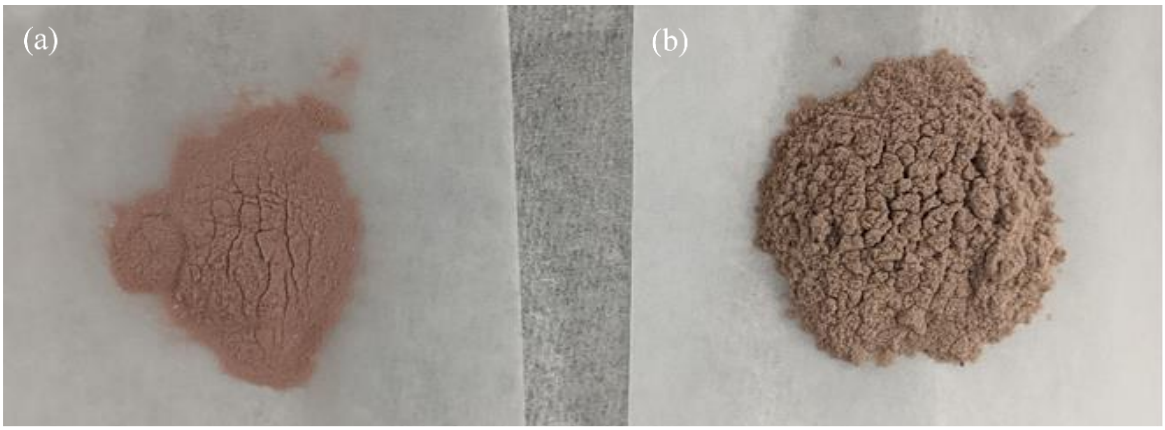

Figure 28. Photos comparing the bulk density of the solid precipitates recovered after digestion. (a) 1 g of $CoC_2O \cdot 2H_2O$ after digesting $LiCoO_2$ with 0.46 M $H_2C_2O_4$ and (b) 1 g of $CoC_2O_4 \cdot 2H_2O$ after digesting $LiCoO_2$ with 0.23 M $H_2C_2O_4$ + 0.46 M H_2O_2 (Co:OA ratio = 1:3, S/L ratio = 15 g/L, agitation speed = 600 rpm and T = 100 °C for both digestions).

3.3.8. $LiCoO_2$ in aqueous $H_2C_2O_4 + H_2O_2$ as a function of temperature

The identification of the novel micro-rod morphology for the solid $CoC_2O_4 \cdot 2H_2O$ precipitate in the presence of H_2O_2 provides a mechanism to improve the kinetics of Li extraction from $LiCoO_2$. To observe the effect on the Li extraction kinetics, the optimized concentration of $H_2C_2O_4 + H_2O_2$ from Chapter 2 was used to perform the Li extraction at lower temperatures (55, 65, and 75 °C) as shown in Figure 29.[162] The Li concentration at each temperature was fit with the cSCM defined in Eq. 3.4. The best fit model parameters are shown in Table 13 along with the standard error in regression. The cSCM fits the Li extraction data at each temperature with a low standard error (0.4 to 3.6 min). The values (i.e., nonzero) for τ_R indicate that the rate-limiting step is predominantly the chemical reaction occurring at the surface of the $LiCoO_2$ core; therefore, a significant improvement in the Li extraction kinetics is observed. Under these reaction conditions with $H_2C_2O_4 + H_2O_2$, the Li can be efficiently extracted even at temperatures as low as 65 °C in less than 2 h. The purity of the $CoC_2O_4 \cdot 2H_2O$ precipitated in the presence of $H_2C_2O_4 + H_2O_2$ has been compared with the commercial $CoC_2O_4 \cdot 2H_2O$ precipitate from the $H_2C_2O_4$ only digestions

in Table 14. In all the precipitates, less than 0.2 wt % of Li was present indicating the $CoC_2O_4 \cdot 2H_2O$ to be > 99.7 % pure. The improved kinetics along with the switch from diffusion control through the $CoC_2O_4 \cdot 2H_2O$ product layer to reaction control at the surface of the $LiCoO_2$ core supports the hypothesis that the morphology of the shell formed around the reacting core is critical to this leaching reaction.

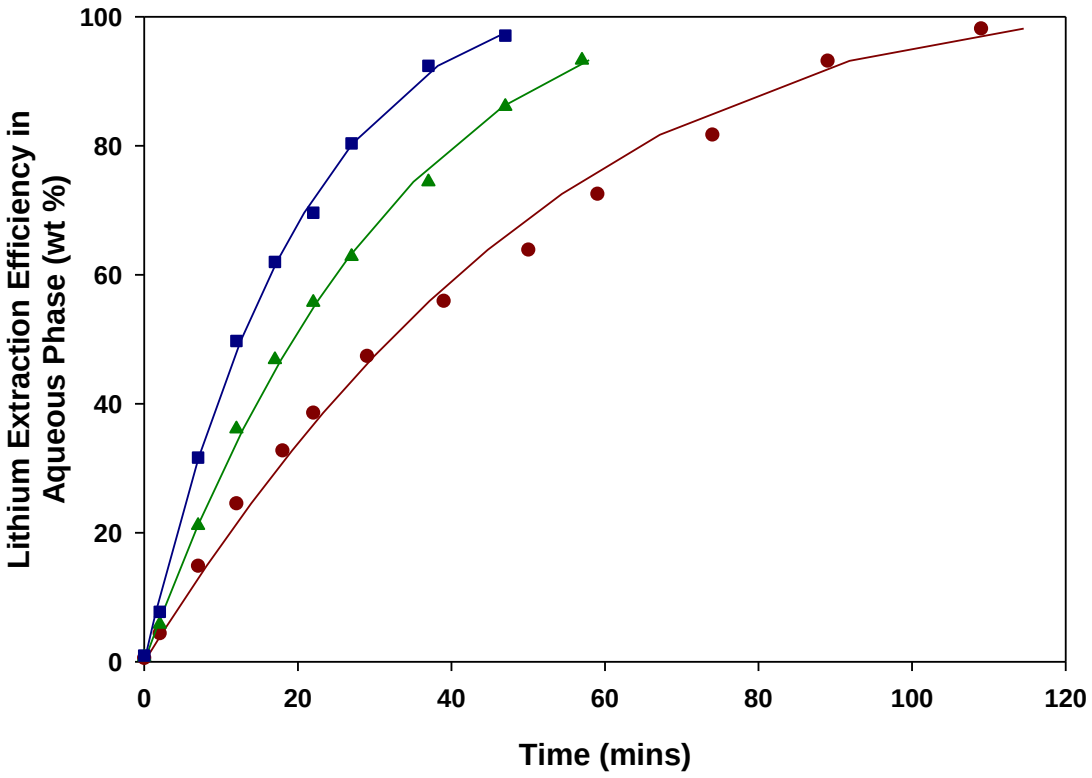

Figure 29. Li extraction efficiency as a function of time in the aqueous phase at Co:OA ratio = 1:1.5, Co:H_2O_2 ratio = 1:3, S/L = 15 g/L, agitation speed = 600 rpm and three temperatures (55 °C - ●, 65 °C - ▲, 75 °C - ■). Each spline curve corresponds to the best fit model.

Table 13. Model parameters for the cSCM shown in Figure 29.

Temperature (°C)	Model parameters for the best fit			Standard Error (min)	Apparent Rate Constant (min^{-1}) $\left(\frac{1}{\tau_R+\tau_P+\tau_F}\right)$
	τ_R (min)	τ_P (min)	τ_F (min)		
75	56.2	9.47	0	0.9	0.015
65	90.4	6.58	0	1.1	0.010
55	155.3	0	0	3.6	0.0064

Table 14. Purity of precipitates recovered in the various metal extraction experiments.

Precipitate Sample – Reaction Conditions	Co (wt %)	Li (wt %)
Commercial $CoC_2O_4 \cdot 2H_2O$	32.21	0.00
Co:OA ratio = 1:3 at 100 °C	32.55	0.00
Co:OA ratio = 1:3 at 90 °C	32.17	0.01
Co:OA ratio = 1:1.5 and Co: H_2O_2 ratio = 1:3 at 65 °C	32.62	0.18
Co:OA ratio = 1:1.5 and Co: H_2O_2 ratio = 1:3 at 55 °C	32.38	0.14

3.3.9. Kinetics Analysis and Apparent Activation Energy

The sum of the cSCM parameters ($\tau_R + \tau_P + \tau_F$) at each temperature can be used to calculate the apparent rate constant (min^{-1}). The apparent activation energy can be determined using the Arrhenius equation as shown in Eq. 3.8

$$\ln(k_a) = \ln(k_a^0) - \frac{E_a}{R}\left(\frac{1}{T}\right) \quad (3.8)$$

where k_a is the apparent rate constant that can be calculated from the inverse sum of the model parameters (τ_R, τ_P, τ_F). The natural logarithm (ln) of k_a can be plotted against $1/T$, and the apparent activation energy (E_a) can be calculated from the slope. The linear fit between $\ln(k_a)$ and $1/T$ for digestions with $H_2C_2O_4$ and $H_2C_2O_4$ + H_2O_2 (shown in Figure 30) indicates that the Arrhenius equation is applicable for both sets of experiments. The apparent activation energy for the Li

extraction with only $H_2C_2O_4$ was estimated to be 61.0 ± 2.5 kJ/mol. The addition of H_2O_2 as an additional reducing agent significantly reduced the apparent activation energy by 33% to 40.9 ± 1.5 kJ/mol. The less dense, more porous $CoC_2O_4 \cdot 2H_2O$ product layer produced in the presence of the H_2O_2 played a critical role in improving the kinetics for this leaching reaction.

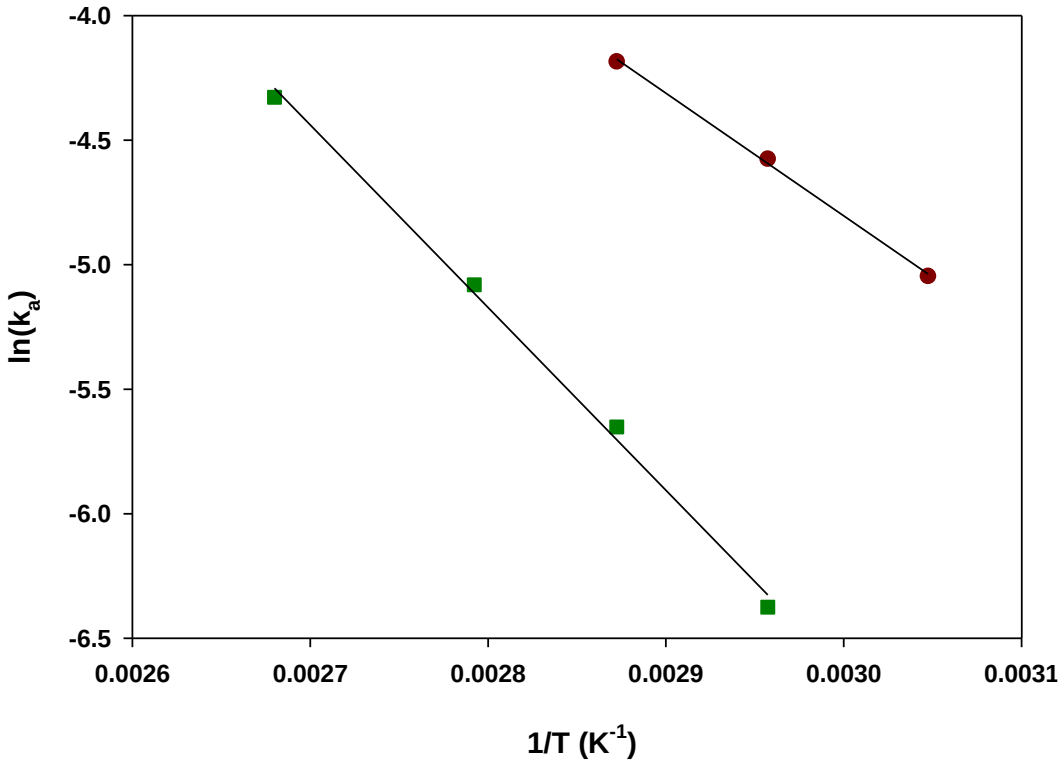

Figure 30. Arrhenius plot and linear fit of the apparent rate constant versus temperature for the Li extraction from $LiCoO_2$ with $H_2C_2O_4$ (Table 12 - ■, slope = -7335.16 K, R^2 = 0.99), and $H_2C_2O_4$ + H_2O_2 (Table 13 - ●, slope = -4923.94 K, R^2 = 0.99).

3.4. Conclusions

In this work, a kinetic model of the Li extraction from $LiCoO_2$ using $H_2C_2O_4$ revealed the diffusion of reactant through the solid $CoC_2O_4 \cdot 2H_2O$ product layer to be rate-limiting. This kinetic analysis was performed using a combined shrinking core model. The existence of a $LiCoO_2$ core and a $CoC_2O_4 \cdot 2H_2O$ shell was confirmed using the combination of PXRD and XPS. The metal extraction performed at 100 °C using 0.46 M oxalic acid leads to an efficient Li and Co extraction

and separation in 1 h. To make this process more energy-efficient, improve Li extraction kinetics, and minimize the amount of $H_2C_2O_4$ required, the reducing agent, H_2O_2, was added. The addition of H_2O_2 reduces the concentration of oxalate ions in solution, which slows the $CoC_2O_4 \cdot 2H_2O$ precipitation and produces a unique micro-rod shaped precipitate. This micro-rod precipitate has a 23% lower bulk density compared to the granular precipitate produced from extractions using only $H_2C_2O_4$. The lower density micro-rod precipitate forms a more porous shell allowing increased diffusion of $H_2C_2O_4$ to the $LiCoO_2$ core. The overall activation energy is significantly reduced by 33% from 61 kJ/mol to 41 kJ/mol by adding H_2O_2 to the $H_2C_2O_4$ digestion. Furthermore, using 0.23 M $H_2C_2O_4$ and 0.46 M H_2O_2 provides an efficient extraction and separation of Li and Co at lower temperatures of 65 to 75 °C in 1 h. This observed phenomenon of improved kinetics and transformation in the rate-limiting step could improve the kinetics for other aqueous hydrometallurgical systems with both soluble and insoluble products. This discovery provides a more energy-efficient and economical oxalate-based, process for critical metals recovery.

Chapter 4. Metal Separation and Precipitation Strategies

Chapter 4

"The greatest threat to our planet is the belief that someone else will save it."
- *Robert Swan (Polar explorer, Environmentalist)*

4.1. Abstract

Recovering metals in the useful form from the aqueous phase is a critical part of a closed-loop metal extraction process. In this chapter, the metal hydroxide and metal carbonate precipitation processes are discussed in detail for the metals present in spent LIBs and ores such as bauxite and ilmenite. The strategies discussed in this chapter were within the scope of this work, but the learnings can be adapted to several similar metal systems. The processes described in this work used oxalate chemistry for metal extraction, and the K-based compounds such as K_2CO_3 and KOH were preferred over Na and NH_4 compounds because of the high aqueous solubility of $K_2C_2O_4$ (36.4 g/100 ml). Using K-based compounds is essential to recover pure precipitate. From the aqueous filtrate recovered in Chapter 2, the Li was precipitated with a 60 % efficiency by adding a stoichiometric amount of K_2CO_3 at a pH > 13. In the presence of excess oxalate, the insoluble $CoC_2O_4 \cdot 2H_2O$ was dissolved in the solution (pH >13) recovered after Li precipitation. The dissolved Co was immediately precipitated as $Co(OH)_2$ at pH > 13. In addition, the selective metal hydroxide precipitation processes for the separation of valuable metals were also discussed. These processes can be utilized for recovering metals in the form of carbonate or hydroxide from the aqueous phase.

4.2. Chemical Separation of Metal Ions

Hydrometallurgical metal extraction is an aqueous chemistry process that leads to a mixture of metal ions in a solution. These metal ions can be separated using various chemical processes such as precipitation, solvent extraction, ion exchange. Metal precipitation is an energy-

efficient and economical process to recover metal efficiently and can be integrated with the closed-loop hydrometallurgical oxalate process conveniently. In this chapter, the precipitation of metal ions as their carbonates or hydroxides are discussed. The precipitated metal carbonates or hydroxides can easily be converted into metal oxides and are preferable in the metal industry.

The oxalate chemistry is unique in its leaching and precipitating properties and can precipitate some of the metals directly, as discussed in Chapter 1. However, to develop a closed-loop process, the recovery of the oxalate ions from the insoluble metal oxalates is critical. This was achieved by dissolving the insoluble metal oxalate compounds and precipitating them in hydroxide form.

4.2.1. Importance of Potassium Compounds in Oxalate Chemistry

To precipitate a metal ion from the aqueous phase, a precipitating reagent was added in an oxalate process. The precipitating reagent must be selected based on the aqueous solubility of the possible side products with $C_2O_4^{2-}$ ions. In a H_2SO_4 process, precipitating reagents like Na_2CO_3 and $(NH_4)_2CO_3$ were preferred for the precipitation of metals from a metal sulfate solution. The side products like Na_2SO_4 and $(NH_4)_2SO_4$ have high aqueous solubility (shown in Table 15) and efficiently recovered the targeted metals.[175,176] But in an oxalate process, the low solubility (Table 15) of the $Na_2C_2O_4$ and $(NH_4)_2C_2O_4$ was an issue in the precipitation of pure metal carbonate products.

In Table 15, the solubilities of potassium compounds are also shown. Among the oxalate compounds, $K_2C_2O_4$ has the highest aqueous solubility, followed by $(NH_4)_2C_2O_4$ and $Na_2C_2O_4$. The addition of K_2CO_3 as a precipitating agent rather than Na_2CO_3 and $(NH_4)_2CO_3$ can precipitate the targeted metal efficiently without any co-precipitate. Therefore, in an oxalate process, K_2CO_3/KOH were the preferred compounds for metal precipitations.

Table 15. Solubilities of possible co-precipitate in the precipitation process.[20]

Compound	Aqueous Solubility at 20 °C (g/100 ml)
Na_2SO_4	16.13
$(NH_4)_2SO_4$	42.9
K_2SO_4	9.95
$Na_2C_2O_4$	3.61
$(NH_4)_2C_2O_4 \cdot H_2O$	5.20
$K_2C_2O_4 \cdot H_2O$	36.4

4.2.2. Metal Hydroxide Precipitation

Metal hydroxide precipitation is a process where the supersaturated metals in the aqueous phase can be removed at a higher pH in their hydroxide form. The solubility of a metal hydroxide was determined by the solubility products (k_{sp}) and the equilibrium between free metal ions, hydroxide ions, and metal hydroxide. In this work, metal recovery processes from mixed metal oxide sources like LIB waste, bauxite, and ilmenite ore are covered. Among the metals within the scope of this work, only Li forms a soluble metal hydroxide with an aqueous solubility of 11 g/100 ml at 20 °C.[20] Most of the other metal ions like Co^{2+}, Ni^{2+}, Mn^{2+}, $Fe^{3+,}$ and Al^{3+} precipitate in the form of metal hydroxides at certain pH. The pH at which the metal hydroxides will precipitate can be estimated using the governing equilibrium and solubility product equations between all the species present in the aqueous phase.[177] Alternatively, it can be modeled through software like Visual MINTEQ, OLI Speciation, or Geochemist's Workbench.

To guide the experiments in this work, an approximate precipitation pH range for metal hydroxide was obtained using the diagrams generated by Kragten in the "Atlas of Metal-ligand Equilibria in Aqueous Solutions."[80] In the work by Kragten, pM vs. pH diagrams are plotted for

various metal-ligand systems at different metal concentrations, where “pM" is defined as the negative logarithm of the free metal ion concentrations in the aqueous phase. The pM vs. pH diagrams for Co^{2+}, Ni^{2+}, Mn^{2+}, Fe^{3+}, $Ti^{4+,}$ and Al^{3+} with the total oxalate concentration of 0.1 M are shown in Figure 31. These diagrams can guide the pH range for metal hydroxide precipitation along with its selectivity. According to Figure 31 (top), from a mixture of Fe^{3+}, $Ti^{4+,}$ and $Al^{3+,}$ Ti^{4+} can be selectively precipitated at pH = 6, after which Fe^{3+} can be precipitated selectively at a pH = 12. The aqueous solution remaining after this will contain a majority of Al^{3+} ions that can be precipitated by acidifying the solution to a pH = 9. It must be noted that the pH range for precipitation will vary with the oxalate concentration and presence of other metal ions. Similarly, from Figure 31 (bottom), it can be concluded that the mixture of Co^{2+}, $Ni^{2+,}$ and Mn^{2+} is difficult to separate using selective metal hydroxide precipitation. The mixture of Co^{2+}, $Ni^{2+,}$ and Mn^{2+} is common in the cathodic waste of NMC based LIBs.

Overall, metal hydroxides are easy to precipitate, but the products are usually low in density with extremely fine precipitate particles resulting in a difficult filtration process. This issue can be resolved by seeding the solution with appropriate metal hydroxide particles to assist in supersaturation. The added seeds will act as the growth site for the additional metal hydroxide particles, resulting in a denser and larger precipitate.

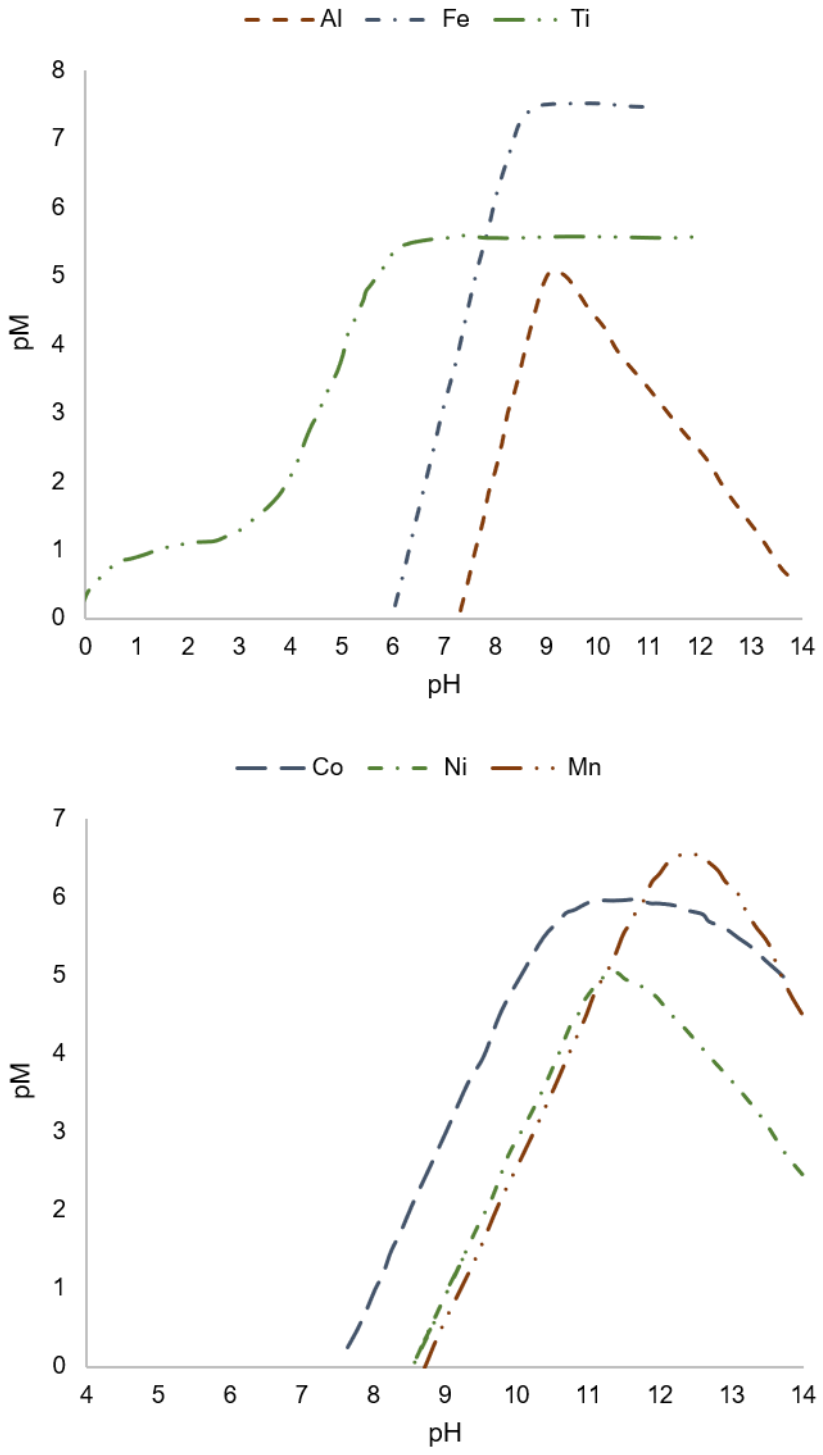

Figure 31. pM vs pH diagram for metals within the scope of this work in presence of 0.1 M oxalate ions. pM is defined as the negative logarithm of the free metal ions concentration in the aqueous phase.

4.2.3. Metal Carbonate Precipitations

Metal carbonate precipitations have been employed commonly for the removal of heavy metals from wastewater.[177,178] In this section, precipitation processes for metals present in LIB waste, bauxite, and ilmenite ore are covered. Most metals like Li^{+}, Co^{2+}, Ni^{2+}, Mn^{2+}, and Fe^{3+} form insoluble metal carbonates, as shown in Table 16. But, for metals such as Al^{3+} and Ti^{4+} (bauxite and ilmenite ore), metal carbonates are not commonly observed, and metal hydroxide precipitations are the best way to recover these from the aqueous phase. The efficient precipitation of metal carbonate requires two important conditions: supersaturation and pH > 12. The pH > 12 is critical because carbonic acid has a pKa_2 = 10.32[179], and at pH > 12, CO_3^{2-} becomes the predominant carbonate species (shown in Figure 32). At pH < 12, metal bicarbonate precipitation will be observed.

The Li can be precipitated efficiently in the form of carbonate for the oxalate-based LIBs recycling process. A major obstacle for Li precipitation in the form of Li_2CO_3 was to achieve a saturated solution. Typically, in a lab-scale recycling process operating at a solid-to-liquid ratio of 50 g/L for LCO or NMC cathode, the Li concentration was 3.50 g/L. The Li concentration was equivalent to an expected Li_2CO_3 concentration of around 19 g/L. From Table 16, in 1 L of an aqueous solution, up to 13.3 g of Li_2CO_3 will be soluble.[20] Hence, Li must be concentrated over multiple cycles of recycling processes before efficient precipitation is performed. After that, the potassium compounds: K_2CO_3 and KOH precipitated Li efficiently, as shown in Eq. 4.1.

$$Li_2C_2O_4(aq) + K_2CO_3(s) \rightleftharpoons Li_2CO_3(s) + K_2C_2O_4(aq) \quad (4.1)$$

Table 16. Solubility of common metal carbonates related to this work.

Compound	Aqueous Solubility at 20 °C (g/100 ml)[20]
K_2CO_3	52.3
Na_2CO_3	17.9
Li_2CO_3	1.33
$CoCO_3$	highly insoluble
$NiCO_3$	highly insoluble
$MnCO_3$	highly insoluble
$FeCO_3$	highly insoluble

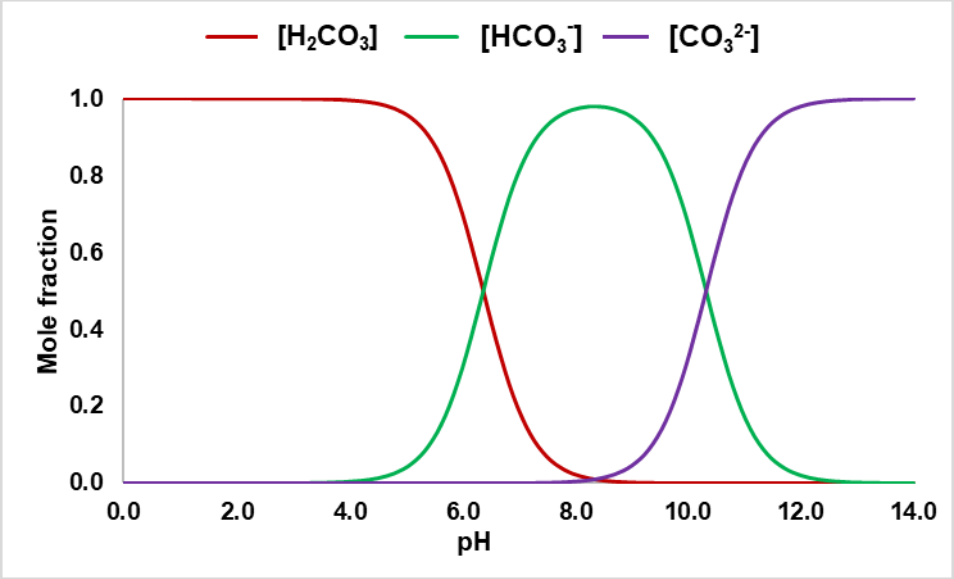

Figure 32. Speciation of carbonic acid at 20 °C for $pKa_1 = 6.37$ and $pKa_2 = 10.32$.

4.2.4. Metal Phosphate Precipitation

Most of the metals that precipitate in the form of carbonates can also be precipitated in the form of their metal phosphates. However, the difficulty in converting the metal phosphates into metal oxides and the eutrophication issues in the waste disposal at the end of the process limit its use. Metal phosphate like Li_3PO_4 is extremely insoluble in the aqueous phase and has a solubility

of 0.027 g/100 ml at 25 °C.[20] The negligible solubility of Li_3PO_4 results in Li^+ to be precipitated efficiently from a typical LIBs recycling leachate (50 g/L S/L ratio). Phosphoric acid has a pKa_1 = 2.0, pKa_2 = 7.20 and pKa_3 = 12.30.[180] Similar to our conclusions for the carbonate precipitation, a pH > 13 was required to precipitate metal phosphates efficiently. The stoichiometric reaction for Li precipitation in the form of Li_3PO_4 is described by Eq. 4.2.

$$3Li_2C_2O_4(aq) + 2K_3PO_4(s) \rightleftharpoons 2Li_3PO_4(s) + 3K_2C_2O_4(aq) \quad (4.2)$$

4.3. Li and Co precipitation in the Oxalate Process

The metal extraction processes from $LiCoO_2$ discussed in Chapters 2 and 3 lead to the Co being precipitated as $CoC_2O_4{\cdot}2H_2O$ whereas Li remains in the solution. The precipitation of Li as Li_2CO_3 from an aqueous oxalate solution is described in Eq. 4.1. All of the metal extractions described in Chapters 2 and 3 were performed at a solid-to-liquid ratio of 15 g/L and resulted in an undersaturated Li solution. To precipitate Li efficiently from this, the aqueous phase was concentrated five times at 105 °C resulting in a Li concentration of 5 g/L. Afterward, KOH and K_2CO_3 were added to recover 60 % of Li as Li_2CO_3. The precipitate was confirmed as Li_2CO_3 using PXRD, as shown in Figure 33. Alternatively, more than 90% of Li was also recovered efficiently in the form of Li_3PO_4 using Eq. 4.2. The Li_3PO_4 precipitate was confirmed using PXRD, as shown in Figure 34.

The precipitation of Co in the form of either hydroxide or carbonate required dissolving $CoC_2O_4{\cdot}2H_2O$ precipitate in the aqueous oxalate phase. This was achieved by utilizing the property of soluble metal oxalate formations in the presence of excess oxalate, as shown in Eq. 4.2.

$$Co^{2+} + 3C_2O_4^{2-} \leftrightarrows CoC_2O_4{\cdot}2H_2O(s) + 2C_2O_4^{2-} \leftrightarrows Co(C_2O_4)_2^{2-} + C_2O_4^{2-} \leftrightarrows Co(C_2O_4)_3^{4-} \quad (4.2)$$

The solubility of $CoC_2O_4 \cdot 2H_2O$ in 1 M $K_2C_2O_4$ solution was determined at different temperatures and summarized in Table 17. However, the solubility limit was insufficient to dissolve the 28 g of $CoC_2O_4 \cdot 2H_2O$ recovered from a $LiCoO_2$ metal extraction at 15 g/L. The 1 M $K_2C_2O_4$ solution had a resulting pH = 8, whereas the aqueous filtrate after precipitation of Li was pH = 13. Therefore, an alternate route was identified where the $CoC_2O_4 \cdot 2H_2O$ was added directly to the high pH solution recovered after Li precipitation. This resulted in a simultaneous dissolution and precipitation of Co in the form of $Co(OH)_2$. The precipitate was confirmed as $Co(OH)_2$ using PXRD, as shown in Figure 35. In this process, KOH constantly needs to be added to maintain the pH around 13. The reactions are summarized in Eqs. 4.3 and 4.4. The complete process of metal recovery and separation for Li and Co extracted from $LiCoO_2$ in the presence of $H_2C_2O_4$ is described in Figure 36.

$$CoC_2O_4 \cdot 2H_2O(s) + K_2C_2O_4(aq) \rightleftharpoons K_2[Co(C_2O_4)_2](aq) \quad (4.3)$$

$$K_2[Co(C_2O_4)_2](aq) + 2KOH(s) \rightleftharpoons Co(OH)_2(s) + 2K_2C_2O_4(aq) \quad (4.4)$$

Table 17. Solubility of $CoC_2O_4 \cdot 2H_2O$ in 1 M $K_2C_2O_4$ at different temperatures

Temperature (°C)	**Solubility (g/100 ml of 1 M $K_2C_2O_4$)**
20	2.09
50	4.48
80	7.76

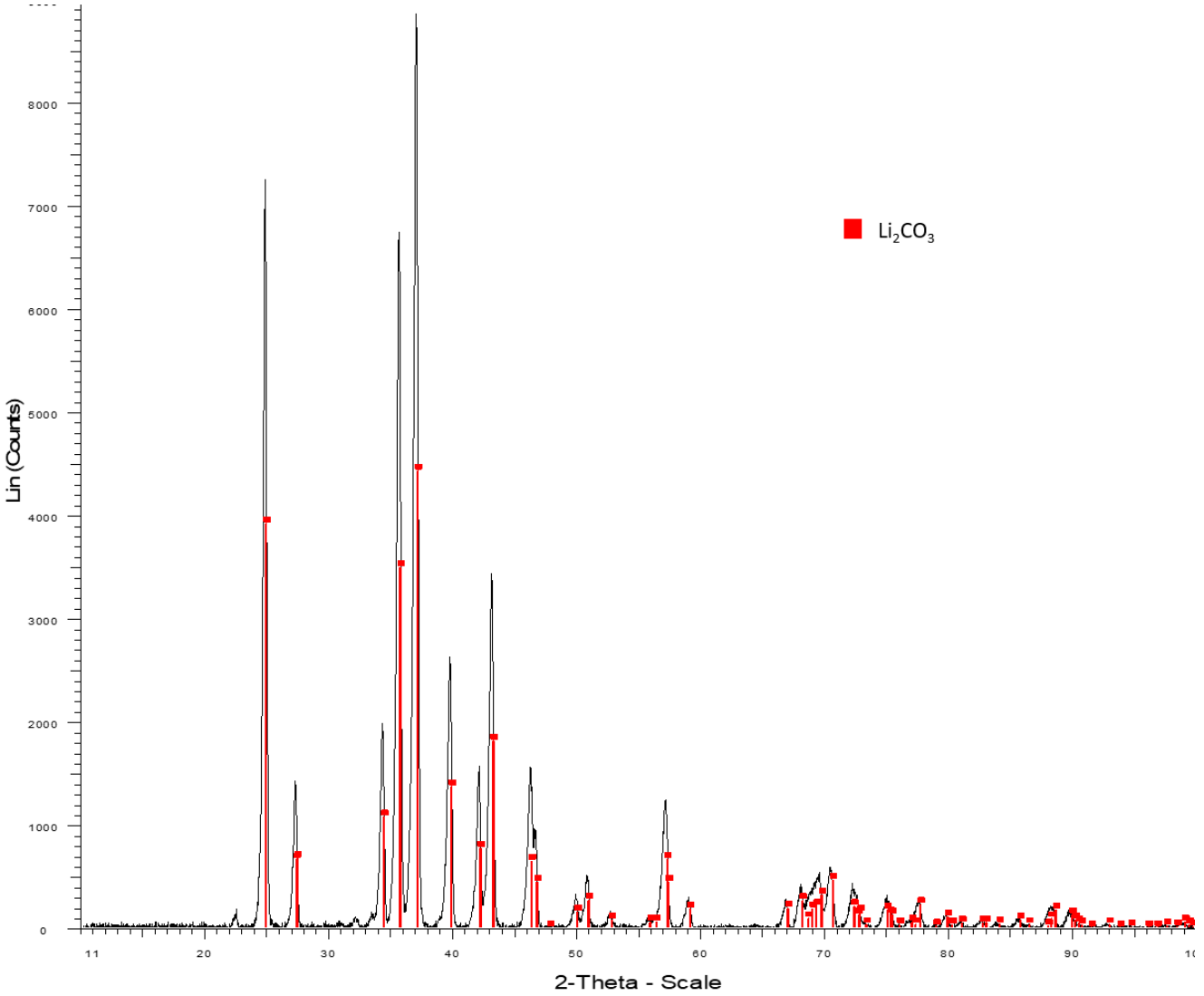

Figure 33. PXRD of precipitate recovered in lithium carbonate precipitation. The collected pattern is corresponding to λ = 1.78897 Å

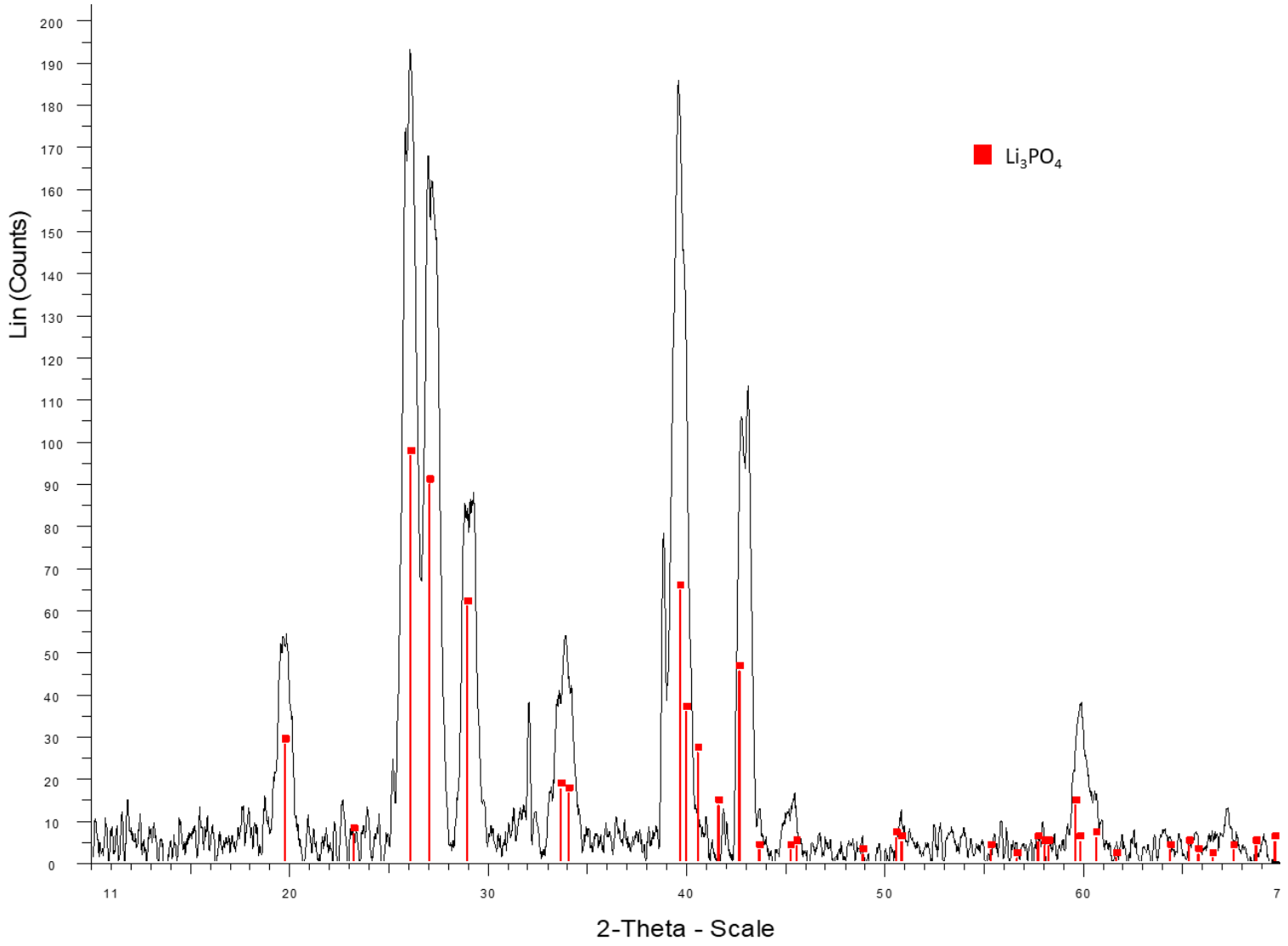

Figure 34. PXRD of precipitate recovered in lithium phosphate precipitation. The collected pattern is corresponding to λ = 1.78897 Å

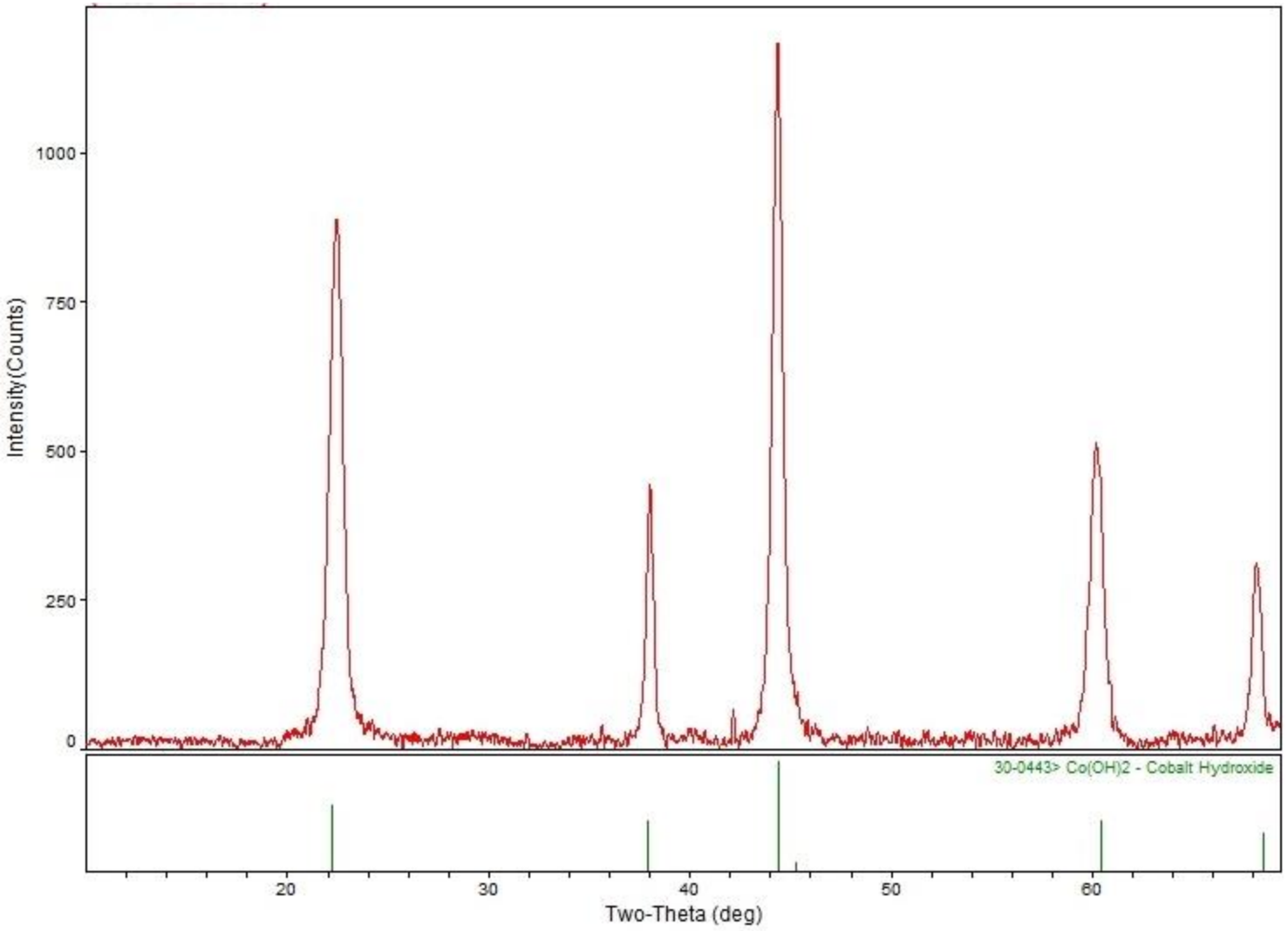

Figure 35. PXRD of precipitate recovered after $CoC_2O_4 \cdot 2H_2O$ dissolution. The collected pattern is corresponding to $\lambda = 1.78897$ Å

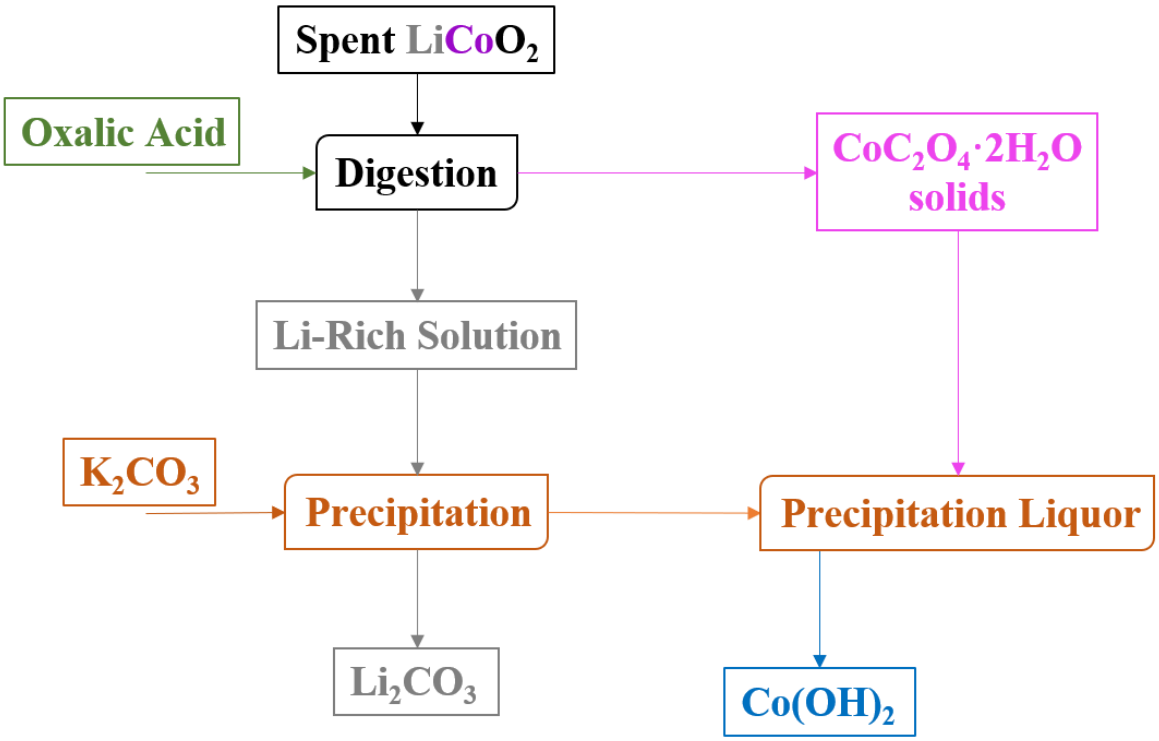

Figure 36. Process flowsheet for Li and Co separation and recovery in presence of $H_2C_2O_4$.

4.3. Thermal Treatment for recovering Co product

In Section 4.2., $CoC_2O_4 \cdot 2H_2O$ was dissolved in the presence of excess $C_2O_4^{2-}$ ions and precipitated $Co(OH)_2$ (Eqs. 4.3 and 4.4). This process is preferable for the complete recovery of $C_2O_4^{2-}$ ions. However, calcination of the $CoC_2O_4 \cdot 2H_2O$ can also synthesize the desired Co product. The thermogravimetric analysis (TGA) of $CoC_2O_4 \cdot 2H_2O$ was performed in the presence of air and nitrogen (100 cc/min) at a ramp rate of 5 °C/min (shown in Figure 37). Based on the weight loss observed following reactions were proposed:

a) Under Air:

$$CoC_2O_4.2H_2O(s) \rightarrow CoC_2O_4(s) + 2H_2O(g) \text{ (Theoretical weight loss = 19.6\%)} \quad (4.5)$$

$$3CoC_2O_4(s) + 2O_2(g) \rightarrow Co_3O_4(s) + 6CO_2(g) \text{ (Theoretical weight loss = 36.4\%)} \quad (4.6)$$

$$2Co_3O_4(s) \rightarrow 6CoO(s) + O_2(g) \text{ (Theoretical weight drop = 2.91\%)} \quad (4.7)$$

b) Under N_2:

$$CoC_2O_4.2H_2O(s) \rightarrow CoC_2O_4(s) + 2H_2O(g) \text{ (Theoretical weight loss = 19.6\%)} \quad (4.8)$$

$$2CoC_2O_4(s) \rightarrow Co(s) + CoO(s) + 3CO_2(g) + CO(g) \text{ (Theoretical weight loss = 51 \%)} \quad (4.9)$$

In the presence of air, calcination of $CoC_2O_4 \cdot 2H_2O$ leads to the formation of Co_3O_4 at a temperature below 800 °C, as shown in Figure 38. In Eq. 4.6., a theoretical weight loss of 36.4% was expected, but the actual weight loss observed during the TGA was around 30%. This could be because of the evolution of a mixture of CO and CO_2 gases rather than only CO_2 as proposed in Eq. 4.6. In the current instrument setup, it was not possible to identify the gaseous species evolving. However, the final product (Co_3O_4) will remain same in both cases. Calcination of the product recovered from Eq.4.6 to a temperature above 800 °C led to the formation of CoO. But, to achieve CoO as a final product, the sample was cooled down in the absence of O_2.

The calcination of $CoC_2O_4 \cdot 2H_2O$ in an inert atmosphere led to the Co and CoO as the final product. The observed weight loss of 45% was close to the expected weight loss of 50% shown in Eq. 4.9. The Eq. 4.9 was proposed after identifying the product recovered from TGA to be a mixture of Co and CoO using PXRD (Figure 39). In Figure 39, Co was observed in an Fm-3m space group with a cubical symmetry and a $P6_3/mmc$ space group with hexagonal symmetry. Another interesting observation was that the unique micro-rod morphology of $CoC_2O_4 \cdot 2H_2O$ observed in the presence of $H_2C_2O_4$ and H_2O_2 (Figure 27) was preserved during the calcination process, as shown in Figures 40 and 41. This can lead to the synthesis of LIB cathodes with a micro-rods morphology as well. The unique 1-D morphology of cathodes can improve the electrochemical capacity and cycling stability of LIBs.[181]

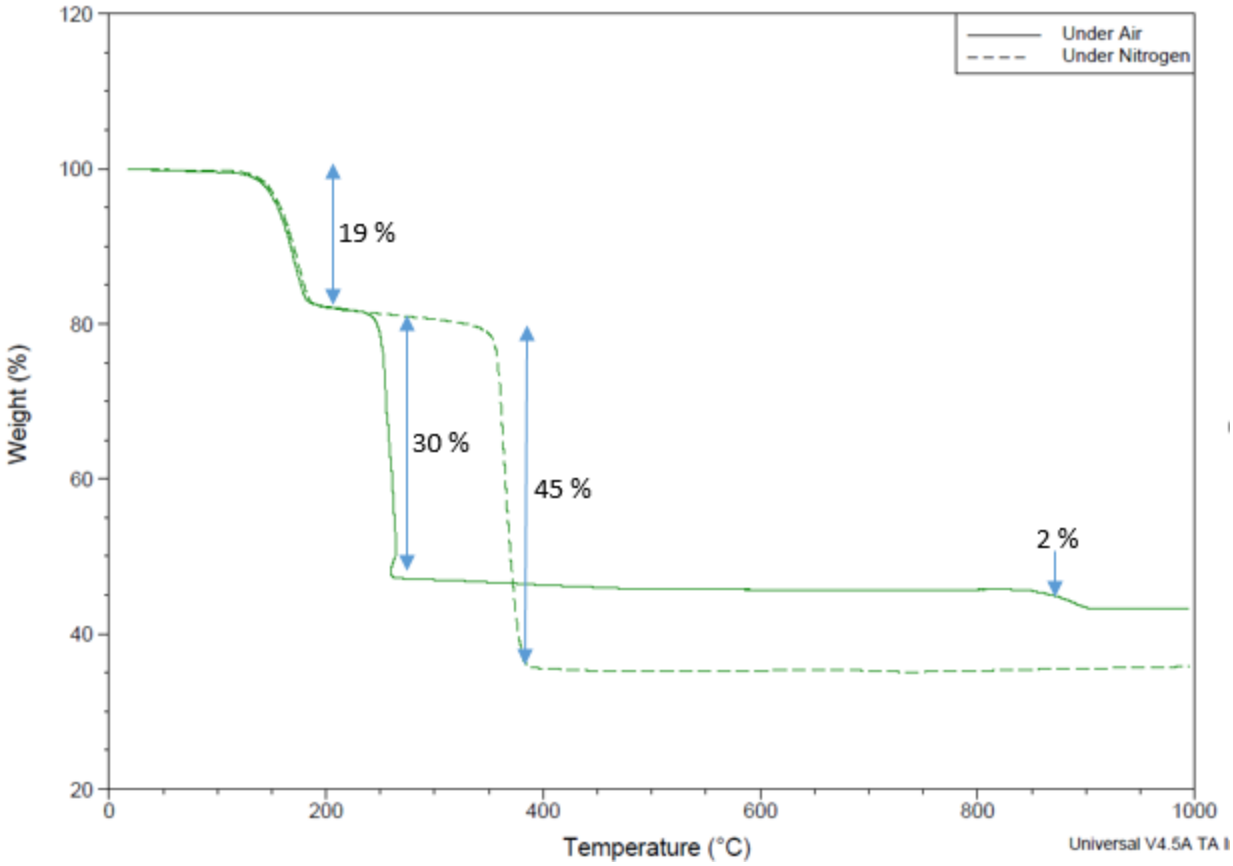

Figure 37. TGA of $CoC_2O_4 \cdot 2H_2O$ in the presence of air and N_2 at a ramp rate of 5 °C/min.

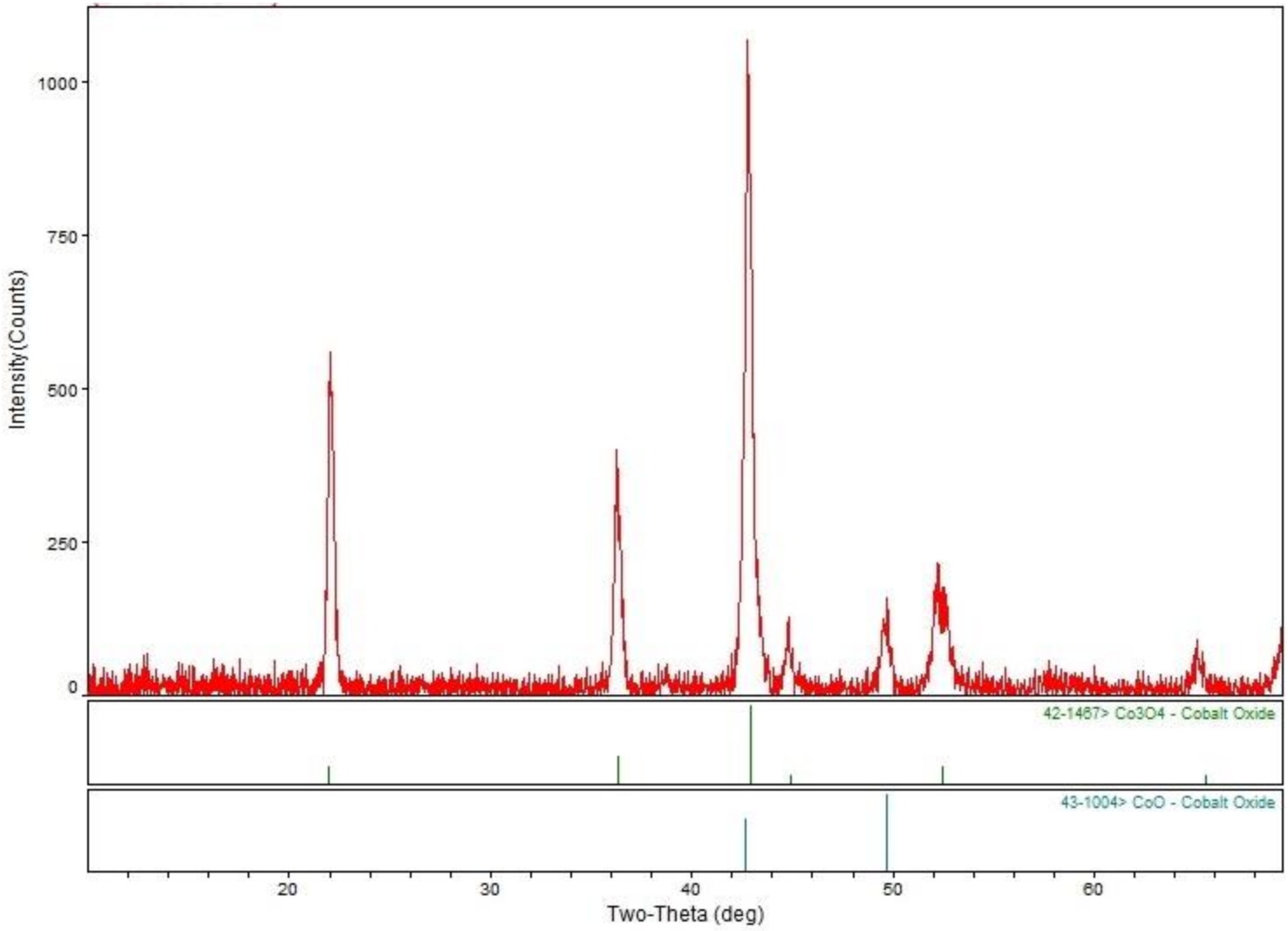

Figure 38. PXRD of solid product recovered after calcining $CoC_2O_4 \cdot 2H_2O$ to 800 °C in the presence of air. The collected pattern is corresponding to $\lambda = 1.78897$ Å.

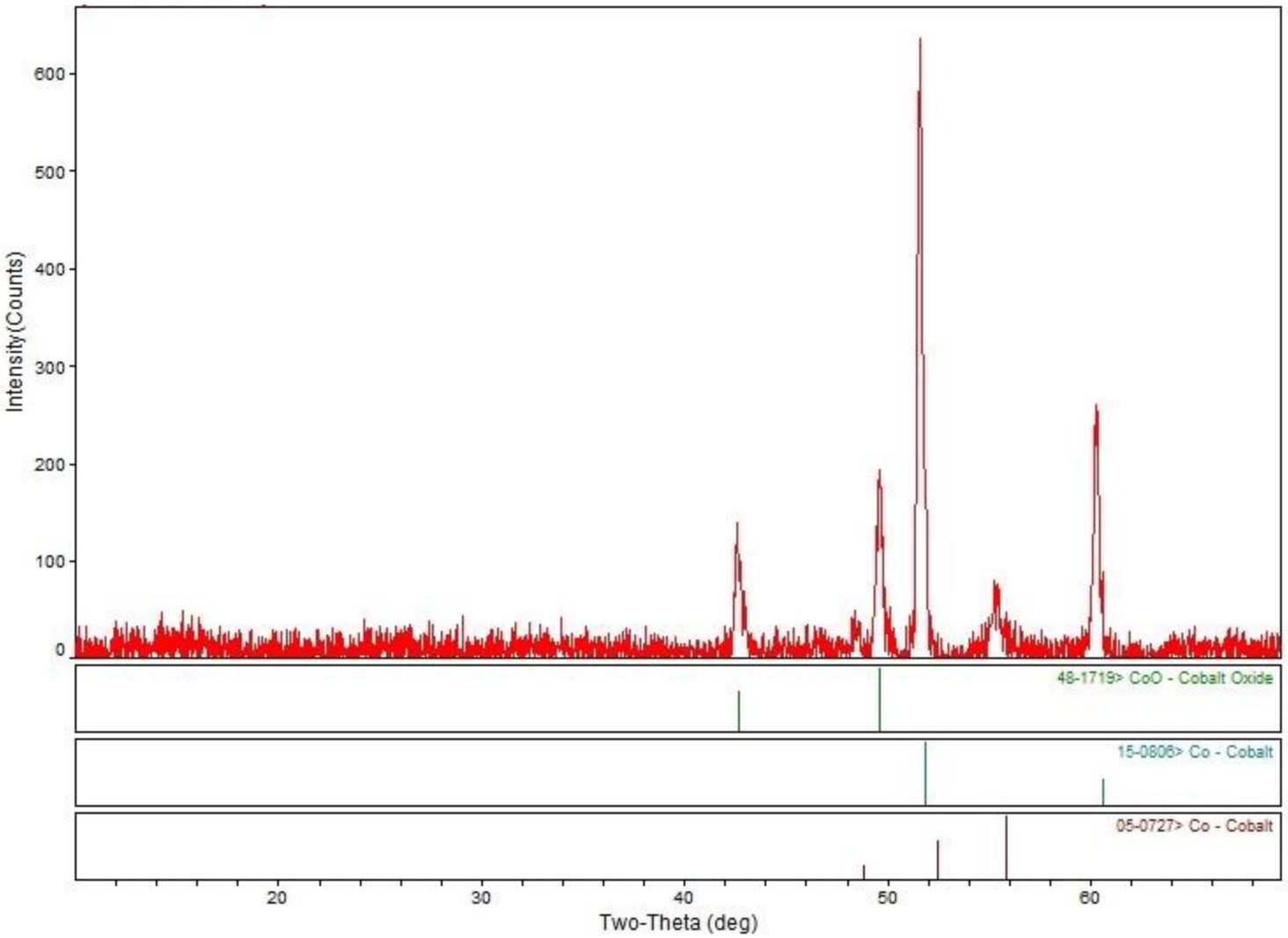

Figure 39. PXRD of solid product recovered after calcining $CoC_2O_4 \cdot 2H_2O$ to 800 °C in the presence of N_2. The collected pattern is corresponding to $\lambda = 1.78897$ Å.

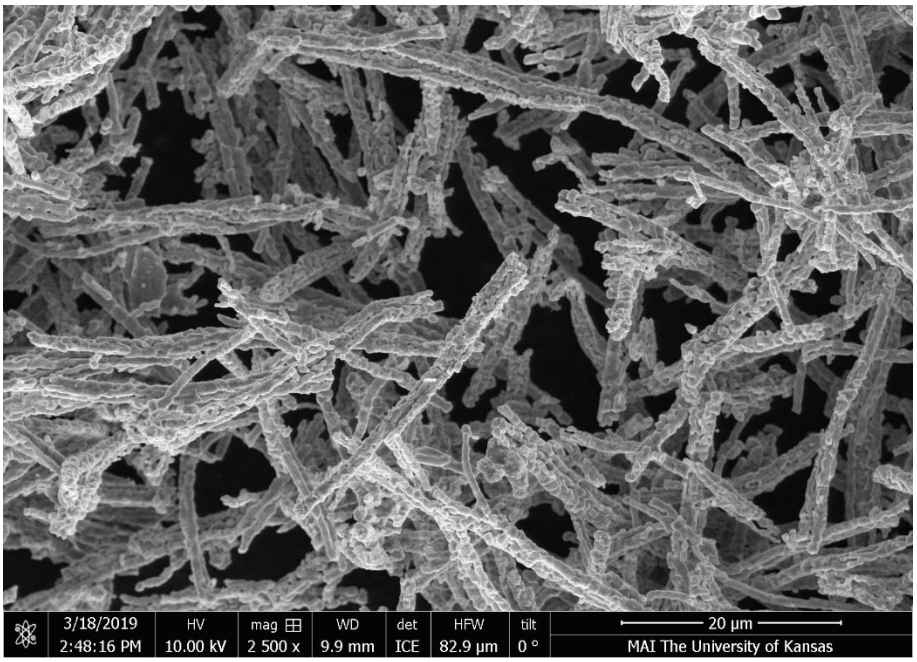

Figure 40. SEM image of Co product synthesized by calcining $CoC_2O_4 \cdot 2H_2O$ to 800 °C in the presence of air.

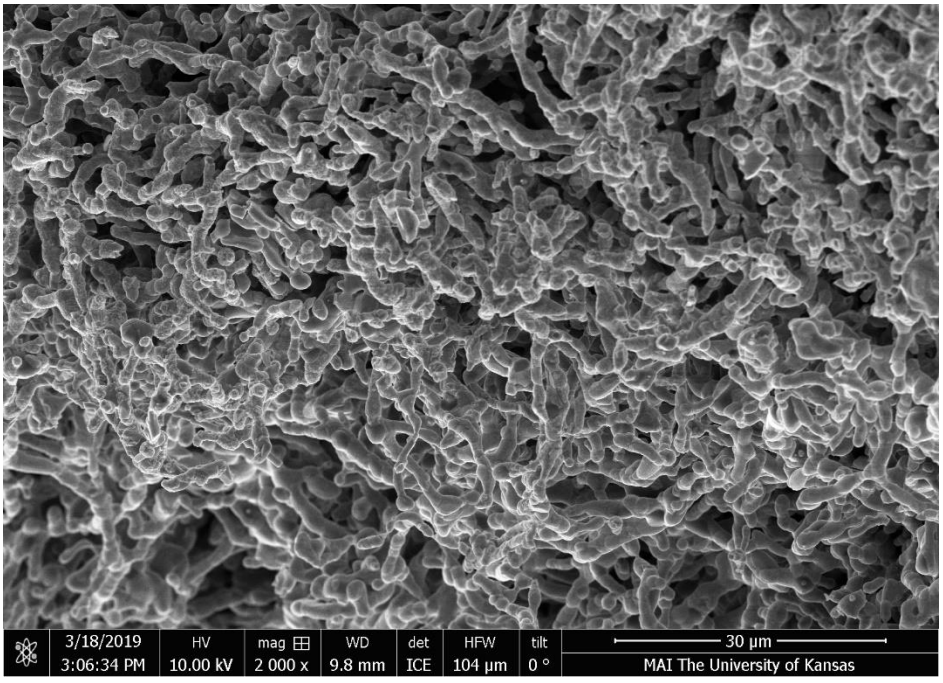

Figure 41. SEM image of Co product synthesized by calcining $CoC_2O_4 \cdot 2H_2O$ to 800 °C in the presence of N_2.

4.4. Conclusions

Recovery of metals in the desired form after extraction is critical for the metal industry. In an oxalate process, potassium compounds like KOH, K_2CO_3, and K_3PO_4 are the preferred precipitation reagents to avoid co-precipitation of side products. In this work, both metal hydroxide and metal carbonate precipitation have been discussed in detail for the metals pertinent to this dissertation. Metal hydroxide precipitations can be performed within a range of pH, and the diagrams by Kragten were used to guide the selective metal hydroxide precipitations. For metal carbonate precipitation, a pH > 13 was preferred because of CO_3^{2-} speciation. But the metal carbonates could not be precipitated selectively because of the similar pH range of precipitation. Metal carbonates can also be calcined into metal oxides and were preferable for Li recovery. The aqueous filtrate recovered in Chapter 2 from $LiCoO_2$ metal extraction was concentrated five times to achieve a Li concentration of 5 g/L for precipitation. The Li in the aqueous phase was precipitated with a 60% efficiency using Li_2CO_3. The Co precipitated in the form of $CoC_2O_4 \cdot 2H_2O$ was dissolved in the pH > 13 solution recovered after Li precipitation. In this pH range, Co^{2+} from the aqueous phase precipitates in the form of $Co(OH)_2$. This led to all the $C_2O_4^{2-}$ initially added with $H_2C_2O_4$ to be in the aqueous phase. Alternatively, the $CoC_2O_4 \cdot 2H_2O$ can be calcined to achieve Co_3O_4 or Co metal as the final product. However, incorporating this approach in the closed-loop process will only lead to 50% acid recovery. The metal recovery processes designed in this chapter and demonstrated for Li and Co recovery are efficient, environmentally-friendly, and economical, and maintains the closed-loop oxalate processes.

Chapter 5. Processes for the Recycling of Oxalate Reagents

Portions of this chapter are adapted from the following article:

Verma, A., Corbin, D.R., & Shiflett, M.B., Lithium and Cobalt Recovery from $LiCoO_2$ using Oxalate Chemistry: Scale-up and Techno-economic Analysis. *Industrial & Engineering Chemistry Research (submitted)*

Chapter 5

"Green chemistry is replacing our industrial chemistry with nature's recipe book. It is not easy, because life uses only a subset of the elements in the periodic table. And we use all of them, even the toxic ones."

- Janine Benyus (Biologist, Nature Nerd)

5.1. Abstract

Commercial hydrometallurgical processes typically use inorganic acids, and a significant amount of caustic waste is generated after metal precipitations and recovery. For an oxalate process, efficient recycling processes for acidic reagents are needed to minimize the waste generations and offset the cost difference with inorganic acids. In this chapter, an ion-exchange resin process using Amberlyst® 15 was developed and optimized to exchange undesired cations with H^+ in a batch setup. The capacity of the Amberlyst® 15 was estimated to be 4.64 meq./g and can efficiently be used to regenerate $H_2C_2O_4$ from the aqueous filtrate recovered after Li and Co precipitation (Chapter 4). Additionally, binoxalate reagents like $NH_4HC_2O_4$ and KHC_2O_4 with applications in the refining of ores can also be regenerated using the optimized ion-exchange resin process. An alternative method utilizing the low solubility of KHC_2O_4 (5.73 g/100 ml) and $KHC_2O_4 \cdot H_2C_2O_4$ (2.97 g/100 ml) was identified to precipitate and recycle them by acidification.

5.2. Motivation

Hydrometallurgical processes using organic acids like oxalic, citric, ascorbic, and succinic acid have been demonstrated at a lab-scale to recover critical metals from spent LIBs.[32,53,54,151-154] These acids have minimal environmental impacts but are expensive compared to inorganic acids. H_2O_2 is commonly used as a reducing agent along with acids to convert Co^{3+} into the stable Co^{2+} form.[31] Oxalic acid ($H_2C_2O_4$) is unique in its reducing and solubility properties and was demonstrated as a sustainable, green, and environmentally-friendly reagent for Li and Co recovery

from $LiCoO_2$ in the previous chapters.[162] To offset the cost of expensive oxalate reagents and minimize waste generation, it is necessary to regenerate and recycle it. To the best of our knowledge, no other hydrometallurgical process has been developed that demonstrates acid regeneration and reuse.

5.3. Possible Methods for Recycling of Oxalate-based Acids

Oxalate-based acids covered in this work contain a $C_2O_4^{2-}$ anion and two single charged cations to maintain electroneutrality. One cation must be H^+ and the second cation is NH_4^+, K^+, Na^+, or H^+. To extract metals from a metal oxide, the presence of H^+ is critical to weaken the metal-oxygen bond and initiate the $C_2O_4^{2-}$ chelation mechanism.[162] Any other cations added during the precipitation step to recover metals also become part of the solution and must be considered during acid recycling. Therefore, it is often preferable to use precipitation reagents containing similar cation as the acids.[16,162] The precipitation processes discussed in Chapter 4 are usually at a pH greater than 12, and acid recycling has to be performed from a basic solution. The regeneration of $H_2C_2O_4$ from a $K_2C_2O_4$ + KOH solution will require an ion exchange method, whereas low solubility reagents like KHC_2O_4 and $KHC_2O_4 \cdot H_2C_2O_4$ can be precipitated by lowering the pH. Both of these approaches are discussed in detail in upcoming sections.

5.4. Regeneration using Ion-exchange Resins

Ion exchange is a technique to exchange the undesirable ions with the required ions using a material like ion-exchange resins or zeolites. Both zeolites and ion-exchange resins have been traditionally used in the water softening industry, with resins being more successful because of higher capacity and efficient regeneration.[182-184] These resins are composed of polymeric matrices with a cationic or anionic functional group permanently bound. The functional groups have a net positive or negative charge to attract the counter ions.[185]

For the regeneration of the acidic reagents, a similar concept as water softening can be applied with the desired pH in the range of 0.5-2 after treatment. During the water softening process, cations like Ca^{2+} or Mg^{2+} are exchanged with either Na^{+} or H^{+} using either weak acid cation exchange resin (for temporary hardness) or strong acid cation exchange resin (for permanent hardness).[186,187] The weak acid cation (WAC) exchange resins employ carboxylic acid (COO^{-}) functional groups and operate in the pH range of 5-9. These resins do not have a high capacity to remove all the ions but can be regenerated efficiently using H_2CO_3 or HCl.[186] The strong acid cation (SAC) exchange resins derive their exchange activity from the sulfonic acid groups (HSO_3^{-}) and operate well in all pH ranges. When used in the H-form during softening, the SAC resins can exchange all the cations with H^{+}. However, to regenerate it, an excess amount of 1-2 M H_2SO_4 is required.[188]

Conceptually, acid regeneration for a hydrometallurgical application is like the water softening process. However, the pH change between feed and output is minimal (pH = 9 to pH = 6) for water softening, whereas a significant change in pH (12 to 1) is desired in this work. To test the hypothesis, a SAC resin: Amberlyst® 15 (Dry, H-form) was selected to perform preliminary studies. The operation mechanism of a strong acid cation exchange resin is explained in Figure 42. The properties of Amberlyst® 15 resins are provided in Table 18.

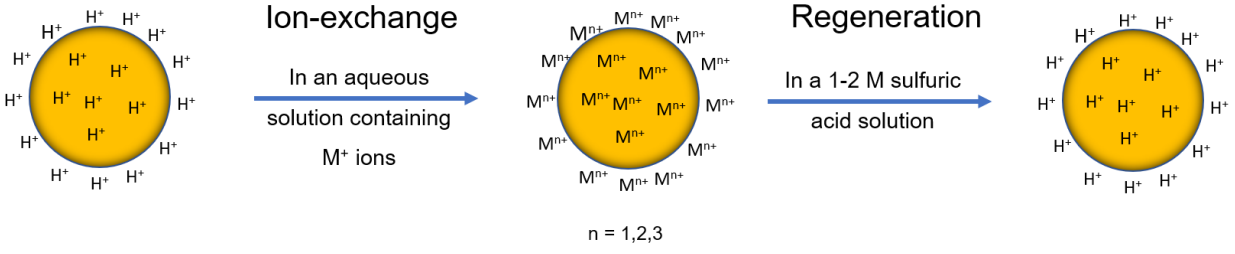

Figure 42. Typical operation of a strong acid cation exchange resin.

Table 18. Typical properties of Amberlyst® 15 from its safety datasheet. [189]

Physical properties	
Copolymer	Styrene-divinyl benzene
Matrix	Macroporous
Type	Strong acid cation
Functional group	Sulfonic Acid
Physical form	Gray, opaque, spherical beads
Nitrogen BET	
Surface area	53 m^2/g
Total pore volume	0.40 cm^3/g
Average pore diameter	300 Å
Chemical properties	
Ionic form	H^+
Maximum operating temperature	120 °C

5.4.1. Preliminary Studies using Amberlyst® 15 in a Batch Setup

Resins activation: The Amberlyst® 15 (Dry, H-form) needs to be activated before performing any ion exchange. Therefore, a sufficient amount of resins were soaked in 1.5 M H_2SO_4 for 2 h to activate the ion exchange sites with H^+. The activated resins were washed with DI water until the effluent was a neutral pH (pH ~ 7). After washing, the activated resins were mixed with the aqueous filtrate for ion exchange.

Preliminary ion-exchange Study with $K_2C_2O_4$: After Li and Co precipitation, as discussed in Chapter 4, the aqueous phase predominantly contained K^+ and the $C_2O_4^{2-}$ initially added during the $H_2C_2O_4$ acid addition. On mixing the resins with the aqueous filtrate, an ion exchange between K^+ and H^+ ion along with a decrease in pH was hypothesized. A 50 ml model solution of pH 13.50 using $K_2C_2O_4$ and KOH was used to test this hypothesis. In the prepared solution, 30 g of activated

resins (wet form) was mixed for 1 h without stirring. The stirring was avoided to minimize damaging the resin beads. The ion-exchange efficiency was calculated by measuring the concentration of remaining K^+ ions in the aqueous phase and subtracting it from the initial K^+ concentration. After 1 h, the pH of the aqueous filtrate decreased to 1.1, with K concentration in the aqueous phase also decreasing from 20 g/L to 0.2 g/L resulting in a 99% exchange efficiency. Based on the speciation of oxalic acid, the aqueous phase at a pH of 1.1 was confirmed to be $H_2C_2O_4$. The results were encouraging and established ion exchange through Amberlyst® 15 as a possible way to recycle the oxalate-based reagents.

5.4.2. Experimental capacity and kinetics of ion exchange using Amberlyst® 15

For the preliminary understanding of ion exchange, experiments were performed in a batch setup rather than a column setup. The theoretical capacity of Amberlyst® 15 was reported as 4.3 meq./g (for Dry, Na^+ form).[188] During the setup of batch experiments, a significant difference between the weight of wet and dry resins was observed. To estimate the difference, the moisture-holding capacity of the Amberlyst® 15 (H^+ form) used in this work was determined to be 55% by drying the wet resins in the air while measuring the weight.

To obtain the experimental exchange capacity of resins for K^+, the resins were activated using the method described in Section 5.4.1. Next, 50 g of wet activated resins were sequentially mixed in the 100 ml batches of 1 M KOH solution until saturated. The experimental capacity for Amberlyst® 15 was found to be 4.64 meq./g, and the results are presented in Table 19. The capacity of the resins was critical for determining the mass of dry resins required to recycle the acid after metal extraction from $LiCoO_2$. Another important parameter is the contact time required between resins and the aqueous phase in the batch setup operation. Hence, the K concentration in the 100 ml of 1 M KOH solution was tracked after mixing with 50 g of wet resins. The

concentration of K in this 1 batch was sufficient to saturate the resin by 80%. The ion exchange (at 20 °C) was completed within the first 15 minutes of contact, as shown in Figure 43. During this ion exchange, pH of the solution decreased from 13.8 to 6.3.

Table 19. Measurement of exchange capacity for Amberlyst® 15 (Dry, H+ form)

Batch No.	**K – concentration in the aqueous phase (g/L)**		**Net exchange (meq. of K)**
	Before resins addition	**After resins addition**	
1	39.10	2.67	93.18
2	39.10	35.55	9.09
3	39.10	38.21	2.27
4	39.10	38.92	0.45
		Total exchange	105 meq. of K
		Dry weight of resins	22.72 g
		Experimental capacity	4.62 meq./g

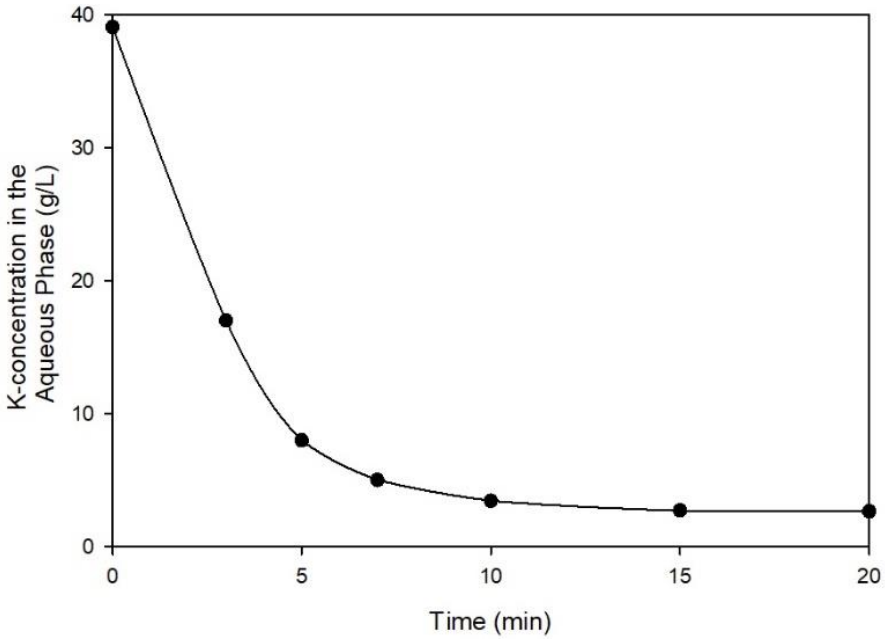

Figure 43. Kinetics of ion exchange with 50 g wet resins in 100 ml of 1 M KOH solution (initial concentration).

5.4.3. Conditions for regeneration of Amberlyst® 15 resins

Another important study was to determine the conditions for regenerating the K-saturated Amberlyst® 15 resins to its original H-form using a batch setup. Approximately 20 g of wet resins (from 50 g wet resins, Table 19) were mixed sequentially with three 40 ml batches of 1.5 M H_2SO_4. The contact time between the resins and 40 ml H_2SO_4 was 30 min. To calculate the regeneration efficiency, the concentration of K in the acidic phase was tracked for every batch, and the results are shown in Table 20. To regenerate 20 g of K-saturated resins into the H-form, at least 120 ml of 1.5 M H_2SO_4 was required. Excess H_2SO_4 was required for the regeneration of SAC resins.[190] In addition, the H_2SO_4 used in the regeneration study shown in Table 20 can be reused for other batch of resins saturated with K^+. To study this hypothesis, 40 ml of 1.5 M H_2SO_4 was mixed with five batches of K-saturated 20 g wet resins. Every resin batch was saturated with approximately 42 meq. of K^+. The results shown in Table 21 conclude that the 40 ml of 1.5 M H_2SO_4 resins can partially regenerate each batch of resin saturated with K^+ ions. After contacting 5 similar batches

of K-saturated resins, 39.27 meq. of K was extracted. The 39.27 meq. of K is 94% of the K present on 20 g saturated resins (1 batch of Table 21). These results were promising, and a process could be designed using recycled and fresh 1.5 M H_2SO_4 for regenerating SAC resins.

Table 20. Regeneration of 20 g wet resins through batches of 1.5 M H_2SO_4

Batch No.	**K – concentration in the H_2SO_4 (g/L)**		**Net exchange (meq. of K)**
	Before resins addition	**After resins addition**	
1 (40 ml – 1.5 M H_2SO_4)	0	19.99	20.45
2 (40 ml – 1.5 M H_2SO_4)	0	14.97	15.31
3 (40 ml – 1.5 M H_2SO_4)	0	4.72	4.83
	Total exchange		40.59 meq. of K
	Amount of K on 20 g saturated resins		42 meq.
	Resin regeneration efficiency		96.6 %

Table 21. Extraction of K^+ in a 1.5 M H_2SO_4 solution (40 ml) from K-saturated resin batches

Batch No.	K – concentration in the H_2SO_4 (g/L)		Net exchange (meq. of K)
	Before resins addition	After resins addition	
1 (20 g - K-Resins)	0	17.26	17.65
2 (20 g - K-Resins)	17.26	28.16	11.15
3 (20 g - K-Resins)	28.16	32.95	4.91
4 (20 g - K-Resins)	32.95	36.32	3.44
5 (20 g - K-Resins)	36.32	38.39	2.11
	Total exchange		39.27 meq. of K

5.5. Regeneration of NH_4^+ based oxalate reagents using Amberlyst® 15

In Section 5.4, the ion exchange process for acid regeneration was demonstrated by exchanging K^+ ions. The NH_4^+ (for $NH_4HC_2O_4$ acid) is another cation that has been used in developing closed-loop processes for Fe and Ti recovery from ilmenite ore.[16,76] For the recovery of $NH_4HC_2O_4$ using ion-exchange resins, 50 ml of 0.30 M $(NH_4)_2C_2O_4$ (pH = 5.70) was used. The $NH_4HC_2O_4$ must be the predominant oxalate species in the aqueous phase for recycling. The radius of NH_4^+ ion (1.48 Å) is similar to the K^+ ion (1.33 Å).[191,192] Because of the similar ionic radii, the ion exchange experiments were performed using the same conditions discussed in the previous section. Therefore, 15 g (wet) of activated Amberlyst® 15 resins were mixed with the 0.30 M $(NH_4)_2C_2O_4$ for 1 h without stirring. After 1 h, the pH of the solution decreased to 2.48. Unlike the previous section, the concentration of NH_4^+ ions in the aqueous phase could not be measured. However, from the oxalate speciation curve (Figure 2), at pH = 2.48, $HC_2O_4^-$ was confirmed to be

the predominant oxalate species. To confirm this, 1 ml of liquid was spread and air-dried on a glass side for 24 h. The resulting crystals were ground and confirmed as $NH_4HC_2O_4 \cdot 0.5H_2O$ using the PXRD shown in Figure 44.

This study was continued further to evaluate whether $H_2C_2O_4$ can also be synthesized by the addition of more resins. To test the hypothesis, 15 g (wet) of activated resins were added in the aqueous solution of pH 2.48 for 1 h. After 1 h, pH decreased to 1.10, and similarly, through air-drying, crystals were generated. These crystals were ground and confirmed to be a 60:40 mixture of $H_2C_2O_4 \cdot 2H_2O$ and $NH_4HC_2O_4 \cdot 0.5H_2O$ using PXRD, as shown in Figure 40. The crystals corresponding to the model 60:40 solution shown in Figure 45 were also prepared through a similar air-drying technique. This study confirms that SAC exchange resins like Amberlyst® 15 can conveniently regenerate the oxalate reagents in the desired acidic form.

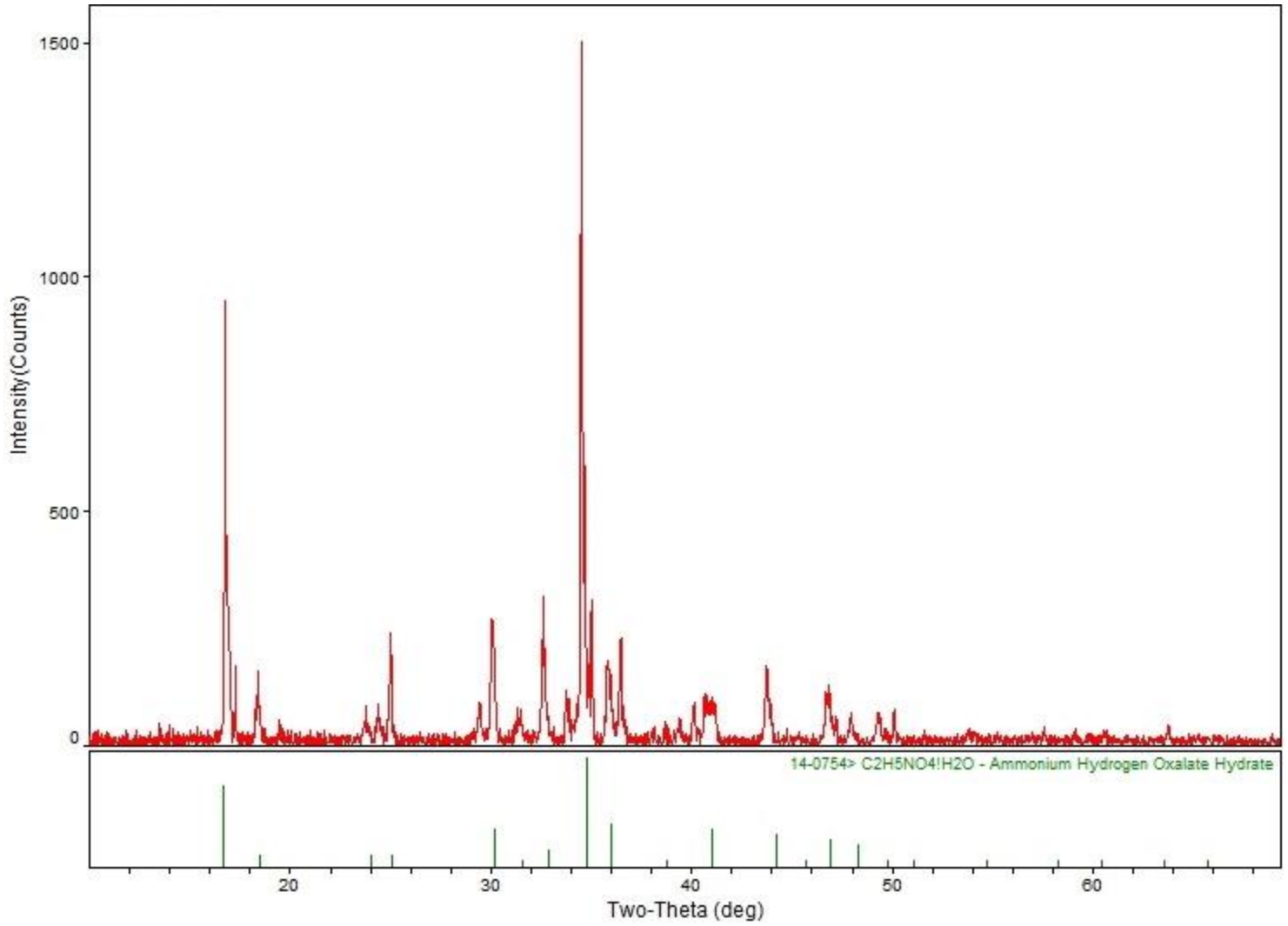

Figure 44. PXRD spectrum of crystals recovered from air-drying the ion exchanged solution (pH = 2.48). The collected pattern is corresponding to $\lambda = 1.78897$ Å

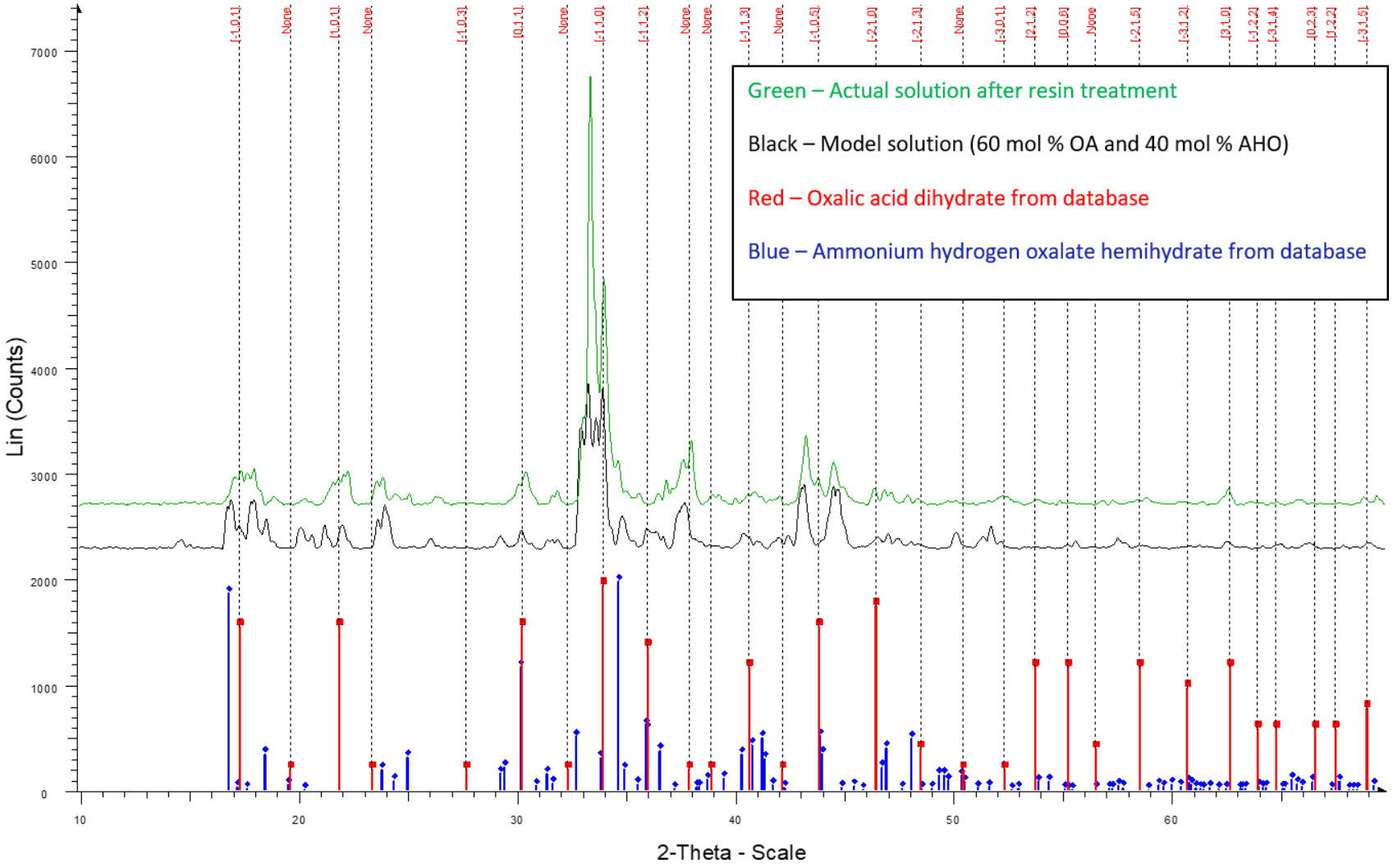

Figure 45. PXRD spectrum of crystals recovered from air-drying ion exchanged solution (pH = 1.10). The spectrum is compared to the crystals generated from the model solution of $H_2C_2O_4 \cdot 2H_2O$ and $NH_4HC_2O_4 \cdot 0.5H_2O$ in a 60:40 wt% ratio. The red and blue patterns are from ICDD database. All patterns are corresponding to $\lambda = 1.78897$ Å

5.6. Regeneration of K^+ based oxalate reagents using precipitation

An alternative approach was identified to recover the K^+ based oxalate reagents on the basis of their aqueous solubility at 20 °C. While performing the ion-exchange experiments of Section 5.4.1, an insoluble white compound was observed in the pH range of 1.5-3.5. This white precipitate contained two different inorganic compounds at a pH of 2.5 and 1.5. Using PXRD, the white compounds at pH = 2.5 and 1.5 were identified as potassium hydrogen oxalate (KHC_2O_4) and potassium tetraoxalate ($KHC_2O_4 \cdot H_2C_2O_4$), respectively. The aqueous solubilities of KHC_2O_4 and $KHC_2O_4 \cdot H_2C_2O_4$ were measured as 5.73 g and 2.97 g per 100 mL of water at 20 °C, respectively. For comparison, the aqueous solubilities of the possible compounds with K^+ and $C_2O_4^{2-}$ ion are summarized in Table 22. The KHC_2O_4 and $KHC_2O_4 \cdot H_2C_2O_4$ have low solubility and was precipitated while acidifying the K-rich oxalate solution.

Table 22. Solubilities of common oxalate compounds relevant to this section.

Compound Formula	Aqueous solubility at 20 °C (g/100 ml)	Reference
KHC_2O_4	5.73 ± 0.33	Experimental
$KHC_2O_4 \cdot H_2C_2O_4 \cdot 2H_2O$	2.97 ± 0.20	Experimental
$K_2C_2O_4 \cdot H_2O$	36.4	193
$H_2C_2O_4 \cdot 2H_2O$	13.3	193

To utilize this unique property, a solution of $K_2C_2O_4$ with $C_2O_4^{2-}$ = 10 g/L was prepared. The $C_2O_4^{2-}$ concentration was based on the saturation limit of $H_2C_2O_4$. To acidify the solution, 98% H_2SO_4 was used. At the pH of 2.5, a white precipitate was observed, and it was confirmed as KHC_2O_4 (Figure 46) using PXRD. Approximately 65% of the $C_2O_4^{2-}$ ion was recovered as

KHC_2O_4. The aqueous phase and the recovered precipitate were acidified further to pH = 1.5, and an increase in the amount of white precipitate was observed. The precipitate recovered at pH = 1.5 was confirmed as $KHC_2O_4 \cdot H_2C_2O_4 \cdot 2H_2O$ using PXRD (Figure 47). About 80% of the initial $C_2O_4^{2-}$ ion was recovered as $KHC_2O_4 \cdot H_2C_2O_4 \cdot 2H_2O$.at pH = 1.50. Using these methods, oxalate reagents are recovered in the solid phase, compared to the aqueous phase recovery from the ion exchange method. However, the cost-effective acid regeneration processes have significant environmental and economic benefits in the ore refining processes, as discussed later.

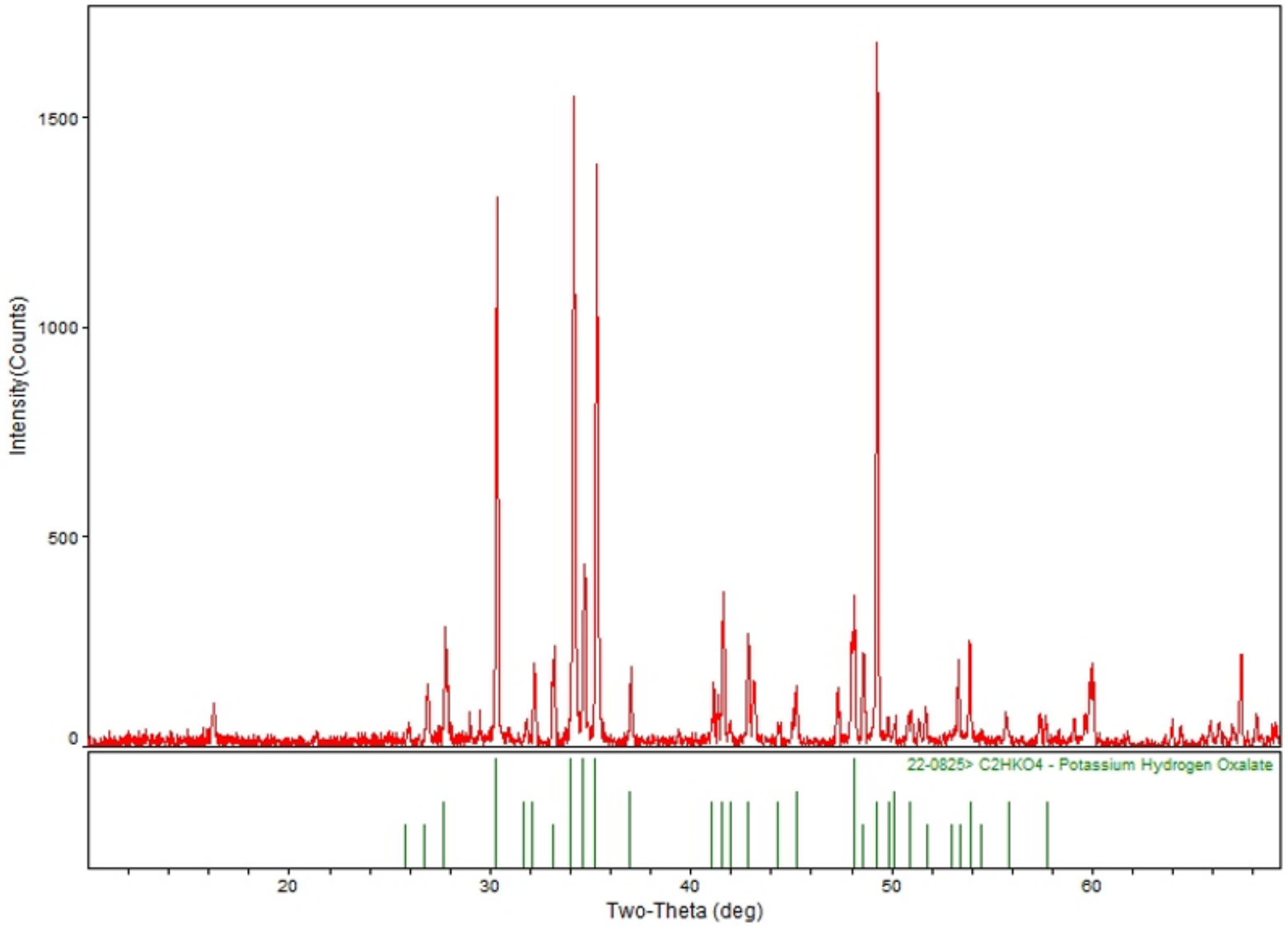

Figure 46. PXRD spectra of solids recovered at pH = 2.50. The collected pattern is corresponding to λ = 1.78897 Å.

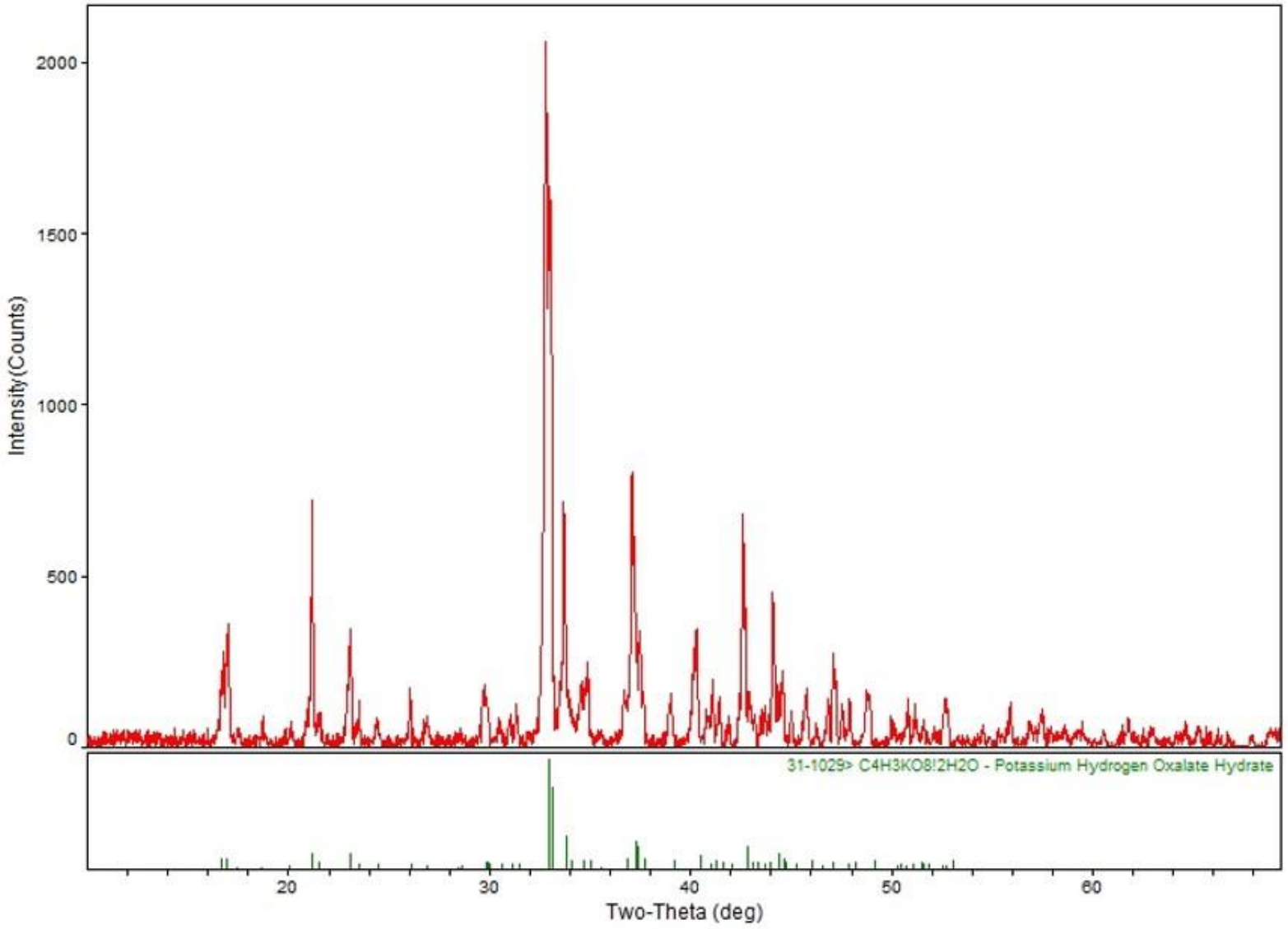

Figure 47. PXRD spectra of solids recovered at pH = 1.50. The collected pattern is corresponding to λ = 1.78897 Å.

5.7. Conclusions

Recycling oxalate reagents after recovery of critical metals is necessary for waste minimization and cost-effectiveness. An ion exchange process using strong acid cation exchange resins replaced the ions such as K^+, NH_4^+ with H^+ to regenerate the oxalic acid and its derivatives. In this chapter, the ion exchange process was optimized for Amberlyst® 15 (Dry, H-form) to exchange K^+ with H^+. The kinetic study revealed that 50 g (wet) of activated resins exchanged 39 g/L of K^+ in around 15 minutes. The K-saturated resins were regenerated efficiently for reuse in a 1.5 M H_2SO_4 solution. This ion exchange process can be implemented for recycling of $H_2C_2O_4$ after Li and Co precipitation and is discussed in Chapter 6. In addition, the regeneration of binoxalate species ($NH_4HC_2O_4$ and KHC_2O_4) was performed through ion-exchange resins with final pH of around 2.5. Alternatively, a solubility-based approach was identified for the regeneration of KHC_2O_4 and $KHC_2O_4{\cdot}H_2C_2O_4{\cdot}2H_2O$. The K^+ based oxalate reagents were precipitated by acidifying the $K_2C_2O_4$ solution to a pH of 1.5-2.5. The oxalate reagents like NH_4H-C_2O_4, $KHC_2O_4{\cdot}H_2C_2O_4$, and KHC_2O_4 have applications in ore refining and will be discussed in Chapter 7. Recycling oxalate reagents is critical to develop closed-loop, economical and environmentally-friendly processes for valuable metal recovery from various mixed metal oxide sources.

Chapter 6. Lithium and Cobalt Recovery from $LiCoO_2$ using Oxalate Chemistry: Scale-up and Techno-economic Analysis

Portions of this chapter are adapted from the following article:

Verma, A., Henne, A.J., Corbin, D.R., & Shiflett, M.B., Lithium and Cobalt Recovery from $LiCoO_2$ using Oxalate Chemistry: Scale-up and Techno-economic Analysis. *Industrial & Engineering Chemistry Research (submitted)*

Chapter 6

"Waste does not exist in nature because ecosystems reuse everything that grows in a never-ending cycle of efficiency and purpose."
- Frans van Houten (CEO, Philips)

6.1. Abstract

Currently, approximately 59% of the lithium-ion batteries (LIBs) contain a lithium cobalt oxide ($LiCoO_2$) cathode. Both lithium (Li) and cobalt (Co) are critical metals, and the efficient recycling of $LiCoO_2$ cathodes through an environmentally-benign process is essential for a stable Li and Co economy. In this chapter, a closed-loop recycling process utilizing oxalic acid ($H_2C_2O_4$) and hydrogen peroxide (H_2O_2) was scaled-up to operate at a solid-to-liquid (S/L) ratio of 38 g/L. The $H_2C_2O_4$ process was operated at 100 °C with Li_2CO_3 and $Co(OH)_2$ as the final products, whereas in the presence of H_2O_2, the metal extraction was operated at 75 °C. After the metal recovery, the $H_2C_2O_4$ was efficiently recycled using an ion exchange process. A techno-economic analysis was performed to compare the oxalate process with H_2SO_4 process operating at 65 °C and S/L = 100 g/L. The $H_2C_2O_4$ and $H_2C_2O_4 + H_2O_2$ processes with 90% recycling of oxalate are equal in cost with the H_2SO_4 process on a per kilogram $LiCoO_2$ production basis. An important difference is the $H_2C_2O_4 + H_2O_2$ process produces 50% less waste than the $H_2SO_4 + H_2O_2$ process. The $H_2C_2O_4$ and $H_2C_2O_4 + H_2O_2$ processes provide the opportunity to recycle oxalate in order to create a closed-loop, economical, and environmentally-friendly process for recovering critical metals such as Li and Co from $LiCoO_2$. The oxalate process offers similar advantages for recycling of other valuable metals from ore processing and waste streams.

6.2. Background and Motivation

Hydrometallurgical processes using organic acids like oxalic, citric, ascorbic, and succinic acid have been demonstrated at a lab-scale to recover critical metals from spent LIBs.[32,53,54,151-154] These acids have minimal environmental impacts but are expensive compared to inorganic acids. H_2O_2 is commonly used as a reducing agent along with acids to convert Co^{3+} into the stable Co^{2+} form. Oxalic acid ($H_2C_2O_4$) is unique in its reducing and solubility properties and was identified as a sustainable, green, and environmentally-friendly reagent in previous chapters.[162] For the hydrometallurgical treatment of $LiCoO_2$ using $H_2C_2O_4$, Li leaches into the solution, whereas Co precipitates out in the form of $CoC_2O_4{\cdot}2H_2O$. This direct separation allows a one-step separation between Li and Co in the recycling process.[12,162]

In Chapters 2, and 3, $H_2C_2O_4$ was shown to be an efficient reagent to separate and recover Li and Co from $LiCoO_2$.[162] In addition, to offset the cost of expensive $H_2C_2O_4$ and minimize waste generation, a closed-loop process was proposed to regenerate the acid after metal precipitations. The $H_2C_2O_4$ regeneration was proposed through a cation exchange process, as discussed in Chapter 5. This chapter extends and improves the study in Chapter 2 to regenerate and reuse 100% of the $H_2C_2O_4$ through a novel closed-loop process. To the best of our knowledge, no other hydrometallurgical process has been developed that demonstrates 100% acid recovery and reuse. In addition, a techno-economic analysis has been performed comparing our developed closed-loop hydrometallurgical processes of $H_2C_2O_4$ and $H_2C_2O_4 + H_2O_2$ with the $H_2SO_4 + H_2O_2$ process for recycling LIBs cathode. The flexibility of the oxalate closed-loop process to recycle NMC cathodes and other metallic impurities (from current collector foils and separators) like Fe, Cu, Al, and Zn have also been discussed. This chapter demonstrates the adaptability and uniqueness of

oxalic acid in developing a closed-loop, green, and environmentally-friendly recycling process for LiBs.

6.3. Demonstration of the closed-loop processes

In this chapter, the metal extraction processes demonstrated in Chapters 2 and 3, were scaled up to the solid-to-liquid (S/L) ratio of 38 g/L from 15 g/L. The Li and Co extraction from $LiCoO_2$ using $H_2C_2O_4$ is a solid-liquid reaction with both solid and liquid products. A S/L ratio determines the amount of solid that can be processed in a 1 L of aqueous reactant. Initially, 15 g/L was chosen on the basis of optimization work performed by Zeng et al.[11] However, it was identified that the S/L ratio could be increased while maintaining the optimized Co:OA ratio (1:3) at high agitation speed (>500 rpm). Hence, the reactor temperature (T) and agitation speed (N_S) were set at 98 °C and 600 rpm, respectively. The molar ratio between $LiCoO_2$ and $C_2O_4^{2-}$ (Co:OA) is critical and was kept constant at Co:OA = 1:3 (1.16 M $H_2C_2O_4$). In the presence of H_2O_2, the molar ratio between $LiCoO_2$, $C_2O_4^{2-}$ and H_2O_2 (Co:OA:H_2O_2) was maintained at Co:OA:H_2O_2 = 1:1.5:3. This corresponds to a concentration of 0.58 M $H_2C_2O_4$ and 1.16 M H_2O_2 to maintain a S/L ratio of 38 g/L. The S/L ratio = 38 g/L was set to avoid crystallization of $H_2C_2O_4$ (may contain Li) in the leachate after cooling to 20 °C.

6.3.1. Materials and Materials Characterization

Lithium cobalt oxide, $LiCoO_2$, (99.8%, Sigma-Aldrich), oxalic acid dihydrate, $H_2C_2O_4 \cdot 2H_2O$, (99.5%, ACROS Organics), lithium nickel-manganese-cobalt oxide, $LiNi_{0.33}Mn_{0.33}Co_{0.33}O_2$, (NMC111, MSE Supplies), and hydrogen peroxide, H_2O_2, (30%, Fisher Chemical) were used for the digestion reactions. Potassium carbonate, K_2CO_3, (99%, ACROS Organics) and potassium hydroxide, KOH, (Pellets 85%, Fisher Chemical) were used for the metal precipitations. Amberlyst® 15 (Dry H-form, strong acid cat ion-exchange resin) and sulfuric acid,

H_2SO_4, (ACS reagent, Fisher Chemical) were used in the regeneration studies. All solutions were prepared in deionized water (18 MΩ-cm).

The metal concentration in the aqueous phase was measured using a Varian/Agilent 725 ES inductively coupled plasma – optical emission spectrometer (ICP-OES). Calibration was performed using the standards prepared from the commercial stock solutions. The 5 wt% HNO_3 was used as diluent for ICP-OES measurements. Solid samples were analyzed on a Bruker D2-phaser powder X-ray diffraction (PXRD) with a Co Kα source (λ = 1.78897 Å), operated at 30 kV and 10 mA. The details about the characterization instruments can be found in Appendix: Section A1

6.3.2. Reactor Setup and Sampling

A 1-L glass reactor was used for all of the hydrometallurgical experiments in this work.[162] A 5 ml plastic syringe with a 20 cm long needle was connected to the sampling port to withdraw solid and aqueous samples. The samples were centrifuged for 5 min at 4000 rpm to separate the aqueous and solid phase. The aqueous phase was diluted with 5 wt% HNO_3 at an appropriate ratio to achieve a concentration of less than 10 ppm for every metal in the aqueous phase.

6.3.3. Precipitation and Acid Regeneration: Experimental

The precipitation and acid regeneration processes were discussed in detail in Chapters 4 and 5. In this section, the experimental details on both processes are covered. For precipitation, the pH of the solution was critical to precipitate metal hydroxides and carbonates from an aqueous solution. KOH pellets (85%) were used to regulate the pH of the solution. During the extraction of Li and Co from $LiCoO_2$ using $H_2C_2O_4$, Li remained in the aqueous phase, whereas Co precipitated as $CoC_2O_4{\cdot}2H_2O$. The Li concentration in the aqueous phase after a 38 g/L metal extraction experiment was 2.70 g/L. The Li_2CO_3 has an aqueous solubility of 13.3 g/L, which

corresponds to the Li concentration of 2.50 g/L; therefore, it is essential to concentrate Li before precipitation. In this work, the aqueous phase was concentrated by four times to achieve a Li concentration greater than 10 g/L. This was achieved by evaporating the water to reduce the 1 L of the aqueous filtrate to 250 ml volume or reusing the same filtrate to perform three additional metal extraction experiments at the S/L ratio of 38 g/L. Once a Li concentration > 10 g/L was achieved, KOH was added to raise the pH > 13, and the Li was precipitated using K_2CO_3. After the removal of Li, $CoC_2O_4 \cdot 2H_2O$ was added slowly (1 g batches) and KOH was used to maintain the pH > 13 to ensure the precipitation of Co in the form of $Co(OH)_2$.

After precipitating Li and Co, the aqueous solution contained only K^+ as the major cation. In this work, Amberlyst® 15 (Dry, H-form), a strong acid cation exchange (SAC) resin, was used to regenerate and recycle $H_2C_2O_4$ in a batch setup. Initially, the resins were soaked in 1.5 M H_2SO_4 for 2 h to activate the ion-exchange sites with H^+. The activated resins were washed with DI water until the effluent was a neutral pH (pH ~ 7). After washing, the activated resins were mixed with the aqueous filtrate for 1-2 h. The aqueous phase predominantly contained K^+ and the $C_2O_4^{2-}$ initially added during the $H_2C_2O_4$ acid addition. The H^+ from the activated resins replaced the K^+ in the solution and $H_2C_2O_4$ was the predominant oxalate species at a pH ~ 1. The ion-exchange efficiency was calculated by measuring the concentration of remaining K^+ ions in the aqueous phase and subtracting it from the initial K^+ concentration. The K-saturated resins were regenerated to the original H-form using 1.5 M H_2SO_4.

6.3.4. Closed-loop Process using $H_2C_2O_4$ at S/L ratio = 38 g/L

Based on the dissolution and precipitation of Co in the form of $Co(OH)_2$, a new closed-loop process shown in Figure 48 was designed for Li and Co extraction and separation from $LiCoO_2$ using $H_2C_2O_4$. As discussed earlier, the hydrometallurgical experiments were performed

at a $LiCoO_2$ to $H_2C_2O_4$ molar ratio of 1:3 (1.16 M $H_2C_2O_4$), S/L ratio of 38 g/L, T = 100 °C, and N_s = 600 rpm. The Li and Co extraction kinetics from this experiment is shown in Figure 49 (Li and Co: Fresh Acid). It is important to note that the Co precipitated in the form of $CoC_2O_4 \cdot 2H_2O$ and was not present in the aqueous phase. The balanced chemical reaction between $LiCoO_2$ and $H_2C_2O_4$ is shown in Eq. 6.1. In Figure 49, efficient Li extraction kinetics were observed within 1 hour and the $LiCoO_2$ corresponding to a S/L ratio of 38 g/L was digested with Li and Co separated in the aqueous and solid phases, respectively.

$$4H_2C_2O_4(aq) + 2LiCoO_2(s) \leftrightarrows Li_2C_2O_4(aq) + 2CoC_2O_4 \cdot 2H_2O(s) + 2CO_2(aq) \qquad (6.1)$$

The next step after Li and Co separation was to precipitate Li in the form of Li_2CO_3 as shown in Figure 48. The Li concentration in the aqueous phase after the first extraction experiment was 2.65 g/L. The solubility of Li_2CO_3 is 13.3 g/L at 20 °C, and that corresponds to a Li concentration of 2.50 g/L.[20] The difference between the Li concentration in the aqueous phase and soluble Li in the Li_2CO_3 was minimal and efficient precipitation could not be performed. The aqueous phase was concentrated by reusing the solution for another extraction experiment. Additional $H_2C_2O_4$ was required to supplement the $C_2O_4^{2-}$ ions precipitated with $CoC_2O_4 \cdot 2H_2O$. In the lab-scale study performed for this work, the aqueous phase was concentrated by evaporating the water from the aqueous filtrate at 105 °C until the volume was reduced by four times. However, concentrating the solution via evaporation is an energy-intensive process and would not be recommended at commercial-scale. After concentrating the aqueous phase, Li was efficiently precipitated at 80 °C using KOH and K_2CO_3 at a pH = 13.5. The Li concentration in the aqueous phase decreased from 10.5 g/L to 1.3 g/L resulting in an 87 % Li recovery in the form of Li_2CO_3. The precipitate was confirmed as Li_2CO_3 using PXRD, as shown in Figure 50.

The precipitation liquor after separating Li had a high pH (pH > 12), and $CoC_2O_4 \cdot 2H_2O$ was hydrolyzed and precipitated in the form of $Co(OH)_2$ as discussed in Chapter 4. The solid $CoC_2O_4 \cdot 2H_2O$ was added in small batches while maintaining the pH using KOH, and a dark pink precipitate was recovered. The precipitate was confirmed as $Co(OH)_2$ using PXRD (Figure 51).

The precipitated Li_2CO_3 and $Co(OH)_2$ was used to synthesize cathode material through a solid-state reaction. The cathode synthesis involved mixing the solid reactants well and calcining the mixture. $LiCoO_2$ was synthesized from Li_2CO_3 and $Co(OH)_2$ in a 1:2 stoichiometric ratio at 800 °C (Eq 6.2). Other cathode materials like NMC can also be synthesized by adding a stoichiometrically equivalent amount of metal hydroxides along with Li_2CO_3. The $LiCoO_2$ was confirmed using PXRD, as shown in Figure 52.

$$Li_2CO_3 + 2Co(OH)_2 + \frac{1}{2}O_2 \rightarrow 2LiCoO_2 + CO_2 + 2H_2O \quad (6.2)$$

Once Li and Co were separated and recovered in their useful forms, the Amberlyst® 15 resins were used to regenerate the $H_2C_2O_4$. The aqueous solution is predominantly $K_2C_2O_4$ with a total K concentration of around 150 g/L. It should be noted that 1 L of the aqueous phase was concentrated to 250 ml during the Li precipitation, leading to a high K concentration. The $H_2C_2O_4$ was regenerated by mixing 90 g of activated Amberlyst® 15 resins (dry weight) in the $K_2C_2O_4$ solution for 1 h. The mixture was occasionally mixed, but continuous stirring was avoided to minimize damaging the resin beads. The quantity of resins used in this experiment was based on the optimization studies described in Section 5.4. After 1 h, the K concentration in the aqueous phase was reduced to 500 mg/L resulting in a 99.99% exchange efficiency. The pH of the aqueous phase also dropped from 13.6 to 0.48 after the complete ion exchange. A 1.5 M H_2SO_4 solution was used to regenerate the acidic sites in the used resins.

The regenerated acid was diluted to the original volume and 10 % of the initial $H_2C_2O_4$ was added to make up for the acid lost during precipitation and acid regeneration. The metal extraction from $LiCoO_2$ was performed using the regenerated acid at similar reaction conditions. The Li and Co extraction kinetics in the aqueous phase are shown in Figure 49 (Regenerated Acid). The Li extraction kinetics in the aqueous phase was similar to the fresh acid experiment, and >90% of Li was extracted within 1 h and >97% of the Co precipitated in the form of $CoC_2O_4 \cdot 2H_2O$. The precipitate was confirmed using PXRD (Figure 53). Using the regenerated acid, the efficient metal extraction from $LiCoO_2$ demonstrated the novel closed-loop process with essentially 100% acid recovery.

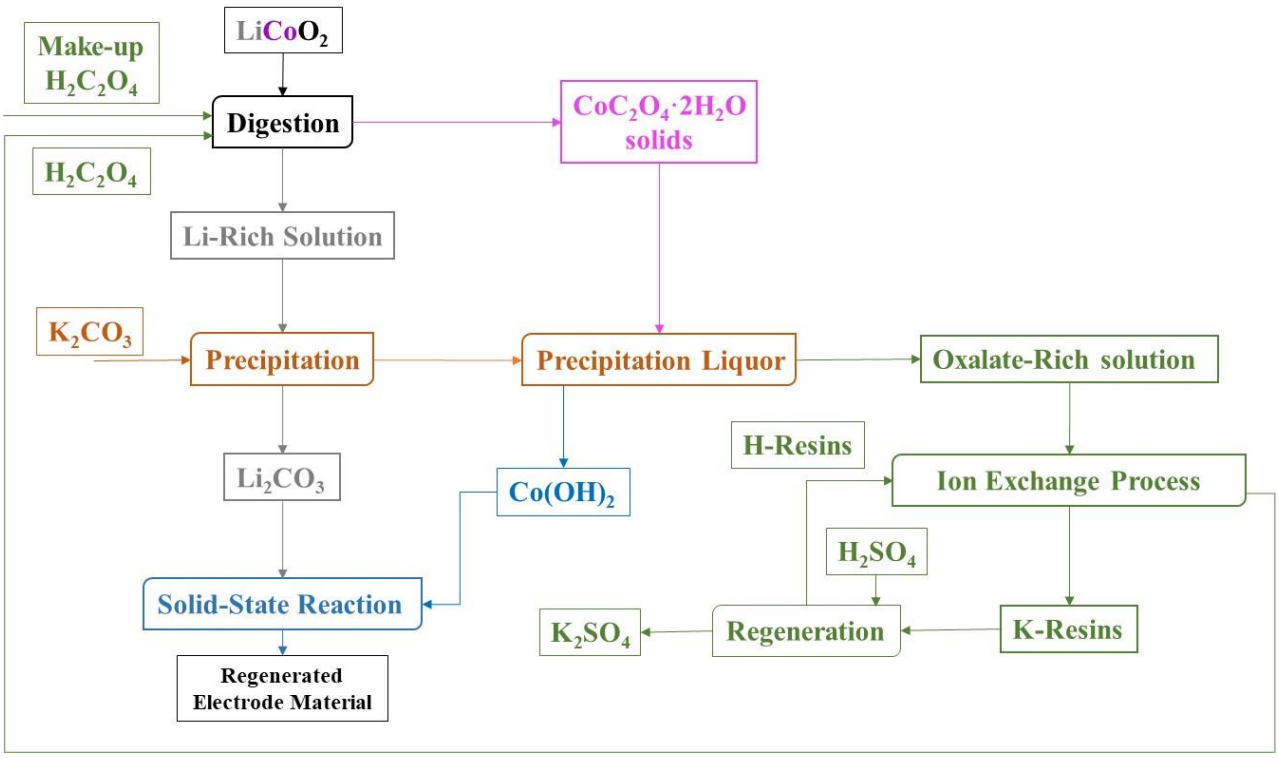

Figure 48. Flowsheet for the proposed closed-loop $LiCoO_2$ recycling process using $H_2C_2O_4$.

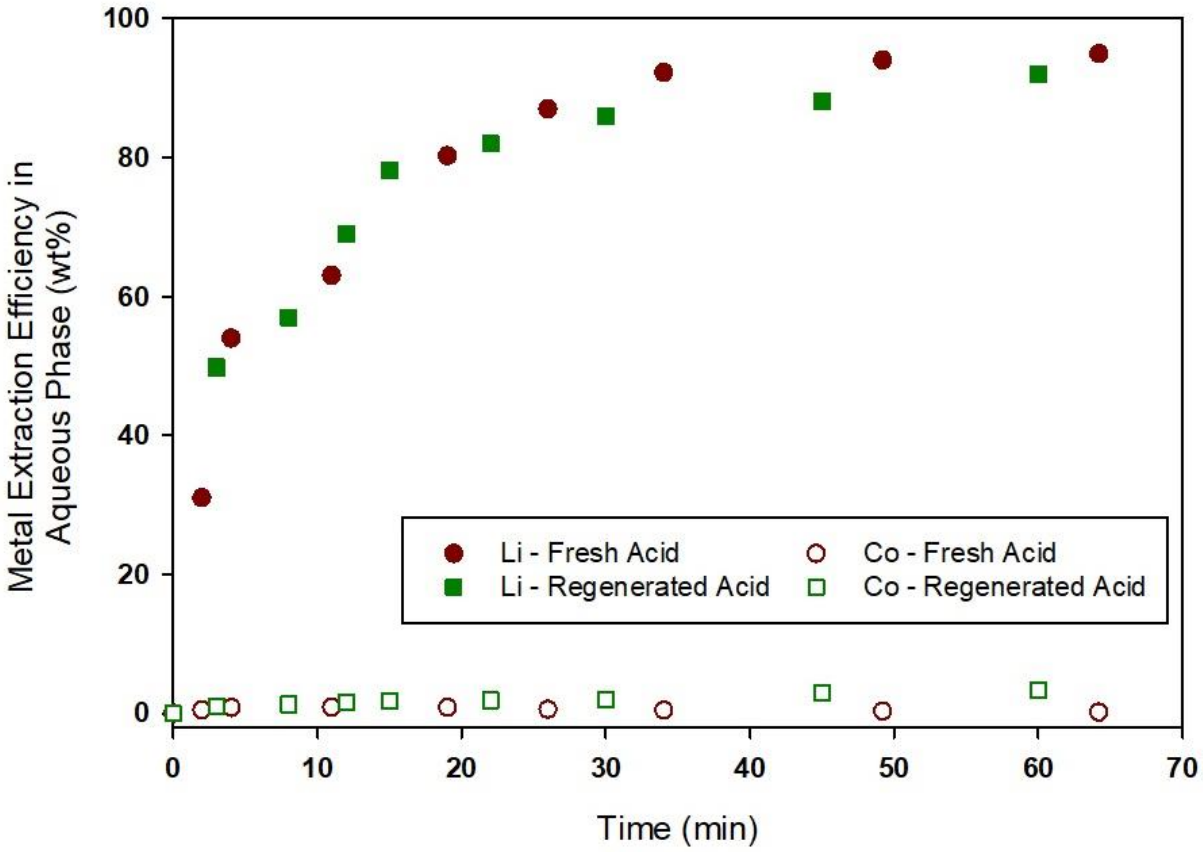

Figure 49. Metal concentration for Li and Co as a function of time in the aqueous phase for fresh and regenerated $H_2C_2O_4$ at Co:OA ratio = 1:3, T = 98 °C, S/L = 38 g/L, and N_S = 600 rpm.

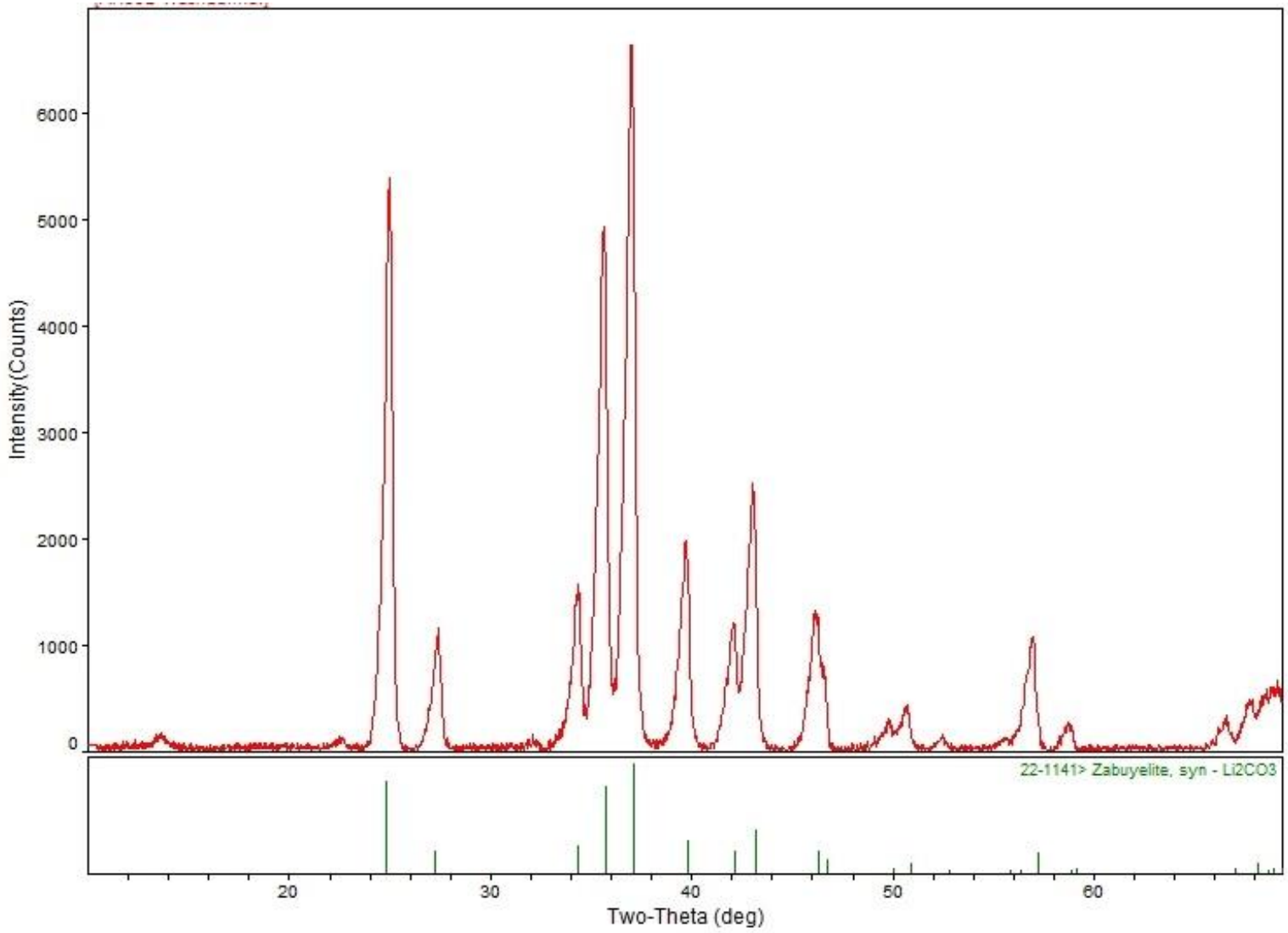

Figure 50. PXRD spectrum of solid recovered during lithium precipitation. The collected pattern is corresponding to λ = 1.78897 Å.

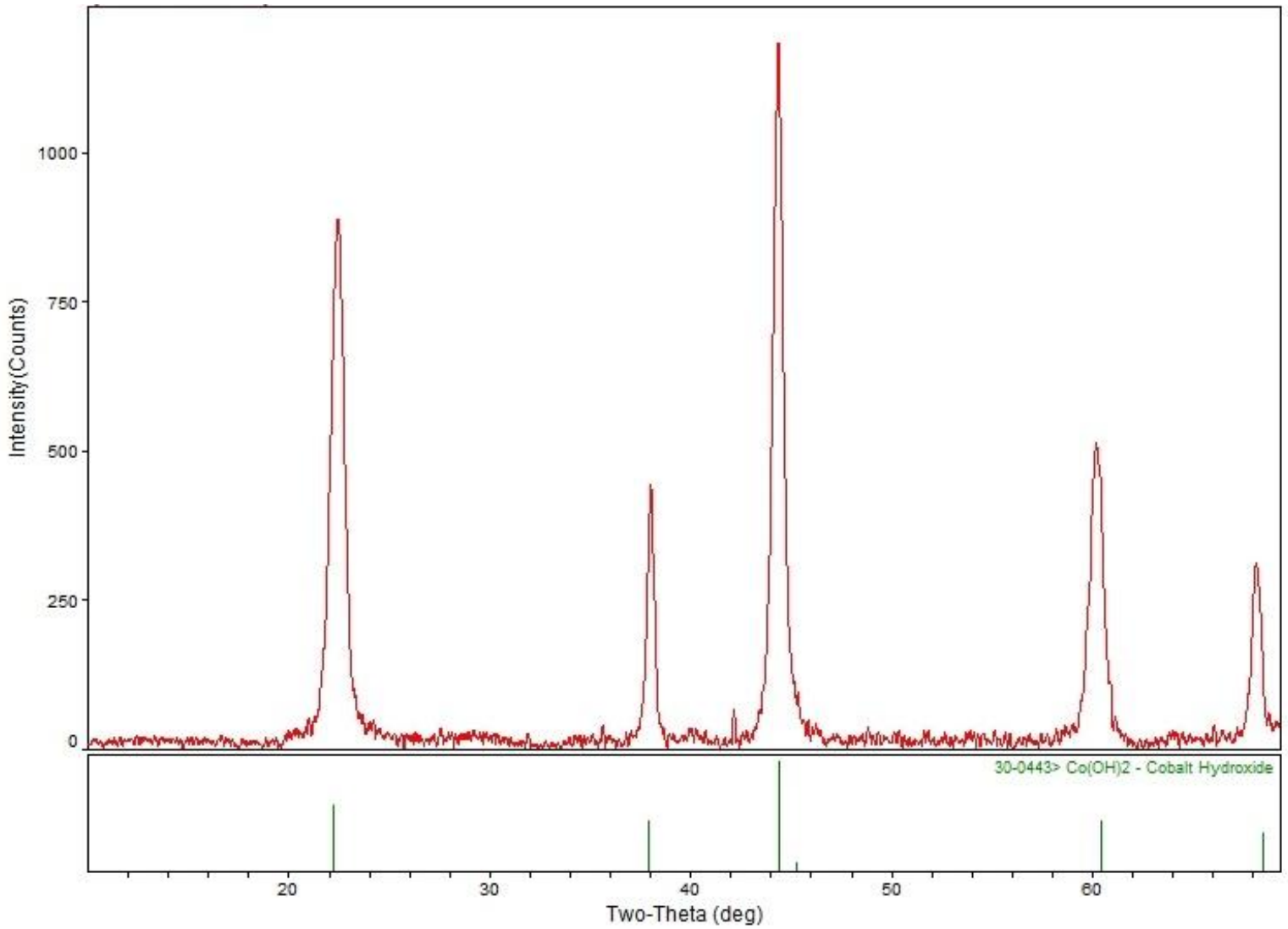

Figure 51. PXRD spectra of solid recovered during cobalt precipitation. The collected pattern is corresponding to λ = 1.78897 Å.

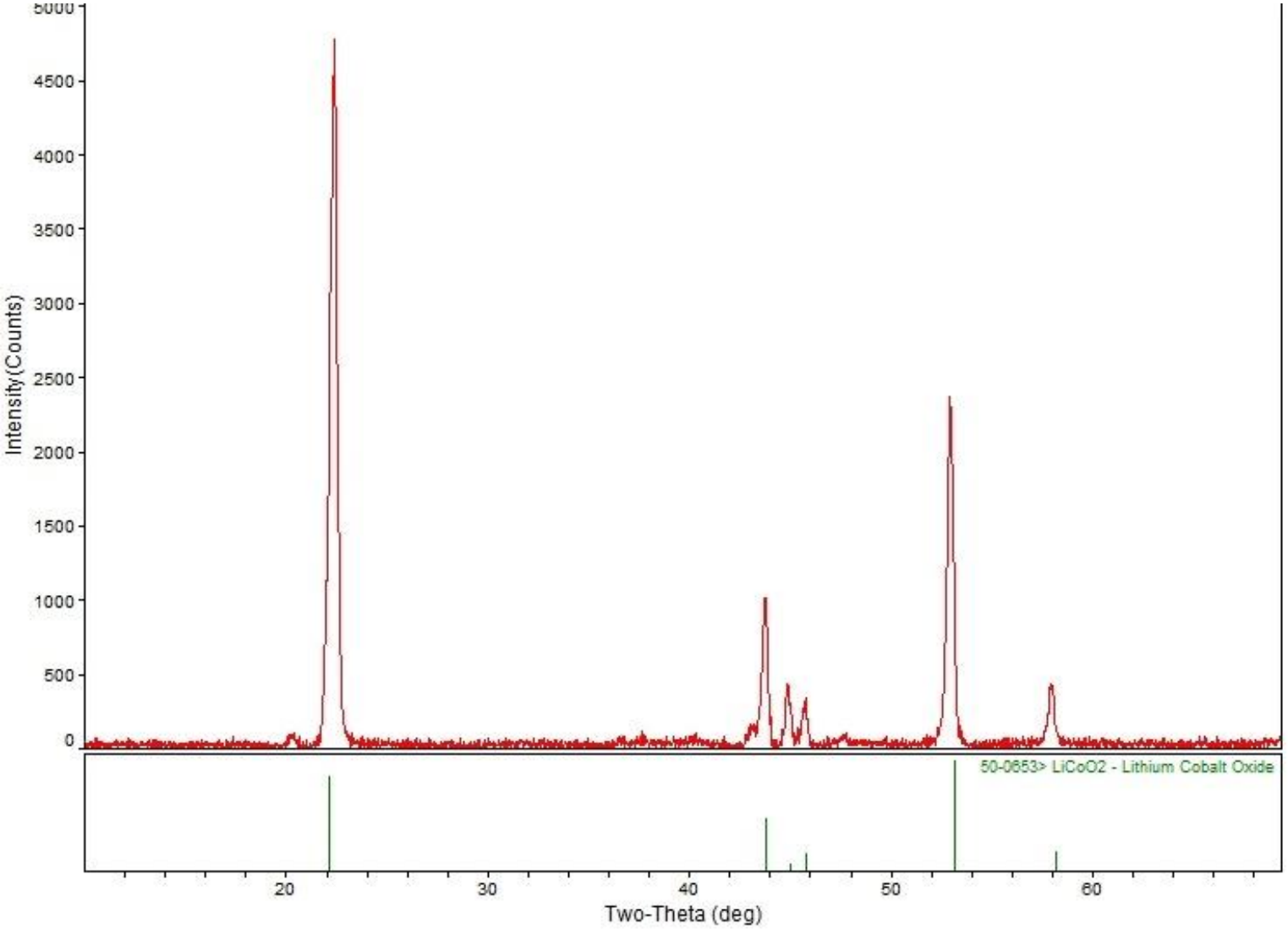

Figure 52. PXRD spectra of solids recovered after the solid-state reaction between Li_2CO_3 and $Co(OH)_2$. The collected pattern is corresponding to $\lambda = 1.78897$ Å.

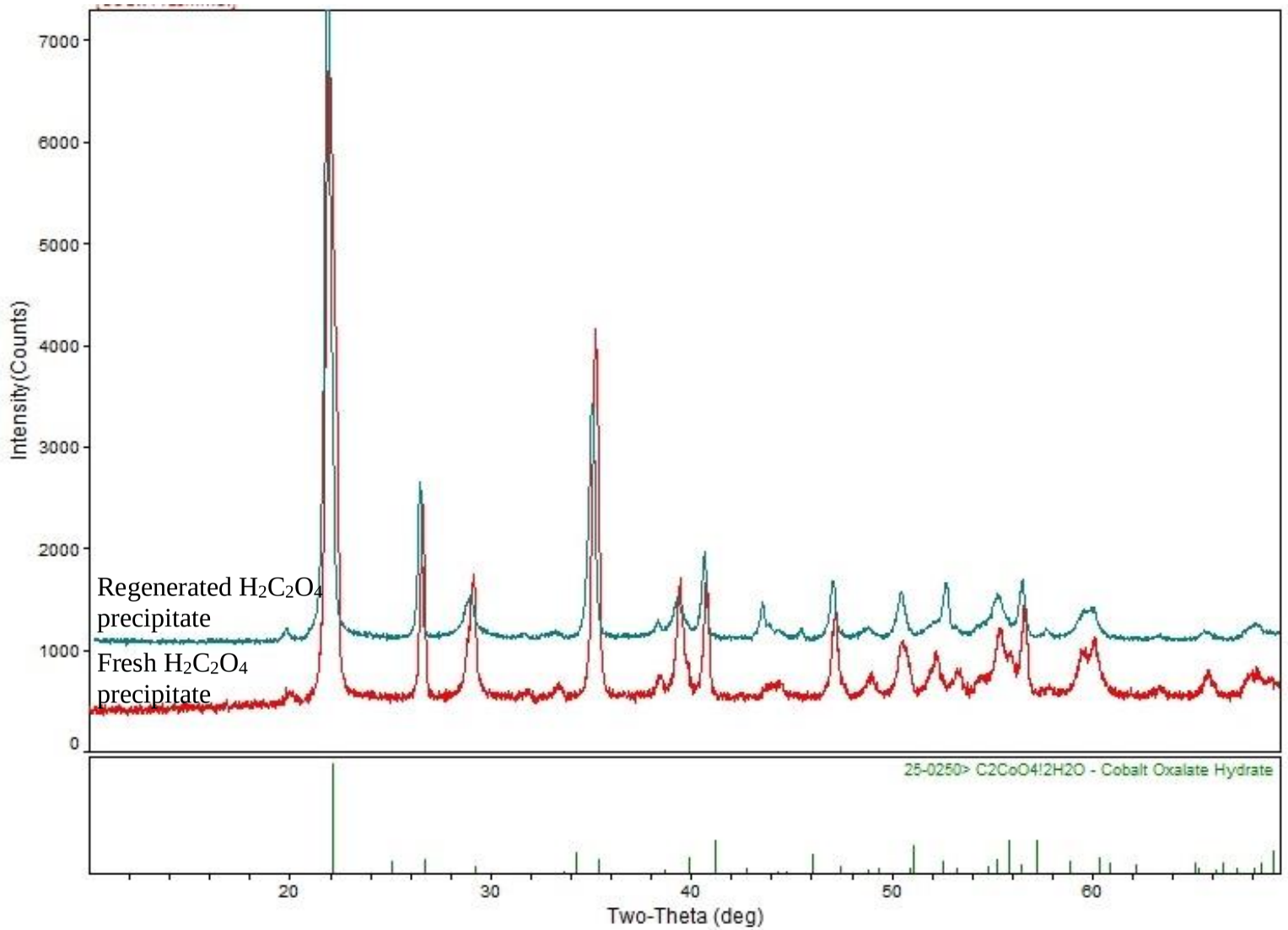

Figure 53. PXRD spectrum of the precipitate recovered from $LiCoO_2$ digestion using fresh and regenerated $H_2C_2O_4$ at S/L ratio = 38 g/L, T = 100 °C and N_s = 600 rpm. The collected pattern is corresponding to λ = 1.78897 Å.

6.3.5. Demonstration of the closed-loop process using $H_2C_2O_4 + H_2O_2$

In Chapter 3, the advantages of a $H_2C_2O_4 + H_2O_2$ process were discussed in detail.[194] A balanced chemical reaction between $LiCoO_2$ and $H_2C_2O_4 + H_2O_2$ is shown in Eq. 6.3. In the presence of H_2O_2, the Li and Co extraction can be performed efficiently in around 1 hour for temperatures in the range of 55-75 °C using a molar ratio of 1:1.5:3 between $LiCoO_2$, $C_2O_4^{2-}$ and H_2O_2 and at a S/L ratio of 15 g/L.[194]

$$4H_2C_2O_4(aq) + 2LiCoO_2(s) \leftrightarrows Li_2C_2O_4(aq) + 2CoC_2O_4{\cdot}2H_2O(s) + 2CO_2(aq) \quad (6.3)$$

In this work, a scaled-up process was developed to extract the metals at a S/L ratio of 38 g/L. Based on the results from Section 6.3.4., a similar closed-loop process could be designed with $H_2C_2O_4 + H_2O_2$ as the extraction reagent, as shown in Figure 54. In the presence of H_2O_2, metal extraction experiments were performed at 75 °C (rather than 100 °C with only $H_2C_2O_4$), and the extraction kinetics are shown in Figure 55 (fresh reagents). More than 90 % Li was extracted into the aqueous phase in around 45 min, and Co extraction in the aqueous phase was also minimal. The PXRD patterns confirming the Co products are provided in Figure 56. The Li and Co precipitations were performed as described in Section 6.3.4. The optimized $H_2C_2O_4 + H_2O_2$ process requires 0.58 M of $H_2C_2O_4$, compared to 1.16 M, described in Section 6.3.4. In addition, the amount of SAC resins required for regeneration was also reduced by 50%. This difference has a significant impact on the overall economics of the process and will be discussed in Section 6.4. The regenerated $H_2C_2O_4$ was diluted to the original volume, and 10% make-up acid along with fresh H_2O_2 was added to perform metal extractions under similar conditions. The Li extraction kinetics observed using the regenerated acid and fresh H_2O_2 (shown in Figure 55 – regenerated acid) were similar to the Li extraction experiments using fresh reagents. The improved kinetics were attributed to the better reduction properties of H_2O_2 than $C_2O_4^{2-}$ ion.

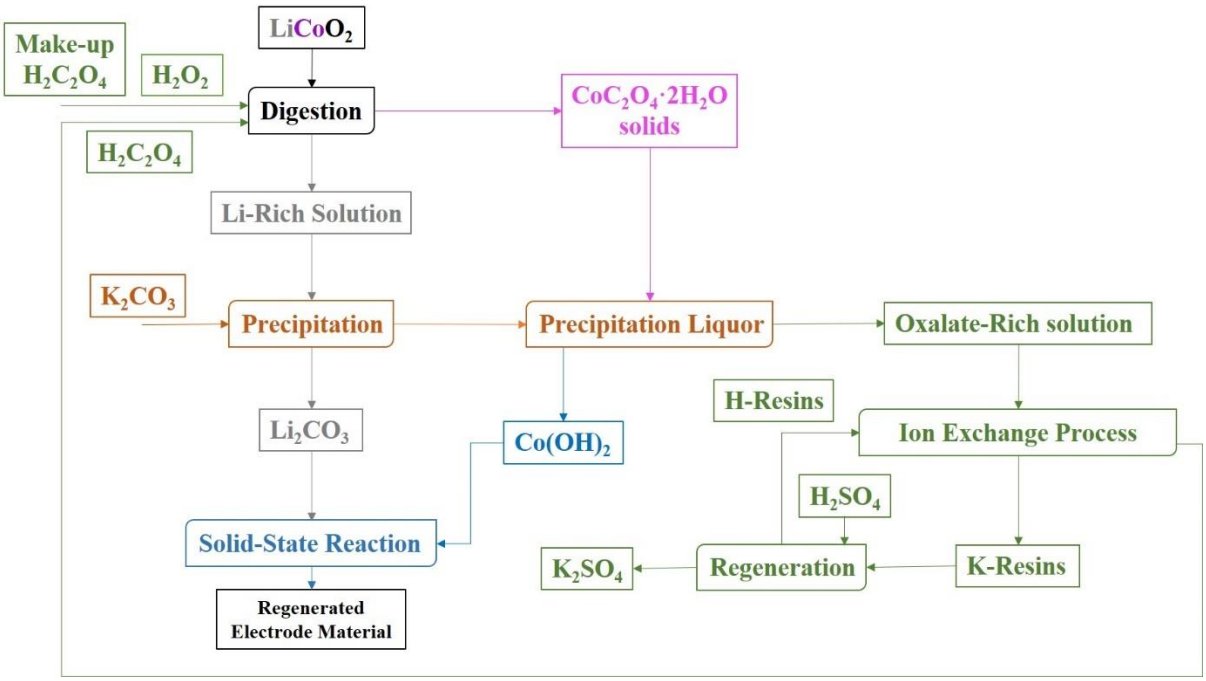

Figure 54. Flowsheet for the proposed closed-loop $LiCoO_2$ recycling process using $H_2C_2O_4$ and H_2O_2.

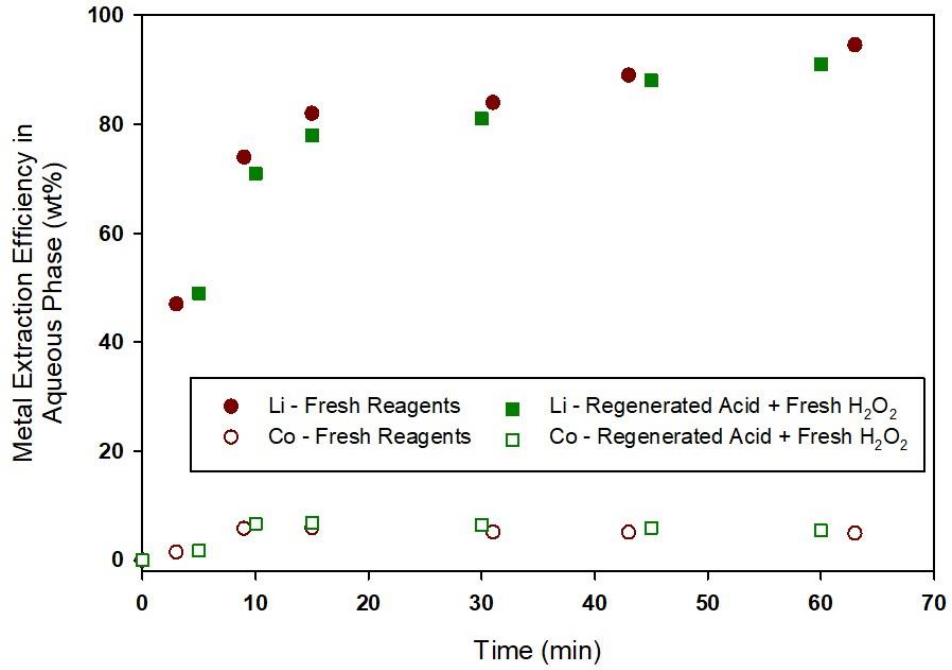

Figure 55. Metal concentration for Li and Co as a function of time in the aqueous phase for fresh and regenerated $H_2C_2O_4$ with H_2O_2 at Co:OA:H_2O_2 ratio = 1:1.5:3, T = 75 °C, S/L = 38 g/L, and N_S = 600 rpm.

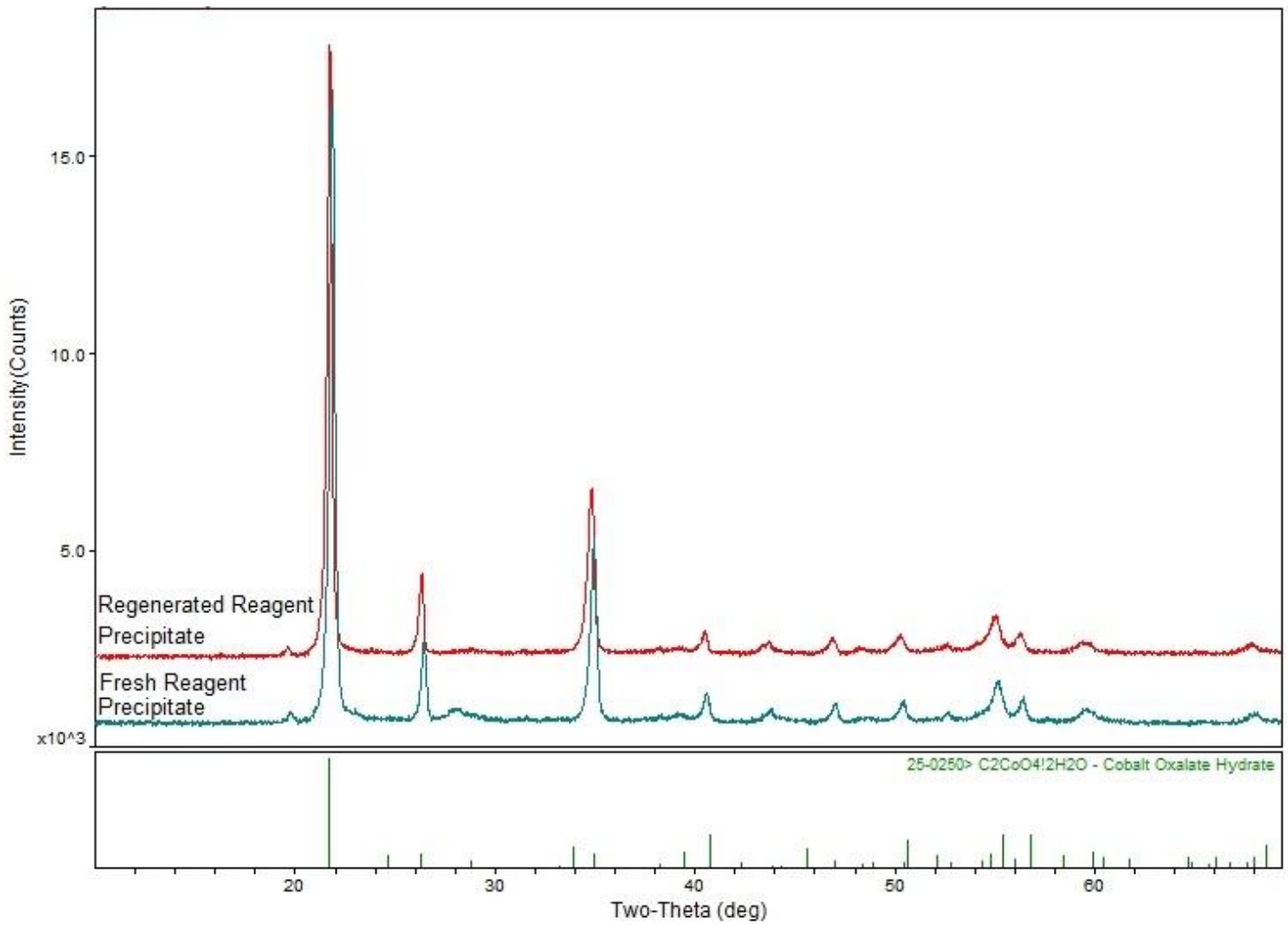

Figure 56. PXRD spectrum of the precipitate recovered from $LiCoO_2$ digestion using fresh and regenerated reagents at S/L ratio = 38 g/L, *T* = 75 °C and *Ns* = 600 rpm. Some peaks (such as 29.5°) are hidden because of the micro-rod morphology of precipitate. All of the patterns are corresponding to λ = 1.78897 Å.

6.4. Techno-economics Analysis

6.4.1. Comparative cost analysis between different processes

To understand the economic impacts of the closed-loop, environmentally-friendly oxalate-based process, a preliminary techno-economic model was developed to compare the H_2SO_4 process with two oxalate-based proposed processes. The three different cases used in this study are A) $LiCoO_2$:$H_2C_2O_4$ in a molar ratio of 1:3 at 100 °C, 1 h and 38 g/L S/L ratio, B) $LiCoO_2$:$H_2C_2O_4$:H_2O_2 in a molar ratio of 1:1.5:3 at 75 °C, 1 h and 38 g/L S/L ratio, and C) LIB black mass in 2 M H_2SO_4 + 5 vol% H_2O_2 at 60 °C, 2 h, and 100 g/L S/L ratios. Case A and B are the conditions used in this work for the oxalate process, and the conditions for case C were obtained from Kim et al.[195]

For the energy analysis, the residence time of reaction was considered to be 1 h for cases A and B and 2 h for case C. The composition of feed for cases A and B was $LiCoO_2$, whereas case C was LIB black mass of NMC cathode. In the work by Kim et al., 100 g of black mass resulted in a total of 0.72 moles of Ni, Mn, and Co metals in the aqueous phase.[195] The 100 g of NMC111 is approximately 1 mole of Ni, Mn, and Co metals stoichiometrically, and it was assumed that the LIB black mass for case C contains 75% of the cathode material. A comparison of these processes is shown in Table 23 based on the cost of reagents for metal extraction ($/kg of cathode material, referred to as $/kg$_{cm}$ from here on) and the energy cost ($/kg$_{cm}$).

The energy cost included the energy required to achieve and maintain the required temperature for the reaction time. The average natural gas price for commercial usage of 7.49 $/MMBtu has been used in the energy cost calculations of this section.[196] A 90% boiler efficiency and an average fluctuation of 2 °C/min in the aqueous phase temperature was assumed for the estimation. The reagent costs required in the downstream processes of separation of metals were

not included in this comparative analysis. Due to variable sources of cathode material, the cost of spent cathode material was also not included in this analysis. However, the black mass paste cost was reported as $100-200 per metric ton, which contained around 50 wt% of carbon, and the rest was spent or unspent metal oxides, along with miscellaneous pieces of plastics and other metals.[197] The bulk prices of chemical reagents used in this analysis are provided in the Table 24.

Table 23. Cost comparison between cases A, B, and C for 1st cycle.

	Price ($/kg$_{cm}$)*		
	Case A: $H_2C_2O_4$	**Case B: $H_2C_2O_4$ + H_2O_2**	**Case C: H_2SO_4 + H_2O_2**
Total energy cost	0.12	0.09	0.11
Cost of acid	1.9	1.0	0.7
Cost of reducing agent	0.0	0.7	0.5
Total Cost	2.00	1.80	1.30

* $/kg$_{cm}$ = Price in $ for processing 1 kg of cathode material

Table 24. Bulk prices of the chemical reagents used in the techno-economic analysis.

Chemical compound	Bulk Price ($/ton)	Source**
Oxalic Acid	500	https://www.alibaba.com/product-detail/Factory-supply-99-6-min-purity_1600175710615.html
Hydrogen Peroxide	340	https://www.alibaba.com/product-detail/35-50-Food-grade-H2O2-hydrogen_1553021671.html
Potassium Hydroxide	700	https://www.alibaba.com/product-detail/CAS-No-1310-58-3-industrial_60814472991.html
Potassium Carbonate	900	https://www.alibaba.com/product-detail/Potassium-Carbonate-Carbonate-Factory-Supply-Fertilizer_1700008076146.html
Strong Acid Cation Exchange Resin*	3000-7000	https://www.alibaba.com/product-detail/Catalyst-Resin-equal-to-AMBERLYST-35WET_62528139106.html
Sulfuric Acid	250	https://www.alibaba.com/product-detail/Premium-quality-Sulphuric-Acid-98-best_62012768376.html
Cobalt Hydroxide	30000	https://www.alibaba.com/product-detail/Cobalt-Hydroxide-Cobalt-Hydroxide-Cobalt-Hydroxide_60398573285.html
Lithium Carbonate	1350	https://www.marketwatch.com/story/lithium-demand-to-grow-at-average-annual-rate-of-30-in-2021-23-bacanora-says-commodity-comment-271631179864

* The prices of strong acid cation-exchange resins were found to be varying from 3000 to 7000 $/ton. Therefore, 5000 $/ton was used in the techno-economic analysis

** Links accessed on 10/28/2021

The recycling of $H_2C_2O_4$ for another metal extraction using the ion-exchange resin process was a novelty of this work. The SAC resins typically have a lifetime of over 10 years; therefore, in the economic comparisons, it was assumed that the resins could be regenerated after each cycle and reused again to recycle $H_2C_2O_4$. In this analysis, 1 kg of cathode material, and 100 cycles were assumed for economic comparisons shown in Table 25. A 90 % $H_2C_2O_4$ recycling efficiency was assumed based on experiments with the ion-exchange resins, and an additional 10% $H_2C_2O_4$ make-up was added, as discussed in Sections 6.3.4. and 6.3.5. The bulk prices of reagents used in the

analysis are shown in Table 24. In Table 23 (1 cycle, no acid recycling), the total cost of the $H_2C_2O_4$ (case A) and $H_2C_2O_4$ + H_2O_2 (case B) are in the similar range ($2/kg and $1.8/kg), but the H_2SO_4 + H_2O_2 (case C, $1.3/kg) process was 30% cheaper. The lower cost is due to the operation of case C at a S/L ratio of 100 g/L by Kim et al.,[195] whereas cases A and B were operated at a S/L ratio of 38 g/L. In the case of recycling 90% of $H_2C_2O_4$ (shown in Table 25) both cases A and B have the reagent cost in similar range as case C ($130/100 kg_{cm}). This observation proves the significance of acid recycling for an inorganic acid process. In addition, the E-factor defined by Eq. 6.4 were used to compare all three cases as shown in Table 26.

$$\text{E-factor} = \frac{\text{Total waste produced (kg)}}{\text{Total product (kg)}} \tag{6.4}$$

For an ideal process, E-factor should be zero. In case A and case B, H_2SO_4 acid used for the recycling of $H_2C_2O_4$ was the major waste stream. This waste acid has a high K concentration and could be used as a fertilizer after appropriate neutralization which would reduce the E factor even further.[198,199] However, for this analysis, the H_2SO_4 containing K was assumed to be a waste. For case C, the aqueous phase remaining after metal recovery was considered a waste. The pH of this waste stream for case C was assumed to be around 13-13.5 because of the metal hydroxide precipitations performed. Among the cases discussed in this section, case B ($H_2C_2O_4$ + H_2O_2) has the lowest E-factor with comparable economics with the H_2SO_4 + H_2O_2 process. Additional improvements in waste minimization could lower the E factor even further for the oxalate process and should be explored.

Table 25. Cost comparison between cases A, B, and C over 100 cycles.

	Price ($/100 kg_{cm})*		
	Case A: $H_2C_2O_4$	**Case B: $H_2C_2O_4 + H_2O_2$**	**Case C: $H_2SO_4 + H_2O_2$**
Total energy cost	12	9	11
Cost of SAC resins (bulk price = $3/kg)	23	11	0
Cost of SAC resins (bulk price = $5/kg)	38	19	0
Cost of SAC resins (bulk price = $7/kg)	53	27	0
Cost of acid (including make-up)	21	11	65
Cost of reducing agent	0	71	54
Cost of H_2SO_4 for regeneration of resins	56	28	0
Total Cost	127 ± 15	138 ± 9	131

* \$/100 kg_{cm} = Price in \$ for processing 100 kg of cathode material

Table 26. Comparison of waste production and E-factor between cases A, B, and C over 100 cycles.

	Case A: $H_2C_2O_4$	**Case B: $H_2C_2O_4 + H_2O_2$**	**Case C: $H_2SO_4 + H_2O_2$**
Total waste produced (kg/100 kg_{cm})	1500	750	1300
Expected pH of waste	1.5-2.0	1.5-2.0	13-13.5
Total product (kg/100 kg_{cm})	132	132	132
E-factor	11.3	5.6	9.8

6.4.2. Profit analysis for oxalate processes

The LIB recycling process was driven by the value associated with the transition metal products, particularly Co. The battery chemistries are continuously evolving to reduce the dependence on Co in the cathode; therefore, the profit associated with any recycling technologies was the most sensitive to the market price of products such as $Co(OH)_2$. The impact of the variable market price

of $Co(OH)_2$ was analyzed on the profit margin of both processes ($H_2C_2O_4$ and $H_2C_2O_4 + H_2O_2$) developed in this work. Currently, the market price of $Co(OH)_2$ is around 30 $/kg (Table 24). For the analysis, this market price was considered the best-case, and $5/kg was considered the worst-case scenario. The worst-case scenario also explains the economic impact of using the oxalate process to recycle a NMC cathode or even a Co-free cathode. The total input cost includes the costs described in Table 25, and the reagents required for metal precipitations. It was also observed that the net profit is sensitive to the number of cycles the resins can be reused. In order to understand this impact, the number of times the resins could be reused was varied from 10 to 150 (e.g., Table 25, 100 cycles). The variation in the net profit with varying cobalt hydroxide market price (best-case to worst-case) and SAC resins expected life (number of recycling cycles) for $H_2C_2O_4 + H_2O_2$ process are shown in Figure 57. In the case of $H_2C_2O_4$ as the extraction reagent the net profit was approximately 5% lesser in every case. For the worst-case scenario, the $H_2C_2O_4$ process becomes profitable after 25 cycles and for $H_2C_2O_4 + H_2O_2$ the process is profitable at even 10 cycles. Overall, the $H_2C_2O_4 + H_2O_2$ process was marginally more profitable and had a smaller E-factor than the only $H_2C_2O_4$ process. The $H_2SO_4 + H_2O_2$ process discussed in the previous section was not compared because of the variability in the metal separation strategies.

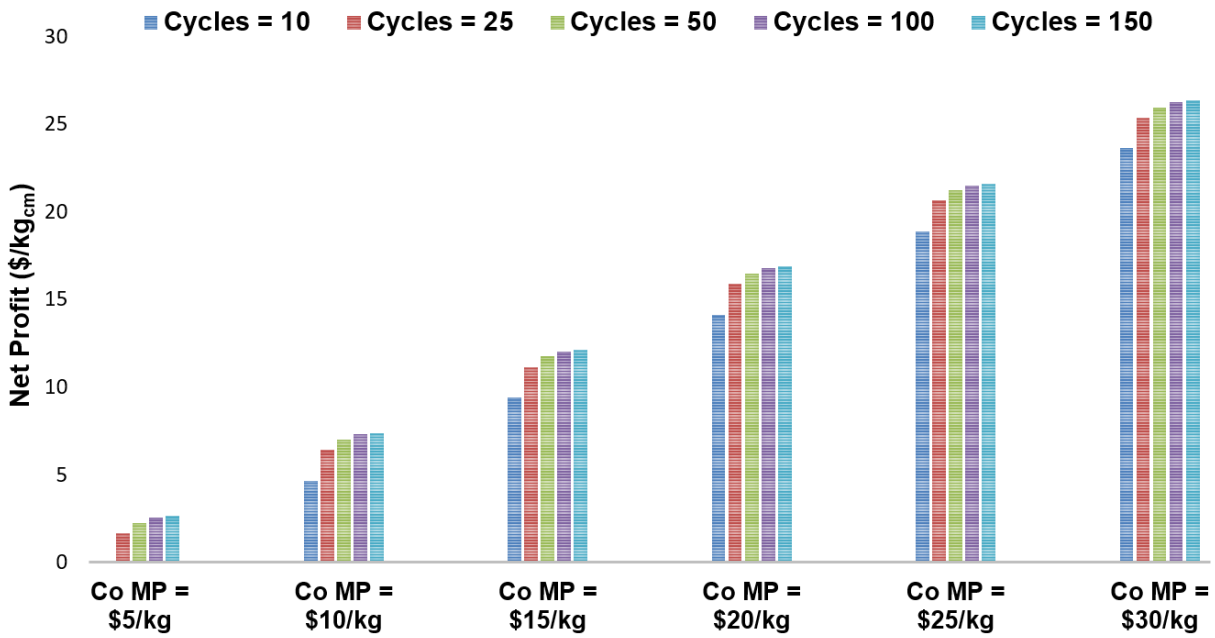

Figure 57. Net profit sensitivity towards the market price of $Co(OH)_2$ and number of cycles for the metal extraction using $H_2C_2O_4$ + H_2O_2. Co MP corresponds market price of $Co(OH)_2$.

6.5. Flexibility of the closed-loop oxalate chemistry process for other metal recovery

In this dissertation (Chapters 3, 4 and 6), the separation and recovery of Li and Co metals from a $LiCoO_2$-based cathode using oxalate chemistry are covered. The cathode chemistry in LIB production is continuously evolving to reduce Co content and replace with other metals such as Ni and Mn. Furthermore, other low-cost metals such as Al, Cu, and Zn along with the graphite might be present in the LIBs waste. To showcase the flexibility of the oxalate process for separating additional metals, an alternative process shown in Figure 58 was proposed. To prove that the cathode chemistries involving Ni, Mn and Co can be recycled conveniently using $H_2C_2O_4$, metal extraction experiments were performed with on a $LiNi_{0.33}Mn_{0.33}Co_{0.33}O_2$ (NMC) material. The NMC cathode has a similar structure to $LiCoO_2$ and using similar metal extraction conditions (T = 100 °C, NMC:OA:H_2O_2 = 1:1.5:3, N_S = 600 rpm and S/L ratio = 15 g/L), >90% Li was extracted

into the aqueous phase and a mixed insoluble metal oxalate containing Ni, Mn and Co metals was recovered in the solid phase.

The process in Figure 58 utilized the property of amphoteric metal hydroxides such as Al, Cu, and Zn to separate them from the NMC material hydroxides at higher pH. Similar to the processes demonstrated in this chapter, Li has to be precipitated before the addition of the NMC oxalate. If any Fe^{3+} and Al^{3+} impurities are present, they can be selectively precipitated in the form of their respective metal hydroxides, as demonstrated in our previous work for bauxite ore.[200] The higher solubility of $Li(OH)_2$ compared to Fe and Al hydroxides will retain Li in the aqueous phase for Li_2CO_3 precipitation. In the oxalate-rich basic solution after Li precipitation, the solid product comprising insoluble metal oxalates and graphite can be added slowly. In the presence of excess oxalate ions, insoluble metal oxalates should dissolve, leaving graphite as the residue. The pH can be controlled to precipitate NMC hydroxide from the mixture selectively. This process is based on our understanding of the oxalate and hydrolysis chemistry.

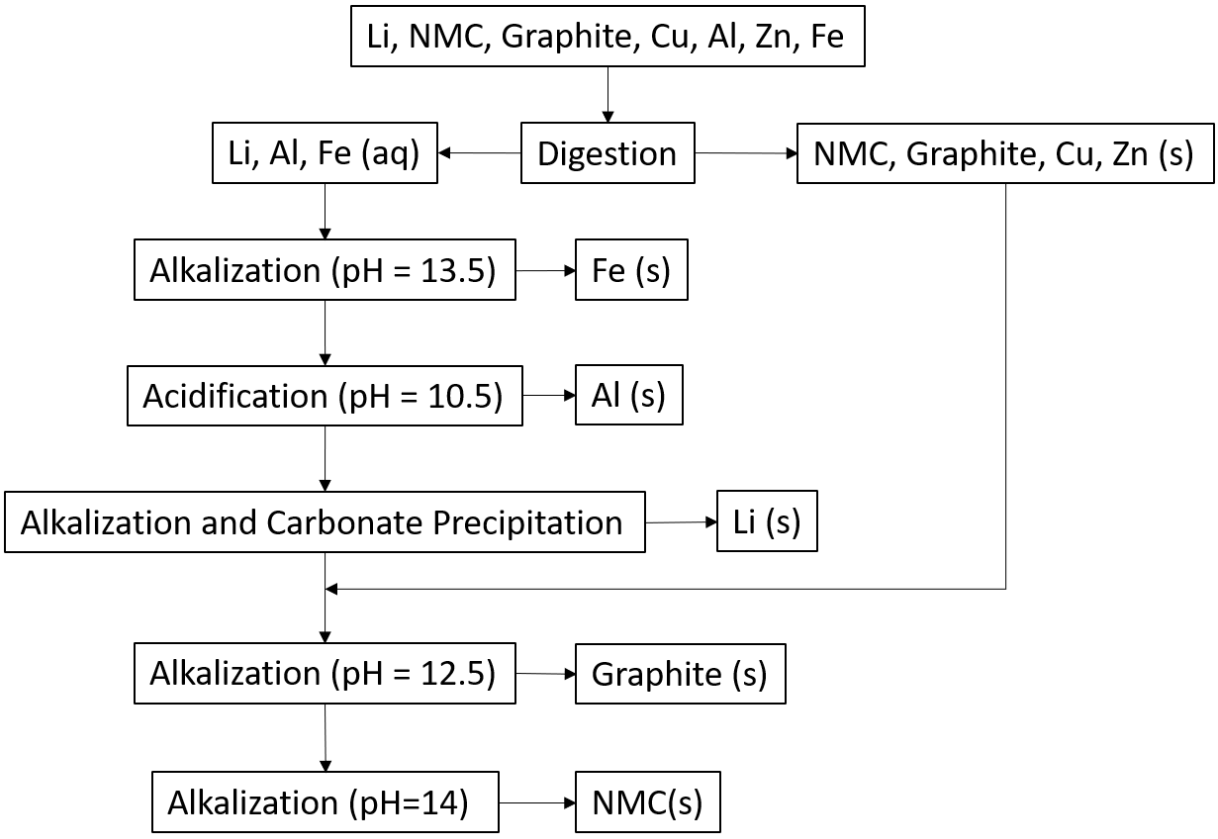

Figure 58. Proposed process for extending the oxalate process to recycle LIB cathodes with various metal impurities.

6.6. Conclusions

In summary, oxalate chemistry can create a closed-loop and environmentally-friendly LIB recycling process that was economical compared with the incumbent H_2SO_4 process. In this chapter, a closed-loop process was designed for recycling 100 % of the $H_2C_2O_4$ used after an efficient metal extraction and precipitation. The optimized conditions for the Li and Co extraction from $LiCoO_2$ (from Chapters 2 and 3) were scaled-up to a solid-to-liquid ratio of 38 g/L using $H_2C_2O_4$ and $H_2C_2O_4 + H_2O_2$ reagents. The $H_2C_2O_4$ process can completely extract and separate Li and Co within 1 hour at 100 °C, whereas $H_2C_2O_4 + H_2O_2$ can perform a similar extraction at 75 °C. The Li present in the aqueous phase can be efficiently precipitated to Li_2CO_3 using potassium

carbonate. The precipitated $CoC_2O_4 \cdot 2H_2O$ was dissolved and reprecipitated in the form of $Co(OH)_2$ and a 100 % recovery of $C_2O_4^{2-}$ ions in the aqueous phase was achieved. An ion exchange process was designed using strong acid cation-exchange resins to regenerate the $H_2C_2O_4$ from $C_2O_4^{2-}$ ions in the aqueous phase.

A preliminary techno-economic analysis of the $H_2C_2O_4$ and $H_2C_2O_4 + H_2O_2$ processes was performed to evaluate the economic and environmental impacts. The analysis concluded with the 80-90% recycling of $H_2C_2O_4$ in the $H_2C_2O_4$ and $H_2C_2O_4 + H_2O_2$ processes are cost competitive with the H_2SO_4 process. To understand the environmental impact, the amount of waste generation and E-factor was estimated. The $H_2C_2O_4 + H_2O_2$ process has an E-factor of 5.5, whereas $H_2C_2O_4$ and H_2SO_4 processes have an E-factor of approximately 10. The 50 % reduction in waste generated with similar economic impacts makes the $H_2C_2O_4 + H_2O_2$ process the most sustainable for the recovery of critical metals such as Li and Co from waste LIB cathodes. In addition, other valuable metals in LIBs such as Ni and Mn form insoluble metal oxalate dihydrates. These compounds can be dissolved and precipitated selectively in excess oxalates without impurity metals like Al, Cu, and Zn. The low cost and efficient metal separation combined with 50% lower waste generation relative to the H_2SO_4 process make the oxalate processes quite attractive for the recovery of critical metals from LIBs. The closed-loop processes discussed in this work can also be used to sustainably recover critical and precious metals from other sources such as ores like bauxite, ilmenite, spent catalysts, and rare-earth containing materials.

Chapter 7. Extraction of Aluminum and Iron from Bauxite using Oxalate Chemistry

Portions of this chapter are adapted from the following published article:

Verma, A., Corbin, D.R., & Shiflett, M.B., Extraction of Aluminum and Iron from Bauxite: A Unique Closed-Loop Ore Refining Process utilizing Oxalate Chemistry. *AIChE Journal*, **2021**, (*in press)*

Chapter 7

"There must be a better way to make the things we want,
a way that doesn't spoil the sky, or the rain or the land."
- Paul McCartney (English Songwriter)

7.1. Abstract

Bauxite ore is the world's primary source of Al metal. The Bayer process holds an exclusive status worldwide for the extraction of alumina from bauxite. This process is efficient for alumina extraction, but a massive amount of "red mud" waste is generated. The red mud waste is caustic and is mainly composed of iron oxides. In this chapter, three oxalate reagents: potassium hydrogen oxalate (KHC_2O_4), potassium tetraoxalate ($KHC_2O_4 \cdot H_2C_2O_4$), and oxalic acid ($H_2C_2O_4$) were investigated for the development of a closed-loop Al and Fe extraction process from NIST SRM 600 – Australian Darling range bauxite ore. KHC_2O_4 and $KHC_2O_4 \cdot H_2C_2O_4$ can be synthesized by mixing $K_2C_2O_4$ and $H_2C_2O_4$ at 1:1 and 1:3 molar ratios, respectively. More than 90% of Al was extracted into the aqueous phase in less than 2 h with 0.50 M $C_2O_4^{2-}$ at 100 °C for all three reagents. The rate of Al extraction was similar at the operating pH = 1.0, 1.5, and 2.5. The rate of Fe extraction was highest for KHC_2O_4 with an operating pH = 2.5. The Fe can be selectively precipitated by hydrolyzing the aqueous phase to a pH = 13.80. After separating the Fe precipitate, the resulting filtrate can be acidified to a pH = 10.50 for efficient Al precipitation. By acidifying the Al and Fe free filtrate to a pH = 2.50, approximately 60% of initial $C_2O_4^{2-}$ can be precipitated and recovered as KHC_2O_4. Additional acidification to a pH = 1.50 can precipitate 80% of the $C_2O_4^{2-}$ as $KHC_2O_4 \cdot H_2C_2O_4$. The acid recovery can be even more efficient using an ion-exchange process. Greater than 90% of the aqueous acid can be recovered and recycled using a strong acid cation exchange resin. The proposed closed-loop process is an energy-efficient, cost-effective,

environmentally-friendly route for extracting commercially valuable metals such as Al and Fe from bauxite ores and other sources.

7.2. Background and Motivation

Aluminum is a lightweight, durable, recyclable metal with its primary use in the production of high strength alloys in combination with other metals like Ni, Zn, Cu, and Mn. These alloys are used in a broad range of industries that vary from automobile manufacturing to aeronautical applications.[201] The primary source of Al is aluminum oxide (alumina) present in bauxite ore. More than 90% of globally mined bauxite is used for Al production. On average, a bauxite ore contains 30-60 wt% of alumina, the rest being a mixture of iron oxides and quartz.[202] Commercially, bauxite is refined using the Bayer process to produce smelter-grade alumina that is then converted to Al metal using the Hall–Héroult process.[201,203]

In bauxite, Al is present in the form of aluminum oxide trihydrate like gibbsite ($Al_2O_3 \cdot 3H_2O$ or $Al(OH)_3$) and monohydrate minerals such as boehmite ($Al_2O_3 \cdot H_2O$ or γ-AlO(OH)) and diaspore ($Al_2O_3 \cdot H_2O$ or α-AlO(OH)). Other minerals which can be found in bauxite include hematite (Fe_2O_3) and quartz (SiO_2). The Bayer process involves the digestion of crushed bauxite in concentrated NaOH solution at high temperatures. The Al present in the ore reacts with NaOH to form water soluble sodium aluminate ($NaAlO_2$) leaving behind an insoluble solid residue (red mud). However, the dissolution of SiO_2 and Al in concentrated NaOH solution makes the Bayer process inefficient for low-grade bauxite ores (greater than 10 wt% SiO_2 content).

The bauxite refining industry faces a global environmental issue because of the disposal problems associated with the caustic bauxite tailings commonly referred to as red mud.[204,205] The red mud is discharged from the process as an alkaline slurry with a pH > 12. It primarily consists of bauxite tailings like iron oxide (Fe_2O_3) and quartz (SiO_2).[206] Typically, about 1.0-1.5 tons of red

mud are produced per ton of alumina in the Bayer process.[207] For the disposal of red mud, methods like landfills, deep-sea dumping, or storage in open ponds or reservoirs are utilized. The high alkalinity of the red mud pollutes the land and threatens plant growth and wildlife.[208,209] With the growing demand for Al, the disposal methods of red mud are an issue that needs global attention. In the past two decades, there have been numerous red mud incidences because of its disposal. The most disastrous incident occurred in Hungary in 2010, when the Ajka refinery dam collapsed, resulting in red mud flooding the nearby area. The release of approximately 1 million cubic meters of red mud contaminated more than 40 square kilometers of land and led to 9 deaths and 122 severely injured.[210,211]

To solve the problems associated with red mud, either environmentally-friendly techniques have to be utilized to dispose of red mud responsibly, or it can be eliminated at the source by developing a closed-loop bauxite refining process. Numerous researchers have worked on the recovery of valuable metals from red mud using both pyrometallurgy and hydrometallurgy.[212-216] Pyrometallurgy is energy intensive, whereas hydrometallurgical processes using inorganic acids (e.g., sulfuric acid and nitric acid) poses significant environmental risk from the emission of SO_X and NO_X. The large amount of acid initially involved for neutralizing the caustic red mud and the handling of effluents create an additional burden on the red mud processing.[210] In this chapter, a closed-loop hydrometallurgical approach for bauxite refining with minimal waste to eliminate the concerns associated with red mud has been discussed. In our alternative approach for bauxite refining, oxalic acid ($H_2C_2O_4$) and two of its derivatives with potassium oxalate ($K_2C_2O_4 \cdot H_2O$): potassium hydrogen oxalate (KHC_2O_4) and potassium tetraoxalate ($KHC_2O_4 \cdot H_2C_2O_4$) are investigated as reagents to extract Al and Fe from bauxite.

The oxalate ion is a bidentate ligand with excellent chelation properties. The $H_2C_2O_4$ and its derivatives (KHC_2O_4 and $KHC_2O_4 \cdot H_2C_2O_4$) utilize the chelation property along with the acidity to extract metals from the metal oxides. The $H_2C_2O_4$ has been used to extract metals from various sources ranging from spent lithium-ion battery cathodes[12,162] to ores such as laterite[77] and scheelite.[86,87] Corbin et al. developed two environmentally-friendly closed-loop processes for extraction of Fe and Ti from ilmenite using ammonium hydrogen oxalate ($NH_4HC_2O_4$)[16] and trimethylammonium hydrogen oxalate ($(NH(CH_3)_3)HC_2O_4$).[76] The $H_2C_2O_4$ and its derivatives can be advantageous for metal separations in an aqueous medium. Most of the divalent (M^{2+}) metal ions are known to form insoluble metal oxalate compounds, whereas monovalent (M^{+}) and trivalent (M^{3+}) metal ions form soluble metal oxalates.[2,150] The difference in the aqueous solubility can be utilized to separate metal oxalate compounds.

In this chapter, a standard bauxite material from the Australian Darling range (NIST SRM600) has been used to investigate the feasibility of a closed-loop Al and Fe recovery process using $H_2C_2O_4$, KHC_2O_4, and $KHC_2O_4 \cdot H_2C_2O_4$. The easy separation of SiO_2 from Al_2O_3 and Fe_2O_3 is a major advantage of using an acidic process. The Al and Fe from their respective metal oxides are leached into the aqueous phase, whereas SiO_2 remains in the solid phase. The Al and Fe extracted in the aqueous phase can be separated using selective hydrolysis, and pH conditions have been optimized for efficient separation. However, the $H_2C_2O_4$ and $K_2C_2O_4$ are more expensive than inorganic acids such as H_2SO_4 and HNO_3.[162] To offset the cost of oxalate-based acids and make this process economical, an ion-exchange resin and a pH-based separation have been developed to recover the oxalate-based acids in their original form. To the best of our knowledge, this is the first study on the extraction of metals from bauxite using oxalic acid and its derivatives.

This novel closed-loop process is an environmentally-friendly and economical route for recovering Al and Fe from bauxite ore.

7.3. Extraction of Al and Fe using Oxalate Reagents

To understand the extraction of metals from NIST SRM 600 bauxite ore using aqueous $H_2C_2O_4$ (OA), KHC_2O_4 (KHO) and $KHC_2O_4 \cdot H_2C_2O_4$ (KTO), the temperature, agitation speed, and S/L ratio were kept constant at T = 100 °C, N_s = 600 rpm, and 15 g/L respectively, for all the experiments in this section unless specified otherwise. The S/L ratio can be optimized after understanding the mechanism. NIST SRM 600 bauxite contains Al in the form of gibbsite ($Al_2O_3 \cdot 3H_2O$), along with hematite (Fe_2O_3) and quartz (SiO_2). A chemical analysis of SRM 600 bauxite was obtained from NIST and provided in the Table 27.

7.3.1. Materials

In this study, NIST SRM 600 – Bauxite, Australian-Darling Range, $H_2C_2O_4 \cdot 2H_2O$ (ACROS Organics, 99.5%), $K_2C_2O_4 \cdot H_2O$ (Alfa Aesar^{TM}, 98.8%), and deionized water were used for the metal extraction experiments. Potassium hydroxide, (KOH Pellets, Fisher Chemical) and Fe metal powder (20 mesh, Alfa Aesar^{TM}, 99%) were used for metal precipitation and hydrolysis, respectively. Sulfuric acid (H_2SO_4, Fisher Scientific, 98%) was used for acidification and regeneration of oxalate.

7.3.2. Characterization

The metal concentrations in the solid and aqueous phase were measured using an inductively coupled plasma – optical emission spectrometer (ICP-OES). A Varian/Agilent 725 ES ICP-OES with simultaneous CCD detector was used for the measurements, and a Varian/Agilent SP3 autosampler was used to sequence multiple samples. The aqueous phase samples were diluted 100 times with 5 wt% HNO_3 before analyzing them by ICP. Elemental compositions of the solid

phases were identified using X-Ray fluorescence (XRF) using a Malvern Panalytical Zetium (1 kW) instrument with a Rh anode and a 75 μm Be window with a duplex detector. Phase identification and crystallinity measurements were performed on a Bruker D2 phaser powder X-ray diffraction (PXRD) with a Co Kα radiation source (λ = 1.78897 Å). The source voltage and current were set at 30 kV and 10 mA, respectively. The data were collected in the 2θ range of 10−70° with a step size of 0.02° and dwell time of 0.40 s per step. XRD patterns were analyzed using MDI Jade 6 software.

Table 27. Certificate of Analysis of NIST SRM 600
(at https://www-s.nist.gov/srmors/certificates/600.pdf on 08/19/2021)

Constituent	Certified Value (Percent by Weight)	Estimated Uncertainty
Al_2O_3	40.0	0.4
Fe_2O_3	17.0	0.3
SiO_2	20.3	0.4
TiO_2	1.31	0.04
ZrO_2	0.060	0.009
P_2O_5	0.039	0.007
V_2O_5	0.060	0.007
Cr_2O_3	0.024	0.004
CaO	0.22	0.02
MgO	0.05	0.01
MnO	0.013	0.004
ZnO	0.003	0.002
K_2O	0.23	0.02
Na_2O	0.022	0.007
SO_3	0.155	0.006
Loss on Ignition	20.5	0.2

7.3.3. Reactor Setup and Sampling

The metal extraction experiments were carried out in a 1-L glass reactor with similar configurations used for the Li and Co extraction from $LiCoO_2$. A detailed reactor schematic can be found in the Appendix, Section A.1.[162] The reactor temperature and agitation speed (N_s) were set at 98 °C and 600 rpm, respectively, for all the experiments in this work. The temperature and agitation speed values were optimized to maximize the kinetics and avoid any diffusion limitation. Samples were withdrawn from the reactor at specific intervals using a 20 cm long needle connected to a 5 mL syringe. The withdrawn samples were centrifuged in a Falcon® tube for 5 min at N_s = 4000 rpm to separate out the solids. The aqueous phase was diluted with 5 wt% nitric acid solution at a ratio of 1:10 for the measurement of Al and Fe concentrations.

7.3.4. Metal Extraction, Hydrolysis, and Acid Regeneration: Experimental

Metal extraction experiments were carried out by mixing the oxalate reagents and heating them to a set temperature and then adding the required amount of bauxite. Aqueous $H_2C_2O_4$ with or without $K_2C_2O_4$ was used in each experiment. The $H_2C_2O_4$ and $K_2C_2O_4$ molar ratio is critical for the synthesis of KHC_2O_4 and $KHC_2O_4{\cdot}H_2C_2O_4$. The reaction parameters for an efficient hydrometallurgical extraction are the acid concentration, temperature, solid-to-liquid ratio (S/L), and agitation speed. As mentioned in the previous section, the temperature and agitation speed were kept constant, while the effect of acid concentration was studied for all three oxalate reagents ($H_2C_2O_4$, KHC_2O_4, and $KHC_2O_4{\cdot}H_2C_2O_4$). The effect of increasing the S/L ratio was studied only with $KHC_2O_4{\cdot}H_2C_2O_4$. Once the Al and Fe metals were extracted into the aqueous phase, the Fe was precipitated as $Fe(OH)_3$ via hydrolysis by increasing the pH using KOH. After removal of the Fe, the Al was precipitated from the solution by lowering the pH to an appropriate range by adding either H_2SO_4 or $H_2C_2O_4$. The specific range of pH for efficient precipitation of Al and Fe is

discussed in the results and discussion section. The precipitation experiments were performed at 20 °C to maximize the precipitation efficiency using minimum energy.

The oxalate reagents were regenerated using two methods. The first approach involved using a strong acid cation exchange resin such as Amberlyst® 15 H-form to decrease the pH. In this chapter as well, the batch process was used for the acid regeneration by mixing the activated resins with the filtrate while monitoring the pH. After achieving the desired pH, the resins were regenerated by soaking them in a 1.5 M sulfuric acid solution. In the presence of a strong acid, the resins regain their initial H-form. The regenerated resins were washed with DI water until the effluent was pH neutral before performing another ion exchange. The washing step removed any excess acid present on the resin beads. The washed and regenerated resins can be repeatedly used for additional metal precipitation. The second method for regenerating the oxalate reagents involved acidification of the filtrate post metal precipitation to the initial pH using H_2SO_4. The acidification will precipitate either KHC_2O_4 or $KHC_2O_4 \cdot H_2C_2O_4$, depending on the pH range. To minimize the amount of water added, 98 wt% H_2SO_4 was used in the acidification process. This pH-based process utilizes solubility differences for separation and is discussed in detail in the results and discussion section. Both of the acid regeneration processes have been discussed in detail in Chapter 5.

7.3.5. Synthesis of Potassium Hydrogen Oxalate and Potassium Tetraoxalate

The $H_2C_2O_4$ is a diprotic acid with $pKa_1 = 1.23$ and $pKa_2 = 4.19$ at 20 °C. Both KHC_2O_4 and $KHC_2O_4 \cdot H_2C_2O_4$ contain the binoxalate anion ($HC_2O_4^-$). Based on the speciation of oxalic acid, $H_2C_2O_4$ is the predominant species below a pH = 1.23, $HC_2O_4^-$ is the predominant species between pH = 1.23 and 4.19, and $C_2O_4^{2-}$ is the predominant species above pH = 4.19.[150] The KHC_2O_4 can be synthesized using a 1:1 molar ratio of $H_2C_2O_4$ and $K_2C_2O_4$, as shown in Eqs. 7.1

and 7.2. The KHC_2O_4 is sparingly soluble in the resulting solution shown in Eq. 7.1. at 20 °C, and a white precipitate was observed. The precipitate was filtered and identified as KHC_2O_4 using PXRD.

$KHC_2O_4 \cdot H_2C_2O_4$ is another derivative of $H_2C_2O_4$ that can be synthesized by mixing $H_2C_2O_4$ and $K_2C_2O_4$ in a 3:1 molar ratio, as shown in Eq. 7.2. The $KHC_2O_4 \cdot H_2C_2O_4$ was also found to be sparingly soluble in the resulting solution shown in Eq. 7.2. at 20 °C. A white precipitate was observed, filtered, and identified using PXRD as $KHC_2O_4 \cdot H_2C_2O_4 \cdot 2H_2O$. These two derivatives provide an alternative to $H_2C_2O_4$ with moderate acidity and similar chelation properties. The low solubility of these acids in comparison to the $H_2C_2O_4$ provides a convenient means to recover the acids after metal extraction.

$$H_2C_2O_4(aq) + K_2C_2O_4(aq) \rightleftharpoons 2KHC_2O_4(aq) \quad (7.1)$$

$$3H_2C_2O_4(aq) + K_2C_2O_4(aq) \rightleftharpoons 2KHC_2O_4 \cdot H_2C_2O_4(aq) \quad (7.2)$$

The solubilities of KHC_2O_4 and $KHC_2O_4 \cdot H_2C_2O_4$ were measured as 5.8 g and 3.0 g per 100 mL of water at 20 °C, respectively. The $NH_4HC_2O_4$ and $NaHC_2O_4$ were synthesized for measuring the solubilities in water at 20 °C. The solubilities of common oxalate compounds have been shown in Table 3, Chapter 1. The potassium-based oxalate compounds are unique because of the low solubility of KHC_2O_4 and $KHC_2O_4 \cdot H_2C_2O_4$ and the high solubility of $K_2C_2O_4$. The high solubility of $K_2C_2O_4$ is critical for separating pure metals (e.g., Al and Fe) during the hydrolysis step without any impurity.

7.3.6. Kinetics of Al and Fe Extraction

The kinetics of Al and Fe extraction from NIST SRM 600 bauxite have been studied using aqueous $H_2C_2O_4$ (OA), KHC_2O_4 (KHO) and $KHC_2O_4 \cdot H_2C_2O_4$ (KTO) reagents. A major difference

between the three oxalate reagents is the reaction pH. The OA is the most acidic, followed by the KTO and then KHO. The acidity of the reagent is critical for breaking the metal-oxygen bonds via hydrogen bonding that initiates the extraction of metals from metal oxides.[14] Figure 59 summarizes the Al and Fe extraction kinetics for NIST SRM 600 bauxite using OA.

The Fe extraction rate was significantly improved by increasing the OA concentration from 0.50 M to 0.75 M, whereas the Al extraction rate increased slightly. The Al extraction rate was faster than Fe, at both 0.50 M and 0.75 M OA, indicating a preference towards Al in the acidic pH range of 0.75-1.2. Greater than 90% of the Al was extracted in 1 h for at both 0.50 M and 0.75 M OA, while about 1.5 h was required for extracting 90% of the Fe. However, when similar extractions were performed using 0.50 M KHO and 0.75 M KHO (Figure 60), the rate of Fe extraction was faster than Al. For both 0.50 M and 0.75 M KHO, less than 1 h was required to extract greater than 90% of the Fe. This observation indicates the importance of the $HC_2O_4^-$ in Fe extraction. The KHO behaves as a pH buffer; therefore, when increasing the concentration of KHO, the pH remains the same, and no significant changes in metal extraction kinetics were observed. OA is the most acidic and effective at Al extraction from bauxite ore; however, the difficulty is regenerating the acid after precipitation of the Al and Fe. For this reason, the moderately acidic KTO is the preferred acid, which can be easily regenerated after Al and Fe precipitation. The stoichiometric reactions for the extraction of trivalent metal (M^{3+} like Al^{3+}, Fe^{3+}) from its oxide (M_2O_3) using OA, KHO and KTO are shown in Eqs. 7.3-7.5.

$$M_2O_3 + 6(H_2C_2O_4 \cdot 2H_2O) \rightleftarrows 2[M(C_2O_4)_3]^{3-} + 15H_2O + 6H^+ \quad (7.3)$$

$$M_2O_3 + 6(KHC_2O_4) \rightleftarrows 2[M(C_2O_4)_3]^{3-} + 3H_2O + 6K^+ \quad (7.4)$$

$$M_2O_3 + 6(KHC_2O_4 \cdot H_2C_2O_4 \cdot 2H_2O) \rightleftarrows 2[M(C_2O_4)_3]^{3-} + 15H_2O + 3K^+ + 3H^+ \quad (7.5)$$

KTO is a double salt of OA and KHO and comprises two moles of $C_2O_4^{2-}$ per mole of KTO. Hence, 0.25 M KTO (0.50 M $C_2O_4^{2-}$) was used to perform the Al and Fe extraction from NIST SRM 600 bauxite at a 15 g/L S/L ratio. In the KHO study, no significant difference was observed in the rate of metal extraction at a higher $C_2O_4^{2-}$ concentration due to essentially the same pH; therefore, only 0.25 M KTO was studied in detail. In Figures 59 and 60, the 0.50 M $C_2O_4^{2-}$ concentration led to an efficient extraction of Fe and Al using 15 g/L S/L ratio of ore; therefore, a higher S/L ratio of 20 g/L with 0.25 M KTO was attempted, as shown in Figure 61. The Al and Fe extraction kinetics for 20 g/L was slower in comparison to 15 g/L experiments because of the decreased concentration of $C_2O_4^{2-}$ per metal ion. However, greater than 95% of Al and Fe was extracted in 2.5 h at 20 g/L S/L ratio, which makes this process energy-efficient. An important observation was the rates of Al extraction for OA, KTO, and KHO at the 0.50 M $C_2O_4^{2-}$ concentration were similar (Figure 62), which confirms the negligible effect of pH on Al extraction kinetics. This could be because of operating the metal extraction in the presence of excess acid. To understand this phenomenon, ore was digested in 0.50 M $K_2C_2O_4$, and no Al extraction was observed, confirming the importance of acidity to initiate the extraction. The elemental composition shown in Table 28 after the extraction experiments indicates less than 10% of Al and 2% of Fe remain in the solid residue. The typical mass of solid residue recovered was 2.5 g from 15 g of ore digested in 1 L of acid. From the elemental composition of the ore and remaining solid residue shown in Table 28, it can be seen that in addition to Al and Fe, some other metals such as Zr and Mg are also leached into the aqueous phase. The residues recovered in the experiments shown in Figures 59-62 were also confirmed using PXRD to be primarily quartz (SiO_2). The PXRD patterns for the NIST SRM 600 and the solid residues from the bauxite digestion using 0.50 M OA, 0.50 M KHO, and 0.25 M KTO are shown in Figures 63 and 64, respectively.

The Fe and Al extraction from bauxite can also be performed using other derivatives of oxalic acid like ammonium hydrogen oxalate ($NH_4HC_2O_4$). Ammonium compounds are more acidic than the potassium compounds. However, as seen in Figure 62, Al extraction kinetics was same for an optimal amount of acidity. To confirm this, 0.50 M $NH_4HC_2O_4$ was used to extract Fe and Al from NIST SRM 600, and very similar extraction kinetics as 0.50 M KHO was observed. However, because of the low aqueous solubility of $(NH_4)_2C_2O_4$, ammonium reagents were not considered as a metal extraction reagent in this dissertation.

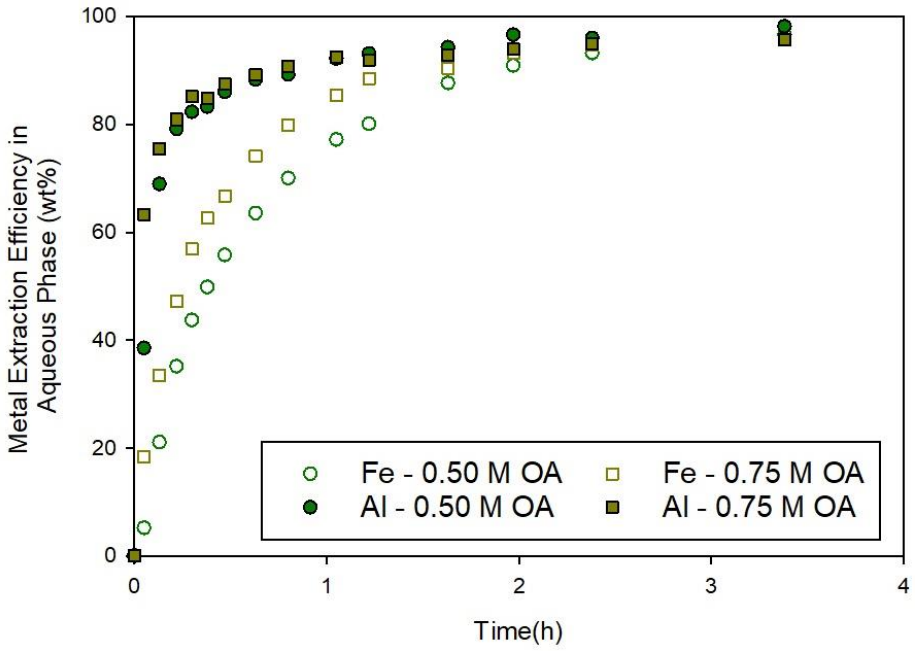

Figure 59. Metal concentration for Al and Fe as a function of time in the aqueous phase for 0.50 M and 0.75 M OA at T = 100 °C, S/L = 15 g/L and Ns = 600 rpm.

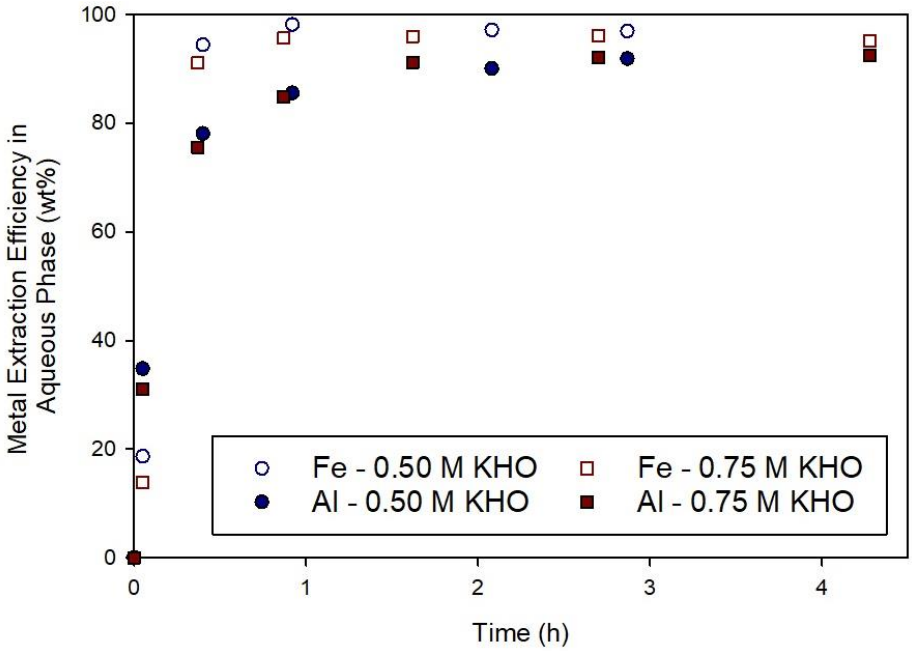

Figure 60. Metal concentration for Al and Fe as a function of time in the aqueous phase for 0.50 M and 0.75 M KHO at T = 100 °C, S/L = 15 g/L and N_s = 600 rpm.

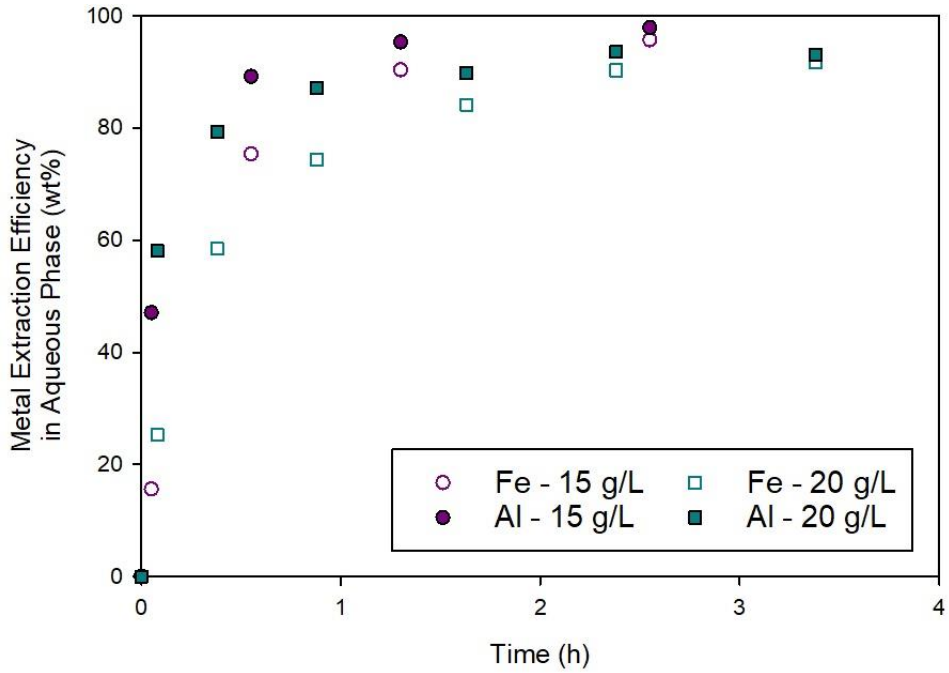

Figure 61. Metal concentration for Al and Fe as a function of time in the aqueous phase for 0.25 M KTO at T = 100 °C, S/L = 15 g/L and 20 g/L and N_s = 600 rpm.

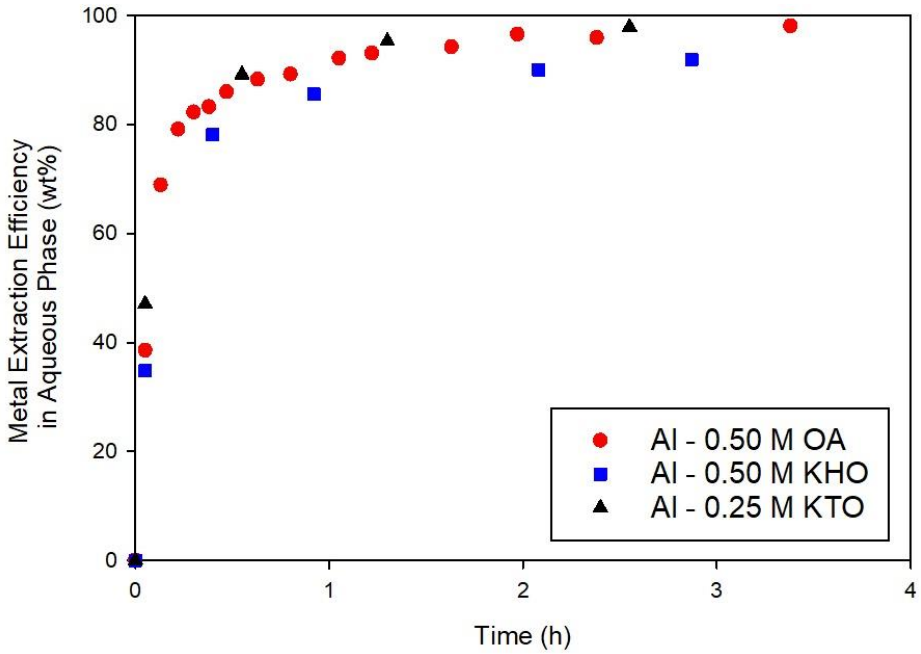

Figure 62. Al concentration as a function of time in the aqueous phase for 0.50 M OA, 0.50 M KHO and 0.25 M KTO at T = 100 °C, S/L = 15 g/L and N_s = 600 rpm.

Table 28. Elemental composition of NIST SRM 600 and the solid residues remaining after refining of NIST SRM 600.

Extraction reagent and conditions	Concentration (wt%)									
	Al	**Fe**	**Si**	**Ti**	**Zr**	**Ca**	**K**	**P**	**Mg**	**O**
NIST SRM 600	33.80	13.52	6.20	0.87	0.32	0.24	0.22	0.22	0.14	44.28
0.50 M KHO – 15 g/L	9.70	1.06	34.05	2.81	0.34	0.60	0.82	0.24	0.02	50.54
0.75 M KHO – 15 g/L	8.00	0.94	35.61	2.56	0.29	0.68	0.73	0.24	0.02	50.70
0.25 M KTO – 15 g/L	9.16	1.09	34.51	3.17	0.32	0.08	0.82	0.28	0.03	50.69
0.25 M KTO – 20 g/L	9.45	2.05	33.39	3.23	0.36	0.08	0.74	0.26	0.02	50.21

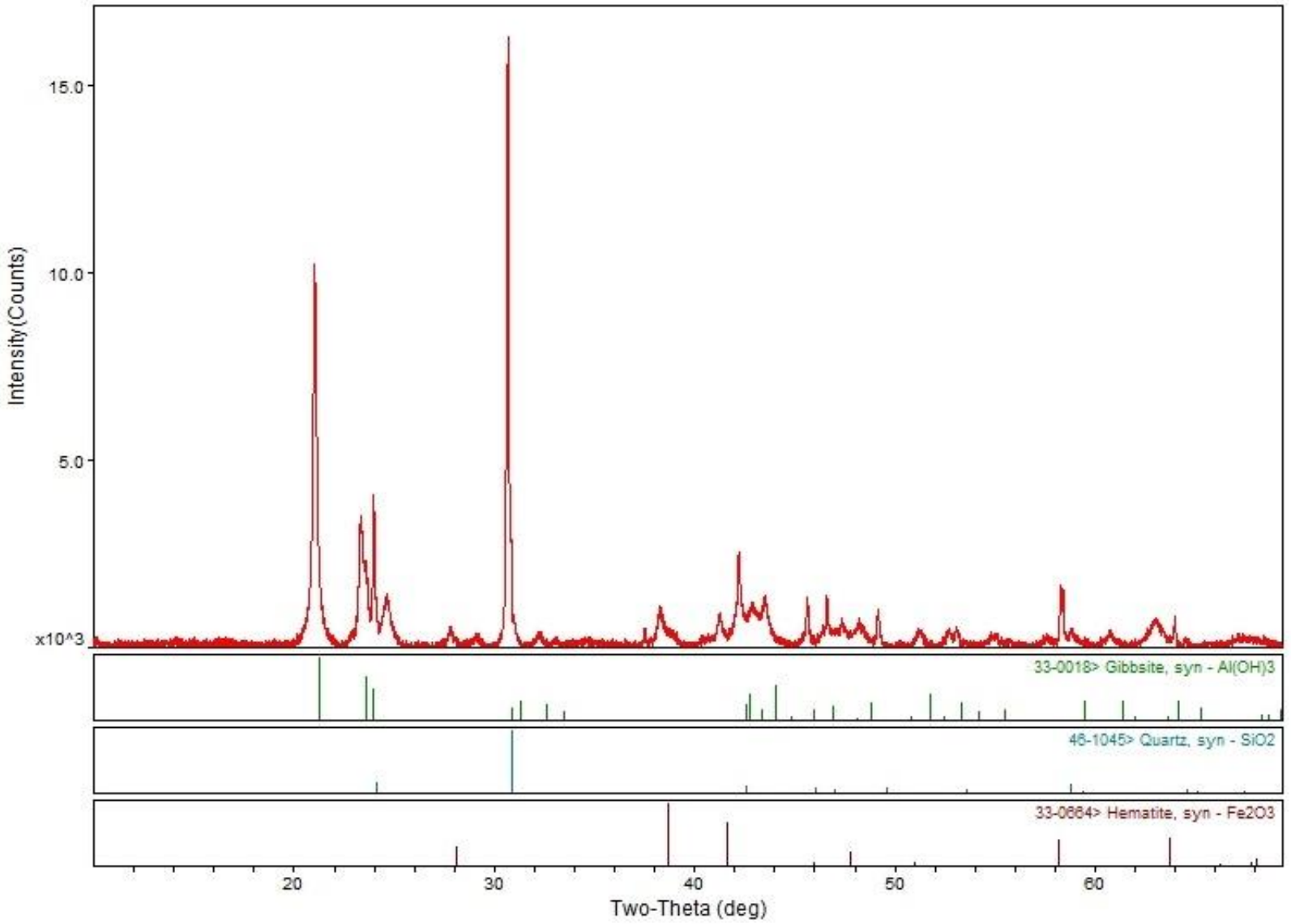

Figure 63. PXRD spectrum of NIST SRM 600 bauxite. The collected pattern is corresponding to λ = 1.78897 Å.

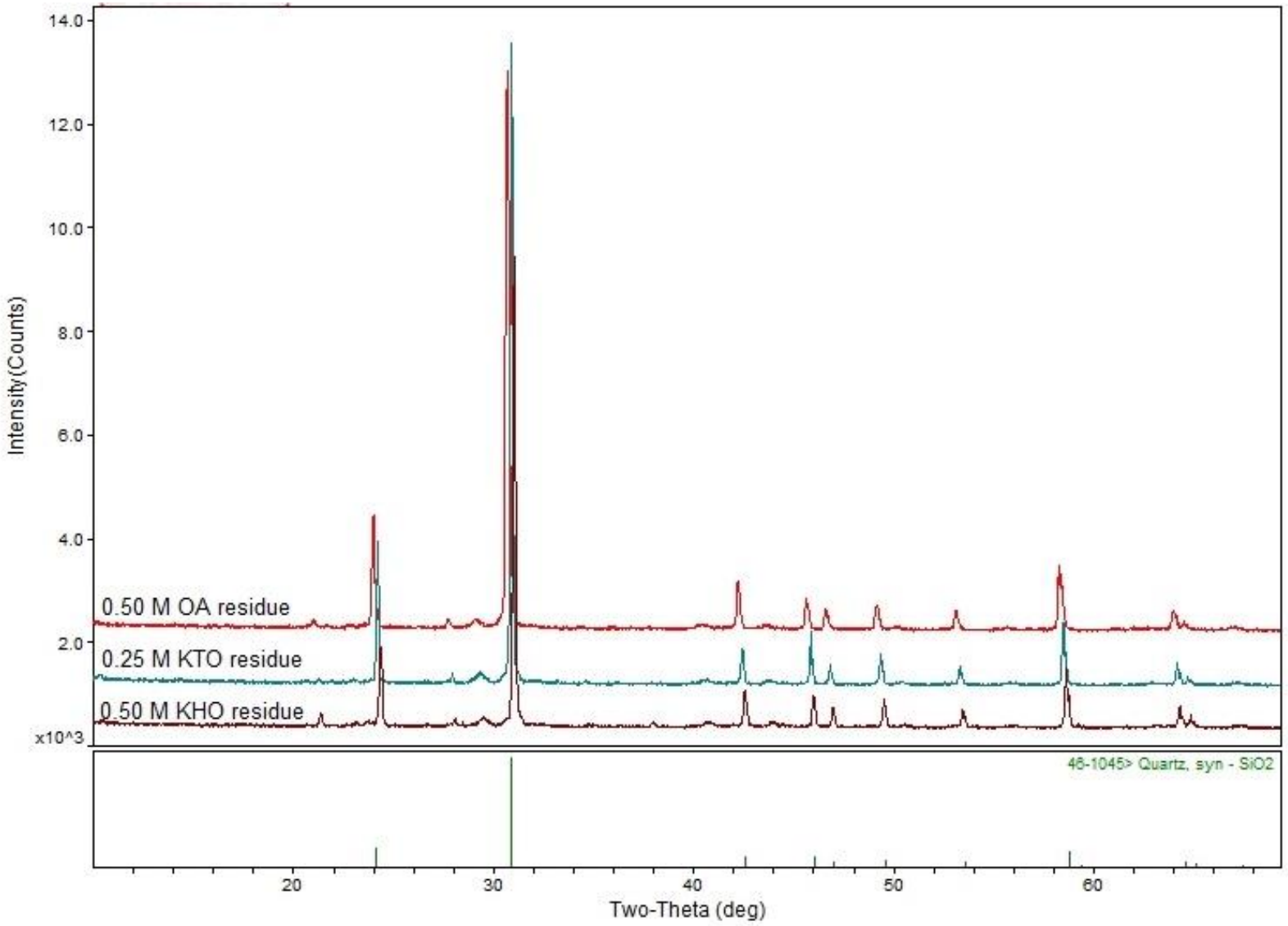

Figure 64. PXRD spectra of solids from NIST SRM 600 refining processes at S/L ratio = 15 g/L, T = 100 °C and Ns = 600 rpm. All of the patterns are corresponding to λ = 1.78897 Å.

7.4. Refining of Sargent-Welch Bauxite using Potassium Hydrogen Oxalate

The composition of a bauxite ore varies with the geographical location from which it is mined. NIST SRM 600 is an Al ore with high Fe and moderate Si content. To broaden the understanding of oxalate chemistry for Al extraction, Sargent-Welch (SW) bauxite ore was used. The SW ore was analyzed using XRF and contains 80% Al_2O_3, 9% SiO_2, 8% Fe_2O_3 and 3% TiO_2. However, only Al_2O_3 was confirmed using XRD (shown in Figure 65), and other metals were hypothesized to be present in a mixed metal oxide phase with Al. To extract Al from the SW ore, 0.50 M and 0.75 M KHO was used at T = 100 °C, N_s = 600 rpm, and S/L ratio = 15 g/L. The Al extraction kinetics has been reported in Figure 66. The metal extraction was ran for 8 h during the initial two extraction experiments. However, because of the slow kinetics, the reaction time was increased up to 24 h.

For all three cases presented in Figure 66, more than 80% of Al was extracted into the aqueous phase. The Al extraction kinetics using 0.50 M KHO was slower compared to 0.75 M KHO and plateaued at around 82% of extraction efficiency. This observation was expected because of low Si content (inert material) and effectively high amount of leachable metal in the ore. On increasing the acid concentration to 0.75 M, 90% Al extraction was achieved in 8 h, and additional 5% extraction was observed by increasing the reaction time to 24 h. The acid concentration was not increased further, but it can be expected that around 1 M KHO will be sufficient to extract Al efficiently from SW ore. This study indicates that depending on the composition and phases present in the ore, any metal extraction process needs to be modified for an efficient extraction of target metal. The solid residue remaining after the 0.75 M KHO – 24 h extraction was analyzed using PXRD (Figure 66) and indicates minor amount of Al present along with the suspected mixed Al-Si-O phase.

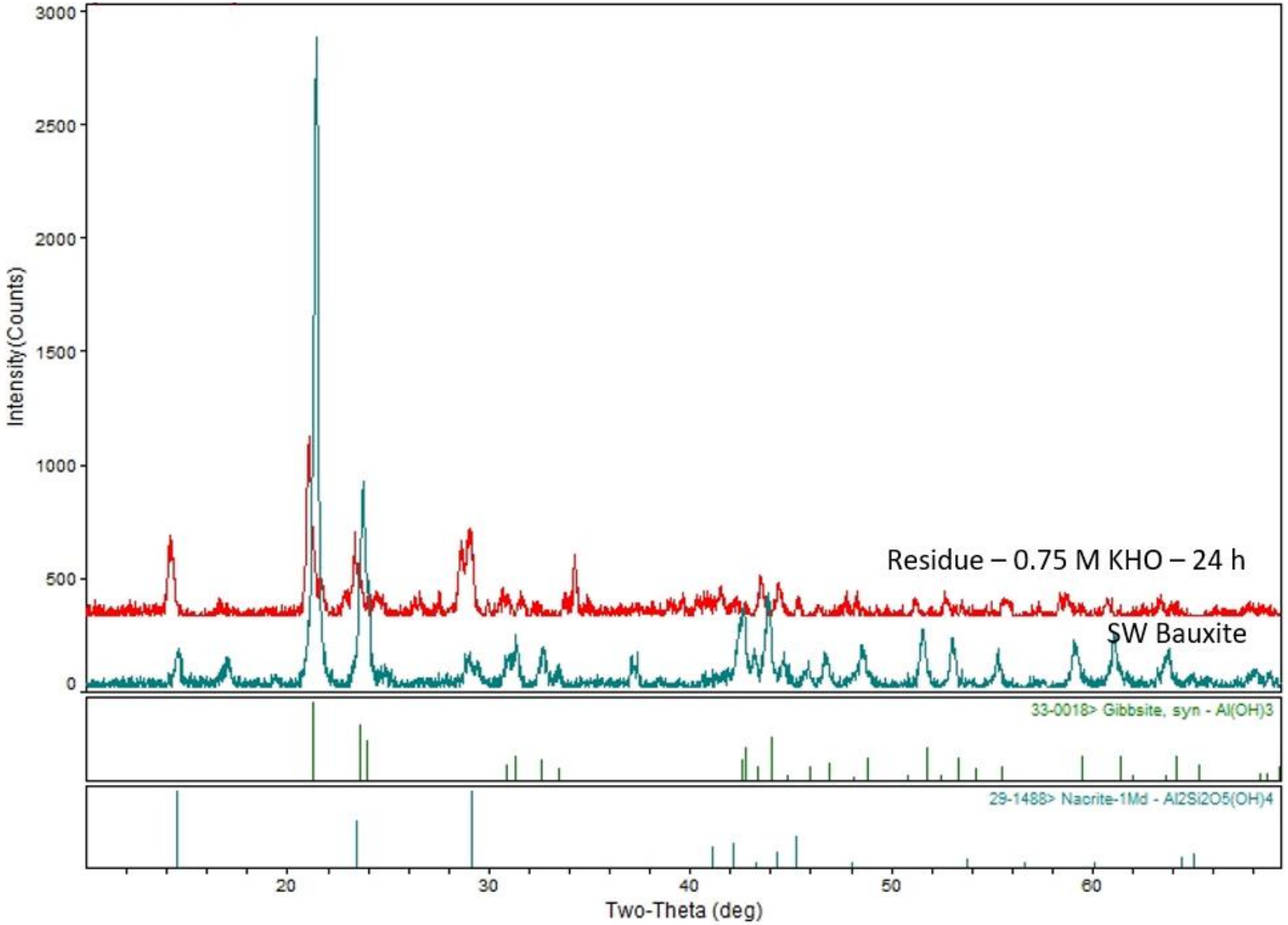

Figure 65. PXRD of Sargent-Welch (SW) bauxite and the solid residue recovered after metal extraction using 0.75 M KHO for 24 h. All of the patterns correspond to $\lambda = 1.78897$ Å.

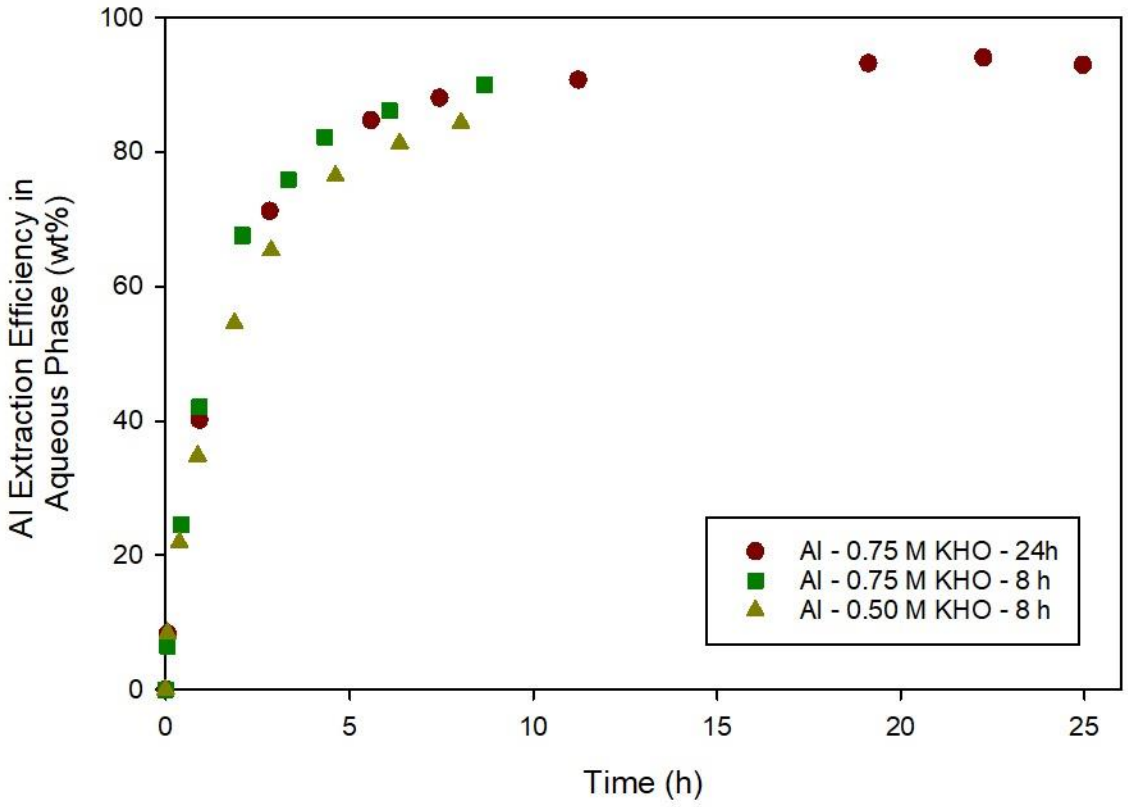

Figure 66. Al concentration as a function of time in the aqueous phase for 0.50 M and 0.75 M KHO at T = 100 °C, S/L = 15 g/L and Ns = 600 rpm.

7.5. Separations of Al and Fe from the Aqueous Phase

The oxalate-based acids (OA, KHO, and KTO) provide an efficient extraction (greater than 95 wt%) for Al and Fe into the aqueous phase and an easy separation for the remaining solid residue which is primarily made of SiO_2. The next step is to efficiently recover the Al from the aqueous phase and minimize any co-precipitation of Fe or other impurities.

The Al and Fe in the NIST SRM 600 bauxite ore are both present in the +3 oxidation state. The Al and Fe can be hydrolyzed to precipitate as metal hydroxides (discussed in Chapter 4). To selectively precipitate these metals, the pH must be optimized. The "Atlas of metal-ligand equilibria in aqueous solutions" by J. Kragten provides the pH range required for precipitation of $Fe(OH)_3$ and $Al(OH)_3$ using 0.1 M $C_2O_4^{2-}$ solution as shown in Figure 67.[80] The $Al(OH)_3$ is amphoteric in nature and can act as a Lewis acid that binds with OH^- ions to form a water-soluble

$Al(OH)_4^-$ ion.[217] Hence, the concentration of Al^{3+} metal in the aqueous phase decreases during hydrolysis up to about a pH = 9, but starts increasing as precipitate dissolves at higher pH. This trend is clearly visible in Figure 67 (dashed blue line). The $Fe(OH)_3$ precipitation begins before the $Al(OH)_3$ (indicated by the red solid line in Figure 67) but is not amphoteric and can be precipitated efficiently at high pH.

To precipitate Al and Fe effectively without any impurities, the basicity of the aqueous phase was increased to a pH of about 14 using KOH. To avoid the precipitation of insoluble metal oxalates, the base KOH is preferred versus NaOH. The high solubility of $K_2C_2O_4$ enables the efficient precipitation of Al and Fe. Greater than 99% of the Fe precipitates at a pH of about 14, while the majority of the Al remains in solution. Any remaining Al can be separated by lowering the pH to about 10.5 using H_2SO_4 or $H_2C_2O_4$. The approach is described in Table 29 for filtrate recovered after refining bauxite ore using OA, KTO, and KHO. Under these concentrations, pH = 10.5 was found to be optimum for Al precipitation. Using this approach, Al can be precipitated without any Fe impurity. The elemental composition of Al and Fe precipitates recovered from the aqueous filtrate of 0.25 M KTO extraction are shown in Table 30. A similar elemental composition was observed for the precipitates recovered from the aqueous filtrate after extracting Al and Fe using 0.50 M OA and KHO. It should be noted that around 10% of total Al precipitates with the Fe. The precipitate recovered at pH = 13.85 is approximately 62% iron hydroxide and 25% aluminum hydroxide whereas the precipitate recovered at pH = 10.56 after acidification is 96% aluminum hydroxide. To recover this additional Al, the Fe precipitate can be dissolved in an acidic oxalate solution (similar to the oxalate reagent initially used), and the approach described in Table 29 can be repeated to separate the remaining Al without any Fe impurity.

Iron precipitation (yellow precipitate) was also observed in the presence of visible light when aqueous filtrates were stored in clear glass bottles. This yellow precipitate was confirmed as $FeC_2O_4 \cdot 2H_2O$ using PXRD (Figure 69). The photoreduction of iron(III) oxalate complex to iron(II) oxalate complex has been reported by numerous researchers.[218-220] Mangiante et al. described this photoreduction through Eq. 7.6.[220] The observation of yellow precipitate from the complex could be attributed to the low pH (pH = 0.93-2.47) of the aqueous phase. In this pH range $H_2C_2O_4$ and $HC_2O_4^-$ are the predominant forms of oxalate ions.[150] The lack of $C_2O_4^{2-}$ combined with the low solubility of $FeC_2O_4 \cdot 2H_2O$ (0.078 g/100 g H_2O at 20 °C)[193] leads to the precipitation of $FeC_2O_4 \cdot 2H_2O$.[221] The kinetics of the photoreduction of Fe^{3+} was slow but efficient, as shown in Figure 68. It is clear from Figure 68 and Eq. 7.6 that bauxite filtrates should be stored in the dark to avoid any Fe precipitation and decomposition of $C_2O_4^{2-}$.

$$2Fe(C_2O_4)_3^{3-} \xrightarrow{h\nu} 2Fe(C_2O_4)_2^{2-} + 2CO_2 + C_2O_4^{2-} \quad (7.6)$$

Table 29. Methodology for selective precipitation of Al and Fe.

Acid concentration (Initial pH)	Procedure (Final pH)	Fe remaining in the aqueous phase (%)	Al remaining in the aqueous phase (%)
0.50 M OA (0.93)	KOH addition (13.87)	0.001	93.2
	H_2SO_4 addition (10.52)	0.002	0.16
0.25 M KTO (1.51)	KOH addition (13.85)	0.002	92.8
	H_2SO_4 addition (10.56)	0.002	0.15
0.50 M KHO (2.47)	KOH addition (13.88)	0.001	92.6
	H_2SO_4 addition (10.48)	0.001	0.24

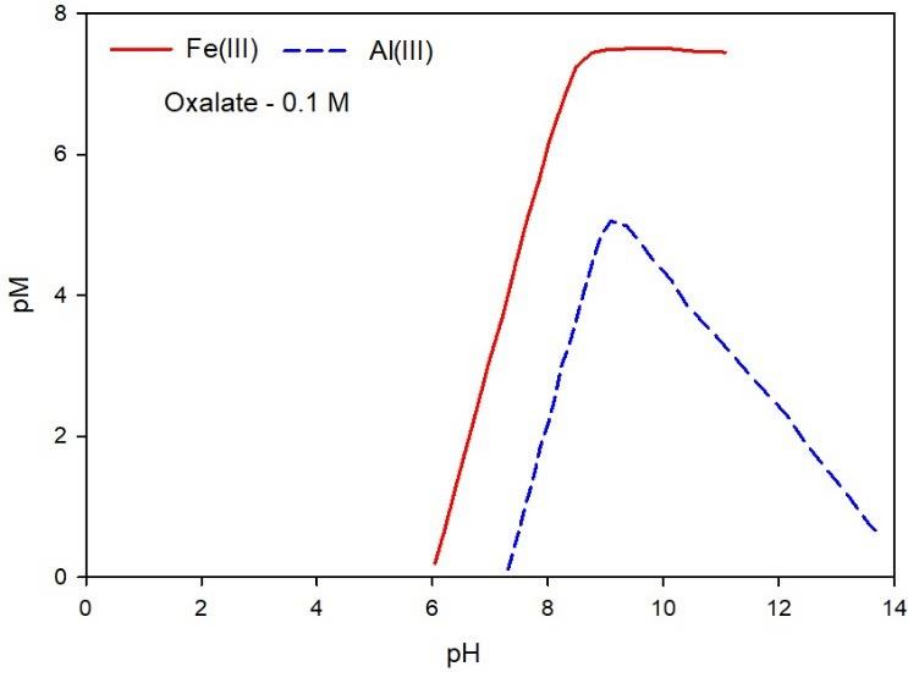

Figure 67. pM versus pH diagram for Fe(III) and Al(III) with 0.1 M oxalate ions. pM is defined as the negative log of the metal ions concentration in the aqueous phase.

Table 30. Elemental composition of Al and Fe precipitate recovered from the filtrate of 0.25 M KTO experiment at T = 100 °C, S/L = 15 g/L, and N_s = 600 rpm.

Precipitate from the aqueous filtrate of 0.25 M KTO extraction	**Concentration (wt%)**									
	Al	**Fe**	**Si**	**Ti**	**Zr**	**Ca**	**K**	**P**	**Mg**	**O**
pH = 13.85	11.06	27.29	1.49	0.76	0.16	2.25	0.32	0.40	0.20	55.63
pH = 10.56	33.89	0.05	0.61	ND	ND	0.47	0.14	0.33	ND	57.60

Note: ND - Not determined

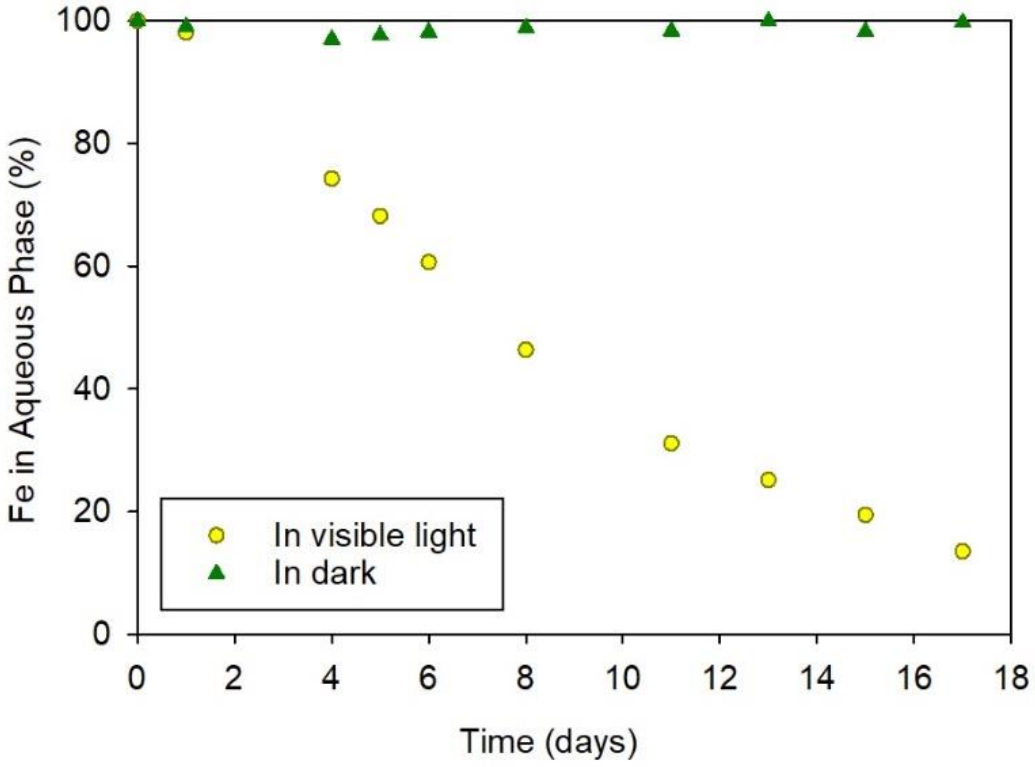

Figure 68. Effect of visible light on the concentration of Fe in the aqueous phase.

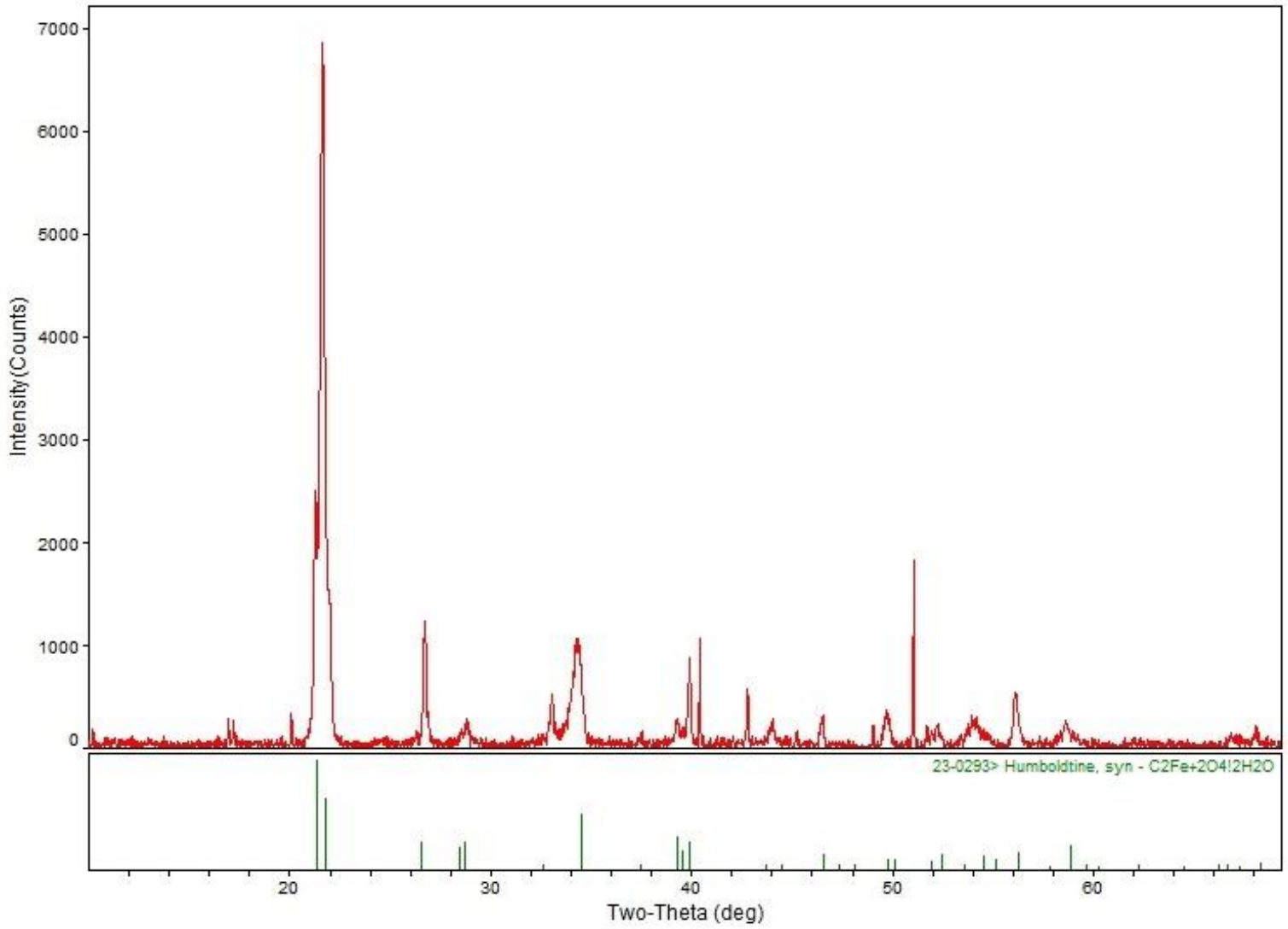

Figure 69. PXRD spectrum of the yellow precipitate (in presence of light) from the filtrate recovered after bauxite refining. The collected pattern is corresponding to $\lambda = 1.78897$ Å.

7.6. Recycling of Oxalate Reagents and Process Economics

A critical step for improving the economics of a metal extraction process is the recycling of the acids used for leaching. For the regeneration of KTO, KHO and OA, an ion-exchange resin was used to regenerate the acid and recycle it for future metal extraction. The precipitation of Al and Fe using KOH and $H_2C_2O_4$ produces K^+ ions as the major cation in the aqueous phase. A strong acid cation exchange resin like Amberlyst® 15 H-form was used to exchange the K^+ with H_3O^+ ions for regeneration of the oxalate reagents used in this study. The overall closed-loop process is shown in Figure 70. The amount of activated H-form resin added to the aqueous phase (containing K^+) determines the final pH. The KHO was regenerated to a pH of about 2.50 and KTO is produced at a pH of about 1.50. The regeneration of OA required a pH of about 1.0 and utilized the most resin. The ideal pH after the ion-exchange treatment should be close to the initial pH needed for the metal extraction process. A small amount of $H_2C_2O_4$ or $K_2C_2O_4$ is likely required to achieve the same starting oxalate concentration, but overall a significant amount of oxalate can be recycled; therefore, reducing the amount of fresh acid required and closing the loop on acid recovery and reuse. In the preliminary studies, around 30 g of Amberlyst-15 H-form (dry) was used to regenerate OA (pH = 1.2) from 1-L of filtrate recovered after Al precipitation at a pH of about 10.9. The recovery process using ion-exchange resins has been described in Chapter 5 in detail.

The alternative method for regenerating the oxalate-based reagents involves the acidification of the post precipitation filtrate using H_2SO_4 (shown in Figure 71). Similar to the ion-exchange resin approach, the final pH is critical in achieving the regenerated oxalate reagent. In this approach, the low solubility of potassium containing oxalate reagents is beneficial for precipitation, and the precipitated reagents can be efficiently filtered and separated. For the

operating conditions described in this work, the aqueous phase will be oversaturated with KHO and KTO and undersaturated for OA; therefore, only KHO and KTO will precipitate. In the preliminary studies, approximately 65% of the initial $C_2O_4^{2-}$ ion was recovered in the form of KHO by acidifying the post precipitate filtrate to a pH = 2.5 using H_2SO_4. Further, reducing the pH to 1.5 led to the recovery of 80% of the initial $C_2O_4^{2-}$ ion in the form of KTO. The precipitates were confirmed as KHO and KTO using PXRD, as shown in Figures 72 and 73, respectively. The closed-loop process is summarized in Figure 71. Decreasing the pH below 1.5 during acidification led to the dissolution of precipitate in the aqueous phase. This happens because of the higher solubility of OA compared to KTO. The approach shown in Figure 71 is advantageous because no resins are required, but the inability in regeneration of OA is a drawback.

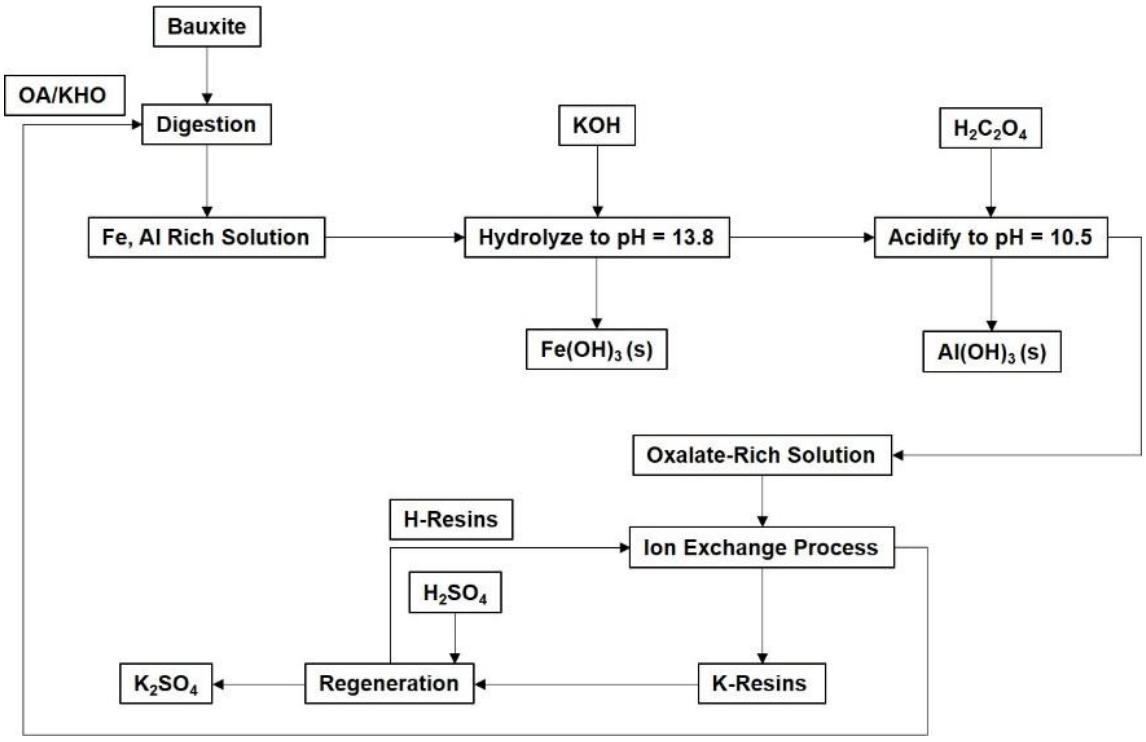

Figure 70. Flowsheet for the proposed closed-loop bauxite refining process using ion-exchange resins.

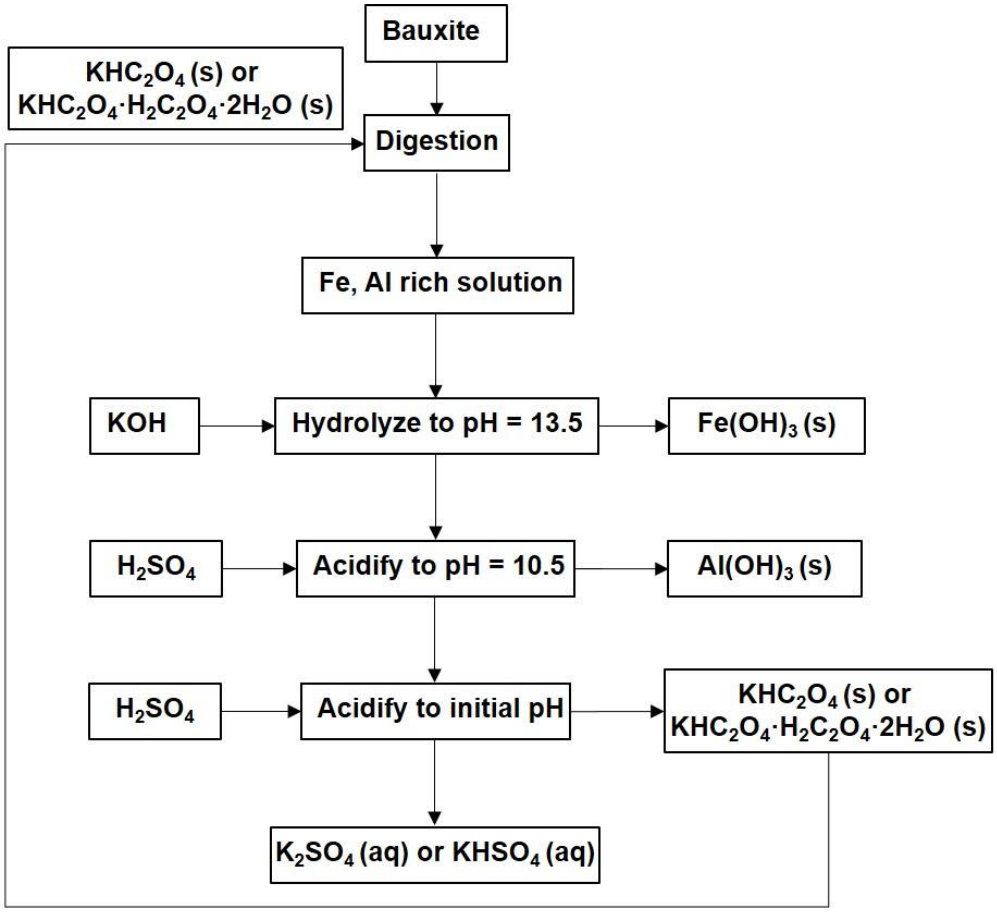

Figure 71. Flowsheet for the proposed bauxite refining process using oxalate precipitation.

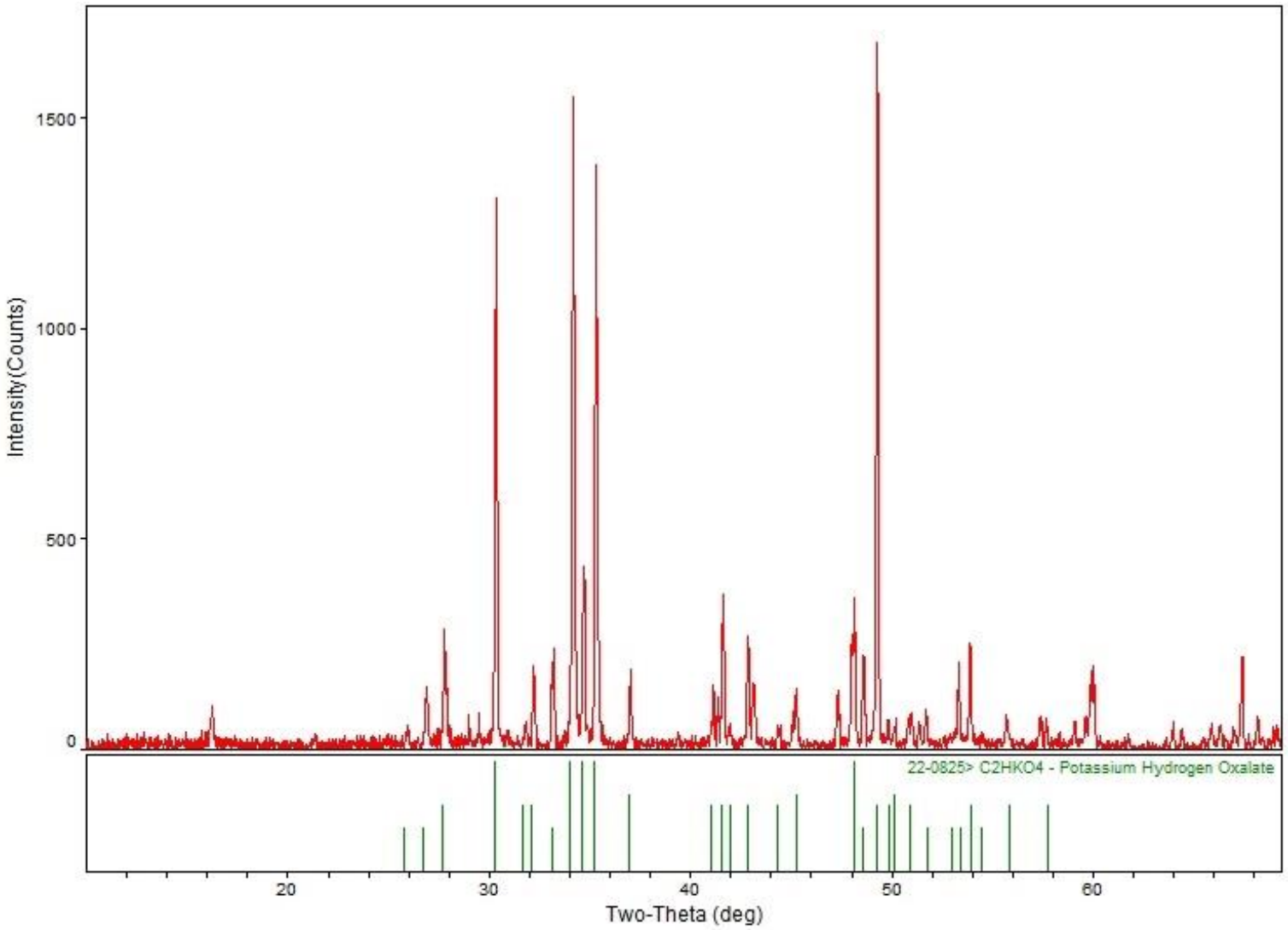

Figure 72. PXRD spectrum of the precipitate recovered on acidifying the filtrate recovered after metal precipitation to pH = 2.50. The collected pattern is corresponding to λ = 1.78897 Å.

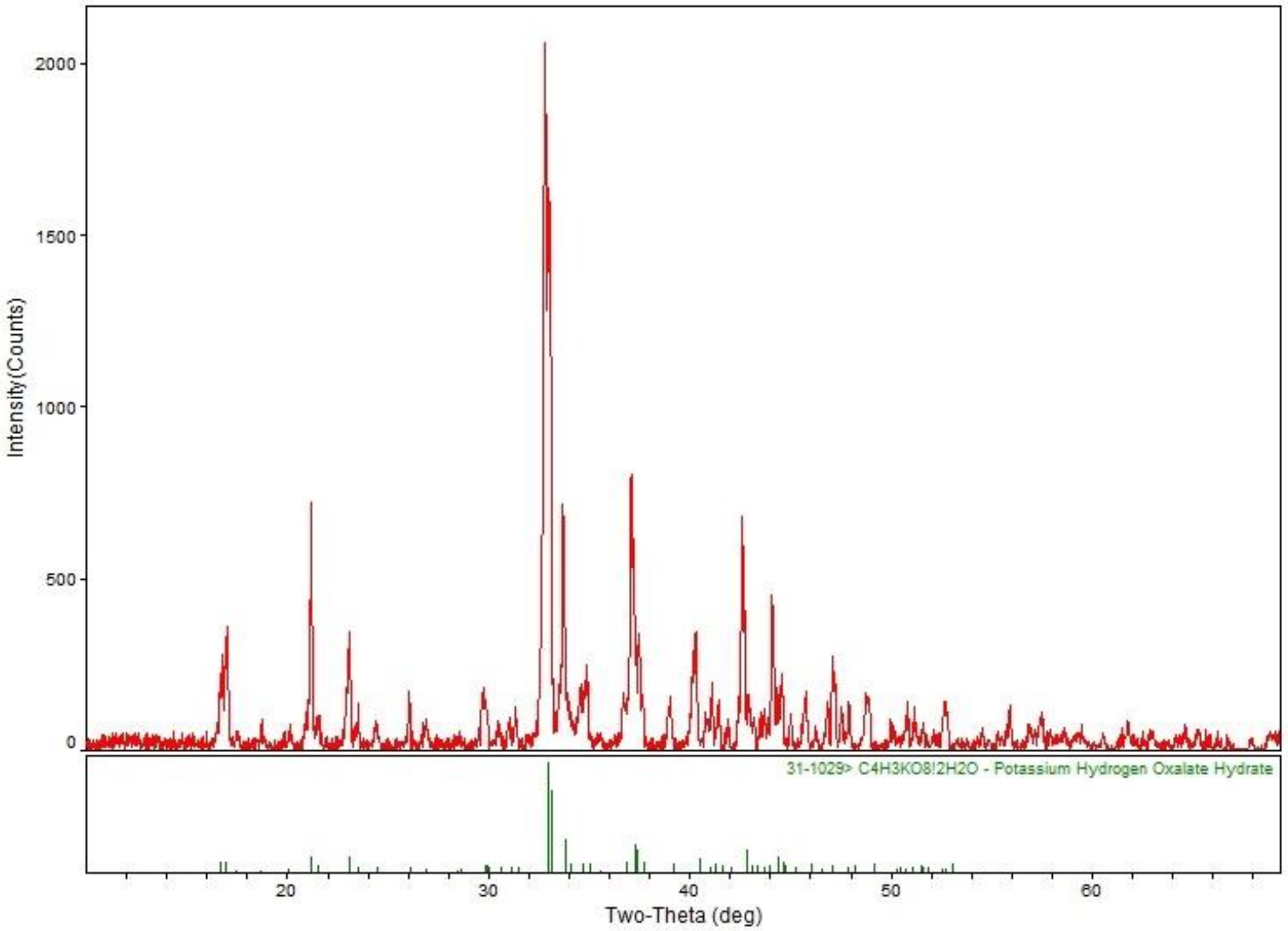

Figure 73. PXRD spectrum of the precipitate recovered on acidifying the filtrate recovered after metal precipitation to pH = 1.50. The collected pattern is corresponding to λ = 1.78897 Å.

The products of the proposed oxalate processes are Al_2O_3, Fe_2O_3 and SiO_2 (may be impure). These metal oxides have high demand and reliable primary and secondary resources. This is reflected in the low bulk costs of these products, as shown in Table 31. Therefore, the economics of an Al and Fe extraction from bauxite using oxalate reagent is highly dependent on the acid recycling efficiency. To understand its impact, the reagent costs for three cases with 70%, 80%, and 90% recycling efficiencies are compared to the market price of products achieved from 100 g of NIST SRM 600 ore. The results for the KHO process are shown in Tables 32 and 33. In this section, the recycling of acid via an ion-exchange resin process has not been considered in the process economics because of the high cost associated with it. For the KHO processes, it was observed that at least 90% of acid recycling is required for the input costs to be less than the market value of products considered. However, even after 90% acid recycling the KHO process is 5 times more expensive than the Bayer process (Table 32). This is because of the low S/L ratio (15 g/L) in the KHO process compared to the Bayer process (S/L ratio > 100 g/L).[222] The S/L ratio used in this chapter needs to be optimized to improve the economics. For Li and Co extraction from $LiCoO_2$, the S/L ratio was optimized to be 38 g/L. The KHO process will only be twice expensive than the Bayer process if S/L ratio of 38 g/L is achieved. Additionally, the particle morphology of Fe_2O_3 can be innovated to increase its value and increase the profit of the oxalate processes.

Table 31. Current market price of products proposed in the bauxite refining process.

S.No.	Outputs	Mass per kg of NIST SRM 600	Price ($/kg)	Source*
1	Fe_2O_3	0.15	0.10	https://www.alibaba.com/product-detail/Iron-Oxide-Factory-Supply-Iron-oxide_1600278576137.html
2	Al_2O_3	0.35	0.60	https://www.alibaba.com/showroom/aluminium-oxide-price.html
3	SiO_2	0.5	0.61	https://www.alibaba.com/product-detail/Silica-fume-Microsilica-price_60610007145.html

* Links accessed on 10/28/2021

Table 32. Cost of input reagents required in the proposed bauxite refining process using KHO.

	Input cost for 100 cycles ($/100 kg of NIST SRM 600)				
	KHO process for Fe and Al recovery (S/L ratio = 15 g/L)			Bayer process for Al recovery (1 M NaOH)	
	90% acid recycling	80% acid recycling	70% acid recycling	S/L ratio = 100 g/L	S/L ratio = 150 g/L
Oxalic Acid	25	48	71	0	0
KOH	17	27	37	0	0
H_2SO_4	8	8	8	0	0
NaOH	0	0	0	15	11
Total	**50**	**83**	**117**	**15**	**11**

Table 33. Current market value of the products from the bauxite refining process using KHO.

	Market price for 100 cycles ($/100 kg of NIST SRM 600)
Fe_2O_3	1.5
Al_2O_3	21
SiO_2	30
Total	**53 (23 without SiO_2)**

7.7. Application of Oxalate Chemistry for Fe and Ti Extraction from Ilmenite

Ilmenite is a major source of Ti and used in the production of TiO_2. It is a mixed metal oxide ore with the chemical formula as $FeTiO_3$. In this chapter, the developed oxalate processes were extended to extract Fe and Ti from $FeTiO_3$. On the basis of previous work by Corbin et al. following stoichiometric reactions (Eqs. 7.7 and 7.8) can be proposed in the presence of $H_2C_2O_4$ and KHC_2O_4. The metal extractions were carried out using 0.5 M and 1 M oxalate reagents at T = 100 °C, N_s = 600 rpm, and S/L ratio = 15 g/L. The metal extraction kinetics for these cases are shown in Figure 74. In Figure 74, the Ti extraction kinetics and efficiency is higher for $H_2C_2O_4$ compared to the KHC_2O_4. This observation was true for both 0.5 M and 1 M cases. However, in

all four cases only 50-60 % Ti was extracted into the aqueous phase. It should also be noted that in $FeTiO_3$, Fe exists in a +2 oxidation state and precipitates in the form of $FeC_2O_4{\cdot}2H_2O$. Therefore, minimal amount of Fe exists in the aqueous phase. However, it can be seen that with the improved extraction efficiency, the amount of Fe in the aqueous phase also increases. This can be well explained by the chemical equilibrium that exists between $FeC_2O_4{\cdot}2H_2O$ and $Fe(C_2O_4)_2^{2-}$.

$$FeTiO_3 + 2(H_2C_2O_4{\cdot}2H_2O) \rightleftarrows FeC_2O_4{\cdot}2H_2O + TiOC_2O_4 + 2H_2O \quad (7.7)$$

$$FeTiO_3 + 2KHC_2O_4 \rightleftarrows FeC_2O_4{\cdot}2H_2O + TiOC_2O_4 + 2KOH \quad (7.8)$$

But, even with the 1 M $H_2C_2O_4$, only 60% extraction efficiency was observed with the kinetics not reaching a plateau point. The slow kinetics could be because of the formation of an inert shell of $FeC_2O_4{\cdot}2H_2O$ around the reacting core of $FeTiO_3$ along with the difficulties in chelating Fe and Ti from the structure of $FeTiO_3$. Additional studies to study the mechanism of metal extraction from $FeTiO_3$ needs to be performed. However, to obtain a higher extraction efficiency, 2 M $H_2C_2O_4$ was used as an extraction reagent with a reaction time of 27 h as shown in Figure 75. After running the metal extraction for 27 h, 90% Ti was extracted into the aqueous phase with the solid residue majorly composed of $FeC_2O_4{\cdot}2H_2O$ (PXRD shown in Figure 76). The extraction of Fe and Ti from ilmenite ore was performed to demonstrate the flexibility of oxalate reagents for various systems. However, the mechanism of metal extraction is different from $LiCoO_2$ and in-depth study will be required for further exploration.

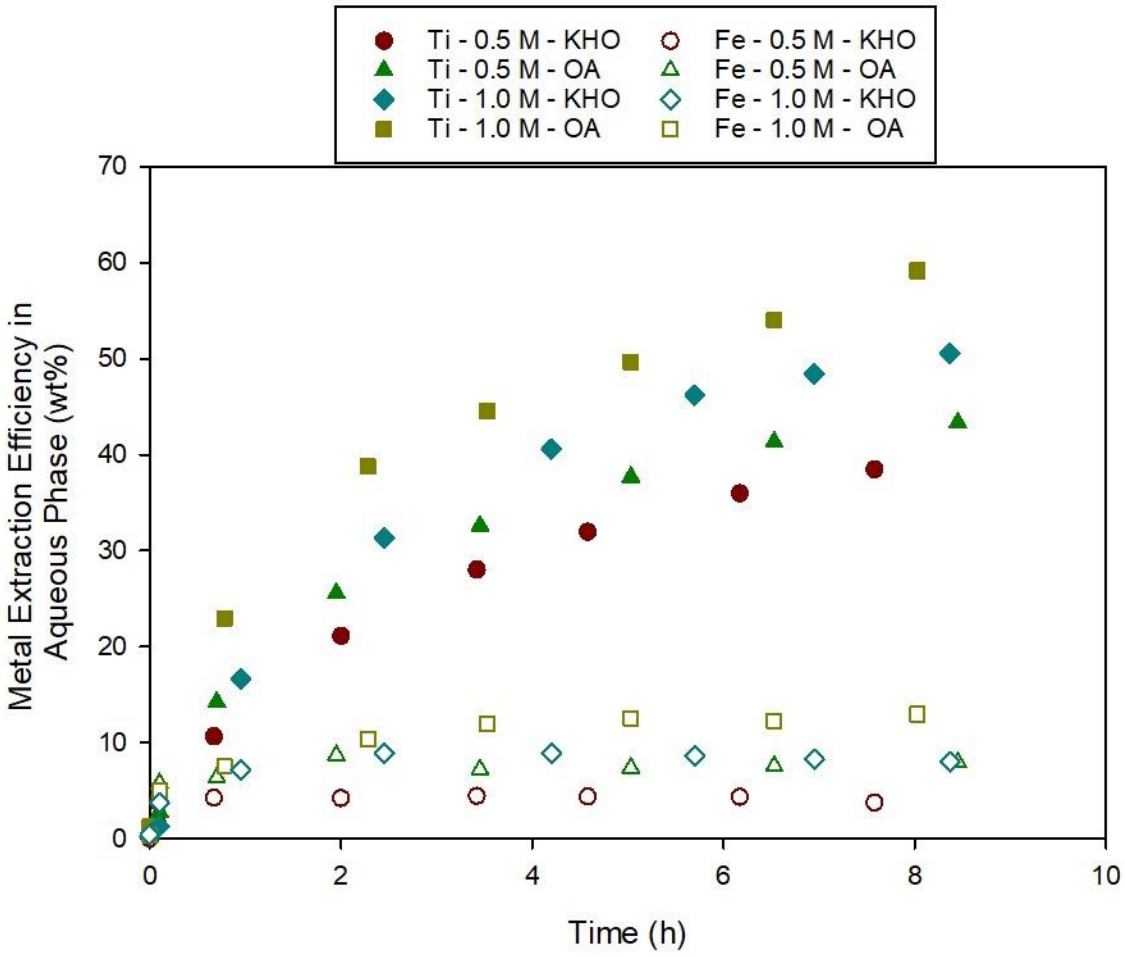

Figure 74. Ti and Fe concentration as a function of time in the aqueous phase for 0.50 M and 1 M oxalate reagents at T = 100 °C, S/L = 15 g/L and Ns = 600 rpm.

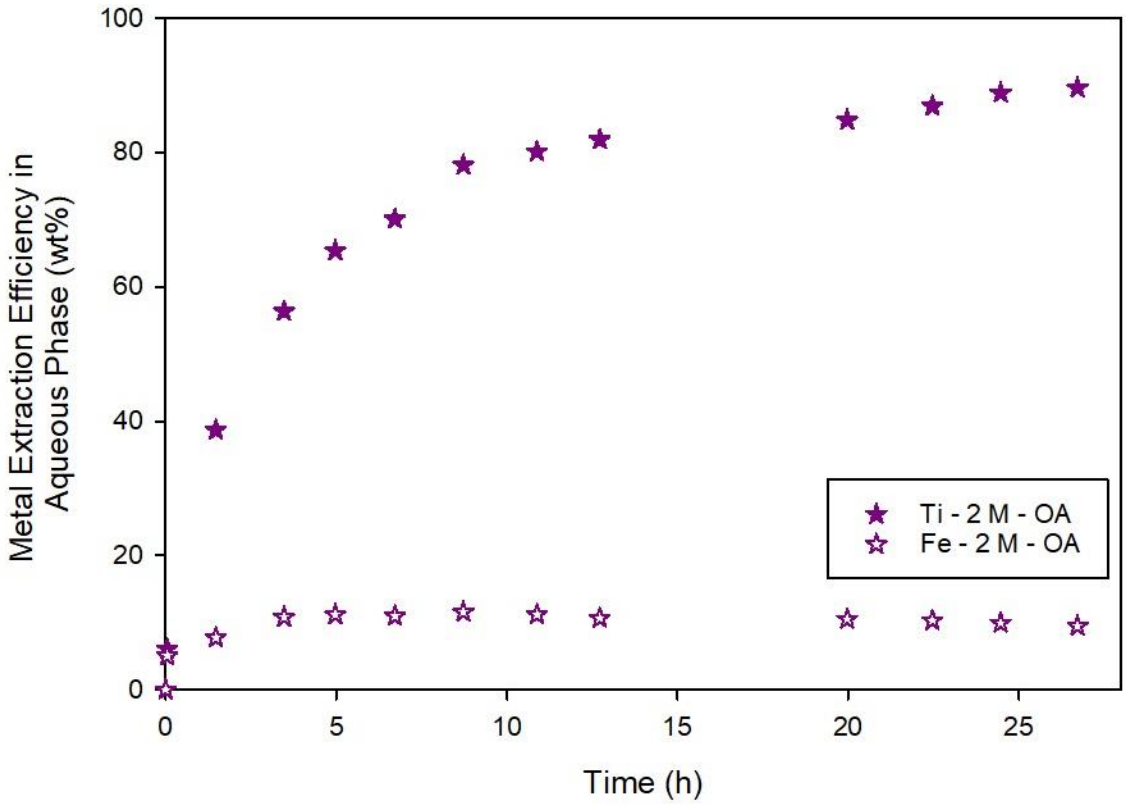

Figure 75. Ti and Fe concentration as a function of time in the aqueous phase for 2 M $H_2C_2O_4$ at T = 100 °C, S/L = 15 g/L and Ns = 600 rpm.

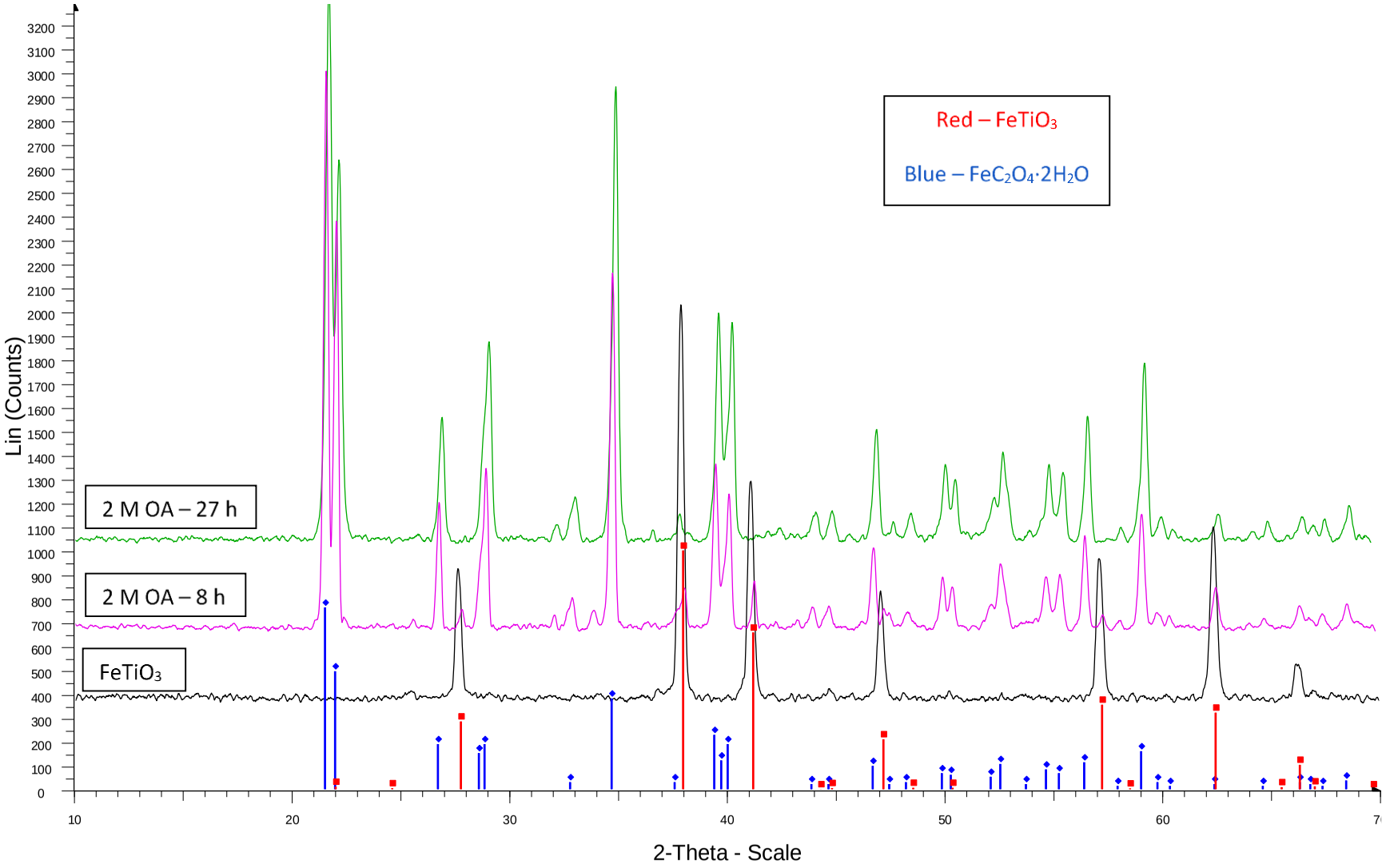

Figure 76. PXRD of $FeTiO_3$ and the solid residue recovered from during the metal extraction using 2 M $H_2C_2O_4$ at 8 and 27 h. All of the patterns are corresponding to λ = 1.78897 Å.

7.8. Conclusions

Commercially valuable metals like Al and Fe can be recovered efficiently from NIST SRM 600 bauxite ore using an environmentally-friendly process based on oxalate chemistry. In this chapter, an efficient Al and Fe extraction process using three oxalate reagents: $H_2C_2O_4$, KHC_2O_4, and $KHC_2O_4 \cdot H_2C_2O_4$ have been demonstrated. The three oxalate reagents were synthesized using various molar ratios of $H_2C_2O_4$ and $K_2C_2O_4$. The amount of $K_2C_2O_4$ determines the reaction pH and the rate of metal dissolution. The kinetics of Al extraction had a negligible dependence on the pH; however, the presence of H^+ ions are necessary for the metal dissolution. The kinetics of Fe extraction was dependent on pH and the fastest rate was measured for KHO at a pH = 2.50. KHO is an effective and safe acid for Al and Fe extraction from bauxite ore compared with the strong acids and bases currently used in the Bayer process. The amphoteric behavior of $Al(OH)_3$ allows selective precipitation of Fe at a pH = 13.80 and Al can be subsequently precipitated by acidifying the filtrate to a pH = 10.50. The efficient extraction of Al and Fe from bauxite ore produces only quartz (SiO_2) as the final residue. On comparing the economics of this process with the Bayer process, a need to increase the S/L ratio was observed. Additionally, some preliminary experiments on applying the proposed bauxite process for refining of Sargent-Welch bauxite with high Al content have also been shown.

In the described processes, 98-99% pure alumina can be produced. A critical step in the proposed process is the recovery and recycling of oxalate. After precipitating and separating the metals, an ion-exchange resin process was developed to regenerate the $H_2C_2O_4$, $KHC_2O_4 \cdot H_2C_2O_4$, or KHC_2O_4 in solution. An alternative approach that acidifies the precipitation filtrate takes advantage of the lower solubility of $KHC_2O_4 \cdot H_2C_2O_4$ and KHC_2O_4. Both reagents were precipitated from the aqueous solution and recovered as solids. The closed-loop process utilizing

oxalate chemistry does not produce any hazardous waste, unlike the alkaline red mud produced in the Bayer process. The simple and novel process using the combination of $H_2C_2O_4$ and $K_2C_2O_4$ provides a safe, efficient, sustainable, and environmentally-friendly route for recovering commercially valuable metals such as Al and Fe from bauxite ore.

Chapter 8. Conclusions and Future Recommendations

Chapter 8

"The real voyage of discovery consists not in seeking new landscapes, but in having new eyes."
- *Marcel Proust (Author)*

8.1. Conclusions

Metals are an important resource with numerous applications worldwide. In U.S., Critical metals like Al (bauxite), Li, Co, Mn, and REEs are vital in various emerging technologies (solar cells, lithium-ion batteries) but have a non-reliable supply. Continuously growing population with the increased level of technological innovation and economic activity has resulted in a rapid increase in resource consumption. Therefore, sustainable use of resources is critical to protect our ecosystem and preserve natural resources for future generations. This dissertation introduces a new array of sustainable critical metal recovery processes using oxalate chemistry.

Oxalate chemistry has tremendous potential to develop sustainable technologies for critical metal recovery from various mixed metal sources like LIB cathodes, ores and REEs containing material. Oxalate ($C_2O_4^{2-}$) anion, which can be derived from organic sources, has minimal to no environmental impact and can be utilized in the synthesis of moderately acidic reagents for developing energy-efficient processes. Oxalates are commonly known for its chelation and metal precipitation properties, but the leaching and reducing properties along with the possibility of soluble metal oxalate complexes are not known. This dissertation establishes oxalate chemistry as a unique and environmentally-friendly approach to extract and separate metals from various minerals and mixed metal oxide sources. The properties of oxalate anion and oxalate reagents have been discussed in detail in Chapter 1. In this dissertation, oxalic acid ($H_2C_2O_4$), ammonium hydrogen oxalate ($NH_4HC_2O_4$), potassium hydrogen oxalate (KHC_2O_4), and potassium

tetraoxalate ($KHC_2O_4 \cdot H_2C_2O_4$) have been demonstrated as reagents to develop closed-loop metal extraction and recovery processes from lithium cobalt oxide ($LiCoO_2$) cathodes, and bauxite ore. In addition, preliminary experiments were also performed on metal extractions from ilmenite ore and lithium nickel-manganese-cobalt oxide cathode.

8.1.1. Recovery and Separation of Li and Co from $LiCoO_2$

Lithium-ion battery cathode chemistry has been continuously evolving over the years with $LiCoO_2$ being the most popular one. The modern cathode chemistries are focused towards replacing the Co content with Ni and Mn while maintaining the layered structure. The recycling of cathode from spent LIBs is essential to develop a secondary source for the critical metals such as Li, Co and Mn and stabilize the LIB economy. In this dissertation, the development of a closed-loop process for efficient recovery and separation of Li and Co from $LiCoO_2$ has been discussed in depth.

In Chapter 2, the mechanism of Li and Co extraction from $LiCoO_2$ was studied to identify the preferable oxalate reagent for efficient recovery. Additional reaction parameters like acid concentration and pH were also optimized. The reaction between $LiCoO_2$ and an acidic oxalate reagent resulted in the precipitation of Co, whereas Li remained in the aqueous phase. To achieve an efficient separation between Li and Co, pH < 1.5 was optimum to avoid the dissolution of insoluble $CoC_2O_4 \cdot 2H_2O$ in the aqueous phase. To maintain an operating pH < 1.5, $H_2C_2O_4$ was preferred over $NH_4HC_2O_4$ because of higher acidity. A green colored intermediate after metal extraction was identified and confirmed as a complex containing $[Co(C_2O4)_3]^{3-}$. From this investigation, Co^{3+} metal extraction, reduction to Co^{2+}, and further precipitation in the form of $CoC_2O_4 \cdot 2H_2O$ were confirmed to occur simultaneously.

In Chapter 3, a combined shrinking core model was developed to study the Li extraction kinetics from $LiCoO_2$ in the presence of $H_2C_2O_4$. The kinetic study revealed the diffusion of aqueous reactant through the solid $CoC_2O_4{\cdot}2H_2O$ product layer to be rate-limiting. The existence of a shrinking $LiCoO_2$ core and an inert $CoC_2O_4{\cdot}2H_2O$ was confirmed with the help of PXRD and XPS. In an $H_2C_2O_4$ process, the reduction of Co^{3+} to Co^{2+} occurs at the expense of $C_2O_4^{2-}$ oxidizing into CO_2. This $H_2C_2O_4$ loss was avoided by the addition of a reducing agent such as H_2O_2. The reaction conditions were optimized, and the kinetics were studied for $H_2C_2O_4 + H_2O_2$ process as well. The addition of H_2O_2 reduces the $C_2O_4^{2-}$ concentration in solution and slows the $CoC_2O_4{\cdot}2H_2O$ precipitation to produce a unique micro-rod structured precipitate. This micro-rod precipitate had a 23% lower bulk density compared to the granular precipitate from extractions using only $H_2C_2O_4$. The lower density micro-rod precipitate forms a porous shell allowing increased diffusion of $H_2C_2O_4$ to the $LiCoO_2$ core. The overall activation energy was significantly reduced by 33% from 61 kJ/mol to 41 kJ/mol by adding H_2O_2 to the $H_2C_2O_4$ extraction process. The observed phenomenon of improved kinetics and transformation in the rate-limiting step could improve the kinetics for other aqueous hydrometallurgical systems with both soluble and insoluble products.

In a hydrometallurgical process using oxalate chemistry, potassium compounds must be used as a precipitation agent to achieve high purity products. The Li dissolved in the aqueous phase was precipitated as Li_2CO_3 using K_2CO_3 and KOH. The Li_2CO_3 was a preferred compound because of low aqueous solubility and an easier route for converting it into Li_2O through calcination. However, the Li must be concentrated in the solution for efficient precipitation. In Chapter 4, the solubility of various Li compounds has been discussed and an effective Li concentration of 10 g/L was identified as an optimum value for >80% precipitation efficiency. The

Li can be concentrated by reusing the aqueous phase for multiple metal extractions before precipitating Li or evaporating the aqueous content. In Chapter 6, the Li precipitation was demonstrated by evaporating the aqueous phase to concentrate it by four times before the addition of K_2CO_3. This led to a precipitation of over 90% Li in the form of Li_2CO_3. The $CoC_2O_4{\cdot}2H_2O$ could directly be calcined into Co_3O_4 and Co, in the presence of air and N_2, respectively. It was also identified that the micro-rod structure of $CoC_2O_4{\cdot}2H_2O$, observed in a $H_2C_2O_4 + H_2O_2$ process was preserved during the calcination process. This unique morphology could be utilized to synthesize 1-D cathode material for LIBs. However, the loss of $C_2O_4^{2-}$ anion during calcination was not preferred. Hence, a novel route was identified, where the $CoC_2O_4{\cdot}2H_2O$ was dissolved in the presence of excess $C_2O_4^{2-}$ anion and precipitated in the form of $Co(OH)_2$. This sequential dissolution and precipitation have been explained in Chapter 4 and was demonstrated in Chapter 6. The aqueous phase recovered after precipitating Li had a high pH and was preferred for $CoC_2O_4{\cdot}2H_2O$ dissolution and precipitation. The $LiCoO_2$ was synthesized through a solid-state reaction between the precipitated Li and Co products.

Recycling oxalate reagent after recovery of critical metals is necessary for waste minimization and cost-effectiveness of the extraction process. In Chapter 5, an ion exchange process using strong acid cation exchange resin was optimized for recycling $H_2C_2O_4$ after Li and Co precipitation. In an ion-exchange process, the amount of resins used was critical in achieving the desired form of oxalate reagent. To recycle the aqueous phase in $H_2C_2O_4$ form, a pH < 1.0 was preferred whereas for KHC_2O_4 and $NH_4HC_2O_4$, pH around 2.5 was preferred. The used resins can be regenerated and reused for multiple recycling processes and was demonstrated for 2 cycles in Chapter 6. A preliminary techno-economic analysis of the $H_2C_2O_4$ and $H_2C_2O_4 + H_2O_2$ processes was performed to evaluate the economic and environmental impacts. The analysis concluded that

the 80-90 % recycling of $H_2C_2O_4$ is necessary for the $H_2C_2O_4$ and $H_2C_2O_4 + H_2O_2$ processes to compete with an H_2SO_4 process economically. To understand the environmental impact, the waste streams were evaluated for estimating E-factor. The $H_2C_2O_4 + H_2O_2$ process has an E-factor of 5.5, whereas $H_2C_2O_4$ and H_2SO_4 processes have an E-factor of approximately 10. The 50% reduction in waste generation with similar economic impacts makes the $H_2C_2O_4 + H_2O_2$ process most sustainable for the recovery of critical metals such as Li and Co from waste LIB cathodes. The novel processes described in this work using oxalate reagent provide an efficient, sustainable, and environmentally-friendly route for recovering and separating critical metals such as Li and Co from $LiCoO_2$.

***Possible Improvements**:* The closed-loop process for Li and Co recovery from $LiCoO_2$ has been optimized and demonstrated in Chapters 2, 3 and 6. However, there are two areas where additional studies will improve the impact of overall process. First, the broader impacts of the micro-rod morphology products (Co_3O_4 and $LiCoO_2$) were not studied in this work. The Co_3O_4 is known as a good catalyst for oxygen reduction reaction and can be used in fuel cell applications. In addition, 1-D cathode products of $LiCoO_2$ could improve the cycling efficiency and overall capacity. The electrochemical characterization of micro-rod structured materials will broaden the impact of the oxalate process. Secondly, the ion exchange process for recycling could be improved further in a column setup, as batch setup has been optimized. The ion exchange in a column is analogous to the infinite number of small batches. This will result in a higher capacity of ion exchange and an improved regeneration for reuse.

8.1.2. Oxalate Process for Bauxite Refining

Bauxite ore is the world's primary source of Al metal. The Bayer process holds an exclusive status worldwide for the extraction of alumina (Al_2O_3) from bauxite. This process is efficient for alumina extraction, but a massive amount of "red mud" waste is generated. The red mud waste is caustic and is mainly composed of iron oxides. In Chapter 7, three oxalate reagents: potassium hydrogen oxalate (KHC_2O_4), potassium tetraoxalate ($KHC_2O_4 \cdot H_2C_2O_4$), and oxalic acid ($H_2C_2O_4$) were investigated for the development of a closed-loop Al and Fe extraction process from NIST SRM 600 – Australian Darling range bauxite ore. These oxalate reagents can be synthesized using different molar ratios of $H_2C_2O_4$ and $K_2C_2O_4$. The efficient Al and Fe extraction was observed for all three reagents at operating at a different pH. The Al extraction kinetics was similar for all three reagents whereas Fe was fastest for KHC_2O_4 (highest operating pH).

To selectively precipitate Fe and Al, fundamentals of metal hydroxide precipitation have been discussed in detail in Chapter 4. It was concluded that the amphoteric properties of $Al(OH)_3$ could be utilized to separate Fe and Al. The selective precipitation was demonstrated in Chapter 7, where at a pH = 13.5, Fe was selectively precipitated leaving Al in the solution. Further, the aqueous phase was acidified to a pH = 10.5 and precipitated Al in the form of $Al(OH)_3$. After precipitating and separating the metals, an ion-exchange resin process was developed to regenerate the $H_2C_2O_4$, $KHC_2O_4 \cdot H_2C_2O_4$, or KHC_2O_4 in solution. An alternative recovery approach utilized the lower solubility of $KHC_2O_4 \cdot H_2C_2O_4$ and KHC_2O_4 in the acidic pH range. Both reagents were precipitated from the aqueous solution in the pH range of 1.5-2.5 and recovered as solids. The closed-loop process utilizing oxalate chemistry does not produce any hazardous waste, unlike the alkaline red mud produced in the Bayer process. The simple and novel process using the

combination of $H_2C_2O_4$ and $K_2C_2O_4$ provides a safe, efficient, sustainable, and environmentally-friendly route for recovering commercially valuable metals such as Al and Fe from bauxite ore.

***Possible Improvements**:* The refining of bauxite ore for efficient recovery of Al and Fe with minimal waste production has been demonstrated in Chapter 7. Bauxite refining using oxalate reagents is a solid-liquid reaction but with only aqueous product. However, the presence of inert SiO_2 in the ore, creates a diffusional resistance for the aqueous oxalate reagent. To improve the kinetics, pre-treatment processes like microwave heating could be performed to generate cracks and pores in the SiO_2 structure. A model similar to the shrinking-core model could be developed for the bauxite refining as well to explain the fundamental kinetics. The solid-to-liquid (S/L) ratio of 20 g/L was the maximum that was attempted in this work. The metal extractions at higher S/L ratio will improve the Fe and Al precipitation efficiency, as well as the recycling of $KHC_2O_4{\cdot}H_2C_2O_4$ and KHC_2O_4. Reusing the aqueous phase for another metal extraction before precipitating metals is an alternative route that could be tried to increase the concentration of metals. In the end, a techno-economic analysis of the oxalate processes should be performed and compared it with the Bayer process.

8.2. Future Work

The oxalate processes demonstrated in this work provide an efficient, cost-effective and environmentally-friendly route to recover metals from mixed metal oxide sources. In this dissertation, closed-loop processes for Li and Co extraction from $LiCoO_2$ for LIBs recycling, and Fe and Al extraction from bauxite ore have been discussed. In this section, strategies to improve

the ion exchange process along with other potential applications of the oxalate process have been discussed.

8.2.1. Ion-Exchange Process

The closed-loop oxalate processes described in this work are environmentally-friendly and economical compared to the inorganic acid processes. However, as discussed in Chapter 6, there is a significant amount of mildly acidic waste that was generated during the regeneration of resins. This problem could be resolved using two different approaches. The first approach involves utilizing the acidic waste containing a high amount of K^+ ions to produce KOH. Chemical reagents like slaked lime ($Ca(OH)_2$) can be added to the acidic waste stream of K_2SO_4 to precipitate gypsum ($CaSO_4$) and produce KOH. But the low concentration of K in the aqueous phase can be a barrier to efficient KOH production and may require additional concentration before the addition of slaked lime. Another approach can be to explore the different types of strong acid cation exchange resins other than Amberlyst® 15. The kinetics, selectivity, and capacity of the ion exchange depend on the crosslinking of the resins. Resins like Dowex® 5WX8 and Purolite® MN500 are 8% and 50% crosslinked compared to 20% crosslinking of Amberlyst® 15. These resins will showcase a different capacity and kinetics for ion exchange. Along with this, operating the ion exchange process in a column setup can also improve the resin regeneration process significantly.

8.2.2. Recycling of NMC Cathodes

NMC111 cathodes ($LiNi_{0.33}Mn_{0.33}Co_{0.33}O_2$) were invented to reduce the Co content in cathodes by replacing it with Ni and Mn. The method for metal extraction from NMC cathode using oxalate chemistry has been briefly discussed in Chapter 6. Additionally, a spent LIB cathode will also contain other additional metals such as Al, Fe, Zn and Cu from foils and current collectors as well as graphite from the anode. In the preliminary experiments on NMC cathodes, oxalate

processes were able to extract Li, Ni, Mn and Co from the cathode. However, the optimization of reaction parameters and kinetic analysis is required. The optimized reaction parameters can be used to extract the metals from an actual battery waste containing additional metals such as Al, Fe, Zn, Cu and graphite. The metal separation strategies and acid recovery processes discussed in Chapters 4 and 5 can be used to separate the metals and develop a closed-loop process with minimum environmental impacts.

8.2.3. Rare-Earths Recovery using Oxalate Chemistry

Rare earth elements (REEs) are a vital component in the high-tech electronic materials and electrical industry. The deposits of naturally occurring REEs are localized in Asia, but the extraction of REEs from secondary resources like electronic waste (e-waste) and spent magnets can be an alternative option. Traditionally, oxalates are known as a precipitation reagent for REEs, but the closed-loop processes developed in this work can also be extended for the extraction of REEs. The REEs are expected to demonstrate pH dependent aqueous solubility as observed with other metals like Co, Ni, Mn and Fe. A thorough literature review along with the solubility experiments on critical REEs should guide the process development of REEs recovery from e-waste using oxalate chemistry.

References

1. Sawada, H.; Murakami, T., Oxalic Acid. In *Kirk-Othmer Encyclopedia of Chemical Technology*, 2000.

2. Krishnamurty, K. V.; Harris, G. M., The Chemistry of the Metal Oxalato Complexes. *Chemical Reviews* **1961,** *61* (3), 213-246. DOI: 10.1021/cr60211a001.

3. Cleland, W. W.; Johnson, M. J., Studies on the Formation of Oxalic Acid by Aspergillus Niger. *Journal of Biological Chemistry* **1956,** *220* (2), 595-606. DOI: 10.1016/S0021-9258(18)65285-8.

4. Kondô, K.; Ameyama, M., Carbohydrate Metabolism by Acetobacter Species. *Bulletin of the Agricultural Chemical Society of Japan* **1958,** *22* (6), 369-386. DOI: 10.1080/03758397.1958.10857508.

5. Dutton, M. V.; Evans, C. S., Oxalate production by fungi: its role in pathogenicity and ecology in the soil environment. *Canadian Journal of Microbiology* **1996,** *42* (9), 881-895. DOI: 10.1139/m96-114.

6. Re, L.; Maurer, B.; Ohloff, G., Ein einfacher Zugang zu 4-hydroxy-2,5-dimethyl-3(2H)-furanon (furaneol), einem Aromabestandteil von Ananas und Erdbeere. *Helvetica Chimica Acta* **1973,** *56* (6), 1882-1894. DOI: 10.1002/hlca.19730560609.

7. Riemenschneider, W.; Tanifuji, M., Oxalic Acid. In *Ullmann's Encyclopedia of Industrial Chemistry*, 2011.

8. Royen, H.; Fortkamp, U., Rare earth elements-purification, separation and recycling. *Environmental Research Institute: Stockholm, Sweden* **2016**.

9. Lakshmanan, V. I.; Sridhar, R.; Halim, M. Process for extraction of rare earth elements. US20130283977A1, 2015.

10. Bard, A. J.; Parsons, R.; Jordan, J., *Standard potentials in aqueous solution*. M. Dekker: New York, 1985.

11. Zeng, X.; Li, J.; Shen, B., Novel approach to recover cobalt and lithium from spent lithium-ion battery using oxalic acid. *Journal of Hazardous Materials* **2015,** *295*, 112-118. DOI: 10.1016/j.jhazmat.2015.02.064.

12. Sun, L.; Qiu, K., Organic oxalate as leachant and precipitant for the recovery of valuable metals from spent lithium-ion batteries. *Waste Management* **2012,** *32* (8), 1575-1582. DOI: 10.1016/j.wasman.2012.03.027.

13. Panias, D.; Taxiarchou, M.; Douni, I.; Paspaliaris, I.; Kontopoulos, A., Dissolution of hematite in acidic oxalate solutions: the effect of ferrous ions addition. *Hydrometallurgy* **1996,** *43* (1), 219-230. DOI: 10.1016/0304-386X(96)00004-7.

14. Panias, D.; Taxiarchou, M.; Paspaliaris, I.; Kontopoulos, A., Mechanisms of dissolution of iron oxides in aqueous oxalic acid solutions. *Hydrometallurgy* **1996,** *42* (2), 257-265. DOI: 10.1016/0304-386X(95)00104-O.

15. Taxiarchou, M.; Panias, D.; Douni, I.; Paspaliaris, I.; Kontopoulos, A., Dissolution of hematite in acidic oxalate solutions. *Hydrometallurgy* **1997,** *44* (3), 287-299. DOI: 10.1016/S0304-386X(96)00075-8.

16. Corbin, D. R.; Griffin, T. P.; Hutchenson, K. W.; Li, S.; Shiflett, M. B.; Torardi, C.; Zaher, J. J. Processes for producing titanium dioxide. US 8137647 B2, 2012.

17. Buttke, L. G.; Schueller, J. R.; Pearson, C. S.; Beyer, K. D., Solubility of the Sodium and Ammonium Salts of Oxalic Acid in Water with Ammonium Sulfate. *The Journal of Physical Chemistry A* **2016,** *120* (32), 6424-6433. DOI: 10.1021/acs.jpca.6b05208.

18. Crouthamel, C. E.; Martin, D. S., The Solubility of Ytterbium Oxalate and Complex Ion Formation in Oxalate Solutions*. *Journal of the American Chemical Society* **1950,** *72* (3), 1382-1386. DOI: 10.1021/ja01159a084.

19. Perry, D. L., *Handbook of inorganic compounds*. CRC Press: Boca Raton, 2011.

20. Rumble, J. R., *CRC handbook of chemistry and physics : a ready-reference book of chemical and physical data*. CRC Press: Boca Raton, 2018.

21. Hall, W. T., The oxalate method for separating calcium and magnesium. *Journal of the American Chemical Society* **1928,** *50* (10), 2704-2707. DOI: 10.1021/ja01397a016.

22. Sarver, L. A.; Brinton, P. H. M. P., The solubilities of some rare-earth oxalates. *Journal of the American Chemical Society* **1927,** *49* (4), 943-958. DOI: 10.1021/ja01403a006.

23. Tuncuk, A.; Stazi, V.; Akcil, A.; Yazici, E. Y.; Deveci, H., Aqueous metal recovery techniques from e-scrap: Hydrometallurgy in recycling. *Minerals Engineering* **2012,** *25* (1), 28-37. DOI: 10.1016/j.mineng.2011.09.019.

24. Li, J.; Xu, Z., Environmental Friendly Automatic Line for Recovering Metal from Waste Printed Circuit Boards. *Environmental Science & Technology* **2010,** *44* (4), 1418-1423. DOI: 10.1021/es903242t.

25. Zheng, X.; Zhu, Z.; Lin, X.; Zhang, Y.; He, Y.; Cao, H.; Sun, Z., A Mini-Review on Metal Recycling from Spent Lithium Ion Batteries. *Engineering* **2018,** *4* (3), 361-370. DOI: 10.1016/j.eng.2018.05.018.

26. Money, R. W.; Davies, C. W., The solubility of barium oxalate in aqueous salt solutions. *Journal of the Chemical Society (Resumed)* **1938,** (0), 2098-2100. DOI: 10.1039/JR9380002098.

27. William, N. S. Vanadyl Oxalate Compounds and Process for Producing Same. US3689515A, 1972.

28. Berckmans, G.; Messagie, M.; Smekens, J.; Omar, N.; Vanhaverbeke, L.; Van Mierlo, J., Cost Projection of State of the Art Lithium-Ion Batteries for Electric Vehicles Up to 2030. *Energies* **2017,** *10* (9). DOI: 10.3390/en10091314.

29. Lee, C. K.; Rhee, K.-I., Preparation of $LiCoO_2$ from spent lithium-ion batteries. *Journal of Power Sources* **2002,** *109* (1), 17-21. DOI: 10.1016/S0378-7753(02)00037-X.

30. Sohn, J.-S.; Shin, S.-M.; Yang, D.-H.; Kim, S.-K.; Lee, C.-K., Comparison of Two Acidic Leaching Processes for Selecting the Effective Recycle Process of Spent Lithium ion Battery. *Geosystem Engineering* **2006,** *9* (1), 1-6. DOI: 10.1080/12269328.2006.10541246.

31. Zeng, X.; Li, J.; Singh, N., Recycling of Spent Lithium-Ion Battery: A Critical Review. *Crit. Rev. Env. Sci. Technol.* **2014,** *44* (10), 1129-1165. DOI: 10.1080/10643389.2013.763578.

32. Aaltonen, M.; Peng, C.; Wilson, B.; Lundström, M., Leaching of Metals from Spent Lithium-Ion Batteries. *Recycling* **2017,** *2* (4), 20. DOI: 10.3390/recycling2040020.

33. Chen, C. H.; Liu, J.; Stoll, M. E.; Henriksen, G.; Vissers, D. R.; Amine, K., Aluminum-doped lithium nickel cobalt oxide electrodes for high-power lithium-ion batteries. *Journal of Power Sources* **2004,** *128* (2), 278-285. DOI: 10.1016/j.jpowsour.2003.10.009.

34. Nitta, N.; Wu, F.; Lee, J. T.; Yushin, G., Li-ion battery materials: present and future. *Materials Today* **2015,** *18* (5), 252-264. DOI: 10.1016/j.mattod.2014.10.040.

35. Meshram, P.; Pandey, B. D.; Mankhand, T. R., Hydrometallurgical processing of spent lithium ion batteries (LIBs) in the presence of a reducing agent with emphasis on kinetics of leaching. *Chemical Engineering Journal* **2015,** *281*, 418-427. DOI: 10.1016/j.cej.2015.06.071.

36. Wang, R.-C.; Lin, Y.-C.; Wu, S.-H., A novel recovery process of metal values from the cathode active materials of the lithium-ion secondary batteries. *Hydrometallurgy* **2009,** *99* (3), 194-201. DOI: 10.1016/j.hydromet.2009.08.005.

37. Li, L.; Lu, J.; Zhai, L.; Zhang, X.; Curtiss, L.; Jin, Y.; Wu, F.; Chen, R.; Amine, K., A facile recovery process for cathodes from spent lithium iron phosphate batteries by using oxalic acid. *CSEE Journal of Power and Energy Systems* **2018,** *4* (2), 219-225. DOI: 10.17775/CSEEJPES.2016.01880.

38. Yang, Y.; Meng, X.; Cao, H.; Lin, X.; Liu, C.; Sun, Y.; Zhang, Y.; Sun, Z., Selective recovery of lithium from spent lithium iron phosphate batteries: a sustainable process. *Green Chemistry* **2018,** *20* (13), 3121-3133. DOI: 10.1039/C7GC03376A.

39. Aikawa, T.; Watanabe, M.; Aida, T.; L. Smith Jr, R., Hydrothermal Leaching of $LiCoO_2$ with Sulfuric Acid, Nitric Acid, and Citric Acid. *KAGAKU KOGAKU RONBUNSHU* **2017,** *43*, 313-318. DOI: 10.1252/kakoronbunshu.43.313.

40. Yuliusman; Fajaryanto, R.; Nurqomariah, A.; Silvia In *Acid leaching and kinetics study of cobalt recovery from spent lithium-ion batteries with nitric acid*, E3S Web of Conferences, 2018; p 03025.

41. Zhang, X.; Bian, Y.; Xu, S.; Fan, E.; Xue, Q.; Guan, Y.; Wu, F.; Li, L.; Chen, R., Innovative Application of Acid Leaching to Regenerate $Li(Ni_{1/3}Co_{1/3}Mn_{1/3})O_2$ Cathodes from Spent Lithium-Ion Batteries. *ACS Sustainable Chemistry & Engineering* **2018,** *6* (5), 5959-5968. DOI: 10.1021/acssuschemeng.7b04373.

42. Ilhan, S. In *Leaching of Spent Ni–Mo Hydrodesulphurization (HDS) Catalyst in Oxalic Acid Solutions*, Proceedings of the 3rd Pan American Materials Congress, Cham, 2017//; Springer International Publishing: Cham, 2017; pp 557-564.

43. Szymczycha-Madeja, A., Kinetics of Mo, Ni, V and Al leaching from a spent hydrodesulphurization catalyst in a solution containing oxalic acid and hydrogen peroxide. *Journal of Hazardous Materials* **2011,** *186* (2), 2157-2161. DOI: 10.1016/j.jhazmat.2010.11.120.

44. Horeh, N. B.; Mousavi, S. M.; Shojaosadati, S. A., Bioleaching of valuable metals from spent lithium-ion mobile phone batteries using Aspergillus niger. *Journal of Power Sources* **2016,** *320*, 257-266. DOI: 10.1016/j.jpowsour.2016.04.104.

45. Wu, W.; Wang, C.; Bao, W.; Li, H., Selective reduction leaching of vanadium and iron by oxalic acid from spent V_2O_5-WO_3/TiO_2 catalyst. *Hydrometallurgy* **2018,** *179*, 52-59. DOI: 10.1016/j.hydromet.2018.05.021.

46. Deng, B.; Wang, B.; Su, S.; Ding, S.; Sun, W., Recovery of iron from pyrolusite leaching slag by a lab-scale circulation process of oxalic acid leaching and ultraviolet irradiation. *Metals* **2018,** *8* (1). DOI: 10.3390/met8010008.

47. Park, Y. M.; Lim, H.; Moon, J.-H.; Lee, H.-N.; Son, S. H.; Kim, H.; Kim, H.-J., High-Yield One-Pot Recovery and Characterization of Nanostructured Cobalt Oxalate from Spent Lithium-Ion Batteries and Successive Re-Synthesis of $LiCoO_2$. *Metals* **2017,** *7* (8), 303.

48. Nayaka, G. P.; Manjanna, J.; Pai, K. V.; Vadavi, R.; Keny, S. J.; Tripathi, V. S., Recovery of valuable metal ions from the spent lithium-ion battery using aqueous mixture of mild organic acids as alternative to mineral acids. *Hydrometallurgy* **2015,** *151*, 73-77. DOI: 10.1016/j.hydromet.2014.11.006.

49. Chen, X.; Luo, C.; Zhang, J.; Kong, J.; Zhou, T., Sustainable Recovery of Metals from Spent Lithium-Ion Batteries: A Green Process. *ACS Sustainable Chemistry & Engineering* **2015,** *3* (12), 3104-3113. DOI: 10.1021/acssuschemeng.5b01000.

50. Hu, C.; Guo, J.; Wen, J.; Peng, Y., Preparation and Electrochemical Performance of Nano-Co_3O_4 Anode Materials from Spent Li-Ion Batteries for Lithium-Ion Batteries. *Journal of Materials Science & Technology* **2013,** *29* (3), 215-220. DOI: 10.1016/j.jmst.2013.01.009.

51. Li, J.; Shi, P.; Wang, Z.; Chen, Y.; Chang, C.-C., A combined recovery process of metals in spent lithium-ion batteries. *Chemosphere* **2009,** *77* (8), 1132-1136. DOI: 10.1016/j.chemosphere.2009.08.040.

52. Chen, L.; Tang, X.; Zhang, Y.; Li, L.; Zeng, Z.; Zhang, Y., Process for the recovery of cobalt oxalate from spent lithium-ion batteries. *Hydrometallurgy* **2011,** *108* (1), 80-86. DOI: 10.1016/j.hydromet.2011.02.010.

53. Li, L.; Lu, J.; Ren, Y.; Zhang, X. X.; Chen, R. J.; Wu, F.; Amine, K., Ascorbic-acid-assisted recovery of cobalt and lithium from spent Li-ion batteries. *Journal of Power Sources* **2012,** *218*, 21-27. DOI: 10.1016/j.jpowsour.2012.06.068.

54. Li, L.; Qu, W.; Zhang, X.; Lu, J.; Chen, R.; Wu, F.; Amine, K., Succinic acid-based leaching system: A sustainable process for recovery of valuable metals from spent Li-ion batteries. *Journal of Power Sources* **2015,** *282*, 544-551. DOI: 10.1016/j.jpowsour.2015.02.073.

55. Li, L.; Dunn, J. B.; Zhang, X. X.; Gaines, L.; Chen, R. J.; Wu, F.; Amine, K., Recovery of metals from spent lithium-ion batteries with organic acids as leaching reagents and environmental assessment. *Journal of Power Sources* **2013,** *233*, 180-189. DOI: 10.1016/j.jpowsour.2012.12.089.

56. Wu, W.; Liu, X.; Zhang, X.; Li, X.; Qiu, Y.; Zhu, M.; Tan, W., Mechanism underlying the bioleaching process of $LiCoO_2$ by sulfur-oxidizing and iron-oxidizing bacteria. *Journal of Bioscience and Bioengineering* **2019,** *128* (3), 344-354. DOI: 10.1016/j.jbiosc.2019.03.007.

57. Chianelli, R. R., Fundamental Studies of Transition Metal Sulfide Hydrodesulfurization Catalysts. *Catalysis Reviews* **1984,** *26* (3-4), 361-393. DOI: 10.1080/01614948408064718.

58. Dhar, G. M.; Srinivas, B. N.; Rana, M. S.; Kumar, M.; Maity, S. K., Mixed oxide supported hydrodesulfurization catalysts—a review. *Catalysis Today* **2003,** *86* (1), 45-60. DOI: 10.1016/S0920-5861(03)00403-6.

59. Masuda, C.; Yonezu, K.; Watanabe, K.; Yokoyama, T., Recovery of Platinum from Spent Reforming Catalyst by Acid Leaching and Coprecipitation. *Procedia Earth and Planetary Science* **2013,** *6*, 435-440. DOI: 10.1016/j.proeps.2013.01.057.

60. Mazurek, K., Recovery of vanadium, potassium and iron from a spent vanadium catalyst by oxalic acid solution leaching, precipitation and ion exchange processes. *Hydrometallurgy* **2013,** *134-135*, 26-31. DOI: 10.1016/j.hydromet.2013.01.011.

61. Erust, C.; Akcil, A.; Bedelova, Z.; Anarbekov, K.; Baikonurova, A.; Tuncuk, A., Recovery of vanadium from spent catalysts of sulfuric acid plant by using inorganic and organic acids: Laboratory and semi-pilot tests. *Waste Management* **2016,** *49*, 455-461. DOI: 10.1016/j.wasman.2015.12.002.

62. Delmas, F.; Nogueira, C.; Dalrymple, I.; Parkes, J., Metals Recovery From Hydrodesulphurization Catalysts. In *Hydrometallurgy '94: Papers presented at the international symposium 'Hydrometallurgy '94' organized by the Institution of Mining and Metallurgy and the Society of Chemical Industry, and held in Cambridge, England, from 11 to 15 July, 1994*, Springer Netherlands: Dordrecht, 1994; pp 1075-1086.

63. Akcil, A.; Vegliò, F.; Ferella, F.; Okudan, M. D.; Tuncuk, A., A review of metal recovery from spent petroleum catalysts and ash. *Waste Management* **2015,** *45*, 420-433. DOI: 10.1016/j.wasman.2015.07.007.

64. Menoufy, M. F.; Ahmed, H. S., Treatment and Reuse of Spent Hydrotreating Catalyst. *Energy Sources, Part A: Recovery, Utilization, and Environmental Effects* **2008,** *30* (13), 1213-1222. DOI: 10.1080/15567030600829048.

65. Al-Sheeha, H.; Marafi, M.; Raghavan, V.; Rana, M. S., Recycling and Recovery Routes for Spent Hydroprocessing Catalyst Waste. *Industrial & Engineering Chemistry Research* **2013,** *52* (36), 12794-12801. DOI: 10.1021/ie4019148.

66. Zou, H.; Gratz, E.; Apelian, D.; Wang, Y., A novel method to recycle mixed cathode materials for lithium ion batteries. *Green Chemistry* **2013,** *15*, 1183-1191. DOI: 10.1039/c3gc40182k.

67. Winterbourn, C. C., Toxicity of iron and hydrogen peroxide: the Fenton reaction. *Toxicology Letters* **1995,** *82/83*, 969-974. DOI: 10.1016/0378-4274(95)03532-X.

68. Lee, F. M.; Knudsen, R. D.; Kidd, D. R., Reforming catalyst made from the metals recovered from spent atmospheric resid desulfurization catalyst. *Industrial & Engineering Chemistry Research* **1992,** *31* (2), 487-490. DOI: 10.1021/ie00002a006.

69. Aung, K. M. M.; Ting, Y.-P., Bioleaching of spent fluid catalytic cracking catalyst using Aspergillus niger. *Journal of biotechnology* **2005,** *116* (2), 159-170. DOI: 10.1016/j.jbiotec.2004.10.008.

70. Santhiya, D.; Ting, Y.-P., Bioleaching of spent refinery processing catalyst using Aspergillus niger with high-yield oxalic acid. *Journal of Biotechnology* **2005,** *116* (2), 171-184. DOI: 10.1016/j.jbiotec.2004.10.011.

71. Valverde Jr, I. M.; Paulino, J. F.; Afonso, J. C., Hydrometallurgical route to recover molybdenum, nickel, cobalt and aluminum from spent hydrotreating catalysts in sulphuric acid medium. *Journal of Hazardous Materials* **2008,** *160* (2-3), 310-317. DOI: 10.1016/j.jhazmat.2008.03.003.

72. Fleming, C. A., Hydrometallurgy of precious metals recovery. *Hydrometallurgy* **1992,** *30* (1), 127-162. DOI: 10.1016/0304-386X(92)90081-A.

73. Sullivan, J. D., Leaching copper from its ores. *Journal of Chemical Education* **1931,** *8* (5), 829. DOI: 10.1021/ed008p829.

74. Posel, J. G. Recovery of nitric acid soluble transition metals from sulfur and iron containing ores of the same. US4038361A, 1976.

75. Agacayak, T.; Zedef, V. In *Leaching of a Turkish Lateritic Nickel Ore in Nitric Acid Solution*, Mine Planning and Equipment Selection, Cham, 2014//; Drebenstedt, C.; Singhal, R., Eds. Springer International Publishing: Cham, 2014; pp 1039-1045.

76. Corbin, D. R.; Hutchison, S. N. Processes for producing titanium dioxide. US 7678350 B2, 2010.

77. Tzeferis, P. G.; Agatzini-Leonardou, S., Leaching of nickel and iron from Greek non-sulphide nickeliferous ores by organic acids. *Hydrometallurgy* **1994,** *36* (3), 345-360. DOI: 10.1016/0304-386X(94)90031-0.

78. Kursunoglu, S.; Kaya, M., Dissolution behavior of Caldag lateritic nickel ore subjected to a sequential organic acid leaching method. *International Journal of Minerals, Metallurgy, and Materials* **2015,** *22* (11), 1131-1140. DOI: 10.1007/s12613-015-1177-9.

79. Sahu, S.; Kavuri, N. C.; Kundu, M., Dissolution kinetics of nickel laterite ore using different secondary metabolic acids. *Brazilian Journal of Chemical Engineering* **2011,** *28*, 251-258. DOI: 10.1590/S0104-66322011000200009.

80. Kragten, J.; Masson, M., *Atlas of metal-ligand equilibria in aqueous solution*. Horwood: Chichester, 1978.

81. Ghosh, S.; Paul, A., Bioleaching of nickel by Aspergillus humicola SKP102 isolated from Indian lateritic overburden. *Journal of Sustainable Mining* **2016,** *15* (3), 108-114. DOI: 10.1016/j.jsm.2016.11.002.

82. Das, A. P.; Swain, S.; Panda, S.; Pradhan, N.; Sukla, L. B., Reductive Acid Leaching of Low Grade Manganese Ores. *Geomaterials* **2012,** *Vol.02No.04*, 4. DOI: 10.4236/gm.2012.24011.

83. Sahoo, R. N.; Naik, P. K.; Das, S. C., Leaching of manganese from low-grade manganese ore using oxalic acid as reductant in sulphuric acid solution. *Hydrometallurgy* **2001,** *62* (3), 157-163. DOI: 10.1016/S0304-386X(01)00196-7.

84. Azizi, D.; Shafaei, S. Z.; Noaparast, M.; Abdollahi, H., Modeling and optimization of low-grade Mn bearing ore leaching using response surface methodology and central composite rotatable design. *Transactions of Nonferrous Metals Society of China* **2012,** *22* (9), 2295-2305. DOI: 10.1016/S1003-6326(11)61463-5.

85. Hazek, M. N. E.; Gabr, A. A., Dissolution of Manganese from Polymetallic Material Using Sulfuric-Oxalic Acid Medium. *American Journal of Analytical Chemistry* **2016,** *Vol.07No.05*, 9. DOI: 10.4236/ajac.2016.75044.

86. Kalpakli, A. O.; Ilhan, S.; Kahruman, C.; Yusufoglu, I., Dissolution behavior of calcium tungstate in oxalic acid solutions. *Hydrometallurgy* **2012,** *121-124*, 7-15. DOI: 10.1016/j.hydromet.2012.04.014.

87. Osthoff, R. C. Process for extracting tungsten values. US2942940A, 1956.

88. Davey, T. R. Method of extracting tungsten values from tungsten containing ores. US4910000A, 1990.

89. Yang, Y.; Wang, X.; Wang, M.; Wang, H.; Xian, P., Recovery of iron from red mud by selective leach with oxalic acid. *Hydrometallurgy* **2015,** *157*, 239-245. DOI: 10.1016/j.hydromet.2015.08.021.

90. Lee, S. O.; Tran, T.; Jung, B. H.; Kim, S. J.; Kim, M. J., Dissolution of iron oxide using oxalic acid. *Hydrometallurgy* **2007,** *87* (3), 91-99. DOI: 10.1016/j.hydromet.2007.02.005.

91. Vakilchap, F.; Mousavi, S.; Shojaosadati, S., Role of Aspergillus niger in recovery enhancement of valuable metals from produced red mud in Bayer process. *Bioresource technology* **2016,** *218*, 991-998. DOI: 10.1016/j.biortech.2016.07.059.

92. Gyliene, O.; Salkauskas, M., Metal recovery from spent electroless plating solutions by oxalate precipitation. *Plating and Surface Finishing* **1995,** *82*, 61-63.

93. Gylienė, O.; Šalkauskas, M.; Juškėnas, R., The use of organic acids as precipitants for metal recovery from galvanic solutions. *Journal of Chemical Technology & Biotechnology* **1997,** *70* (1), 111-115. DOI: doi:10.1002/(SICI)1097-4660(199709).

94. Lee, K. R.; Kim, J.; Jang, J. G., Recovery of zinc in spent pickling solution with oxalic acid. **2017,** *55*, 785-790. DOI: 10.9713/kcer.2017.55.6.785.

95. Yu, B.; Hse, C. Y.; Shupe, T. F. In *Rapid microwave-assisted acid extraction of metals from chromated copper arsenate (CCA)-treated southern pine wood*, In: The 40th Annual Meeting of the International Research Group on Wood Protection. Beijing, China: The International Research Group on Wood Protection. 1-11., 2009; pp 1-11.

96. Wei, M.; Chen, J.; Wang, X., Removal of arsenic and cadmium with sequential soil washing techniques using Na_2EDTA, oxalic and phosphoric acid: Optimization conditions, removal effectiveness and ecological risks. *Chemosphere* **2016,** *156*, 252-261. DOI: 10.1016/j.chemosphere.2016.04.106.

97. Ash, C.; Tejnecký, V.; Borůvka, L.; Drábek, O., Different low-molecular-mass organic acids specifically control leaching of arsenic and lead from contaminated soil. *Journal of Contaminant Hydrology* **2016,** *187*, 18-30. DOI: 10.1016/j.jconhyd.2016.01.009.

98. Shupe, T. F.; Hse, C. Y.; Pan, H. In *New Approach to Remove Metals from Chromated Copper Arsenate (CCA)-Treated Wood*, 2012.

99. Agatzini-Leonardou, S.; Oustadakis, P.; Tsakiridis, P.; Markopoulos, C., Titanium leaching from red mud by diluted sulfuric acid at atmospheric pressure. *Journal of hazardous materials* **2008,** *157* (2-3), 579-586. DOI: 10.1016/j.jhazmat.2008.01.054.

100. Malden, P. J.; Windle, W. Method of improving the whiteness of clays. US3482685, 1969.

101. Hernández, R. A. H.; García, F. L.; Cruz, L. E. H.; Luévanos, A. M., Iron removal from a kaolinitic clay by leaching to obtain high whiteness index. *IOP Conference Series: Materials Science and Engineering* **2013,** *45*, 012002. DOI: 10.1088/1757-899x/45/1/012002.

102. Veglio, F.; Passariello, B.; Barbaro, M.; Plescia, P.; Marabini, A. M., *Drum leaching tests in iron removal from quartz using oxalic and sulphuric acids*. 1998; Vol. 54, p 183-200.

103. Vegliò, F.; Passariello, B.; Abbruzzese, C., Iron Removal Process for High-Purity Silica Sands Production by Oxalic Acid Leaching. *Industrial & Engineering Chemistry Research* **1999,** *38* (11), 4443-4448. DOI: 10.1021/ie990156b.

104. Baumgartner, E.; Blesa, M. A.; Marinovich, H.; Maroto, A. J. G., Heterogeneous electron transfer as a pathway in the dissolution of magnetite in oxalic acid solutions. *Inorganic Chemistry* **1983,** *22* (16), 2224-2226. DOI: 10.1021/ic00158a002.

105. Lee, S.-O.; Kim, W.-T.; Oh, J.-K.; Shin, B.-S., Iron-removal of Clay Mineral with Oxalic Acid. *Shigen-to-Sozai* **1997,** *113* (11), 847-851. DOI: 10.2473/shigentosozai.113.847.

106. Lee, S.-O.; Oh, J.-k.; Shin, B.-S., Dissolution of Iron Oxide Rust Materials using Oxalic Acid. *Shigen-to-Sozai* **1999,** *115* (11), 815-819. DOI: 10.2473/shigentosozai.115.815.

107. Ubaldini, S.; Piga, L.; Fornari, P.; Massidda, R., Removal of iron from quartz sands: A study by column leaching using a complete factorial design. *Hydrometallurgy* **1996,** *40* (3), 369-379. DOI: 10.1016/0304-386X(95)00012-6.

108. Oviedo, C.; Rodríguez, J., EDTA: the chelating agent under environmental scrutiny. *Química Nova* **2003,** *26*, 901-905. DOI: 10.1590/S0100-40422003000600020.

109. Oustan, S.; Heidari, S.; Neyshabouri, M.; Reyhanitabar, A.; Bybordi, A. In *Removal of heavy metals from a contaminated calcareous soil using oxalic and acetic acids as chelating agents*, International Conference on Environment Science and Engineering IPCBEE, 2011; pp 152-155.

110. Ibrahim, L., Experimental study for heavy metals mitigation in polluted soil. *Basic Research Journal of Agricultural Science and Review* **2015,** *4(4)* (2315-6880), 119-126.

111. Tandy, S.; Bossart, K.; Mueller, R.; Ritschel, J.; Hauser, L.; Schulin, R.; Nowack, B., Extraction of heavy metals from soils using biodegradable chelating agents. *Environmental Science & Technology* **2004,** *38* (3), 937-944. DOI: 10.1021/es0348750.

112. Kato, Y.; Ogumi, Z.; Martín, J. M. P., *Lithium-ion Batteries: Overview, Simulation, and Diagnostics*. Jenny Stanford Publishing: Singapore, 2019.

113. Yoshino, A., The birth of the lithium-ion battery. *Angewandte Chemie International Edition* **2012,** *51* (24), 5798-5800. DOI: 10.1002/anie.201105006.

114. Armand, M., Intercalation electrodes. In *Materials for advanced batteries*, Springer: Boston, MA, 1980; pp 145-161.

115. Lazzari, M.; Scrosati, B., A cyclable lithium organic electrolyte cell based on two intercalation electrodes. *Journal of The Electrochemical Society* **1980,** *127* (3), 773. DOI: 10.1149/1.2129753.

116. Advanced information. NobelPrize.org. https://www.nobelprize.org/prizes/chemistry/2019/advanced-information/ (accessed 13 April 2020).

117. Brédas, J.-L.; Buriak, J. M.; Caruso, F.; Choi, K.-S.; Korgel, B. A.; Palacín, M. R.; Persson, K.; Reichmanis, E.; Schüth, F.; Seshadri, R., An Electrifying Choice for the 2019 Chemistry Nobel Prize: Goodenough, Whittingham, and Yoshino. *Chemistry of Materials* **2019,** *31(21)*, 8577-8581. DOI: 10.1021/acs.chemmater.9b04345.

118. Mizushima, K.; Jones, P.; Wiseman, P.; Goodenough, J. B., Li_xCoO_2 (0< x<-1): A new cathode material for batteries of high energy density. *Materials Research Bulletin* **1980,** *15* (6), 783-789. DOI: 10.1016/0025-5408(80)90012-4.

119. Hunter, J. C., Preparation of a new crystal form of manganese dioxide: λ-MnO_2. *Journal of Solid State Chemistry* **1981,** *39* (2), 142-147. DOI: 10.1016/0022-4596(81)90323-6.

120. Schipper, F.; Erickson, E. M.; Erk, C.; Shin, J.-Y.; Chesneau, F. F.; Aurbach, D., Review—Recent Advances and Remaining Challenges for Lithium Ion Battery Cathodes. *Journal of The Electrochemical Society* **2016,** *164* (1), A6220-A6228. DOI: 10.1149/2.0351701jes.

121. Walsh, F., Understanding cathodes and cells. *Transactions of the Institute of Metal Finishing(UK)* **1996,** *74* (2), 2-3.

122. Madian, M.; Eychmüller, A.; Giebeler, L., Current advances in TiO_2-based nanostructure electrodes for high performance lithium ion batteries. *Batteries* **2018,** *4* (1), 7. DOI: 10.3390/batteries4010007.

123. Rougier, A.; Gravereau, P.; Delmas, C., Optimization of the Composition of the $Li_{1-z}Ni_{1+z}O_2$ Electrode Materials: Structural, Magnetic, and Electrochemical Studies. *Journal of The Electrochemical Society* **1996,** *143* (4), 1168-1175. DOI: 10.1149/1.1836614.

124. Itou, Y.; Ukyo, Y., Performance of $LiNiCoO_2$ materials for advanced lithium-ion batteries. *Journal of Power Sources* **2005,** *146* (1), 39-44. DOI: 10.1016/j.jpowsour.2005.03.091.

125. Armstrong, A. R.; Bruce, P. G., Synthesis of layered $LiMnO_2$ as an electrode for rechargeable lithium batteries. *Nature* **1996,** *381* (6582), 499-500. DOI: 10.1038/381499a0.

126. Yabuuchi, N.; Ohzuku, T., Novel lithium insertion material of $LiCo_{1/3}Ni_{1/3}Mn_{1/3}O_2$ for advanced lithium-ion batteries. *Journal of Power Sources* **2003,** *119-121*, 171-174. DOI: 10.1016/S0378-7753(03)00173-3.

127. Shaju, K. M.; Bruce, P. G., Macroporous $Li(Ni_{1/3}Co_{1/3}Mn_{1/3})O_2$: A High-Power and High-Energy Cathode for Rechargeable Lithium Batteries. *Advanced Materials* **2006,** *18* (17), 2330-2334. DOI: 10.1002/adma.200600958.

128. Thackeray, M. M., Manganese oxides for lithium batteries. *Progress in Solid State Chemistry* **1997,** *25* (1), 1-71. DOI: 10.1016/S0079-6786(97)81003-5.

129. Thackeray, M. M.; de Picciotto, L. A.; de Kock, A.; Johnson, P. J.; Nicholas, V. A.; Adendorff, K. T., Spinel electrodes for lithium batteries — A review. *Journal of Power Sources* **1987,** *21* (1), 1-8. DOI: 10.1016/0378-7753(87)80071-X.

130. Nanjundaswamy, K. S.; Padhi, A. K.; Goodenough, J. B.; Okada, S.; Ohtsuka, H.; Arai, H.; Yamaki, J., Synthesis, redox potential evaluation and electrochemical characteristics of NASICON-related-3D framework compounds. *Solid State Ionics* **1996,** *92* (1), 1-10. DOI: 10.1016/S0167-2738(96)00472-9.

131. Armand, M.; Gauthier, M.; Magnan, J.-F.; Ravet, N. Method for synthesis of carbon-coated redox materials with controlled size. US7601318, 2009.

132. Pender, J. P.; Jha, G.; Youn, D. H.; Ziegler, J. M.; Andoni, I.; Choi, E. J.; Heller, A.; Dunn, B. S.; Weiss, P. S.; Penner, R. M.; Mullins, C. B., Electrode Degradation in Lithium-Ion Batteries. *ACS Nano* **2020,** *14* (2), 1243-1295. DOI: 10.1021/acsnano.9b04365.

133. Vetter, J.; Novák, P.; Wagner, M. R.; Veit, C.; Möller, K. C.; Besenhard, J. O.; Winter, M.; Wohlfahrt-Mehrens, M.; Vogler, C.; Hammouche, A., Ageing mechanisms in lithium-ion batteries. *Journal of Power Sources* **2005,** *147* (1), 269-281. DOI: 10.1016/j.jpowsour.2005.01.006.

134. Bai, P.; Li, J.; Brushett, F. R.; Bazant, M. Z., Transition of lithium growth mechanisms in liquid electrolytes. *Energy & Environmental Science* **2016,** *9* (10), 3221-3229. DOI: 10.1039/C6EE01674J.

135. Liu, T.; Lin, L.; Bi, X.; Tian, L.; Yang, K.; Liu, J.; Li, M.; Chen, Z.; Lu, J.; Amine, K.; Xu, K.; Pan, F., In situ quantification of interphasial chemistry in Li-ion battery. *Nature Nanotechnology* **2019,** *14* (1), 50-56. DOI: 10.1038/s41565-018-0284-y.

136. Edge, J. S.; O'Kane, S.; Prosser, R.; Kirkaldy, N. D.; Patel, A. N.; Hales, A.; Ghosh, A.; Ai, W.; Chen, J.; Yang, J.; Li, S.; Pang, M.-C.; Bravo Diaz, L.; Tomaszewska, A.; Marzook, M. W.; Radhakrishnan, K. N.; Wang, H.; Patel, Y.; Wu, B.; Offer, G. J., Lithium

ion battery degradation: what you need to know. *Physical Chemistry Chemical Physics* **2021,** *23* (14), 8200-8221. DOI: 10.1039/D1CP00359C.

137. Zhang, S.; Zhao, K.; Zhu, T.; Li, J., Electrochemomechanical degradation of high-capacity battery electrode materials. *Progress in Materials Science* **2017,** *89*, 479-521. DOI: 10.1016/j.pmatsci.2017.04.014.

138. Jung, R.; Metzger, M.; Maglia, F.; Stinner, C.; Gasteiger, H. A., Oxygen Release and Its Effect on the Cycling Stability of $LiNi_xMn_yCo_zO_2$(NMC) Cathode Materials for Li-Ion Batteries. *Journal of The Electrochemical Society* **2017,** *164* (7), A1361-A1377. DOI: 10.1149/2.0021707jes.

139. Radin, M. D.; Hy, S.; Sina, M.; Fang, C.; Liu, H.; Vinckeviciute, J.; Zhang, M.; Whittingham, M. S.; Meng, Y. S.; Van der Ven, A., Narrowing the Gap between Theoretical and Practical Capacities in Li-Ion Layered Oxide Cathode Materials. *Advanced Energy Materials* **2017,** *7* (20), 1602888. DOI: 10.1002/aenm.201602888.

140. Billy, E.; Joulié, M.; Laucournet, R.; Boulineau, A.; De Vito, E.; Meyer, D., Dissolution Mechanisms of $LiNi_{1/3}Mn_{1/3}Co_{1/3}O_2$ Positive Electrode Material from Lithium-Ion Batteries in Acid Solution. *ACS Applied Materials & Interfaces* **2018,** *10* (19), 16424-16435. DOI: 10.1021/acsami.8b01352.

141. Lux, S. F.; Lucas, I. T.; Pollak, E.; Passerini, S.; Winter, M.; Kostecki, R., The mechanism of HF formation in $LiPF_6$ based organic carbonate electrolytes. *Electrochemistry Communications* **2012,** *14* (1), 47-50. DOI: 10.1016/j.elecom.2011.10.026.

142. Li, W., Review—An Unpredictable Hazard in Lithium-ion Batteries from Transition Metal Ions: Dissolution from Cathodes, Deposition on Anodes and Elimination Strategies. *Journal of The Electrochemical Society* **2020,** *167* (9), 090514. DOI: 10.1149/1945-7111/ab847f.

143. Harper, G.; Sommerville, R.; Kendrick, E.; Driscoll, L.; Slater, P.; Stolkin, R.; Walton, A.; Christensen, P.; Heidrich, O.; Lambert, S., Recycling lithium-ion batteries from electric vehicles. *Nature* **2019,** *575* (7781), 75-86. DOI: 10.1038/s41586-019-1682-5.

144. Meshram, P.; Pandey, B.; Mankhand, T., Extraction of lithium from primary and secondary sources by pre-treatment, leaching and separation: A comprehensive review. *Hydrometallurgy* **2014,** *150*, 192-208. DOI: 10.1016/j.hydromet.2014.10.012.

145. Katwala, A., The spiralling environmental cost of our lithium battery addiction. Wired on Energy: 2018.

146. Nkulu, C. B. L.; Casas, L.; Haufroid, V.; De Putter, T.; Saenen, N. D.; Kayembe-Kitenge, T.; Obadia, P. M.; Mukoma, D. K. W.; Ilunga, J.-M. L.; Nawrot, T. S., Sustainability of

artisanal mining of cobalt in DR Congo. *Nature sustainability* **2018,** *1* (9), 495-504. DOI: 10.1038/s41893-018-0139-4.

147. Chen, M.; Ma, X.; Chen, B.; Arsenault, R.; Karlson, P.; Simon, N.; Wang, Y., Recycling End-of-Life Electric Vehicle Lithium-Ion Batteries. *Joule* **2019,** *3* (11), 2622-2646. DOI: 10.1016/j.joule.2019.09.014.

148. Ciez, R. E.; Whitacre, J. F., Examining different recycling processes for lithium-ion batteries. *Nature Sustainability* **2019,** *2* (2), 148-156. DOI: 10.1038/s41893-019-0222-5.

149. Pinegar, H.; Smith, Y. R., Recycling of End-of-Life Lithium Ion Batteries, Part I: Commercial Processes. *Journal of Sustainable Metallurgy* **2019,** *5* (3), 402-416. DOI: 10.1007/s40831-019-00235-9.

150. Verma, A.; Kore, R.; Corbin, D. R.; Shiflett, M. B., Metal Recovery Using Oxalate Chemistry: A Technical Review. *Industrial & Engineering Chemistry Research* **2019,** *58* (34), 15381-15393. DOI: 10.1021/acs.iecr.9b02598.

151. Li, L.; Ge, J.; Wu, F.; Chen, R.; Chen, S.; Wu, B., Recovery of cobalt and lithium from spent lithium ion batteries using organic citric acid as leachant. *Journal of Hazardous Materials* **2010,** *176* (1), 288-293. DOI: 10.1016/j.jhazmat.2009.11.026.

152. Li, L.; Ge, J.; Chen, R.; Wu, F.; Chen, S.; Zhang, X., Environmental friendly leaching reagent for cobalt and lithium recovery from spent lithium-ion batteries. *Waste Management* **2010,** *30* (12), 2615-2621. DOI: 10.1016/j.wasman.2010.08.008.

153. Golmohammadzadeh, R.; Rashchi, F.; Vahidi, E., Recovery of lithium and cobalt from spent lithium-ion batteries using organic acids: Process optimization and kinetic aspects. *Waste Management* **2017,** *64*, 244-254. DOI: 10.1016/j.wasman.2017.03.037.

154. Nayaka, G. P.; Pai, K. V.; Manjanna, J.; Keny, S. J., Use of mild organic acid reagents to recover the Co and Li from spent Li-ion batteries. *Waste Management* **2016,** *51*, 234-238. DOI: 10.1016/j.wasman.2015.12.008.

155. Shao-Horn, Y.; Croguennec, L.; Delmas, C.; Nelson, E. C.; O'Keefe, M. A., Atomic resolution of lithium ions in $LiCoO_2$. *Nature Materials* **2003,** *2* (7), 464-467. DOI: 10.1038/nmat922.

156. Verma, A.; Johnson, G.; Kore, R.; Corbin, D. R.; Shiflett, M. B. In *Recovery of Metals from Cathode of Lithium-Ion Batteries: A Closed-Loop Approach Using Oxalate Chemistry*, 2019 AIChE Annual Meeting, Orlando. Fl, AIChE: Orlando. Fl, 2019.

157. Verma, A.; Kore, R.; Corbin, D. R.; Shiflett, M. B. In *Role of Oxalate in Metal Separation and Recovery*, 2019 AIChE Annual Meeting, Orlando, Fl, AIChE: Orlando, Fl, 2019.

158. Adamson, A. W.; Sporer, A. H., Photochemistry of Complex Ions. I. Some Photochemical Reactions of Aqueous $PtBr_6^{-2}$, $Mo(CN)_8^{-4}$ and Various Co(III) and Cr(III) Complex Ions. *Journal of the American Chemical Society* **1958,** *80* (15), 3865-3870. DOI: 10.1021/ja01548a016.

159. Vraneš, M.; Gadžurić, S. B.; Zsigrai, I. J.; Dožić, S., Absorption spectra of cobalt(II) chloride and nitrate complexes in aqueous calcium nitrate–ammonium nitrate melts: The influence of solvent composition. *Journal of Molecular Liquids* **2010,** *152* (1), 34-38. DOI: 10.1016/j.molliq.2009.12.002.

160. Banic, N.; Vranes, M.; Abramović, B.; Canadi, J.; Gadžurić, S., Thermochromism, stability and thermodynamics of cobalt(II) complexes in newly synthesized nitrate based ionic liquid and its photostability. *Dalton Trans.* **2014,** *43*, 15515-15525. DOI: 10.1039/C4DT01836B.

161. Majumdar, P. K.; Gupta, A.; Mukherjee, R. K., Electronic absorption spectra of Co^{2+} in trimethylammonium cobalt chloride dihydrate ($(CH_3)_3NH)CoCl_3.2H_2O$ single crystal. *Journal of Physics C: Solid State Physics* **1986,** *19* (25), 4977-4983. DOI: 10.1088/0022-3719/19/25/014.

162. Verma, A.; Johnson, G. H.; Corbin, D. R.; Shiflett, M. B., Separation of Lithium and Cobalt from LiCoO2: A Unique Critical Metals Recovery Process Utilizing Oxalate Chemistry. *ACS Sustainable Chemistry & Engineering* **2020,** *8* (15), 6100-6108. DOI: 10.1021/acssuschemeng.0c01128.

163. Zheng, C.; Jian, R. H.; Pan, J. L.; Zou, C.; Wang, H.; Sheng, Y. Y.; Zhou, Q. F.; Liu, W. Q., Study on the preparation of battery grade cobalt carbonate from PTA oxidation residue. *Integrated Ferroelectrics* **2018,** *189* (1), 65-70. DOI: 10.1080/10584587.2018.1454805.

164. Levenspiel, O., *Chemical Reaction Engineering, John Wiley and Sons Inc*. 1999.

165. Gao, W.; Song, J.; Cao, H.; Lin, X.; Zhang, X.; Zheng, X.; Zhang, Y.; Sun, Z., Selective recovery of valuable metals from spent lithium-ion batteries–process development and kinetics evaluation. *Journal of Cleaner Production* **2018,** *178*, 833-845. DOI: 10.1016/j.jclepro.2018.01.040.

166. Yuliusman; Fajaryanto, R.; Nurqomariah, A.; Silvia, Acid leaching and kinetics study of cobalt recovery from spent lithium-ion batteries with nitric acid. *E3S Web Conf.* **2018,** *67*, 03025. DOI: 10.1051/e3sconf/20186703025.

167. Takacova, Z.; Havlik, T.; Kukurugya, F.; Orac, D., Cobalt and lithium recovery from active mass of spent Li-ion batteries: Theoretical and experimental approach. *Hydrometallurgy* **2016,** *163*, 9-17. DOI: 10.1016/j.hydromet.2016.03.007.

168. Nazemi, M.; Rashchi, F.; Mostoufi, N., A new approach for identifying the rate controlling step applied to the leaching of nickel from spent catalyst. *International Journal of Mineral Processing* **2011,** *100* (1-2), 21-26. DOI: 10.1016/j.minpro.2011.04.006.

169. Morin, D.; Gaunand, A.; Renon, H., Representation of the kinetics of leaching of galena by ferric chloride in concentrated sodium chloride solutions by a modified mixed kinetics model. *Metallurgical Transactions B* **1985,** *16* (1), 31-39. DOI: 10.1007/BF02657485.

170. Mustaffa, D.; Kamarulzaman, N.; Taib, M.; Rusdi, R.; Ibrahim, A. In *Theoretical investigations of Li^{+} and Co^{3+} positions for layered LiCoO2 Lithium ion battery cathode material using first principle method*, AIP Conference Proceedings, AIP Publishing LLC: 2017; p 080005.

171. Dillard, J. G.; Crowther, D. L.; Murray, J. W., The oxidation states of cobalt and selected metals in Pacific ferromanganese nodules. *Geochimica et Cosmochimica Acta* **1982,** *46* (5), 755-759. DOI: 10.1016/0016-7037(82)90027-8.

172. Liu, X.; Jiang, J.; Ai, L., Non-precious cobalt oxalate microstructures as highly efficient electrocatalysts for oxygen evolution reaction. *Journal of Materials Chemistry A* **2015,** *3* (18), 9707-9713. DOI: 10.1039/C5TA01012H.

173. Wang, D.; Wang, Q.; Wang, T., Morphology-Controllable Synthesis of Cobalt Oxalates and Their Conversion to Mesoporous Co_3O_4 Nanostructures for Application in Supercapacitors. *Inorganic Chemistry* **2011,** *50* (14), 6482-6492. DOI: 10.1021/ic200309t.

174. Parkhouse, J. G.; Kelly, A., The Random Packing of Fibres in Three Dimensions. *Proceedings of the Royal Society of London Series A* **1995,** *451*, 737. DOI: 10.1098/rspa.1995.0152.

175. Wang, C.; Wang, S.; Yan, F.; Zhang, Z.; Shen, X.; Zhang, Z., Recycling of spent lithium-ion batteries: Selective ammonia leaching of valuable metals and simultaneous synthesis of high-purity manganese carbonate. *Waste Management* **2020,** *114*, 253-262. DOI: 10.1016/j.wasman.2020.07.008.

176. Chen, X.; Chen, Y.; Zhou, T.; Liu, D.; Hu, H.; Fan, S., Hydrometallurgical recovery of metal values from sulfuric acid leaching liquor of spent lithium-ion batteries. *Waste management* **2015,** *38*, 349-356. DOI: 10.1016/j.wasman.2014.12.023.

177. Patterson, J. W.; Allen, H. E.; Scala, J. J., Carbonate Precipitation for Heavy Metals Pollutants. *Journal (Water Pollution Control Federation)* **1977,** *49* (12), 2397-2410.

178. Schwartz, M. O.; Ploethner, D., Removal of heavy metals from mine water by carbonate precipitation in the Grootfontein-Omatako canal, Namibia. *Environmental Geology* **2000,** *39* (10), 1117-1126. DOI: 10.1007/s002549900082.

179. Reddy, S. K.; Balasubramanian, S., Carbonic acid: molecule, crystal and aqueous solution. *Chemical Communications* **2014,** *50* (5), 503-514. DOI: 10.1039/C3CC45174G.

180. Salz, U.; Mücke, A.; Zimmermann, J.; Tay, F. R.; Pashley, D. H., pKa value and buffering capacity of acidic monomers commonly used in self-etching primers. *Journal of Adhesive Dentistry* **2006,** *8* (3). DOI: 10.3290/j.jad.a11222.

181. Wu, N.; Zhang, Y.; Wei, Y.; Liu, H.; Wu, H., Template-Engaged Synthesis of 1D Hierarchical Chainlike $LiCoO_2$ Cathode Materials with Enhanced High-Voltage Lithium Storage Capabilities. *ACS Applied Materials & Interfaces* **2016,** *8* (38), 25361-25368. DOI: 10.1021/acsami.6b09159.

182. Cinar, S.; Beler-Baykal, B., Ion exchange with natural zeolites: an alternative for water softening? *Water Science and Technology* **2005,** *51* (11), 71-77. DOI: 10.2166/wst.2005.0392.

183. Klein, G.; Villena-Blanco, M.; Vermeulen, T., Ion-Exchange Equilibrium Data in Design of a Cyclic Sea Water Softening Process. *Industrial & Engineering Chemistry Process Design and Development* **1964,** *3* (3), 280-287. DOI: 10.1021/i260011a017.

184. Alexandratos, S. D., Ion-Exchange Resins: A Retrospective from Industrial and Engineering Chemistry Research. *Industrial & Engineering Chemistry Research* **2009,** *48* (1), 388-398. DOI: 10.1021/ie801242v.

185. Kunin, R.; Meitzner, E.; Bortnick, N., Macroreticular Ion Exchange Resins. *Journal of the American Chemical Society* **1962,** *84* (2), 305-306. DOI: 10.1021/ja00861a035.

186. Kunin, R.; Barry, R. E., Carboxylic, weak acid type, cation exchange resin. *Industrial & Engineering Chemistry* **1949,** *41* (6), 1269-1272. DOI: 10.1021/ie50474a028.

187. Entezari, M. H.; Tahmasbi, M., Water softening by combination of ultrasound and ion exchange. *Ultrasonics sonochemistry* **2009,** *16* (3), 356-360. DOI: 10.1016/j.ultsonch.2008.09.008.

188. Kunin, R.; Meitzner, E.; Oline, J.; Fisher, S.; Frisch, N., Characterization of amberlyst 15. macroreticular sulfonic acid cation exchange resin. *Industrial & Engineering Chemistry Product Research and Development* **1962,** *1* (2), 140-144. DOI: 10.1021/i360002a016.

189. AMBERLYST™ 15DRY Polymeric Catalyst: Product Data Sheet. https://www.dupont.com/content/dam/dupont/amer/us/en/water-solutions/public/documents/en/45-D00927-en.pdf.

190. Zhang, P.-J.; Zhao, Z.-G.; Yu, S.-J.; Guan, Y.-G.; Li, D.; He, X., Using strong acid–cation exchange resin to reduce potassium level in molasses vinasses. *Desalination* **2012,** *286*, 210-216. DOI: 10.1016/j.desal.2011.11.024.

191. Huang, L.; Catterall, W. A.; Ehrenstein, G., Selectivity of cations and nonelectrolytes for acetylcholine-activated channels in cultured muscle cells. *The Journal of general physiology* **1978,** *71* (4), 397-410. DOI: 10.1085/jgp.71.4.397.

192. Sidey, V., On the effective ionic radii for ammonium. *Acta Crystallographica Section B: Structural Science, Crystal Engineering and Materials* **2016,** *72* (4), 626-633. DOI: 10.1107/S2052520616008064.

193. Rumble, J. R.; Bruno, T. J.; Doa, M., *CRC handbook of chemistry and physics : a ready-reference book of chemical and physical data*. CRC Press: Boca Raton, 2020.

194. Verma, A.; Corbin, D. R.; Shiflett, M. B., Lithium and cobalt recovery for lithium-ion battery recycle using an improved oxalate process with hydrogen peroxide. *Hydrometallurgy* **2021,** *203*, 105694. DOI: 10.1016/j.hydromet.2021.105694.

195. Kim, S.; Yang, D.; Rhee, K.; Sohn, J., Recycling process of spent battery modules in used hybrid electric vehicles using physical/chemical treatments. *Research on Chemical Intermediates* **2014,** *40* (7), 2447-2456. DOI: 10.1007/s11164-014-1653-2.

196. U.S. Energy Information Administration (EIA). https://www.eia.gov/dnav/ng/ng_pri_sum_dcu_nus_a.htm (accessed 10/17/2021).

197. Curran, P. The Economics Around Lithium-Ion Battery Recycling Are Strong and Growing. https://glginsights.com/articles/the-economics-around-lithium-ion-battery-recycling-are-strong-and-growing/ (accessed 10/02/2021).

198. Almodares, A.; Taheri, R.; Chung, M.; Fathi, M., The effect of nitrogen and potassium fertilizers on growth parameters and carbohydrate contents of sweet sorghum cultivars. *J. Environ. Biol* **2008,** *29* (6), 849-852.

199. Mona, A.; Sabah, M.; Rehab, A., Influence of potassium sulfate on faba bean yield and quality. *Australian Journal of Basic and Applied Sciences* **2011,** *5* (3), 87-95.

200. Verma, A.; Corbin, D. R.; Shiflett, M. B., Extraction of aluminum and iron from bauxite: A unique closed-loop ore refining process utilizing oxalate chemistry. *AIChE Journal (in press)*, e17477. DOI: 10.1002/aic.17477.

201. Hind, A. R.; Bhargava, S. K.; Grocott, S. C., The surface chemistry of Bayer process solids: a review. *Colloids and Surfaces A: Physicochemical and Engineering Aspects* **1999,** *146* (1), 359-374. DOI: 10.1016/S0927-7757(98)00798-5.

202. Hose, H. R., Bauxite Mineralogy. In *Essential Readings in Light Metals: Volume 1 Alumina and Bauxite*, Donaldson, D.; Raahauge, B. E., Eds. Springer International Publishing: Cham, 2016; pp 21-29.

203. Habashi, F., A Hundred Years of the Bayer Process for Alumina Production. In *Essential Readings in Light Metals: Volume 1 Alumina and Bauxite*, Donaldson, D.; Raahauge, B. E., Eds. Springer International Publishing: Cham, 2016; pp 85-93.

204. Power, G.; Gräfe, M.; Klauber, C., Bauxite residue issues: I. Current management, disposal and storage practices. *Hydrometallurgy* **2011,** *108* (1), 33-45. DOI: 10.1016/j.hydromet.2011.02.006.

205. McConchie, D.; Clark, M.; Davies-McConchie, F. In *New strategies for the management of bauxite refinery residues (red mud)*, Proceedings of the 6th international alumina quality workshop, 2002; pp 327-332.

206. Ujaczki, É.; Feigl, V.; Molnár, M.; Cusack, P.; Curtin, T.; Courtney, R.; O'Donoghue, L.; Davris, P.; Hugi, C.; Evangelou, M. W. H.; Balomenos, E.; Lenz, M., Re-using bauxite residues: benefits beyond (critical raw) material recovery. *Journal of Chemical Technology & Biotechnology* **2018,** *93* (9), 2498-2510. DOI: 10.1002/jctb.5687.

207. Zhang, R.; Zheng, S.; Ma, S.; Zhang, Y., Recovery of alumina and alkali in Bayer red mud by the formation of andradite-grossular hydrogarnet in hydrothermal process. *Journal of Hazardous Materials* **2011,** *189* (3), 827-835. DOI: 10.1016/j.jhazmat.2011.03.004.

208. Li Loretta, Y., Properties of Red Mud Tailings Produced under Varying Process Conditions. *Journal of Environmental Engineering* **1998,** *124* (3), 254-264. DOI: 10.1061/(ASCE)0733-9372(1998)124:3(254).

209. Wong, J.; Ho, G., Effectiveness of acidic industrial wastes for reclaiming fine bauxite refining residue (red mud). *Soil science* **1994,** *158* (2), 115-123. DOI: 10.1097/00010694-199408000-00005.

210. Khairul, M. A.; Zanganeh, J.; Moghtaderi, B., The composition, recycling and utilisation of Bayer red mud. *Resources, Conservation and Recycling* **2019,** *141*, 483-498. DOI: 10.1016/j.resconrec.2018.11.006.

211. Mayes, W. M.; Jarvis, A. P.; Burke, I. T.; Walton, M.; Feigl, V.; Klebercz, O.; Gruiz, K., Dispersal and Attenuation of Trace Contaminants Downstream of the Ajka Bauxite Residue (Red Mud) Depository Failure, Hungary. *Environmental Science & Technology* **2011,** *45* (12), 5147-5155. DOI: 10.1021/es200850y.

212. Zhu, D.-q.; Chun, T.-j.; Pan, J.; He, Z., Recovery of Iron From High-Iron Red Mud by Reduction Roasting With Adding Sodium Salt. *Journal of Iron and Steel Research, International* **2012,** *19* (8), 1-5. DOI: 10.1016/S1006-706X(12)60131-9.

213. Rath, S. S.; Pany, A.; Jayasankar, K.; Mitra, A. K.; Kumar, C. S.; Mukherjee, P. S.; Mishra, B. K., Statistical modeling studies of iron recovery from red mud using thermal plasma. *Plasma Science and Technology* **2013,** *15* (5), 459. DOI: 10.1088/1009-0630/15/5/13.

214. Agatzini-Leonardou, S.; Oustadakis, P.; Tsakiridis, P. E.; Markopoulos, C., Titanium leaching from red mud by diluted sulfuric acid at atmospheric pressure. *Journal of Hazardous Materials* **2008,** *157* (2), 579-586. DOI: 10.1016/j.jhazmat.2008.01.054.

215. Uzun, D.; Gülfen, M., Dissolution kinetics of iron and aluminium from red mud in sulphuric acid solution. *Indian Journal of Chemical Technology* **2007,** *14*, 263-268.

216. Çengeloğlu, Y.; Kir, E.; Ersöz, M., Recovery and Concentration of Al(III), Fe(III), Ti(IV), and Na(I) from Red Mud. *Journal of Colloid and Interface Science* **2001,** *244* (2), 342-346. DOI: 10.1006/jcis.2001.7924.

217. Gayer, K. H.; Thompson, L. C.; Zajicek, O. T., The Solubility of Aluminum Hydroxide in Acidic and Basic Media at 25 °C. *Canadian Journal of Chemistry* **1958,** *36* (9), 1268-1271. DOI: 10.1139/v58-184.

218. Parker, C., Induced autoxidation of oxalate in relation to the photolysis of potassium ferrioxalate. *Transactions of the Faraday Society* **1954,** *50*, 1213-1221. DOI: 10.1039/TF9545001213.

219. Pliego, G.; Zazo, J. A.; Casas, J. A.; Rodriguez, J. J., Fate of iron oxalates in aqueous solution: The role of temperature, iron species and dissolved oxygen. *Journal of Environmental Chemical Engineering* **2014,** *2* (4), 2236-2241. DOI: 10.1016/j.jece.2014.09.013.

220. Mangiante, D. M.; Schaller, R. D.; Zarzycki, P.; Banfield, J. F.; Gilbert, B., Mechanism of Ferric Oxalate Photolysis. *ACS Earth and Space Chemistry* **2017,** *1* (5), 270-276. DOI: 10.1021/acsearthspacechem.7b00026.

221. Panias, D.; Taxiarchou, M.; Douni, I.; Paspaliaris, I.; Kontopoulos, A., Thermodynamic Analysis of the Reactions of Iron Oxides: Dissolution in Oxalic Acid. *Canadian Metallurgical Quarterly* **1996,** *35* (4), 363-373. DOI: 10.1179/cmq.1996.35.4.363.

222. Zhu, X.; Jin, Q.; Ye, Z., Life cycle environmental and economic assessment of alumina recovery from secondary aluminum dross in China. *Journal of Cleaner Production* **2020,** *277*, 123291. DOI: 10.1016/j.jclepro.2020.123291.

Appendix

A.1. Experimental Setup and Specifics

This section will cover the details on the experimental setups and sampling procedures used in this dissertation.

A.1.1. Digestion Reactor

To carry out hydrometallurgical experiments, reactor must be made up of an inert material that has good stability with strong acids and oxidant at high temperature and pressure. For the experiments in this work, double-walled glass reactor from ACE glass was used. To integrate the temperature control system, and a sampling system the 1-L glass reactor was enclosed in a heating jacket with a 5-neck DURAN® head from which two thermocouples (sensory and over-temperature), electric agitator, and a reflux condenser were connected. The reflux condenser was connected to a chiller (water bath) operating at 5 °C to avoid the water loss during the metal extraction process. From the fifth neck, a syringe was connected to withdraw solid and aqueous samples for characterization and measuring metal concentrations. A simple schematic of the reactor and the actual image of reactor are shown in Figures A1 and A2.

A.1.2. Aqueous Phase Sampling

As mentioned in the previous section, samples were withdrawn using a plastic syringe, that contains both aqueous and solid phases. Hence, immediate separation of solid particles from acidic aqueous phase is necessary for accurate kinetics measurement. For this purpose, a 0.45 µm nylon syringe filter was used to separate the solid particles from aqueous phase. During some instances, inaccuracies in concentrations were observed when syringe plunger was pushed strongly. This

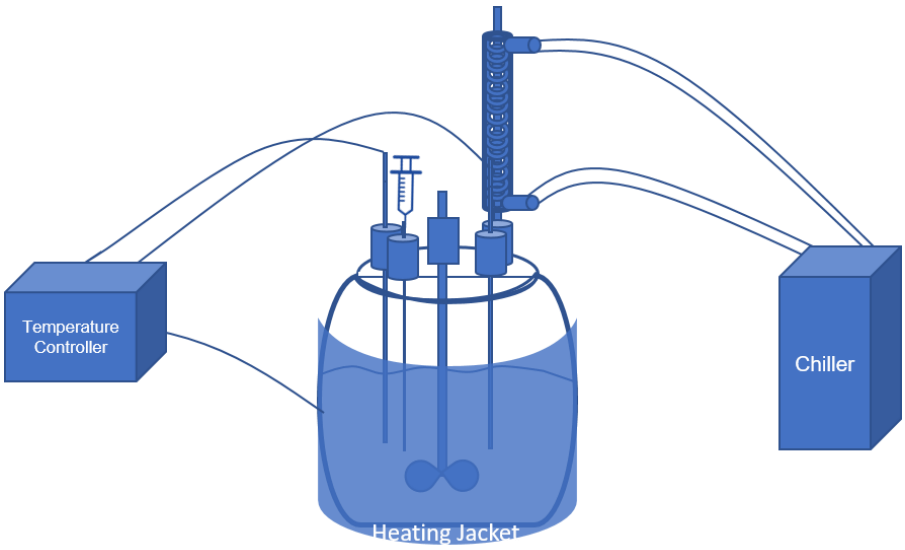

Figure A1. Schematic of the reactor used in hydrometallurgical experiments

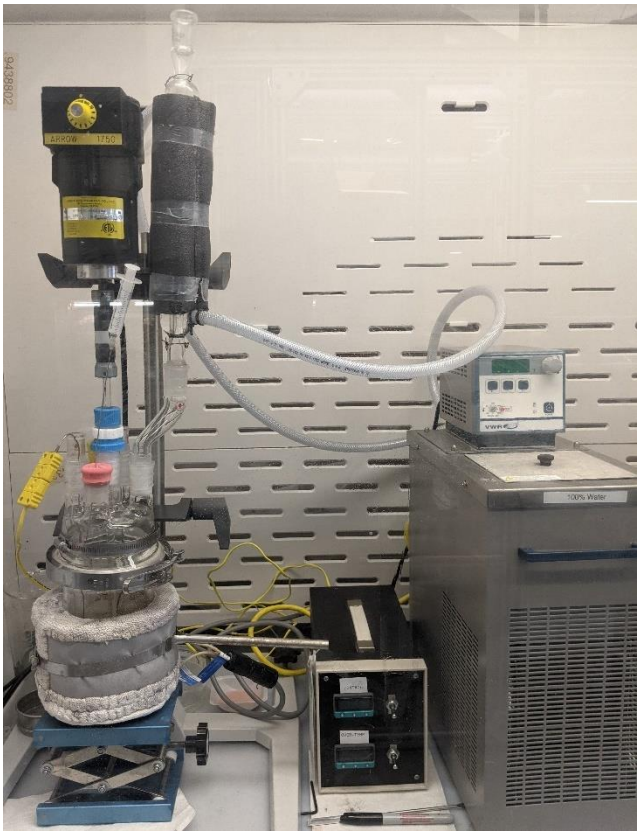

Figure A2. Metal extraction reactor used in hydrometallurgical experiments.

was attributed to the metal leaching from the fine solid particles that passed through the filter.

To avoid any errors, sampling technique was modified. After withdrawing the samples, the samples were immediately transferred to Falcon® tube and the reaction was quenched in the refrigerator. After 1 h, the samples were centrifuged at 3000 rpm for 5 mins. Upon centrifugation, a small amount of liquid (0.1 - 0.2 g) from was withdrawn to perform ICP dilutions.

A.1.3. Solid Phase Sampling

Intermediate solid particles during the hydrometallurgical experiments were required to estimate the metal ratios and observe the phase change through SEM imaging and powder diffraction pattern. The withdrawn solid samples after centrifugation were washed in DI water before filtering it using a 10 µm cellulose filter paper. Further, the solid residue was washed using deionized water until the conductivity of filtrate obtained is low (1-2 µS/cm). The solid residues were air dried before performing any characterization on it.

A.1.4. Hot Filtration Setup

Oxalate reagents have low aqueous solubility and may precipitate during the cooling process. Therefore, hot filtration was performed to avoid the precipitation of reactants with the solid products. To perform a hot filtration, ceramic funnel and vacuum flask were heated at 120 °C in an oven for 1 h. After 1 h, a wet 10 µm cellulose filter paper was used to filter the reactor content. The washing was also done with hot DI water (90 °C).

A.1.5. Microwave Reactor

To estimate the metal concentration in the solid phase, samples were digested in the microwave reactor using freshly prepared aqua regia. Aqua regia can dissolve most of the metals pertinent to this work except Si. For this purpose, Multiwave Pro reactor from Anton Paar (shown in Figure A3) was used to digest the solid samples at 300 W for 30 mins. Usually, 20 mg of solid

samples was mixed with 10 ml of aqua regia in the sample cell. The exact weight ratio between solid and aqueous phase is important to estimate the concentration of metals in the solid phase. The microwave wattage and digestion time could be altered depending on the solid material, but in general the above specified recipe was suitable for most of the material used in this work.

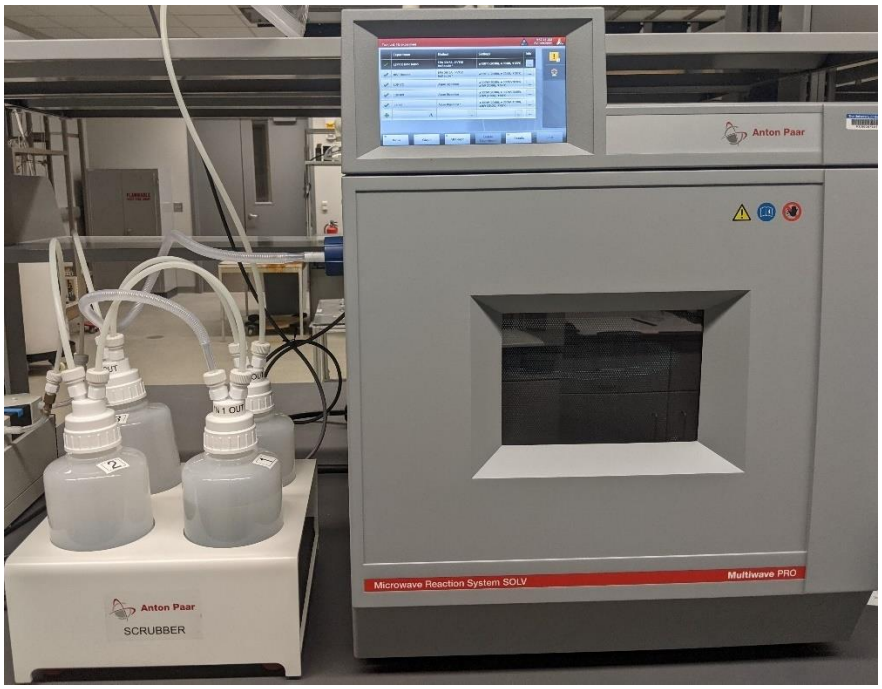

Figure A3. Image of microwave digestion reactor used in this work.

A.2. Characterization Instruments

This section includes a brief theory on characterization instruments used in this work along with the required sample preparation techniques.

A.2.1. Inductively Coupled Plasma – Optical Emission Spectroscopy (ICP-OES)

Instrument name: Varian/Agilent 725-ES ICP

Description: Agilent 725 contains a radially-viewed plasma and is vertically oriented with simultaneous CCD detection, which makes it more suitable for analysis of difficult matrices. It features an echelle polychromator equipped with a custom designed CCD detector producing

continuous wavelength from 167 to 784 nm. Along with that the toleration of undissolved solids is high in radial instruments which is better for analysis of minerals and ores. This instrument is also optimized for cost-efficiency through an efficient RF system, that minimizes the Ar flow required. The sample introduction unit consisted of a quartz-torch, nebulizer, and a spray chamber. An Agilent SPS5 autosampler was used to introduce the solutions to the instrument. The ICP and autosampler is shown in Figure A4.

Operating Principle: ICP-OES is an analytical technique for determination of concentrations of elements in a solution on the basis of atomic spectroscopy. As the name implies, atomic spectroscopy involves both absorption and/or emission of electromagnetic radiation from the atoms of a sample. In general, quantitative information such as concentration is related to the amount of radiation that is emitted (in cases of OES), while qualitative information like elements which are present is related to the wavelengths at which the radiation is emitted. In ICP-OES liquid samples are subjected to high temperatures from plasma that ionizes the sample atoms. Once the atoms or ions are in their excited states, they can decay to lower states through energy emissions. The amount of radiations emitted at specific wavelengths is measured and used to identify the elements and its concentration.

Instrument Calibration: The instrument was calibrated using a tuning solution containing numerous metals of specific concentrations. The commercially purchased tuning solution was diluted at a ratio of 1:10 using 5% HNO_3 before using it during the calibration. Along with the wavelength calibration, torch intensity and position also should be aligned before every measurement.

Sample Preparation: In this instrument, 5 wt% HNO_3 was used as the reference matrix for preparation of samples and standards. Along with that, a 2 wt% HNO_3 solution was used for rinsing

the solution line before calibration and after every measurement. Typically, the aqueous samples were diluted at a ratio that achieved less than 10 ppm concentration for all the desired metals. Hence, dilution ratio was varied on the basis of reaction parameters like solid-to-liquid ratio (S/L) and acid concentration.

Figure A4. Varian/Agilent 725-ES ICP used in this work.

A.2.2. Powder X-ray Diffraction (PXRD)

Instrument name: Bruker D2 Phaser Powder XRD

Description: D2 Phaser is a benchtop XRD fitted with a CoKα (1.78897 Å) radiation source and a LynxEye detector. The source voltage and current were 30 kV and 10 mA, respectively. It is a portable all-in-one design with no requirement of an external water chiller and special power supply. The D2 Phased XRD is shown in Figure A5.

Operating Principle: Any X-ray diffractometer consists of three main elements: a X-ray tube, a sample holder and an X-ray detector along with elements like monochromator and collimator. X-

rays are generated in the X-ray tube by bombarding high speed electrons on a target material. When electrons have sufficient energy to remove inner shell electrons, characteristic X-ray spectra is produced. The spectra produced is characteristic of the target metal used. Typically, Cu is the most common choice for target material, but for characterization of Co and Fe containing samples, Co anode is used to avoid sample fluorescence. Sample fluorescence leads to high background and low intensity in detection as most of the X-ray photons are absorbed by the sample. A monochromator filters the X-rays and with the help of collimator, X-rays are collimated and directed on a sample. As the sample and detector are rotated, 2θ angle is varied and X-rays are detected. For typical powder patterns, intensities are recorded between 2θ values of 5° and 70°. The interaction of the incident X-rays with the sample performs constructive interference (and a diffracted ray) when the Bragg's law is satisfied. Diffraction from different planes of atoms produces a diffraction pattern, and that was used to identify the solid powder.

Sample Preparation and pattern analysis: D2 Phaser XRD instrument have the specific sample disks that should be filled with finely ground powder sample for analysis. The sample holder typically needs roughly 200-300 mg of sample. In the case of small amount of sample, a zero diffraction Si disk could be sprinkled with small amount of powder and the assembly could be placed on the sample holder disk for analysis. The collected powder patterns can be analyzed in either EVA (Bruker) or MDI Jade software. Both available software's are equipped with the ICDD database and allows to fit the collected powder patterns to the patterns in the database.

Figure A5. D2 Phaser PXRD used in this work.

A.2.3. Thermogravimetric Analyzer (TGA)

Instrument Name: TA Instruments SDT Q600 TGA

Description: TA SDT Q600 is a simultaneous analyzer that can measure both heat flow and weight changes in sample as a function of temperature with the maximum operating temperature of 1500 °C. It consists of a high precision dual beam balance with sample pans and a bifilar wound furnace with platinum thermocouple for temperature measurement. Two gas inlets are provided to purge and control the furnace atmosphere during the heating. The instrument is shown in Figure A6.

Operating Principle: A TGA analysis is performed by gradually increasing the temperature of a sample enclosed in the furnace while measuring its weight. The masses of the sample and reference are measured using the sensitivity-calibrated drive coils separately and the weight difference is sent as a signal to record the weight loss. The change in weight of a sample can provide information

about phase transformation, physical adsorption and desorption as well as chemical phenomenon including chemisorptions, thermal decomposition and oxidation or reduction.

Sample Preparation: A 40 µL alumina cup was cleaned with a combination of isopropanol and DI water before filling it with 10-20 mg of sample. The sample was loosely packed in alumina cups for uniformly exposure to the gaseous flow.

Figure A6. Image of TGA instrument used in this work.

A.3. Derivation of Combined-Shrinking Core Model (cSCM)

Shrinking-core model (SCM) visualizes that the reaction between solid and fluid occurs first at the outer skin of the particle. The reaction zone slowly moves into the solid leaving behind completely converted material and an inert solid. The inert solid has been commonly referred as ash and at any time there exists an unreacted core along with an ash. As discussed in Chapter 3, SCM could be applicable for hydrometallurgical processes involving solid and liquid reactants with a solid and liquid product. The solid product formed in these cases is equivalent to ash described in the general SCM model. The model was first developed by Yagi and Kunii, and the kinetic equations

were developed by Levenspiel. A schematic of the solid particle reacting with a fluid and forming inert product layer is shown in Figure A7. For reaction: aA (g) + bB (s) → solid product, the kinetic equations were described as follows for different rate-controlling steps:

For film diffusion controlled, $t = \frac{\rho_s R}{3kC_a} X$ (A.1)

For ash diffusion controlled, $t = \frac{\rho_s R^2}{6DC_a}[1 - 3(1-X)^{\frac{2}{3}} + 2(1-X)]$ (A.2)

For reaction controlled, $t = \frac{\rho_s R}{k'C_a}(1-(1-X)^{\frac{1}{3}})$ (A.3)

If the rate of a process is controlled by all three mechanisms,

$$t = \frac{\rho_s R}{3bkC_a} X + \frac{\rho_s R^2}{6bDC_a}[1-3(1-X)^{\frac{2}{3}} + 2(1-X)] + \frac{\rho_s R}{bk'C_a}(1-(1-X)^{\frac{1}{3}}) \quad (A.4)$$

$$t = \tau_F X + \tau_P[1-3(1-X)^{\frac{2}{3}} + 2(1-X)] + \tau_R(1-(1-X)^{\frac{1}{3}}) \quad (A.5)$$

where, ρ_s is the density of the solid particle, R is the initial radius of the solid particle, C_a is the concentration of the reaction species in the gaseous phase, k is the mass transfer coefficient between the gaseous and solid phase, D is the effective diffusion coefficient of gaseous reactant in the ash layer and k' is the first order rate constant for the surface reaction.

In the above equation, experimental X (conversion of solid particle) vs *t* (time) data can be fitted using a least square minimization problem to obtain the constant parameters (τ_F,τ_P,τ_R). If the reaction is controlled by only one parameter, all the other parameter except that should be zero.

A.3.1. Least Square Minimization Problem for cSCM

$$t = \tau_R\left[1-(1-X)^{\frac{1}{3}}\right] + \tau_P\left[1-3(1-X)^{\frac{2}{3}} + 2(1-X)^{\frac{1}{3}}\right] + \tau_F X \quad (A.6)$$

Eq. A.6 for the cSCM can be transformed into a minimization problem as shown in eq. A.7

$$\Phi = \sum_i\left[\tau_R\left[1-(1-X_i)^{\frac{1}{3}}\right] + \tau_P\left[1-3(1-X_i)^{\frac{2}{3}} + 2(1-X_i)^{\frac{1}{3}}\right] + \tau_F X_i - t_i\right]^2 \quad (A.7)$$

-

Using the least square technique, eq. A.7 can be minimized and τ_R, τ_P and τ_F can be calculated (τ_R, τ_P, $\tau_F > 0$).

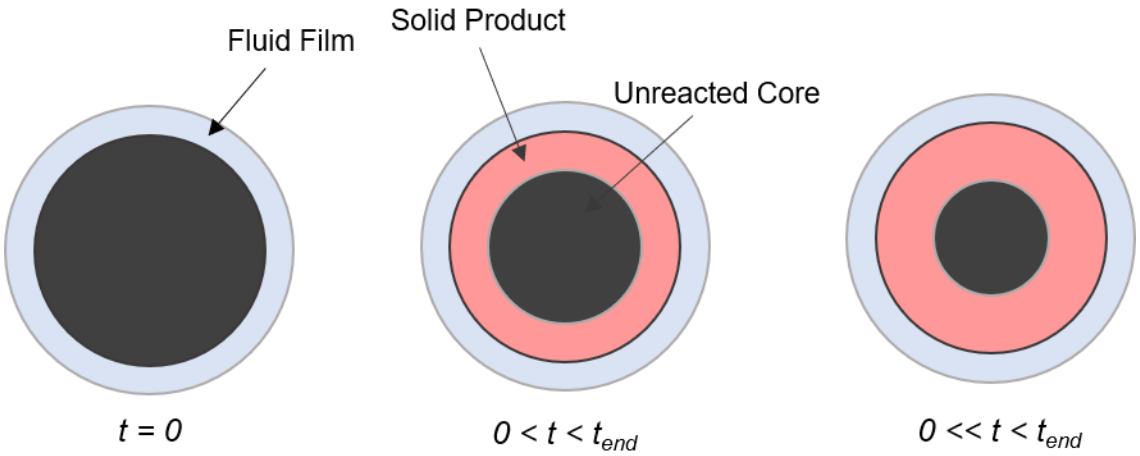

Figure A7. Representation of a solid particle reacting with the fluid and forming a product layer.

A.3.2. Methodology used for cSCM Parameter Estimation

The measured concentration versus time data for a metal can be converted into extraction efficiency (%) using the maximum possible concentration

1. Divide the extraction efficiency (%) for every t_i by 100 to obtain a set of (t_i, X_i)
2. Provide an initial value for τ_R, τ_P and τ_F. The sum of these initial values should be less than or equal to the total reaction time. Assuming an equal control for each rate-limiting step is a good estimate.
3. Substitute the independent variables: t_i and X_i , along with estimated values for τ_R, τ_P and τ_F in eq S2 and calculate Φ.
4. Minimize Φ to obtain calculated τ_R, τ_P and τ_F.

The minimization could be performed either through the problem solver in MS Excel or by using the lsqcurvefit optimization algorithm in MATLAB.

Standard Error Calculation

$$\text{Standard Error} = \sqrt{\frac{\sum_i (t_i - t_{fit,i})^2}{\text{DOF}}} \tag{A.8}$$

Degrees of freedom (DOF) is defined as the number of data points minus the number of parameters in the minimization problem. The value for the standard error should be close to zero for a good fit.